DOCTOR OF PHILOSOPHY

Functional characterisation of Schizosaccharomyces pombe meiotic linear elements

Dafydd, Heledd Fflur

Award date:
2011

Awarding institution:
Bangor University

Functional characterisation of *Schizosaccharomyces pombe* meiotic linear elements

Heledd Fflur Dafydd

Prifysgol Bangor

PhD thesis 2011

Abstract

Sexual reproduction in eukaryotes requires the creation of haploid gametes from diploid cells by a specialized cell division called meiosis. Correct alignment and orientation of the homologues on the metaphase I plate is crucial for the correct reductional segregation of chromosomes during meiosis. In most organisms, homologue alignment is concurrent with, although distinct from, a process called synapsis, which is the close association between the homologues within the context of a proteinaceous structure formed along the entire length of the chromosome, called the synaptonemal complex (SC).

The model yeast system *Schizosaccharomyces pombe* exhibits an SC-free meiosis. In *S. pombe,* proteinaceous structures termed linear elements (LinEs) are formed, which vary in length and are classified accordingly. A major component of LinEs is the Rec10 protein. Different mutations in the *rec10* gene result in distinct defects in the formation and/or development of LinEs alongside varying effects on meiotic recombination.

In this study, we demonstrate the temporal order of LinE formation and maturation, correlated with Rad51 and Hop1 localisation. Cytological analysis of Hop1 localisation revealed the presence of as yet unidentified structures.

A multiple sequence alignment of the C-terminal domain of Rec10 with axial proteins of other organisms exhibited domain homology, with some residues being highly conserved. Based on this, this study generated several *rec10* mutants exhibiting different point mutations within the C-terminal domain of *rec10.* In this study we analysed the temporal profile of LinE development and the recombination proficiency of these mutants.

This study analysed the temporal profile of LinE development in mutants of LinE-associated proteins, previously demonstrated as having altered LinE formation; demonstrating that Rec27 is not required for initiation of LinE formation, as previously proposed.

In addition, we present data that is in agreement with the regions of crossover preference model. We also analyse LinE formation in several *rec10* heterozygous diploids, demonstrating semi-dominance of some *rec10* mutant alleles.

Acknowledgements

I would like to thank K. Tanaka for strains and J. Loidl for the Hop1-ab.
Thank you to Jenny Wells and Ramsay MacFarlane for the opportunity to discuss unpublished data. Diolch i Mantais am y cyfle i astudio ym Mangor, ac i Deri Tomos am ei arweiniad.
I would also like to thank Ramsay for the opportunity of working in his laboratory, for all his advice, guidance and patience along the way. Thanks also to Dave for always being around to put a smile on my face and to Alessa and Becky for countless lunches, sympathetic ears and your friendship. Thanks to all members of 'G30', as well as the technical and administrative staff, who have been both supportive and helpful.
Diolch i fy nheulu annwyl; Dad & Mam, am eich gofal tyner, eich cyfeillgarwch, eich hyder ynof fi a'ch cefnogaeth – yn ogystal â'r cannoedd o baneidiau a sgyrsiau dros y misoedd/blynyddoedd diwethaf! Mared a Gwion, am eich cwmni a'r hwyl ac am garu fi jest fel ydwi ☺! Rich, am fod ar gael bob amser i roi gwên ar fy ngwyneb i.
Diolch arbennig hefyd i Cati ag Andres - muchas gracias! Dave & Tina, Derek & Betty, David & Rachel a Thelma – diolch am eich cyfeillgarwch ac am bob gweddi ar hyd y ffordd.

CODAF FY LLYGAID TUA'R MYNYDDOEDD; O BLE DAW CYMORTH I MI?
DAW FY NGHYMORTH ODDI WRTH YR ARGLWYDD, CREAWDWR NEFOEDD A DAEAR.
NID YW'N GADAEL I'TH DROED LITHRO, AC NID YW DY GEIDWAD YN CYSGU.
NID YW CEIDWAD ISRAEL YN CYSGU NAC YN HUNO.
YR ARGLWYDD YW DY GEIDWAD, YR ARGLWYDD YW DY GYSGOD AR DY DDEHEULAW;
NI FYDD YR HAUL YN DY DARO YN Y DYDD, NA'R LLEUAD YN Y NOS.
BYDD YR ARGLWYDD YN DY GADW RHAG POB DRWG, BYDD YN CADW DY EINIOES.
BYDD YR ARGLWYDD YN GWYLIO DY FYND A'TH DDOD YN AWR A HYD BYTH.

Abbreviations

ADCR	ATP-dependent chromatin remodelling factor
ATP	adenosine-5'-triphosphate
CO	crossover
CRE	cAMP-responsive-element
DAPI	4'-6-diamidino-2-phylindole
sHJ	single Holliday Junction
dHJ	double Holliday junction
DMSO	dimethyl sulfoxide
DNA	deoxyribonucleic acid
DSB	double-strand break
DTT	1,4-dithio-DL-threitol
EDTA	ethylenediaminetetraacetic acid
EM	electron microscope
EMM2	Edinburgh minimal media
EMM2-N	Edinburgh minimal media without Nitrogen
EtOH	ethanol
FACS	fluorescence activated cell sorting
HAT	histone acetyl transferase
HJ	Holliday junction
HR	homologous recombination
kb	kilobase
LinE	linear element
MI	meiosis I
MII	meiosis II
MES	(2-(*N*-morpholino) ethane sulfonic acid)
MM	minimal media
MM-N	minimal media without nitrogen
MNase	micrococcal nuclease
MRN	Mre11-Rad50-Nbs1
MRX	Mre11-Rad50-Xrs2
NB	nitrogen base

NCO	non-crossover
ncRNA	non-coding RNA
NHEJ	non-homologous end joining
PBS	phosphate buffered saline
PC	polycomplex
PI	propidium iodide
PMSF	phenylmethylsulfonyl fluoride
SC	synaptonemal complex
SDS	sodium dodecyl sulfate
SMC	structural maintenance of chromosomes
SPA	sporulation agar
SPB	spindle pole body
SSA	single strand annealing
SUMO	small ubiquitin-related modifier
TE	tris EDTA
YEL	yeast extract liquid
YEA	yeast extract agar

Index

Figures List

Chapter 1

Chapter 3

Chapter 4

Chapter 5

Chapter 6

Chapter 7

Chapter 8

List of Tables

Chapter 2

Chapter 5

Chapter 7

Chapter 1

1.1 Introduction

Sexual reproduction in eukaryotic organisms requires the production of haploid cells (gametes) from diploid parental cells. Gametes are formed through a specialised type of cell division known as meiosis. Meiosis consists of a single round of DNA replication followed by two subsequent rounds of chromosome segregation. During meiosis I (MI) (Figure 1.1), homologous chromosomes pair, recombine, then segregate to opposite poles, with the sister chromatids remaining associated with each other via meiosis-specific chromatid cohesion. This is the reductional division and results in a halving of the cell's DNA content. During meiosis II (MII) it is the sister chromatid that segregate to opposite poles (resembling the equational segregation exhibited in mitosis) (see Figure 1.1). Diploidy is restored by the fusion of two gametes during sexual reproduction, culminating in the production of a genetically unique diploid zygote (reviewed in YANOWITZ 2010).

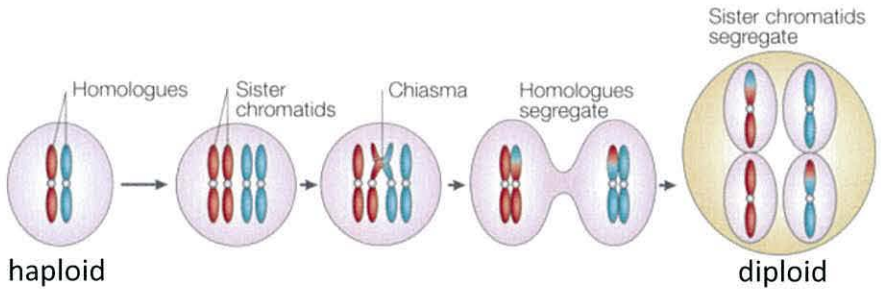

Figure 1.1 The meiotic divisions. During meiosis, the parental homologous chromosomes undergo pre-meioitic DNA replication, which yields pairs of sister chromatids. The sister chromatids are held together along their entire length by meiotic cohesins.
Homologous chromosomes pair, align and recombine. This recombination can lead to the formation of physical associations between the homologues – termed chiasmata, which serve to retain the association of homologous chromosomes until their faithful segregation during MI. The segregation of homologues is known as the reductional division as it halves the DNA content of each cell. Centromeric cohesion is retained between the sister chromatids throughout MI to ensure that they do not separate prematurely. When centromeric sister-chromaitd cohesion is subsequently lost, sister-chromatids are 'allowed' to separate (MII). The equational division during MII results in the formation of four haploid daughter cells. Figure adapted from MARSTON & AMON (2004).

Meiosis is a fundamentally important process for many living creatures. It not only produces the haploid gametes essential for sexual reproduction, it also maintains genetic diversity by the reciprocal exchange of genetic material during meiotic recombination. Genetic diversity is a must within any species population – ensuring long-term survival in accordance with the 'survival of the fittest' hypothesis.

1.2 The sub-stages of meiosis

Meiosis has been artificially divided into many different stages to distinguish the sequence of chromosomal and cellular events, although it occurs *in vivo* as a continuous process. Meiosis includes a single round of DNA replication, followed by the two main stages of chromosome segregation, MI and MII. MI is separated into four main stages; prophase I, anaphase I, metaphase I and telophase I. Prophase I consists of five sub-stages:

Leptotene	Replicated chromosomes condense and become visible.
Zygotene	Homologous chromosomes pair and begin to synapse. Telomeres cluster to one end of the nucleus as chromosomes take on the bouquet-like configuration (thought to aid the alignment of homologous chromosomes).
Pachytene	Homologous chromosomes are fully synapsed within the context of a proteinacious structure called the synaptonemal complex (SC); chromosomes begin to crossover at distinct recombination nodules (chiasmata).
Diplotene	The SC begins to degrade. Homologous chromosomes condense, but remain associated via chiasmata.
Diakinesis	The SC has completely dissociated. Homologous chromosomes condense further, but remain firmly attached via chiasmata

During metaphase I, microtubules emanating from opposite spindle poles of the cell attach to the kinetochores of the homologous chromosomes as they align on the metaphase I plate. The microtubule attachments ensure correct chromosomal alignment, and subsequent segregation at anaphase I. The nuclear envelope encapsulates the two new haploid daughter cells at telophase I, and the chromosomes decondense, although sister-chromatids remain attached. There is no S-phase between MI and MII. During prophase II, the chromatin condenses again, and chromosomes become more defined. The chromosomes align at the metaphase II plate, and sister-chromatids segregate in the equational segregation at anaphase II. Telophase II exhibits the formation of nuclear envelopes encompassing the 4 new daughter cells.

1.3a Meiosis in *S. pombe*

S. pombe is a preferentially haploid organism although it can exist as a diploid under certain conditions. It consists of 3 chromosomes: chromosome 1 = 5.7 Mb; chromosome 2 = 4.6 Mb; chromosome 3 = 3.5 Mb. In stress-free conditions, haploid *S. pombe* cells grow vegitively, alternating between growth (including DNA replication) and subsequent mitotic division (Figure 1.2). Having only 3 chromosomes, *S. pombe* is still able to generate a substantial number of viable spores in the absence of meiotic recombination. This fact makes *S. pombe* a valuable experimental tool, facilitating the study of meiotic recombination-deficient mutants.

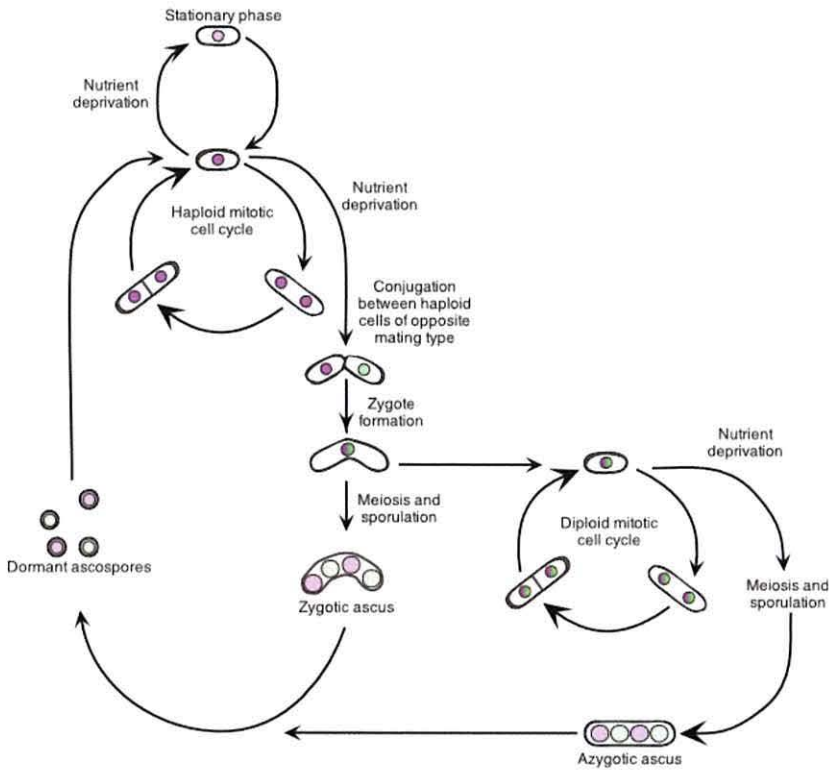

Figure 1.2 Life cycle of *S. pombe*. The magenta and green represent the two opposite mating types (h^+ and h^-) of *S. pombe*. These colours are lighter in spores and stationary phase to indicate genetic inactivity. In diploids, both colors are present to indicate that the *S. pombe* diploid nucleus contains both h^+ and h^- determinants.
Figure adapted from NURSE *et al.*, 1997.

Environmental factors, such as low nitrogen levels can trigger meiosis in *S. pombe. S. pombe* can exhibit a zygotic, or azygotic meiosis. A number of pathways are involved with entry into meiosis in *S. pombe* (Figure 1.3). Zygotic meiosis is induced when haploid cells expressing *mat1* mating pheromone heterozygosity (*mat1-P*/h^+ and *mat1-M*/h^-) conjugate under conditions of environmental stress, and their nuclei fuse (karyogamy), generating a diploid cell. *S. pombe* utilises a number of mitogen-activated protein kinase (MAPK) signal transduction cascades in meiosis. Each MAPK cascade consists of three enzymes: MAPKKK (activated by extracellular stimuli), phosphorylates a MAPKK on its serine and threonine residues; MAPKK, activated by serine/threonine phosphorylation, phosphorylates a MAPK on its threonine and tyrosine residues; and MAPK. Mating pheromone signals received by either the Mam2 or Map3 G-protein coupled receptors activate the Byr2 (MAPKKK), Byr1 (MAPKK) Spk1 (MAPK)

cascade (NEIMAN *et al.*, 1993), which ultimately results in Ste11 phosphorylation and activation (KJÆRULFF *et al.*, 2005). Whilst 'stress' in the form of nitrogen limitation (SHIOZAKI & RUSSELL, 1996) and carbon starvation (MORIGASAKI *et al.*, 2008) activate the stress activated protein kinase (SAPK) Wak1/Win1-Wis1-Spc1 MAPK protein kinase cascade which ultimately results in phosphorylation of Atf1 (transcription factor) (WILKINSON *et al.,* 1996).

Azygotic meiosis is induced in a cell that is already diploid, in response to conditions of environmental stresses.

Lowering of glucose (carbon source) and/or nitrogen cause these diploids to:

1. Activate the stress activated protein kinase (SAPK) Wak1/Win1-Wis1-Spc1 MAPK protein kinase cascade.
2. Inactivate the protein kinase Pka1 (repressor of Ste11) by lowering the cAMP concentration levels by activity of adenylate cyclase (ISSHIKI *et al.,* 1992).

These two pathways culminate in the induction of *ste11* transcription (SUGIMOTO *et al.,* 1991). Ste11 is a meiotic transcription factor (SUGIMOTO *et al.,* 1991), involved in the induction of *mat1-P* and *mat1-M* expression – their co-expression resulting in Mei3 activation (WILLER *et al.,* 1995). Mei3 acts as a substrate for Pat1 (mitotic negative regulator of meiosis) – inhibiting its kinase activity. The inhibition of Pat1 subsequently permits activation of Mei2 (an RNA binding protein) – which is vital for meiotic induction (NURSE 1985). Dephosphorylation of Mei2, by inhibition of Pat1 kinase, is sufficient to permit entry into meiosis (PENG *et al.,* 2003). Ste11 regulates the activation of Cdc10 and Rep1 (also known as Rec16) (CUNLIFFE *et al.,* 2004). These two proteins form a meiosis-specific complex that transcriptionally activates genes known to be required for meiotic replication and recombination (SUGIYAMA *et al.,* 1994).

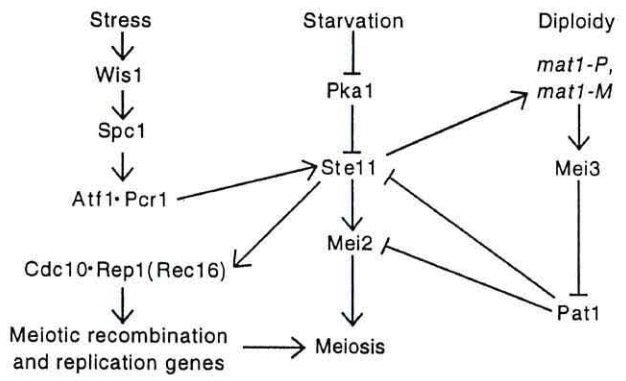

Figure 1.3 Controlling entry into meiosis in *S. pombe*. Arrows indicate activation of one protein by the other; straight lines indicate inhibition or repression of one protein by the other. Figure is adapted from (DAVIS and SMITH 2001).

1.3b Pat1 kinase

Pat1 kinase is a mitotic protein, negatively regulating meiosis. Itself being negatively regulated by Mei3, Pat1 suppresses the activation of Mei2, an RNA-binding protein that controls the transition between meiotic G_1 and S-phase. Although azygotic meiosis is known to be more synchronous than a zygotic meiosis, a mutation in *pat1* can produce an even more synchronous meiosis – a useful tool for temporal analysis of meiosis. When shifted from 25°C (permissive temperature) to the restrictive temperature (37°C), the *pat1-114* temperature sensitive mutant (IINO and YAMAMOTO 1985) triggers entry into meiosis without the need for many of the prerequisite mechanisms usually required for meiotic induction. *pat1-114* thermally triggered meiosis may even be induced from G_2 (WATANABE *et al.*, 2001).

1.4a Cohesion

Cohesins are a very important family of proteins, serving to retain sister chromatid / homologous chromosome cohesion during mitosis and meiosis (NASMYTH 2001). Retention of cohesion generates the tension required to ensure the correct alignment of chromosomes prior to their segregation; subsequent cleavage of cohesion via a protease named separase, frees the chromosomes for migration towards opposite poles of the nucleus. Cohesins have also been

implicated in the regulation of gene expression in yeast (GARTENBERG 2009), mouse (WENDT and PETERS 2009) and the fruit fly (DORSETT 2009).

1.4b Mitotic Cohesion

There are four core units involved in mitotic cohesion: two structural maintenance of chromosome (SMC) proteins, Smc1 and Smc3; a kleisin family protein, Scc1 (also known as Mcd1 in *Saccharomyces cerevisiae*, and Rad21 in *S. pombe*); and Scc3 (Psc3 being the *S. pombe* ortholog)(NASMYTH and HAERING 2005). Pds5 also appears to be associated, although less tightly bound to the mitotic cohesin complex (HARTMAN *et al.,* 2000). It is proposed that the two SMC proteins dimerize. The Scc proteins bind to each other, and serve to connect the Smc heterodimer, resulting in the formation of a large proteinaceous ring (Figure 1.4).

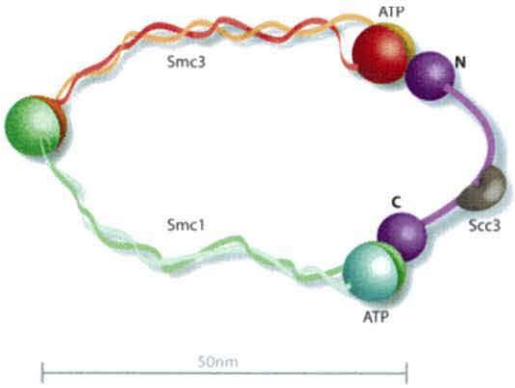

Figure 1.4 Structure of the cohesin complex. Smc1 (green) and Smc3 (orange) form a hinged heterodimer. The C- and N- terminal of Scc1 (purple) associates with Smc1 and Smc3 respectively; forming a closed-ring structure. Scc3 (grey) binds directly with Scc1. Figure adapted from FEENEY *et al.*, 2010.

Current data supports a model that proposes that this cohesin ring encircles both sister chromatids, directly mediating sister chromatid cohesion – known as 'The Ring Model' (GRUBER *et al.,* 2003). However, in a second hypothesis, 'The Handcuff Model', each sister chromatid is encircled by its own cohesin ring, the

two cohesin rings then associate with one another, facilitating cohesion of the DNA strands (FEENEY *et al.,* 2010) (Figure 1.5).

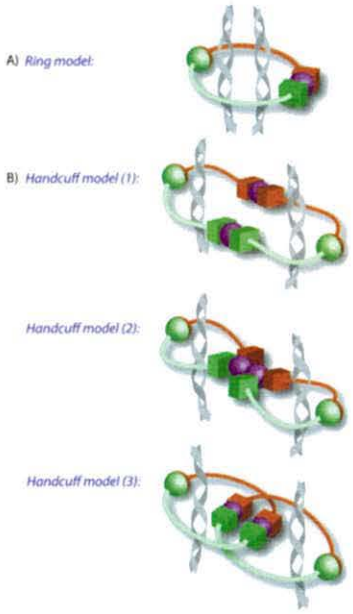

Figure 1.5 Models of sister-chromatid cohesion via the cohesin ring. (A), shows the ring model, in which a single cohesin ring encircles both sister chromatids. (B) 1, 2 and 3 show variations of the handcuff model, in which each sister chromatid is encircles by a cohesin ring, and it is the association of the two cohesin rings that facilitates sister-chromatid cohesion. Figure adapted from FEENEY *et al.*, 2010.

Cohesin associates with DNA at the end of G1 phase in lower eukaryotes (GUACCI *et al.*,1997; MICHAELIS *et al.,* 1997) this process occurs earlier in mammalian cells, cohesin associating with DNA following the reformation of the nuclear envelope during telophase (DARWICHE *et al.,* 1999). Loading of cohesin requires the aid of loading factor Scc2-Scc4 (CIOSK *et al.,* 2000), which is proposed to facilitate the 'opening' of the cohesin ring via ATP hydrolysis (ARUMUGAM *et al.*, 2000). Eco1 acetyl transferase (Eso1 in *S. pombe*) facilitates the establishment of cohesion during S-phase (IVANOV *et al.,* 2002). Cohesion is maintained throughout G_2. In *S. pombe* and metozoa, loss of cohesion has been observed as a regulated two-step process; arm cohesion is lost at the end of prophase in a pathway independent of

Rad21 (Scc1) cleavage (DARWICHE *et al.,* 1999; SCHMIDT *et al.,* 2009; WAIZENEGGER *et al.,* 2000). Both sister chromatid kinetochores are captured by microtubules emanating from opposite poles of the nucleus during metaphase. Tension is generated between sister chromatids as the microtubules attempt to pull the kinetochores of the sister chromatids apart whilst pericentromeric cohesion of sister chromatids tries to retain their association. This tension stabilizes kinetochore-microtubule attachments, and ensures the correct orientation of sister-chromatids in preparation for their subsequent segregation (DEWAR *et al.,* 2004). At the onset of anaphase, the Scc1 subunit of cohesin is cleaved by a specific protease termed separase, triggering equational chromatid disjunction (NASMYTH 2001; UHLMANN 2003). A regulatory mechanism, termed the spindle assembly checkpoint ensures that cleavage is blocked until all kinetochore-microtubule attachments have been formed (WAIZENEGGER *et al.,* 2000; UHLMANN *et al.,*1999; UHLMANN *et al.,* 2000). Separase is kept inactive by its association with an inhibitory chaperone protein called securin. Once the spindle assembly checkpoint has been inactivated, securin is targeted for degradation, leaving separase free to completely remove cohesin complexes along the entire length of the chromosome.

1.4c Meiotic Cohesion

First identified in *S. pombe* by mutations exhibiting reduction in meiotic recombination at the *ade6* locus (PONTICELLI and SMITH 1989), Rec8 and Rec11 are meiotic, sister-chromatid cohesion proteins, localizing to the chromosomes around the time of pre-meiotic replication (WATANABE and NURSE 1999). During meiosis, Rad21 (Scc1) is partly replaced by Rec8, although not completely removed from the chromosomes. (PARISI *et al.,* 1999; KLEIN *et al.,* 1999; WATANABE and NURSE 1999). Rec11 (meiosis-specific) and Psc3 (Scc3) (expressed during both mitosis and meiosis) are present during fission yeast meiosis. Rec11 forms a complex with Rec8 along the chromosome arms [this complex is Rec11-dependent (KITAJIMA *et al.,* 2003)]. Psc3 is present alongside Rec8 in the centromeres (KITAJIMA *et al.,* 2003). This Rec8-Psc3 centromeric complex is essential for the orientation of sister kinetochores at MI ad MII (WATANABE and NURSE 1999). Sister chromatids must remain associated during MI to ensure that

they are segregated to the same pole, before being released from each other during MII facilitating sister chromatid segregation. These two different types of segregation require a different mechanism of cohesion and cleavage than that seen during mitosis. Cohesion is established during DNA replication. Therefore, the cohesion established during pre-meiotic S-phase must be sufficient to serve faithfully during both rounds of meiotic segregation. In order to do so, meiotic cohesion complexes are abolished in a temporal, region-specific manner. Deletions of *S. pombe rec8* and *rec11* genes results in a region-specific reduction in meiotic recombination exhibiting a reduction of ~500 fold at the *ade6-M26* locus and reduction factors of 10 or less at other loci/intervals (DEVEAUX and SMITH 1994; KRAWCHUK *et al.,* 1999). These observations infer that cohesion is required for meiotic recombination (ELLERMEIER and SMITH 2005).

MI sees the formation of physical links between homologous chromosomes (chiasmata). During which, a sister chromatid from one homologue becomes covalently attached to a sister chromatid from the other homologue. The formation of chiasmata during MI provides the necessary opposing tension to that created by the spindle. This tension, alongside cohesion of the sister chromatids ensures the correct orientation of homologous chromosomes at metaphase I, aligning them for their subsequent segregation during anaphase I. Sister-chromatid cohesion along the chromosomes arms must therefore be lost at anaphase I in order for chiasmata to be resolved, resulting in the segregation of homologous chromosomes to opposite poles. In *S. pombe*, Rec8-Rec11 cohesion is lost during anaphase I – permissively facilitating homologue segregation. However, the Rec8-Psc3 cohesion complex retains centromeric cohesion, keeping sister chromatid mono-polar attachments during MI, preventing their miss-segregation due to premature separation (YOKOBAYASHI *et al.*,2003). During MII, centromeric cohesion between the sister chromatids provides the tension needed against the microtubule forces, ensuring correct orientation. Centromeric cohesion is abolished during anaphase II when sister chromatids migrate to opposite poles of the cell. Interestingly in fission yeast, in the absence of Rec8, Rad21 recruits to the centromeres (YOKOBAYASHI *et al.,* 2003). However, Rad21 associated centromeres do not form monopolar attachment of sister kinetochores. This infers that monopolar attachment of

sister chromatids is specifically controlled by the cohesin Rec8 in fission yeast (Figure 1.6) (WATANABE and NURSE 1999).

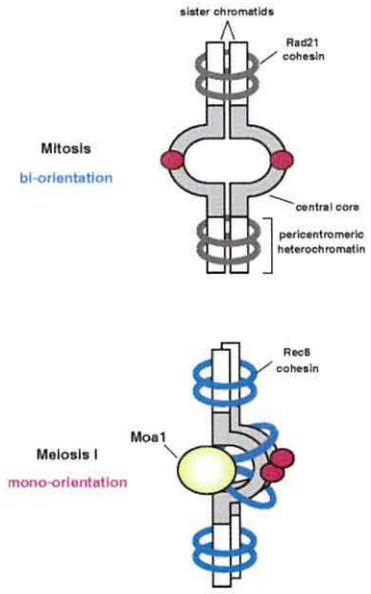

Figure 1.6 Rec8 regulates kinetochore mono-orientation during fission yeast meiosis. During mitosis, Rad21-cohesin preferentially associates with pericentromeric heterochromatin, but not at the central core, allowing the bi-orientation of sister kinetochores (red ovals). During meiosis, Rec8-cohesin associates with the central core alongside pericentromeric heterochromatin, facilitating the mono-orientation of sister kinetochores. Moa1 is a meiosis-specific kinetochore protein thought to facilitate the formation of Rec8-dependent cohesion at the central core region. Figure adapted from SAKUNO & WATANABE, 2009.

1.4d Protecting meiotic cohesion

The protection of centromeric cohesion during MI is central to the faithful segregation of homologous chromosomes. During mitosis, Rad21 is cleaved by Cut1 (mitotic separase) to allow sister chromatid segregation. Similarly, Rec8 is cleaved by a separase, but the presence of a 'protective' protein at meiotic centromeres protects Rec8 from cleavage at these sites (KITAJIMA *et al.*, 2004). In fission yeast, protection of Rec8 centromeric cohesion during MI is largely due to the localisation of a protein named Shugoshin (Sgo1) [Figure 1.7 – meaning 'guardian spirit' in Japanese (KITAJIMA *et al.*, 2004)] to pericentromeric chromosome regions at metaphase I. Sgo1 protects the Rec8-Psc3 cohesin complex from degradation during MI in those regions (KITAJIMA *et al.*, 2004). Sgo1 shares sequence similarity to MEI-S332 (KATIS *et al.*, 2004), a protein required for centromeric cohesion maintenance during MI in *Drosophila melangoster*

(MOORE *et al.,* 1998). This protective protein is widely conserved amongst eukaryotes, with homologues identified in *S. cerevisiae* (KATIS *et al.,* 2004), and humans (WATANABE and KITAJIMA 2005). This allows sister chromatids to recombine and subsequently resolve chiasmata, whilst retention of cohesion at the centromere holds homologues together, permitting segregation of homologues rather than sister chromatids during MI.

Fission yeast also expresses another paralogue of Shugoshin – Sgo2, expressed during both meiosis and mitosis. Sgo2 is not required for protection of Rec8 centromeric cohesion during meiosis, but does play an important role in facilitating the correct segregation of chromosomes during meiosis (KITAJIMA *et al.,* 2004; RABITSCH *et al.,* 2004). Recent studies have also demonstrated a role for Sgo2 in the activation of the tension-sensing spindle assembly checkpoint during both meiosis and mitosis (KAWASHIMA *et al.,* 2007).

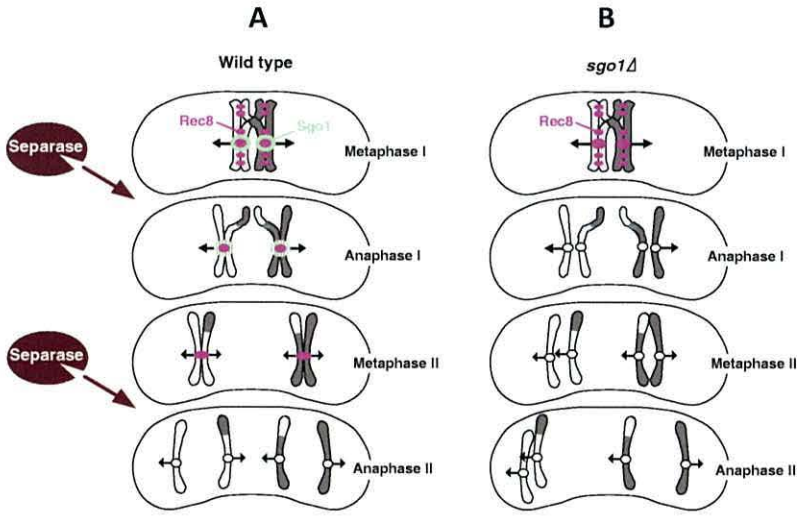

Figure 1.7 Centromeric cohesion protection. (**A**) Wild-type profile of Sgo1 centromeric cohesion protection during meiosis; resulting in a temporally ordered loss of cohesion, firstly along the chromosome arms (anaphase I), and subsequently at centromeric regions (anaphase II). This ensures faithful segregation of chromosomes at both meiotic divisions. (**B**) Meiotic divisions in the absence of Sgo1 centromeric cohesion protection protein exhibits aberrant segregation due premature to loss of centromeric cohesion. Figure adapted from WATANABE, (2004).

1.4e Other roles of the cohesin complex

Alongside establishing cohesion, the meiotic cohesins play a critical role in the formation axial elements – precursory structures to the mature SC that mediates chromosome synapsis (KLEIN *et al.,* 1999). In many organisms, formation of axial elements coincides with the longitudinal compaction of chromosomes (ZICKLER and KLECKNER 1999). *rec8* null mutants exhibit abolition of SC formation, reciprocal recombination, sister-chromatid monopolar attachments and centromeric cohesion (CHELYSHEVA *et al.,* 2005;DEVEAUX and SMITH 1994; KLEIN *et al.,* 1999; PARISI *et al.,* 1999; WATANABE and NURSE 1999).

Rec8 and Rec11 have been shown to modulate chromosome compaction in *S. pombe* (DING *et al.,* 2006). Although Rec8 and Rec11 are both essential for the formation of LinEs (LORENZ *et al.,* 2004) (*S. pombe* SC axial counterparts) during meiosis, their role in chromosome compaction is independent of LinE formation (DING *et al.,* 2006). Studies in *S. pombe* have also demonstrated a role for the cohesin complex in the prevention of recombination and stabilisation of heterochromatin (NONAKA *et al.,* 2002).

Doll *et al.*, (2008) proposed a model for some of the steps that govern the G1-to-S-phase transition during azygotic meiosis in *S. pombe.* The model infers that Rec8 has a central role in stimulating the transition via activation of a yet unidentified regulatory protein (DOLL *et al.,* 2008). Rec11 on the other hand, alongside other meiotic proteins (Meu13, Rec10, Rec12, Rec14, Rec6, Rec7, Rec15) is thought to stall the transition via inhibition of the yet unidentified regulatory protein (DOLL *et al.,* 2008). The model proposes that control of activating or deactivating the unknown regulatory factor is by the interaction of the Rec8 and Rec11 cohesins with chromatin (DOLL *et al.,* 2008).

1.5a Chromosome Pairing

Chromosome pairing is defined as the co-alignment of homologous chromosomes – being more closely associated to each other within the nucleus than random distribution would facilitate.

Pairing of homologous chromosomes during meiosis is vital in facilitating favourable conditions for meiotic recombination, which is, in turn, essential for the faithful segregation of homologous chromosomes during MI. Pairing is also

observed outside the context of meiosis. Pre-meiotic pairing is defined as pairing of chromosomes prior to the onset of pre-meiotic S-phase. Examples of pre-meiotic pairing include: the Rabl-configuration of chromosomes during meiosis (described in more detail in section 1.5b), which has been observed in both budding and fission yeast (CHIKASHIGE *et al.,* 1997), *D. melangoster* (MARSHALL *et al.,* 1996) and mammals (CREMER *et al.,* 2001); and a domain organization, whereby separate chromosomes tend to occupy certain territories within the nucleus (TANABE *et al.,* 2002), for example, it has been demonstrated that homologous chromosomes in *S. pombe* are associated before entry into meiosis – arranged in three distinct chromosomal territories (SCHERTHAN *et al.,* 1994). The presence of pre-meiotic pairing infers that the meiotic pairing of homologous chromosomes is initiated from an already highly organized pre-meiotic nucleus (WELLS *et al.,* 2006).

1.5b The bouquet formation

One evolutionarily conserved method of homologue pairing involves the clustering of telomeres on the nuclear envelope (NE) during early prophase – observed in most eukaryotes, including *S. cerevisiae* (TRELLES-STICKEN *et al.,* 1999) and *S. pombe* (CHIKASHIGE *et al.,* 1994). This chromosomal arrangement has been termed the bouquet formation.

The mitotic nucleus exhibits a polarized organisation of chromosomes, termed the Rabl configuration: during anaphase, the chromosome centromeres are drawn toward the spindle pole, leaving the telomeres 'dragging' behind at the other side of the newly formed nucleus.

Meiosis, however exhibits the characteristic bouquet chromosomal arrangement. The arrangement of chromosomes observed during meiosis is not thought to be a modification of the Rabl configuration seen during mitosis, but rather, a drastic nuclear re-arrangement (BASS *et al.,* 1997) - including the re-positioning of other nuclear components, e.g., nuclear pores (COWAN *et al.,* 2001).

During zygotene, pairing and synapsis of homologues occurs. It is at the onset of zygotene that the bouquet formation is first observed in *S. cerevisiae*, alongside the formation of the SC (HARPER *et al.,* 2004).

As the chromosomes re-locate to form the bouquet structure, all the telomeres move in a highly regulated fashion (HARPER *et al.,* 2004), to attach to the inner NE, and it is this cluster-like structure that has been named according to its resemblance to a bouquet of flowers. During the bouquet stage, centromeres are distributed across one pole of the nucleus, whilst the telomere cluster is located on the opposite side of the nucleus. At pachytene, the bouquet formation disperses, inferring that the pathway leading to the clustering of telomeres is reversed or switched off (HARPER *et al.,* 2004).

During early prophase in *S. pombe,* the bouquet formation is formed in response to secretion of mating pheromones P factor and M factor from haploid cells of opposite mating type (Figure 1.8). Telomeres cluster and associate with the spindle pole body (SPB) prior to conjugation of the mating cells (CHIKASHIGE *et al.,* 1997). The generation of the bouquet formation requires two meiosis-specific proteins, Bqt1 and Bqt2 in order to 'glue' the telomeres to the SPB. In addition, loss of Taz1 and Rap1 (proteins regulating telomere length) and Kms1 and Sad1 (SPB component), result in failure of complete telomere clustering (COOPER *et al.,* 1998), and compromised SPB integrity (SHIMANUKI *et al.,* 1997) respectively. The temporal order of telomere-association and centromere-dissociation ensures that the SPB remains attached to the centromeres, telomeres or both during this nuclear re-arrangement (CHIKASHIGE *et al.,* 1997).

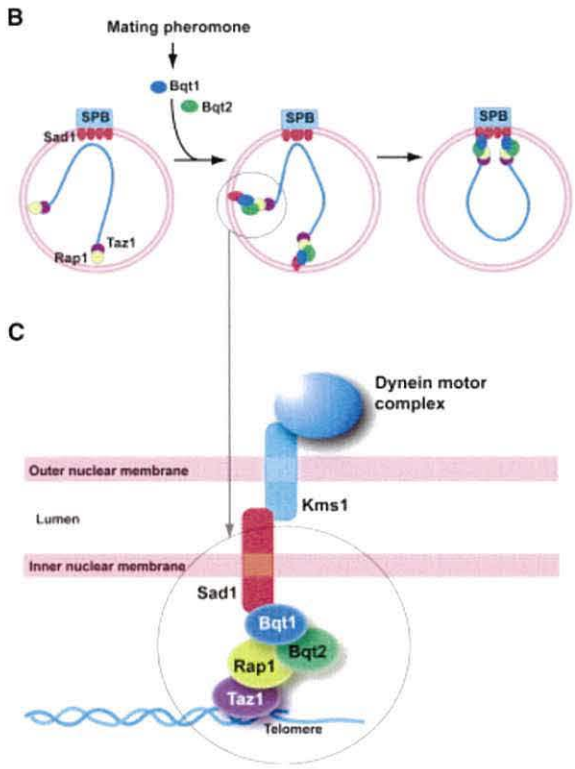

Figure 1.8 Re-arrangement of chromosomes from the Rabl-configuration to the bouquet formation in *S. pombe*. (B) left hand nucleus: mitotic nucleus, exhibiting Rabl-configuration whereby centromeres are located at SPB; Centre nucleus: mating pheromone signalling induces Bqt1 and Bqt2 to locate to telomeres; right hand nucleus: Bqt1 and Bqt2 associated telomeres are tethered to the SPB. (C), localisation pattern of proteins at the telomere-SPB association. Figure adapted from CHIKASHIGE *et al.*, 2006.

The bouquet structure was initially proposed to be involved in homologue pairing, as mutants failing to form the bouquet structure show aberrant homologue pairing (DING *et al.,* 2004). However, recent data infers a different role(s). The timing of bouquet formation (at zygotene) seems to be too late for it to be the main initiator of homologous chromosome pairing (ZICKLER and KLECKNER 1998). It has been suggested that the most important feature of the bouquet formation is the initiation of chromosomal movements, and not the bouquet configuration itself (KOSZUL and FISCHER 2009). The movements of the chromosomes into the bouquet configuration could 'iron out' any knots or tangles they may have that could hamper the faithful completion of pairing, full synapsis and recombination (ZICKLER 2006; KOSZUL *et al.,* 2008; KOSZUL and KLECKNER 2009).

1.5c Chromosome pairing - Horsetail stage in *S. pombe*

S. pombe exhibits a prolonged prophase I. During this time, the nucleus takes on a distinctive elongated tear-drop-like morphology, recognised as the horsetail-nucleus. Led by the SPB, the nucleus oscillates back and forth within the cell. This leads to a polarized orientation of chromosomes within the cell (the SPB-associated telomeres occupying the narrower leading end of the horsetail nucleus, whereas the centromeres reside on the opposite side of the cell (CHIKASHIGE *et al.,* 1994; CHIKASHIGE *et al.,* 1997). This movement causes the nucleus to elongate, facilitating the organisation, pairing and alignment of homologous chromosomes (DING *et al.,* 2004). The alignment of homologues reduces the risk of recombination between non-homologous loci which bear similar sequences, which could culminate in chromosomal deletions (NIWA *et al.,* 2000; CROMIE and SMITH 2008). This oscillation is thought to last approximately 2 hours, before the nucleus stops in the centre of the cell. The cell then traverses into metaphase I as chromosomes begin to condense in preparation for subsequent segregation. The horsetail stage is defined as the period between completing karyogamy and the end of nuclear oscillation (DING *et al.,* 2004). In *S. pombe* the horsetail stage is the only chance that homologous chromosomes get to align, pair and recombine (CHIKASHIGE *et al.,* 1997), as it is immediately followed by meiosis I segregation. It is proposed that the function of the bouquet structure in *S. pombe* is to effectively 'grab' all the chromosomes and attach them to the SPB simultaneously, with the oscillatory movement of the nucleus then vigorously shaking the homologues into alignment (HARPER *et al.,* 2004). Mutations in *taz1*, *kms1* and *dhc1*, affect horsetail movement and also exhibit a reduced recombination frequency, suggesting that the horsetail movement in *S. pombe* enhances recombination, but is not an essential pre-requisite, as some levels of recombination are observed in the absence of horsetail movement. (NIMMO *et al.,* 1998; SHIMANUKI *et al.,* 1997; COOPER *et al.,* 1998; YAMAMOTO *et al.,* 1999). It is possible that the prolonged prophase, telomere-clustering and nuclear oscillation exhibited by *S. pombe* compensates for the lack of SC, aiding the maintenance of a polarised configuration of homologous chromosomes (DING *et al.,* 2004).

1.5d Chromosome pairing – kissing homologues

Telomeres are clustered at the SPB during meiosis, their close proximity facilitating the pairing of telomere-proximal regions (CHIKASHIGE *et al.*, 1994) (DING *et al.*, 2004). An increased pairing frequency is also observed at centromere-proximal regions (SCHERTHAN *et al.*, 1994). Pairing of fission yeast homologous chromosomes during meiosis however, does not happen uniformly along their entire lengths – a phenomenon also reported in other organisms (reviewed in ROEDER 1997). Pairing of telomere-centromere interstitial regions is transient – homologous loci associating and dissociating from each other during prophase – known as chromosomal 'kissing' (DING *et al.*, 2004). During the horsetail stage, the distance between homologous chromosomes decreases, and the frequency of homologous loci associations increases (DING *et al.*, 2004), with the stabilisation of these transient associations facilitated by meiotic crossover recombination (ROCKMILL *et al.*, 1995).

Meu13 is known to be a factor involved in a region-specific control of meiotic pairing in *S. pombe* (NABESHIMA *et al.*, 2001). Loss of *meu13* results in pairing defects at the onset of meiotic prophase – inferring that Meu13 is required for the initial stages of pairing (NABESHIMA *et al.*, 2001; WELLS *et al.*, 2006). Meu13 is thought to be involved in inducing pairing of homologous chromosomes in a pathway independent to meiotic recombination (NABESHIMA *et al.*, 2001). Hop2 is the *S. cerevisiae* Meu13 orthologue. Hop2 has roles in mediating chromosome pairing and prevention of SC formation between non-homologous chromosomes (LEU *et al.*, 1998).

Hop2 is thought to form a stable heterodimer with Mnd1, and plays a key role in the stabilisation of Dmc1- and Rad51- mediated homologous pairing (CHI *et al.*, 2007; PEZZA *et al.*, 2007).

1.6 DNA double-strand breaks

Non-preprogrammed double-strand breaks (DSBs) are a dangerous form of DNA damage, which if left unrepaired can potentially result in chromosomal fragmentation. There are several choices of DSB repair pathways. The cell can choose to simply 'stick' the two ends of the DSB back together by means of non-homologous DNA end joining (NHEJ), or single-strand annealing (SSA). However,

loss of DNA is often a side effect of these forms of DSB repair, therefore an alternative mechanism must be employed to ensure that no genetic information is compromised or lost during DSB repair. This mechanism is known as homologous recombination (HR). During HR, the broken chromosome invades a homologous un-broken DNA duplex (sister-chromatid, or homologous chromosome), and uses it as a template to synthesise the DNA lost during DSB formation. Mitotically growing cells use recombination to repair damaged DNA – with sister chromatids being the preferred choice for repair (KADYK and HARTWELL 1993). Homologous chromosomes are the preferred partner choice during meiotic recombination.

1.7a Meiotic recombination

Meiotic homologous recombination is an essential process for meiotic DSB repair and meiotic chromosome alignment, in addition to its importance for the maintenance of genetic diversity, which may be vital to the long-term survival of the species. It is also essential for correct segregation of meiotic homologous chromosomes during MI. Miss-segregation of homologues (MI) or sister chromatids (MII) can result in the aneuploidy in the 4 daughter cells produced. If an aneuploid zygote is produced, its viability is dependent on many factors including which chromosome is affected or the number of chromosomes gained/lost. A few of the most common examples of viable aneuploidy seen in humans include trisomy of chromosome 13 (Patau syndrome), 18 (Edward syndrome) and 21 (Down syndrome).

1.7b Meiotic DSB formation

During leptotene, homologous chromosomes first begin to become paired, and align. With the exception of the fruit fly *D. melangoster*, *C. elegans*, and *S. pombe* the alignment of homologous chromosomes as this stage is dependent on programmed DSBs (reviewed in HENDERSON and KEENEY 2005). DSBs are crucial during meiosis, as they are proposed to initiate meiotic recombination (YOUNG *et al.,* 2004). DSB initiation of homologous meiotic recombination is widely conserved (KAN *et al.,* 2011).

Similarly to *S. cerevisiae*, in *S. pombe,* DSBs appear after DNA replication (CERVANTES *et al.,* 2000); however, it is an interesting observation that DSBs are still observed in situations where DNA replication is diminished, as long as the replication checkpoint is also inactivated (TONAMI *et al.,* 2005).
A model, introduced in 1983 (SZOSTAK *et al.,* 1983), suggests that a DSB in one of the homologous chromosomes serves as a trigger for meiotic recombination (Figure 1.9).

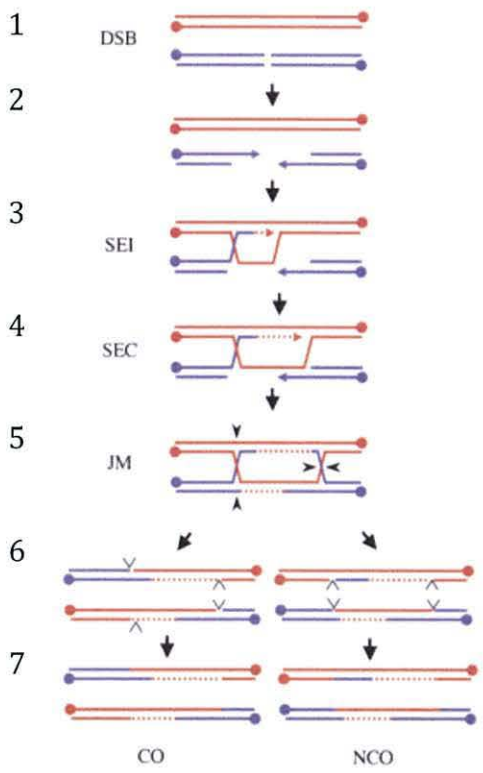

Figure 1.9 Meiotic recombination via the double strand break repair pathway. 1 - formation of DSB in one homologue by Spo11 (*S. cerevisiae*) / Rec12 (*S. pombe*); 2 – resectioning of 5' ends of DSB via MRX (*S. cerevisiae*) / MRN (*S. pombe*) complex, resulting in the overhang of the 3' free ends of the DSB; 3 – one of the overhanging 3' ends invades its homologous chromosome (single end invasion (SEI)) forming a D-loop, and proceeds to synthesise DNA using its intact homologue as a template; 4 – the D-loop is extended by the synthesis of DNA, when the D-loop reaches the origin of the DSB, second end capture (SEC) occurs as the newly synthesised strand re-anneals with the re-sected strand it was originally joined to; 5 – joint molecule (JM), or double Holliday junction (dHJ) is formed; 6 + 7 – differential cleavage result in formation of crossover (CO) or non-crossover (NCO) products. Figure adapted from HOLLINGSWORTH & BRILL, 2004.

In *S. cerevisiae*, a topoisomerase II-related protein - Spo11, initiates DSB formation (KEENEY *et al.,* 1997). Spo11 forms a dimer, breaks the phosphodiester bonds in the two DNA strands of the chromosome, and its Y135 tyrosine active site covalently links Spo11 to the 5' ends of the broken DNA (KEENEY *et al.,* 1997). It is thought that Rec8 governs the localisation of Spo11 to the chromosome axes during meiosis (BERCHOWITZ and COPENHAVER 2010), and it subsequent transition from the axes to the chromatin loops where it initiates DSB formation (KUGOU *et al.,* 2009).

Other proteins associated with Spo11 function in *S. cerevisiae*, include the meiosis-specific proteins Mei4, Rec102, Rec104 and Rec114 (KASSIR *et al.,* 2003), Ski8 (ARORA *et al.,* 2004) and Mer2 (ENGEBRECHT *et al.,* 1991). The interactions and roles of these proteins remain fairly poorly understood, but they are proposed to work in three functionally distinct subgroups; Spo11-Ski8, Rec102-Rec104 and Mer2-Mei4-Rec114 (MALEKI *et al.,* 2007). Mei4-Rec114 localisation to chromatin loops has been correlated with DSB formation sites (MALEKI *et al.,* 2007). All of these proteins (Spo11, Mei4, Rec102, Rec104, Rec114, Ski8 and Mer2) have been observed as remaining associated to the chromatin subsequent to the formation of the DSB (HENDERSON *et al.,* 2006; ARORA *et al.,* 2004; PRIELER *et al.,* 2005; LI *et al.,* 2006; MALEKI *et al.,* 2007). It is not known why they remain attached, and the dynamics of their dissociation is also unknown.

In *S. pombe*, Rec6, Rec7 (homologue to *S. cerevisiae* Rec114), Rec10, Rec12, Rec14 (homologue of *S. cerevisiae* Ski8), Rec15, Rec24, Rec25, Rec27 and Mde2 are all required for DSB formation and meiotic recombination (CERVANTES *et al.,* 2000; MARTIN-CASTELLANOS *et al.,* 2005; ELLERMEIER and SMITH 2005). Rec10 is required for the loading of Rec7 (LORENZ *et al.,* 2006). Therefore Rec7 is dependent on the proteins required for Rec10 loading; Rec8, Rec11, Rec25 and Rec27 (LORENZ *et al.,* 2006; MARTIN-CASTELLANOS *et al.,* 2005). Mutations in *rec8, rec10* and *rec11* leads to a region-specific reduction, though not complete abolition, of meiotic recombination (ELLERMEIER and SMITH 2005).

S. pombe Rec12 is the homologue of the highly conserved *S. cerevisiae* Spo11 protein. Rec12 is responsible for formation of DSBs via its Tyrosine-98 residue (KEENEY *et al.,* 1997; CERVANTES *et al.,* 2000). In *S. pombe, rec12* mutants result in genome-wide loss of recombination and DSB formation (DE VEAUX *et al.,* 1992;

DAVIS and SMITH 2003; YOUNG *et al.,* 2002). Rec12 catalyzed DSBs are essential for meiotic recombination (KAN *et al.,* 2011). Rec12 and its associated proteins are believed to congregate to initiate DSB formation during meiotic G^1 (DOLL *et al.,* 2008). It is therefore essential for their activity to be inhibited until G^1 and meiotic S-phase are successfully completed. Mde2, activated by the transcription factor Mei4, is proposed to effectively release Rec12 for DSB formation (GREGAN *et al.,* 2005). Rec12 utilises a conserved topo-isomerase-like mechanism to catalyze the formation of meiotic DSBs (KAN *et al.,* 2011). Rec12 is also thought to have an unknown function later in recombination, subsequent to the formation of DSBs (KAN *et al.,* 2011).

1.7c DSB processing

In order to facilitate strand invasion Spo11 must be effectively removed from the DNA at the DSB site. Removal of Spo11 is induced by the endonucleolytic activity of the highly conserved MRX (Mre11-Rad50-Xrs1) complex (USUI *et al.,* 1998) and Sae2 (NEALE *et al.,* 2005). The MRX complex is evolutionarily conserved and known to function in telomere maintenance and DNA damage checkpoint activation in both meiotic and mitotic cells (MURAKAMI, 2008). Mre11, a nuclease and component of the MRX complex resections the 5' ends of the DSB. Strand transfer proteins Rad51 and Dmc1 are then recruited to the free protruding 3' ends and mediate invasion of the DNA duplex of the unbroken homologue. It has been proposed that the MRX complex associates to known DSB sites prior to actual DNA breakage, inferring that its localisation is not based upon reaction to DNA damage (in the form of DSBs) – this proposal allows for prompt processing of DSBs, bypassing the requirement for DNA damage response (BORDE *et al.,* 2004).

Cleavage by *S. cerevisiae* Spo11 is thought to be asymmetrical on either side of the DSB – generating two Spo11-oligonucleotide molecules of different lengths (NEALE *et al.,* 2005). This asymmetrical cleavage is proposed to create an orderly accessibility to the 3' ends – suggesting that subsequent proteins are differentially loaded in a manner as to promote invasion of the homologous chromosome for preferential DSB repair (NEALE *et al.,* 2005).

The *S. pombe* homologues of MRE11, RAD50 and XRS1 (MRX complex proteins) are Rad32 (TAVASSOLI *et al.,* 1995), Rad50 (HARTSUIKER *et al.,* 2001) and Nbs1 (UENO *et al.,* 2003) respectively. These three proteins are thought to form a complex in *S. pombe* (MRN complex) similarly to their MRX-complex counterparts (YOUNG *et al.,* 2004). In *S. pombe*, removal of Rec12 is Rad32- and Ctp1- (*S. cerevisiae* Sae2 homologue) – dependent (HARTSUIKER *et al.,* 2009). Mutants deficient in MRN nucleases exhibit an accumulation of Rec12-DNA structures (YOUNG *et al.,* 2002). The regulation of Rec12 removal (Figure 1.10) is different to that seen in the removal of Spo11 in *S. cerevisiae* (MILMAN *et al.,* 2009). Unlike *S. cerevisiae*, the cleavage of Rec12 in fission yeast is thought to be symmetrical, giving rise to Rec12-oligonucleotide fragments of the same length (ROTHENBERG *et al.* 2009). The symmetrical cleavage of Rec12 may suggest that the differential loading of Rad51 and Dmc1 (strand invasion proteins, described in more detail in section 1.6d) proposed for *S. cerevisiae*, does not occur in *S. pombe* (ROTHENBERG *et al.,* 2009). The removal of Rec12 in fission yeast appears to occur approximately an hour after DSBs are seen at their most abundant (MILMAN *et al.,* 2009), compared with the removal of Spo11 in *S. cerevisiae* which occurs immediately following DSB formation (NEALE *et al.,* 2005). It is interesting to note here that the *S. pombe* MRN complex is not required for the formation of DSBs, unlike *S. cerevisiae* where loss of the MRX complex results in loss of DSB formation (YOUNG *et al.,* 2004). Correlation of these data indicates that the requirement of the MRX complex for DSB formation in budding yeast explains the prompt removal of Spo11 after DSB formation, as it is already present at the site of the DSB; fission yeast DSB formation on the other hand is MRN-complex independent, therefore the recruitment of the MRN complex to the DSB site subsequent to DSB formation may explain the delay seen between DSB formation and Rec12 removal in *S. pombe* (MILMAN *et al.,* 2009).

The DNA is resected by the MRN complex in the 5'-3' direction (FARAH *et al.,* 2009) with interaction from the Ctp1 protein (SARTORI *et al.,* 2007). The MRN complex consists of three proteins: Rad50, an ATPase and member of the structural maintenance of chromosomes (SMC) family of proteins (CROMIE and SMITH 2008). Rad50 has a long coiled-coil hairpin like structure, allowing it to co-ordinate events at both sides of a meiotic DSB (CROMIE and SMITH 2008); Rad32, a

nuclease regulated by Rad50 is required for DSB processing; and the regulatory protein, Nbs1. Recent studies have demonstrated a temperature-sensitivity phenotype of Nbs1 (MILMAN *et al.,* 2009). It is proposed that Rad32 and Rad50 may be able to retain partial functionality in the absence of Nbs1 at low temperatures, and that Nbs1 offers stabilisation or activation of Rad32 and Rad50 at higher temperatures (MILMAN *et al.,* 2009).

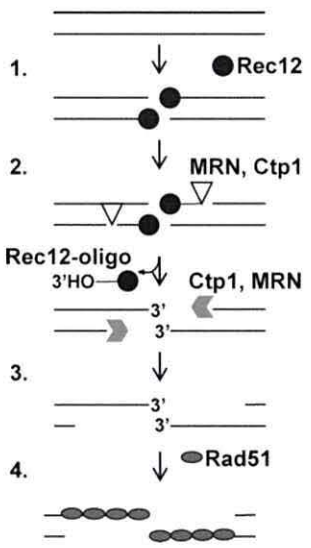

Figure 1.10 Removal of Rec12 in *S. pombe*. (1) - Rec12 (alongside its associate proteins) bind to the DNA to generate a DSB – remaining covalently bound to the DNA after DSB formation; (2) – Rad32 and Ctp1 induce the removal of Rec12 from the DSB site, resulting in the formation of Rec12-oligonucleotide fragments of similar size; (3) – Ctp1 resects the 5'ends of the DSB, leaving protruding 3' DNA overhangs; (4) – Rad51 coats the 3' overhangs, in preparation for the invasion of its homologous chromosome. Figure adapted from MILMAN *et al.*, 2009.

In both *S. cerevisiae* and *S. pombe*, sites of DSBs have also been associated with areas exhibiting a more open chromatin structure – Mre11, but not Rad50 or Xrs2, has been linked to changes in chromatin morphology in these regions (OHTA *et al.,* 1998).

1.7d(i) Strand Invasion

In *S. cerevisiae*, Spo11 is thought to remain associated with the cleaved 5' DNA end of the DSB until strand exchange is initiated, if not a bit longer (NEALE *et al.,* 2005). Strand invasion involves the free, protruding 3' end strand of the DSB

literally 'invading' its neighbouring homologue in search of a homologous complementary sequence. This 'invasion' creates a structure termed the displacement loop (more commonly known as the D-loop); the invading strand displacing one of the strands of its homologous chromosome. Rad51 and Dmc1 are RecA (*Escherichia coli* archetypal strand exchange protein) homologues (BISHOP 1994; BISHOP *et al.,* 1992) involved in meiotic recombination strand invasion.

1.7d(ii) Rad51

The *rad51* gene is expressed in both mitotic and meiotic cells, and orthologues have been found in cells of all eukaryotes studied. Rad51 plays a role in the DNA repair pathway during both types of cell division so far. *rad51* mutants do form DSBs in meiosis, but they are not subsequently repaired – severely reducing meiotic recombination and spore viability - indicating the essential nature of Rad51 in meiotic DSB repair (YOUNG *et al.,* 2004).

In *S. cerevisiae*, Rad52, and the Rad55-Rad57 complex (KHASANOV *et al.,* 1999) induce loading of Rad51 onto single-stranded DNA, in fact Rad51 loading shows a strict dependence upon Rad52 (for review, see KROGH and SYMINGTON 2004). Another accessory complex required for efficient Rad51 activity in *S. pombe* is Swi5-Sfr1 (note: *rad51* is termed *rhp51* in *S. pombe*)(ELLERMEIER *et al.,* 2004). A single deletion of either the Rad55-Rad57 complex or the Swi5-Sfr1 complex has only a mild effect on DSB repair (YOUNG *et al.,* 2004), whereas a deletion of both complexes reduced DSB repair comparable to that seen in a *rad51* deletion (HYPPA *et al.,* 2008). This suggests that the two complexes act in different sub-pathways of Rad51-dependent DSB repair in S-phase (Figure 1.11) (GRISHCHUK and KOHLI 2003; ELLERMEIER *et al.,* 2004).

Fission yeast has two Rad52 homologues – Rad22 and Rti1 (also known as Rad22B)(VAN DEN BOSCH *et al.,* 2001). Rad22 is important for the survival of vegetative cells, and for the faithful completion of meiosis, whilst Rti1 is only required during meiosis (OCTOBRE *et al.,* 2008). Rad22 and Rti1 have been previously demonstrated to interact (VAN DEN BOSCH *et al.,* 2002), and the timing of their appearance alongside their localisation patterns infers a role in DSB repair (OCTOBRE *et al.,* 2008).

Rad22 and Rti1 are proposed to mediate inter-sister DSB repair (HYPPA and SMITH 2010). *rad22* and *rti1* mutants exhibit a reduction in inter-chromosomal recombination, but no such loss of inter-homolog events (HYPPA and SMITH 2010). Loss of Rad51 results in a reduction in crossover frequency, but a much stronger reduction in gene-conversion (non-crossover) events (GRISHCHUK *et al.,* 2004). These data suggest that Rad51 is primarily active in a pathway resulting in non-crossover products.

1.7d(iii) Dmc1

Dmc1 was first identified in *S. cerevisiae* as a gene that caused meiotic defects when mutated (BISHOP *et al.,* 1992); mutations in *dmc1* result in defective strand invasion (HUNTER and KLECKNER 2001), and accumulation of resected DSBs (BISHOP *et al.,* 1992). Dmc1 functions in a repair pathway independent of Rad51 in both budding and fission yeasts (BISHOP *et al.,* 1999; GRISHCHUK *et al.,* 2004). *dmc1* mutants, unlike in *rad51* mutants, can form and repair DSBs. *dmc1* mutants are also proposed to exhibit high spore viability, although recombination frequency is somewhat reduced (FUKUSHIMA, 2000; GRISHCHUK and KOHLI 2003; ELLERMEIER, 2004; YOUNG *et al.,* 2004). The Swi5-Sfr1 Rad51-accessory complex also induces Dmc1 activity (Figure 1.11)(FERRARI *et al.,* 2009).
Indications are that Dmc1 is only required for inter-homolog DSB repair, and has a locus-dependent requirement, only being needed at hotspot-poor intervals – possibly dictated by chromatin structure (HYPPA and SMITH 2010). Swi5-Sfr1 is thought to mediate inter-homolog DSB repair across the genome (HYPPA and SMITH 2010) – as mutants in either of these proteins result in near exclusive inter-sister DSB repair.
Both Rad22-Rti1 and Swi5-Sfr1 complexes mediate DSB repair partner choice by control of Rad51 and Dmc1 access to the single-stranded resected DNA (HYPPA and SMITH 2010).

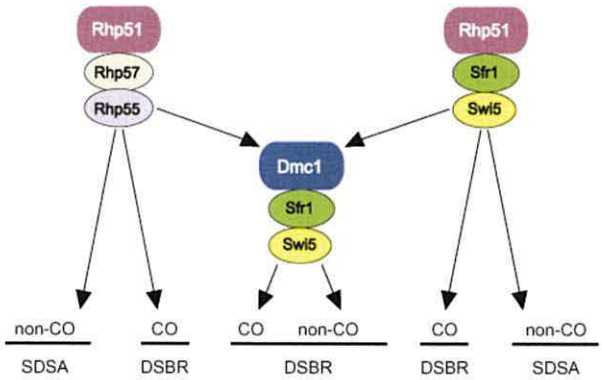

Figure 1.11 Activation of strand-invasion proteins in *S. pombe*. This figure shows the two sub-pathways of Rad51 (Rhp51), and the exclusively inter-homologue pathway of Dmc1. Figure adapted from HARUTA *et al.*, 2008.

1.7e Second end capture

The exposed 3' ends of the invading strands then proceed to synthesise DNA using the homologous chromosome as a template to ensure no genetic information is lost due to DSB formation. This DNA synthesis lengthens the D-loop structure. Second end capture occurs when the DNA synthesis ceases, and the 3' ends re-attach onto the exposed, re-sected 5' ends of their original strands. In *S. cerevisiae*, this predominantly results in the formation of structures termed double Holliday Junctions (dHJ) (Figure 1.12); composed of a pair of homologous chromosomes joined by an extended D-loop. *S. cerevisiae* exhibits both double- and single HJs (CROMIE *et al.,* 2006), although the major pathway seems to utilise dHJ.

S. pombe on the other hand predominantly exhibits a single Holliday Junction (sHJ) at processed DSB sites (Figure 1.12). The few dHJs that are exhibited in *S. pombe* are proposed to arise from two independent recombination events that have occurred in close proximity to each other – absence of crossover interference (discussed below) allows for this in *S. pombe* (CROMIE *et al.,* 2006).

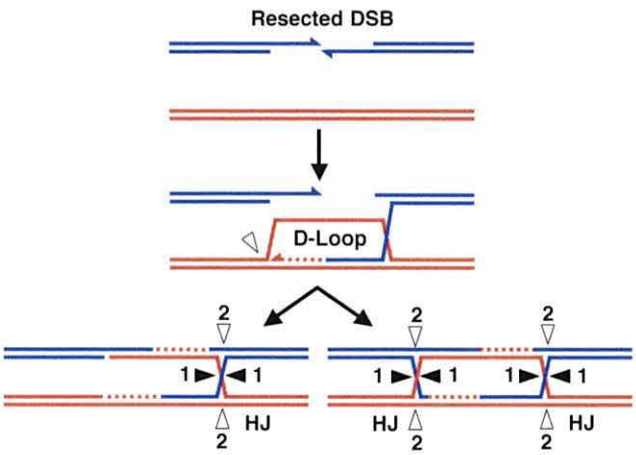

Figure 1.12 Formation of single- and double- Holliday Junctions. A single HJ is produced if the D-loop created by the invading strand is cut before second end capture is completed (left hand image). A dHJ is created when the D-loop remains uncut, and second-end capture is completed (right hand 2 images). The formation of crossover *vs.* non-crossover products is determined by which DNA strands are cleaved. Figure adapted from CROMIE & SMITH, 2008.

1.8a Holliday Junction resolution

The genetic outcome of recombination is dependent on how a HJ is resolved (Figure 1.13), with the possibility of forming CO or NCO products. CO products exhibit exchange of DSB flanking sequences along with a region of gene-conversion, whilst NCO products exhibit only gene conversion. The symmetrical nature of the dHJ suggests that no bias should be found between resolving to CO or NCO products. However, in *S. cerevisiae*, meiotic dHJs are exclusively resolved into CO products (ALLERS and LICHTEN 2001; HUNTER and KLECKNER 2001; BORNER *et al.,* 2004). This particular CO-creating pathway in *S. cerevisiae* is dependent upon ZMM proteins (Zip1, Zip2, Zip3, Zip4, Msh4, Msh5, and Mer3 (WHITBY 2005).

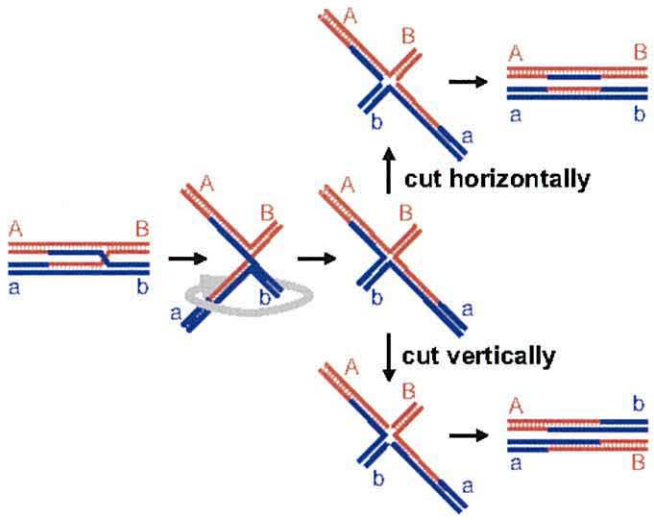

Figure 1.13 Differential resolution of Holliday Junctions. Demonstrating the production of crossover (bottom image) and non-crossover (top image) products via the differential cleavage of DNA strands.

Resolution of the HJ is catalysed by specialized nucleases, for example the Mus81-Eme1 complex, which is implicated in eukaryotic HJ resolution (Boddy *et al.,* 2001; Chen *et al.,* 2001), although its preferred substrates are in fact D-loops and un-ligated HJs (Osman *et al.,* 2003; Gaskell *et al.,* 2007; Gaillard *et al.,* 2003). Mus81 and Eme1 were first identified in humans and in *S. pombe* as candidates for processing of HJs (Boddy *et al.,* 2001; Chen *et al.,* 2001; Ciccia *et al.,* 2003). *S. pombe* Mus81 was initially identified as a substrate for Cds1 kinase (Boddy *et al.,* 2000). *S. pombe* mutants exhibiting complete lack of Mus81 or Eme1 produce inviable spores due to defects in MI chromosome segregation (Boddy *et al.,* 2000). In contrast, deletion of *MUS81* in *S. cerevisiae* results in only a modest decrease in spore viability – these data inferring possible different roles for Mus81 in fission and budding yeast meiosis (de los Santos *et al.,* 2003). In *S. pombe* Mus81-Eme1 appears to be the only HJ resolvase (Boddy *et al.,* 2001). HJs accumulate in *mus81* mutants in *S. pombe* (Cromie *et al.,* 2006). Unlike the archetypal HJ resolvase RuvC (*E. coli*), fission yeast Mus81-Eme1 appears to cleave HJs asymmetrically (Osman *et al.,* 2003). Crossover events are down 8-fold in an *S. pombe* mutant lacking Mus81 (Boddy *et al.,* 2001), however gene-conversion (non-crossover) events seem to be unaffected (Osman *et al.,* 2003;

SMITH *et al.,* 2003). These data infer that crossovers, but not gene conversions are dependent upon Mus81.

Another HJ resolvase, is the human GEN1 (orthologous to *S. cerevisiae* YEN1) protein (IP *et al.,* 2008). *S. pombe* does not exhibit a GEN1 orthologue, which explains the essential nature of the Mus81-Eme1 complex during meiosis in *S. pombe* (IP *et al.,* 2008). Interestingly however, ectopic expression of the human GEN1 protein rescues the meiotic phenotype of a *mus81Δ* mutant in *S. pombe*, leading to the proposal that GEN1 is able to play a functional role in HJ resolution *in vivo* (LORENZ *et al.,* 2010).

1.8b(i) Crossovers

Crossovers are generated at DSBs by meiotic recombination between homologous chromosomes. The number of DSBs formed far outweighs the number of CO formed. In *S. cerevisiae*, sites of DSB are known to coincide with COs. Two factors govern the generation of crossovers from DSB sites; firstly the choice of sister chromatid or homologous chromosome for repair of the DSB (crossovers only arising from homologous chromosome repair), and secondly that inter-homolog repair of DSBs does not always result in COs. It was proposed (SZOSTAK *et al.,* 1983) that alternate resolution of the dHJ was the deciding factor between forming CO or non-crossover (NCO) products. However, recent evidence proposes two separate pathways for formation of CO and NCO products respectively. The decision between following a CO or NCO pathway occurs very early on – possibly even prior to strand invasion (BISHOP and ZICKLER 2004). dHJ resolution is thought to always result in formation of CO, and a separate pathway called synthesis-dependent strand annealing (SDSA) (Figure 1.14) generates NCO products (ALLERS and LICHTEN 2001; CROMIE *et al.,* 2001; HUNTER and KLECKNER 2001; SMITH *et al.,* 2003).

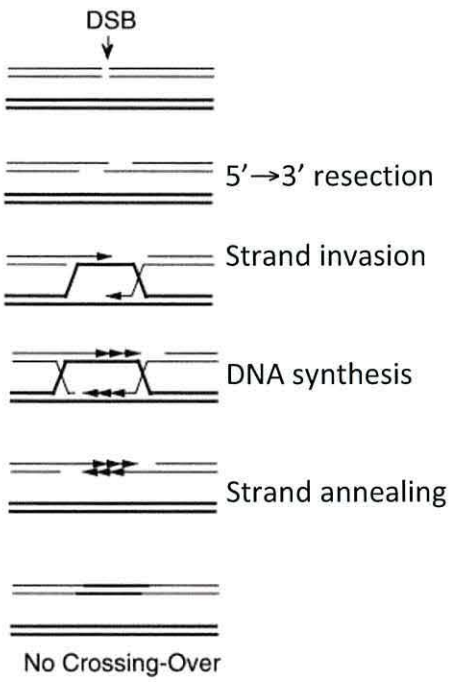

Figure 1.14 Synthesis-dependent strand annealing. A simple model whereby the protruding 3' end primes DNA synthesis, using its homologue as a template. The new D-loop unwinds, and the DNA strands re-anneal to their original partners. Figure adapted from PAQUES & HABER, 1999.

1.8b(ii) Regulating crossovers

Chromosomes that do not CO frequently miss-segregate. The frequency and distribution of meiotic crossovers is tightly controlled, so as to minimise the chance of a chromosome not exhibiting a CO event (BORNER *et al.,* 2004). Sites of crossing over are controlled by intra- and inter-chromosomal non-random distribution of COs. Inter-chromosomal non-random distribution is known as 'the obligate crossover', or 'crossover assurance'– by which each pair of homologous chromosomes receives at least one 'obligate' crossover despite the fact that the average number of crossovers per chromosomes is low (typically1-3 per chromosome) (JONES 1984). Intra-chromosomal non-random distribution of COs is often referred to as crossover interference (BORNER *et al.,* 2004) – where crossovers are more widely spaced than one would expect by random distribution - the distance of interference varying on a species-to-species basis (MARTINI *et al.,* 2006). Regulating CO events in this manner ensures at least one CO per chromosome (BORNER *et al.,* 2004). Interference is not observed between

NCO events – their distribution not significantly different to that expected from a random distribution (MANCERA *et al.,* 2008). However, recent studies on a genome-wide approach suggest that NCO and COs seem to exhibit some interference with each other (MANCERA *et al.,* 2008).

Crossover interference is due to a post-DSB formation choice of CO against NCO pathway. A reduction in DSB formation does not result in a reflective reduction in CO frequency (MARTINI *et al.,* 2006) – CO frequency is maintained at the expense of NCO events (MARTINI *et al.,* 2006). This regulation of CO frequency is known as crossover homeostasis. These findings suggest that CO events are pre-designated to an appropriate number and distribution of DSBs, independent of the number of DSBs present, and that all other DSBs are repaired via an alternative NCO pathway (MARTINI *et al.,* 2006). *Caenorhabditis elegans* exhibits perfect interference, having only one CO per pair of homologous chromosomes, all mediated in an Msh4-Msh5-dependent manner (MENEELY *et al.,* 2002). Many organisms (humans, *S. cerevisiae, A. thaliana*) exhibit two distinct CO pathways. The primary pathway mediates approximately 80% of total COs; it is sensitive to crossover interference and characterized by the Msh4-Msh5 heterodimer. The other pathway does not exhibit crossover interference, and is Mus81-Eme1-dependent and facilitiates the remaining ~20% of COs (DE LOS SANTOS *et al.,* 2003).

In *S. pombe*, COs are observed at a relatively constant frequency throughout the genome (YOUNG *et al.,* 2002). Unlike *S. cerevisiae*, where COs coincide with DSBs, COs in *S. pombe* are not observed more frequently at sites of known high levels of DSBs (YOUNG *et al.,* 2002). There is evidence to suggest that this may be due to partner choice bias in hotspot-rich and hotspot-poor regions (HYPPA and SMITH 2010) – low-level DSBs being preferentially repaired with the homologue, whilst the sister is the preferred repair mechanism in DSB hotspots. This partner-choice bias would explain the constant frequency of COs seen throughout the *S. pombe* genome (HYPPA and SMITH 2010).

It is important to note that *S. pombe* does not exhibit crossover interference (MUNZ 1994), although surprisingly crossover homeostasis is exhibited – its mechanisms remain unknown (KAN *et al.,* 2011). Fission yeast normally exhibits approximately 45 COs per meiosis (MUNZ 1994) [~95% of which are Mus81-

Eme1-dependent (CROMIE *et al.,* 2006; SMITH *et al.,* 2003)]; however, recent data proposes that a single CO event per chromosome pair is sufficient for high-fidelity chromosome segregation in *S. pombe* (KAN *et al.,* 2011). The additional COs are thought to be regulated by Rec12, to ensure a high probability that each pair of chromosomes will receive at least one CO (KAN *et al.,* 2011). Rec12 has been proposed to be directly involved in deciding between a CO and NCO recombination pathway in *S. pombe* (KAN *et al.,* 2011).

1.9 Partner choice for repair of DSBs

During meiosis, a chromosome has 3 choices of partner for DSB repair – a sister chromatid, alongside the two sister chromatids of its homologue. Recombinational repair of DSBs during meiosis in *S. cerevisiae*, occurs at approximately a 3:1 (inter-homologue:inter-sister) ratio (SCHWACHA and KLECKNER 1994). DSBs in mitotic cells on the other hand, are almost exclusively repaired with sister chromatids (KADYK and HARTWELL 1992). This preference is proposed to be mediated by the cohesin-dependent close proximity of sister-chromatids during mitosis (SJOGREN and STROM 2010). We know that sister-chromatid cohesion is also exhibited during meiosis, therefore it has been inferred that there must be a process/processes, which resists the mitotic tendency for inter-sister repair, and/or promote meiotic inter-homologue repair. In *S. cerevisiae*, several proteins act specifically in inter-homolog DSB repair - lack of Dmc1, Red1, Hop1, Rad51, Rad55 or Rad57 results in reduction of inter-homolog DSB repair, but not of inter-sister DSB repair (SCHWACHA and KLECKNER 1994; SCHWACHA and KLECKNER 1997). Mnd2-Hop2 and Hop1-Red1-Mek1 complexes appear to promote inter-homolog DSB repair (NIU *et al.,* 2007; TSUBOUCHI and ROEDER 2002). Regulation of meiotic inter-sister DSB repair by Mek1 supression of Rad51 strand invasion is specific to sister chromatids (CALLENDER and HOLLINGSWORTH 2010). Rec8 is not required for inter-sister DSB repair, but specifically promotes inter-homolog DSB repair (CALLENDER and HOLLINGSWORTH 2010).

In *S. pombe,* inter-sister recombination is preferred over inter-homologue recombination (CROMIE *et al.,* 2006), with inter-sister events outweighing inter-homologue repair 3:1 at the *mbs1* recombination hotspot (CROMIE *et al.,* 2006).

S. cerevisiae employs a barrier against inter-sister recombination to ensure an inter-homologue bias during DSB repair (NIU *et al.,* 2005). Inter-homologue bias in budding yeast may be utilised as another mechanism to ensure the 'obligate crossover'. Absence of inter-homologue bias for DSB repair in fission yeast may be for the same reason as crossover interference is absent - random distribution of crossovers seems to 'do the trick'; therefore inter-homologue bias is simply not needed (CROMIE *et al.,* 2006).

1.10a Recombination hotspots

Some areas of the genome have higher instances of meiotic recombination than other areas. First identified as regions exhibiting a higher-than-average intensity of recombination (GUTZ 1971), these limited loci are termed recombination hotspots. Studies in *S. cerevisiae* showed that DSBs occurred primarily within GC-rich and intergenic regions (GERTON *et al.,* 2000). *S. pombe* DSBs also appear to form primarily within intergenic regions (CROMIE *et al.,* 2007); so-much-so that intergenic regions were proposed to strongly predict areas of DSB formation, but there is no correlation between DSBs and GC-rich regions in the fission yeast. *S. pombe* exhibits a genome-wide preference of DSB localization to areas of non-coding RNA (ncRNA) (WAHLS *et al.,* 2008). Recombination hotspots are thought to be evolutionarily unstable (PRYCE and MCFARLANE 2009), due to the hotspot being more frequently converted – a phenomenon known as the recombination hotspot paradox (PINEDA-KRCH and REDFIELD 2005).

1.10b *S. pombe ade6-M26* recombination hotspot

In *S. pombe,* a single G-to-T base-pair nonsense mutation (*M26*) in the 5' end of the *ade6* gene has created a meiosis-specific recombination hotspot that has been and continues to be a very useful tool for the study of recombination. The mutation generates a heptameric sequence (5'-ATGACGT-3') (PONTICELLI *et al.,* 1988; SZANKASI *et al.,* 1988) that exhibits a ~13-fold increase in recombination (GUTZ 1971). Substitution of any of the 7 base pairs results in loss of hotspot activity (SCHUCHERT *et al.,* 1991). *S. pombe* exhibits closely related sequences in its wild type genome, and 15 of these loci were tested and found to be hotspots for meiotic recombination (STEINER and SMITH 2005).

The *ade6-M375* mutation is a G-to-T single base pair nonsense mutation in the codon preceeding *ade6-M26* (PONTICELLI *et al.,* 1988; SZANKASI *et al.,* 1988). The *ade6-M26* mutation exhibits a 10-15-fold increase in meiotic recombination, whilst the *ade6-M375* does not exhibit this hotspot phenotype (GUTZ 1971). This renders the *ade6-M375* mutation an excellent control allele for *ade6-M26* hotspot activity, as it does not bind Atf1-Pcr1.

The hotspot activity of *ade6-M26* is dependent on its chromosomal context i.e. when the whole *ade6-M26* gene is 'cut-and pasted' into another location on the genome, hotspot activity can be maintained, or the move can often result in hotspot activity being lost (PONTICELLI and SMITH 1992; VIRGIN *et al.,* 1995).

The heptameric sequence is a binding site for the Atf1-Pcr1 'stress-response' transcription factor; generating Atf1-Pcr1-dependent chromatin remodelling (MIZUNO *et al.,* 1997), which is essential for hotspot activity (WAHLS and SMITH 1994; YAMADA *et al.,* 2004). In the case of *ade6*, Atf1-Pcr1 is not however, required for 'basal' recombination (DAVIS and SMITH 2001). Atf1-Pcr1 also binds to other sites termed CRE (cAMP response element). These sites share the consensus sequence 5'-NTGACGT(C/A)-3', and were shown to be meiotic recombination hotspots (STEINER and SMITH 2005).

A 13 base pair DNA sequence motif (CCNCCNTNNCCNC) has been identified as being over-represented in approximately 40% of human recombination hotspots (MYERS *et al.*, 2010). PRDM9 is a zinc-finger protein, expressed during early meiosis. It is proposed as being a striking candidate for binding to this 13 base pair motif, with direct sequence specificity. It is inferred to regulate hotspot activity through chromatin modification via its conserved central domain that harbours H3K4 methyltransferase activity [widely observed in hotspot regions] (MYERS *et al.*, 2010).

1.11 Chromatin transition

Eukaryotic cells contain proteins named histones that compact the mass of chromosomal DNA into the tiny space within the nucleus. The protein-DNA complex is called chromatin. Chromatin is composed of repeating units of 8 DNA-associated histone proteins – historically described as resembling beads on a string. This compact packaging of DNA renders it inaccessible for molecules that

need to associate with the DNA for processes such as transcription, replication and recombination. Therefore, the DNA is made accessible by a family of proteins known as chromatin remodelers. Ease of accessibility to the DNA is a pre-requisite for hotspot activation (MIZUNO *et al.,* 1997). Chromatin at sites of known meiotic recombination hotspots in both budding and fission yeasts have demonstrated a heightened sensitivity to micrococcal nuclease (MNase) – this infers a correlation between chromatin accessibility and initiation of meiotic recombination (OHTA *et al.,* 1994). The process of chromatin morphological alteration has been termed the chromatin transition (OHTA *et al.,* 1994).
The chromatin configuration surrounding the *ade6-M26* hotspot is altered during early meiosis, becoming more sensitive to micrococcal nucleases (MNase) (MIZUNO *et al.,* 1997). This chromatin alteration is vital for the activation of recombination at the *ade6-M26* hotspot (HIROTA *et al.,* 2008). The chromatin alterations surrounding *ade6-M26* have been also been implicated as playing a vital role in transcriptional regulation in response to environmental stresses (HIROTA *et al.,* 2004). There are two main pathways of chromatin alteration: firstly, acetylation of histone amino termini by histone acetyltransferase (HAT) – increased acetylation being indicative of a more relaxed chromatin configuration (GRANT *et al.,* 1998); secondly, the movement of nucleosomes from one place to another (TRAVERS 1999) via ADCR factors. Many proteins are required for wild-type chromatin alteration, including: HAT; Gcn5 (its loss resulting in partial hotspot activity) (YAMADA *et al.,* 2004) and Ada2 both essential for acetylation of histone H3 (HIROTA *et al.,* 2008); ATP-dependent chromatin remodelling factor (ADCR); Hrp3; Snf22 (its loss resulting in a severe reduction in hotspot activity)(YAMADA *et al.,* 2004). Tup11, Tup12 and Hrp1 inhibit chromatin alteration at *ade6-M26* (HIROTA *et al.,* 2003; YAMADA *et al.,* 2004). Steiner *et al.* 2009 propose a model by which hotspots in fission yeast occur when a hotspot sequence motif (e.g. CRE sequence) and an open, permissive chromatin configuration intersect (STEINER *et al.,* 2009) – see PRYCE and MCFARLANE, 2009 for review.

1.12 Chromosome synapsis

Chromosome synapsis is a distinct process describing the pairing of homologous chromosomes within the context of a proteinaceous structure called the synaptonemal complex (SC) (Figure 1.15).

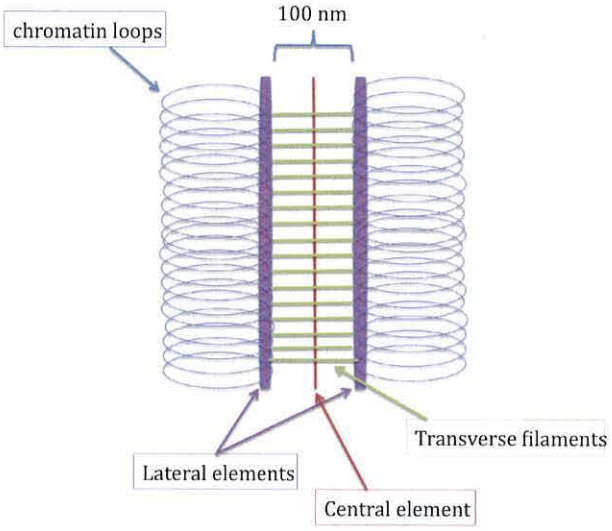

Figure 1.15 The synaptonemal complex. See section 1.12 for more detailed description.

The homologous chromosomes are held together within the context of the SC until completion of exchanging genetic material (PAGE and HAWLEY 2004). Synapsis is known to be distinct from chromosomes pairing, as chromosomal homology is not a pre-requisite for synapsis (PAWLOWSKI *et al.*, 2004). The SC is a long tripartite proteinaceous structure, composed of two axial elements (which mature into the electron dense lateral elements) and a less dense central element, all joined by transverse filaments. The SC is a highly conserved structure across a wide variety of species (VON WETTSTEIN 1984).

During early prophase, a proteinaceous structure termed the axial element begins to develop along the central core of the sister chromatids. When homologous chromosomes pair, the axial element from each pair of sister chromatids become closely associated with each other, and transverse filaments are produced to connect the axial elements (which have now matured into lateral elements) to each other via the central element. The transverse filaments

keep the lateral elements at a uniform distance (~100 nm) from each other. This forms the tri-partite structure of the central core of the SC, which is flanked at either side by homologous chromosomes. The DNA of the homologues is organised into a series of loops. Most of the chromatin looping from the homologues lies outside the context of the SC, associating with their respective lateral element only via the base of each chromatin loop. The central region of the SC does not contain any DNA. The DNA anchoring the chromosomes to the SC is made up of several kinds of DNA repeat sequences, termed 'lateral element-associated repeat sequences (LEARS)' (HERNANDEZ-HERNANDEZ *et al.,* 2008). The chromatin structure of these DNA repeat sequences is thought to facilitate their recruitment to the SC, and possibly even aid SC stability (HERNANDEZ-HERNANDEZ *et al.,* 2008). The frequency of chromatin loop associations along the SC is approximately 20 loops per micron of SC axis length (ZICKLER 1999). This number is relatively well conserved amongst a variety of organisms regardless of genome size or SC length (ZICKLER 1999). Differing chromatin loop sizes, to maintain the regularity of chromatin loop-to-SC association frequencies (KLECKNER 2006), accommodates these differences in genome and SC sizes. Humans serve as a good example of this intra-species difference. The length of the SC in a human female is approximately twice as long as that seen in a human male; in correlation with this, the chromatin loops in a human female are approximately half the size as those exhibited in a human male (TEASE and HULTEN 2004).

The role of the SC is unclear, but its absence from some organisms (e.g., *S. pombe*) indicates that it is not a pre-requisite for meiosis or meiotic recombination (CROMIE and SMITH 2008).

1.13 SC proteins

1.13a Zip proteins

Zip1 was identified via the isolation of mutants defective in SC formation in *S. cerevisiae* (SYM and ROEDER 1995). It is thought to be the main component of the SC central region, localising along the entire lengths of chromosomes during pachytene (SYM *et al.,* 1993); with SCP1 being the human orthologue (ZICKLER

1999). Evidence of Zip1 being a dominant feature of the SC central region includes the association of Zip1 to fully synapsed lateral elements, but not to the precursory, un-synapsed axial elements, moreover intimate synapsis of homologous chromosomes is lost in a *zip1* null mutant (although homologue pairing is still exhibited) (SYM *et al.,* 1993). Further evidence indicates that Zip1/SCP1 is the main component of the SC transverse filaments; *zip1* mutations which affect the length of the protein have exhibited corresponding variations in the width of the SC, from one lateral element to the other (SYM and ROEDER 1995). It has been hypothesised that these proteins (Zip1/SCP1) dimerize, and lie 'head-to-head' spanning the width of the SC (thus determining its uniform width), with the central element being formed from the globular amino-terminal domains at the 'head' of each protein (ROEDER 1997)(Figure 1.16).

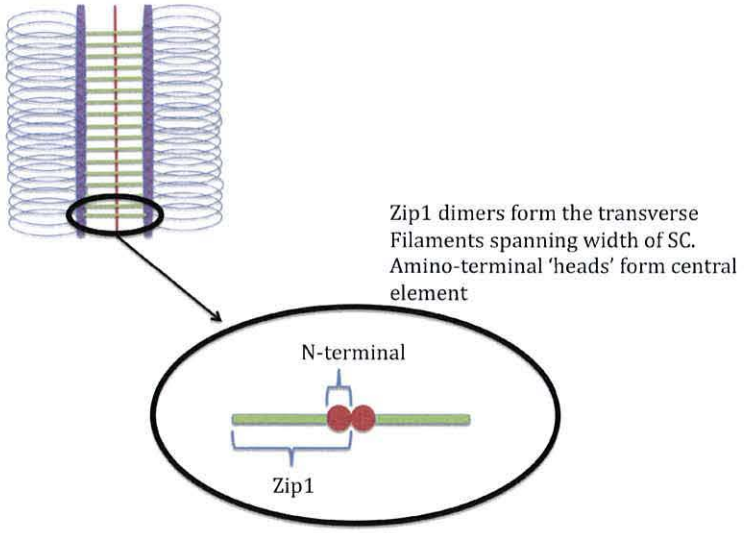

Figure 1.16 Zip1 dimerisation forms transverse filaments of SC. See section 1.12 for more details.

Zip2 facilitates SC elongation (CHENG *et al.,* 2006), a process thought to be Spo11-dependent (TSUBOUCHI *et al.,* 2008; TSUBOUCHI and ROEDER 2005).
zip1 mutants form functional chiasmata, and exhibit only a slight reduction in SCC (SYM and ROEDER 1994). However, in *zip1* mutants, crossover interference is completely abolished (SYM and ROEDER 1994). This indicates that one of the functions of Zip1, as part of the SC central core is to regulate the distribution of crossovers (SMITH and ROEDER 1997). Zip1 is also known to mediate centromere

coupling between non-homologous chromosomes during early prophase (TSUBOUCHI and ROEDER 2005) – although this has not yet been related to SC assembly (HENDERSON and KEENEY 2005). *S. cerevisiae* Zip2, Zip3 and Zip4 have recently been implicated as having roles in the polymerization of transverse filaments (LYNN *et al.*, 2007). Zip3 initiates SC formation (CHUA and ROEDER 1998). Zip3-dependent SUMO modifications are required for SC formation (CHENG *et al.*, 2006).

1.13b Red1, Hop1 and Mek1

RED1 was identified in *S. cerevisiae*, as a mutant that makes inviable meiotic products (ROCKMILL and ROEDER 1988). Loss of the meiosis specific Red1 protein results in a failure to form a SC, or any of its precursory structures. Red1 is a component of the SC axial element, which later mature into lateral elements (ZICKLER 1999). Red1 localises to unsynapsed axial elements, and with the mature lateral elements of the SC (SMITH and ROEDER 1997). Red1 staining is not observed along the continuous length of the chromosomes and is thought to serve to nucleate the formation of axial/lateral elements (SMITH and ROEDER 1997). Red1 binds to chromosomes at the same positions as cohesin binding is observed (BLAT *et al.*, 2002). Red1 is required for wild-type levels of recombination (MAO-DRAAYER *et al.*, 1996); (ROCKMILL and ROEDER 1990), and faithful chromosome disjunction (ROCKMILL and ROEDER 1990).
Hop1 is a meiosis-specific protein that localizes to chromosomes (HOLLINGSWORTH *et al.*, 1990). Hop1 and Red1 are thought to physically interact with one another (ROCKMILL and ROEDER 1990). Hop1 and Red1 localize to the same chromosomal sites during the early stages of meiotic prophase (SMITH and ROEDER 1997). The localization of Hop1 is Red1-dependent, implying that Red1 has an earlier role in SC formation than Hop1 (SMITH and ROEDER 1997). Whilst *red1* mutants fail to form any detectable SC (ROCKMILL and ROEDER 1990), *hop1* mutants are able to form short stretches of axial elements (HOLLINGSWORTH and BYERS 1989; LOIDL *et al.*, 1994)– consistent with Hop1 loading being Red1-dependent. However, some levels of recombination are still observed in the absence of Red1 (ROCKMILL and ROEDER 1990), showing that Hop1 is multi-functional, and not all its functions are Red1-dependent (SMITH and ROEDER 1997). Over-expression of *RED1* leads to

suppression of *HOP1* – suggesting that they interact with one another (HOLLINGSWORTH and JOHNSON 1993).

Mek1 is a serine-threonine protein kinase that functions in conjunction with Red1 and Hop1 to promote inter-homologue recombination, by preventing inter-sister DSB repair (BAILIS and ROEDER 1998; NIU *et al.,* 2005; NIU *et al.,* 2007). Mec1- and Tel1- dependent phosphorylation of Hop1 activates Mek1 (CARBALLO *et al.,* 2008). Dimerization of Mek1 is Hop1-dependent (NIU *et al.,* 2005).

In *S.cerevisiae*, Hop1, Red1 and Mek1 are involved in the promotion of homologous chromosome repair preference versus sister chromatid repair (NIU *et al.,* 2007). Hop1 is thought to inhibit Dmc1-independent repair of DSBs (NIU *et al.,* 2005) rather than positively promote inter-homolog repair (CARBALLO *et al.,* 2008).

Red1, Hop1 and Mek1 are all known to act downstream of the 9-1-1 complex. The 9-1-1 complex recognizes, and binds to DSB sites (LYDALL *et al.,* 1996). 9-1-1 activity results in the phosphorylation of Red1 and Hop1 (HONG and ROEDER 2002; CARBALLO *et al.,* 2008), Hop1 in turn activates Mek1 (CARBALLO *et al.,* 2008). Red1 interacts with two subunits of the 9-1-1 complex (Mec3 and Ddc1) via its C-terminal domain (EICHINGER and JENTSCH 2010). The interaction of Red1 with these two 9-1-1 proteins (Ddc1 in particular) is crucial for a successful meiosis (EICHINGER and JENTSCH 2010), and it is proposed to be essential for checkpoint activation and SC formation (EICHINGER and JENTSCH 2010). This data infers that Red1 operates within the meiotic checkpoint signaling pathway, and that the 9-1-1 checkpoint complex is connected to the SC via Red1 (EICHINGER and JENTSCH 2010).

1.14 Synaptonemal polycomplexes

Many different organisms exhibit aggregation of SC-like material, which have been termed polycomplexes (PCs) (GOLDSTEIN 1987). PCs resemble a parallel stack of SCs (SYM and ROEDER 1995), and are most commonly observed after the dissociation of the SC (ZICKLER 1973) – consistent with being products of SC decomposition. They have also been observed before SC formation (ZICKLER 1973). PCs exhibit many different morphologies that indicate that they are not merely stacked discarded SCs (ZICKLER 1999). In *S. cerevisiae*, over-expression of

the SC central core protein Zip1 induces the formation of PCs, and it is also a major component of these structures (SYM and ROEDER 1995). The PCs formed by Zip1 over-expression are not affected by the absence of either Hop1 or Red1 – proteins associated with SC axial/lateral elements (SYM and ROEDER 1995). This infers that PCs are composed of proteins associated with the SC central core only (SYM and ROEDER 1995). In yeast mutants that fail to form full SCs the level of PCs is significantly higher than seen in wild-type nuclei – suggesting that the unused SC central core proteins in these mutants aggregate to form PCs (ALANI *et al.,* 1990; LOIDL *et al.,* 1994; BISHOP *et al.,* 1992). In *S. cerevisiae,* high levels of PC accumulation have been observed in mutants lacking in: SC structural components (*red1, hop1, zip2, zip3);* recombination proteins (*spo11*); mutants exhibiting prophase block (*clb5, clb6*)(CHENG *et al.,* 2006).

1.15a Linear Elements

The fission yeast *S. pombe* is unusual as it is one of few organisms that have an SC-less meiosis (BAHLER *et al.,* 1993); alongside *Tetrahymena thermophila* and *Aspergillus nidulans.* Instead, during early meiotic prophase, *S. pombe* forms structures termed linear elements (LinEs), which are proposed to be minimal structures required for proper chromosome function during MI (BAHLER *et al.,* 1993). The temporal development of the SC is used as a guideline to define different stages of prophase I in other organisms – the lack of SC in *S. pombe* however, make these divisions of prophase I using these criteria impossible. LinEs were first observed by silver staining under the electron microscope (EM), with their morphology and the timing of their appearance being comparable to that of the lateral elements of the SC (BAHLER *et al.,* 1993). Although visibly comparable to the lateral elements of the SC, LinEs do not form along the entire length of the chromosome (MOLNAR *et al.,* 2003), with their chromosomal localisation sites remaining elusive. It also remains unclear whether there is some kind of structural difference between the chromatin that associates with LinEs and the chromatin that lacks LinE association - or if all chromatin has the same probability of becoming LinE associated (LOIDL 2006). Unlike the SC, there are no visible transverse filaments adjoining the LinEs of *S. pombe* (LORENZ *et al.,* 2004). Significant levels of meiotic recombination can occur in the absence of

LinEs (WELLS *et al.,* 2006), in fact all evidence suggests that LinEs formation is independent of homologue pairing (LOIDL 2006). Rec10, Rec25, Rec27, Mek1 and Hop1 are proteins that have all been identified as LinE components – Rec10, Mek1 and Hop1 having homologues in *S. cerevisiae* (LORENZ *et al.,* 2004; DAVIS *et al.,* 2008).

1.15b LinE Classification

LinEs were initially classified according to the observed variations in their lengths, and their temporal morphological differences as observed by silver staining under an electron microscope, during meiotic prophase (BAHLER *et al.* 1993) (Figure 1.17). Time-course experiments revealed that the differing LinE morphologies observed appears to reflect different stages of LinE development (MOLNAR *et al.,* 2003) – see Figure 1.18 for schematic representation of LinE development.

Currently, classification of Rec10 immuno-stained LinEs (Figure 1.17) is the preferred method of LinE morphological quantification:

Class Ia	small dot-like foci
Class Ib	small oblong/elongated foci
Class IIa	long thread-like structures that appear to form overlapping networks
Class IIb	densely stained 'bundles' of structures – typically only 1-2 separate structures observed per nucleus.
Late time-point Class Ib	a cross between class Ib and IIa. Small, elongated foci mixed with fragmented longer thread-like structures. Proposed as representing LinE degradation.

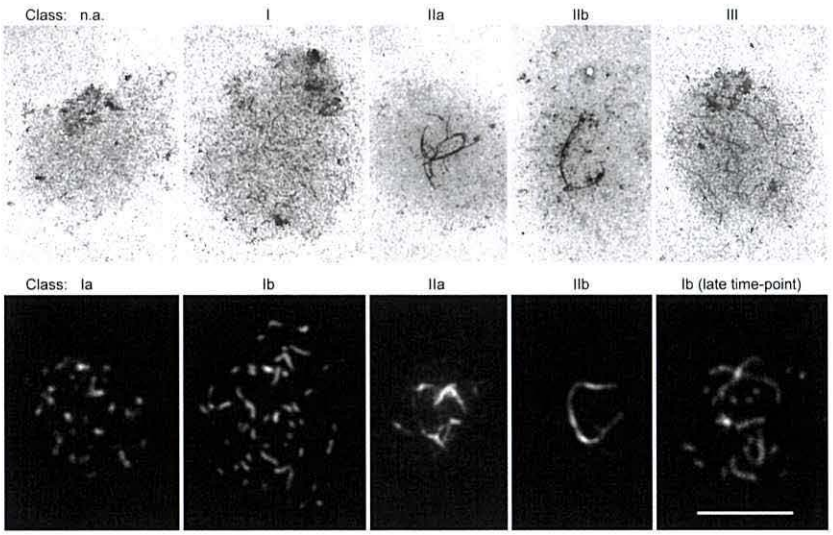

Figure 1.17 Classification of LinEs. Top row - silver-stained LinEs viewed under the electron microscope. Classification (noted above the images) is according to Bahler et al., 1993. Bottom row – Rec10 immuno-stained LinEs viewed under the fluorescence microscope. Classification (noted above the images) is according to Lorenz et al., 2004. Rec10 immunostaining allows a finer distinction in LinE classification and observation of smaller structures, due to less background interference in comparison to the EM images.
Figure adapted from LORENZ *et al.*, 2004.

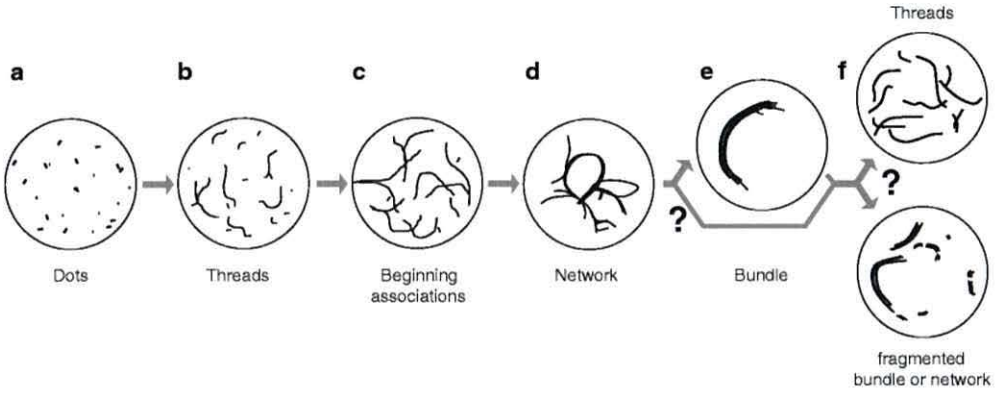

Figure 1.18 Schematic representation of different LinE classes. Diagram represents the current model of temporal LinE development and maturation. 'a' represents class Ia; 'b' represents class Ib; 'c' and 'd' represent class IIa; 'e' represents class IIb; 'f' represents late timepoint class Ib. Figure adapted from LOIDL, 2006.

1.16 Rec10

The main component of LinEs is the meiosis-specific protein Rec10 (LORENZ *et al.*, 2004). Rec10 is essential for LinE formation (ADAMS *et al.*,2003; LORENZ *et al.*, 2004). Detection of Rec10 positive immunofluorescent staining is used for LinE visualisation (LORENZ *et al.*, 2004). Rec10 is required for meiotic recombination throughout the genome (ELLERMEIER and SMITH 2005), although the *rec10-109* missense mutant exhibits reduction in recombination in a region-specific manner (DEVEAUX and SMITH 1994). Like Rec12, Rec10 is essential for meiosis-specific DSB formation (ELLERMEIER and SMITH 2005). *rec10* mutants exhibit wild-type horsetail movement, and are therefore presumed to exhibit normal telomere clustering (MOLNAR *et al.*, 2003). The decrease in chromosome pairing in a *rec10* mutant has been attributed to lack of LinEs suggesting they are required for pairing (MOLNAR *et al.*, 2003); although it is known that recombination is needed for pairing, and so loss of pairing may be due to the reduced recombination observed in *rec10* mutants rather than LinEs (WELLS *et al.*, 2006).

The C-terminus of Rec10 shows a limited sequence similarity to *S. cerevisiae* Red1 (axial element protein) C-terminal domain (ROCKMILL and ROEDER 1988; SMITH and ROEDER 1997; LORENZ *et al.*, 2004). The C-terminus of both proteins contains a lysine-rich region predicted to contain nuclear targeting signals (LORENZ *et al.*, 2004). The C-terminal of Red1 is thought to code a region that mediate Red1-homo-oligomerization (WOLTERING *et al.*, 2000). Rec10 is proposed to help determine recombination sites – nucleating at designated recombination sites, (such as sites exhibiting a more open chromatin configuration) and subsequently recruiting Rec7, which in turn initiates recombination by recruitment of Rec12 (LORENZ *et al.*, 2006).

Rec10 has also been implicated as an important factor for full activation of the *M26* hotspot heptamer, in a context-dependent manner (PRYCE *et al.*, 2005).

1.17 LinE-associated proteins

1.17a Rec25 and Rec27

Rec25 and Rec27 are meiosis specific proteins, identified as part of a large scale screening of *S. pombe* meiotically upregulate genes (MUG) (MARTIN-CASTELLANOS *et al.,* 2005). Both proteins are required for detectable DSB formation, efficient pairing of homologous chromosomes, and are important, yet not essential for meiotic recombination (MARTIN-CASTELLANOS *et al.,* 2005). Rec25 is known to promote meiotic recombination in a region-specific manner, and acts within the same pathway as the meiotic cohesin Rec8 (DAVIS *et al.,* 2008). Rec25 and Rec27 are both proposed as being essential for the localisation of Rec10 during LinE formation, and both proteins are shown to co-localise with Rec10 during the formation of LinEs with a similar classification pattern (small dots later maturing into longer thread-like structures) (DAVIS *et al.,* 2008).

1.17b Hop1 and Mek1

S. pombe Hop1 exhibits limited sequence similarity to *S. cerevisiae* Hop1, which is a component of the SC precursory axial elements (HOLLINGSWORTH *et al.,* 1990). Hop1 localises to wild-type LinEs in fission yeast – but not along the entire length of the Rec10 structures (MOLNAR *et al.,* 2003). Hop1 localisation to LinEs is Rec10-dependent (MOLNAR *et al.,* 2003) – echoing to the Red1-dependency of Hop1 in *S. cerevisiae.*

Like the *S. cerevisiae* homologue, fission yeast Mek1 is not thought to be a structural component of LinEs (or the SC in *S. cerevisiae*), but does localise to them (LORENZ *et al.,* 2004).

S. pombe hop1 and *mek1* mutations have an effect on spore viability, chromosome pairing and recombination between homologous chromosomes (LATYPOV *et al.,* 2010). *hop1* and *mek1* mutations do not however, result in abolition of LinE formation (LORENZ *et al.,* 2004). Hop1 and Mek1 both contribute to high levels of DSB formation (LATYPOV *et al.,* 2010).

1.17c Rec7

Rec7 (homologue to *S. cerevisiae* Rec114 (MOLNAR *et al.*, 2001)) is expected to be one of the earliest recombination factors to localise to the chromatin, subsequently recruiting and activating Rec12 (LORENZ *et al.*, 2006). Rec7 foci virtually all localise to LinEs, with the number of foci increasing as LinEs mature (LORENZ *et al.*, 2006). LinE formation is however, not Rec7-dependent (LORENZ *et al.*, 2006). Rec7 foci are still seen to localise to aberrantly formed LinEs (eg. In *rec8, mek1* and *hop1* mutants), with a reduced number of foci, reflecting the aberrant nature of the LinEs (LORENZ *et al.*, 2006). Rec7 foci are not visible in nuclei before LinEs appear – and are therefore concluded to appear later than Rec10 (LORENZ *et al.*, 2006). Localisation of Rec7 to LinEs defines them as sites where recombination is likely to occur (LORENZ *et al.*, 2006). Rec7 foci are not observed in *rec10Δ* strain – although western blot analysis concludes that *rec7* is still expressed (LORENZ *et al.*, 2006). These data suggests that Rec7 aggregation is Rec10-dependent (LORENZ *et al.*, 2006).

DSB formation is greatly reduced in a *rec7* mutant (CERVANTES *et al.*, 2000). Rec7 is essential for both intra- and intergenic recombination (DEVEAUX and SMITH 1994), and wild-type meiosis progression (MOLNAR *et al.*, 2001).

Rec7 is present in the nucleus prior to karyogamy (MOLNAR *et al.*, 2001), where up to 3 foci were visualised (possibly a connection between these numbers and the 3 chromosomes exhibited by a haploid cell). Prophase 1 exhibits multiple Rec7 signals (up to 50 foci) – suggested to correspond well with the observed number of crossovers during meiosis in *S. pombe* (approximately 45) (MUNZ 1994). This proposes a role for Rec7 in the protein complexes that assemble at sites of meiotic recombination initiation (MOLNAR *et al.*, 2001). The number of foci subsequently reduces before meiosis I, although some Rec7 foci are still seen after meiosis 1, which suggests a possible involvement in the regulation of other meiotic processes (MOLNAR *et al.*, 2001).

1.17d Rad51 and Linear Elements

In *S. pombe*, Rad51 (strand exchange protein) foci are not visible in *rec10Δ* strains (LORENZ *et al.*, 2006). Rad51 foci numbers are somewhat reduced in mutants exhibiting aberrant LinE formation, e.g., *rec8, hop1*, but are still seen to

localise to LinEs (LORENZ *et al.,* 2006). However, Rad51 foci are abundantly present in a *rec10-*155 mutant, which fails to form any detectible LinEs (WELLS *et al.,* 2006). Therefore, Rad51 foci are *rec10-* but not LinE- dependent (WELLS *et al.,* 2006).

Rad51 foci seem to be most abundant (mean number of foci~24, maximum number of foci ~54) in nuclei exhibiting long thread-like (class IIa) LinEs (LORENZ *et al.,* 2006) – this possibly indicative of the stage when most recombination occurs (LORENZ *et al.,* 2006). Although Rad51 foci are seen to localise to LinEs, the localisation is variable, and a clear localization pattern in conjunction with LinE development has not been established (LORENZ *et al.,* 2006). One proposal is that Rad51 foci transiently form on LinEs, with Rad51 foci that do not localise to LinEs being due to detachment of Rad51 from LinEs, or partial disintegration of LinEs before meiotic recombination has ended (LORENZ *et al.,* 2006). It is also possible that a small number of meiotic recombination events occur outside the context of the LinEs (LORENZ *et al.,* 2006). However, based on the localisation of Rad51, it has been proposed that DSBs form and are initially processed within the spatial context of LinEs (LORENZ *et al.,* 2006). Rec7 and Rad51 were shown not co-localise (LORENZ *et al.,* 2006), however these data were collected from a *rec7*::GFP strain which did not yield wild-type recombination levels, therefore these results should be interpreted with caution . Rad51 foci formation is Rec12-dependent, with Rad51 foci only exhibited very sporadically in a *rec12* mutant (LORENZ *et al.,* 2006).

1.18 Requirements for LinE formation

Several meiotic proteins are known to be required for the correct formation of LinEs. In *S. cerevisiae*, Rec8 (meiotic cohesin) is part of the core SC structure (KLEIN *et al.,* 1999), but in *S. pombe*, Rec8 is not seen to co-localise with LinEs. However, in *S. pombe*, loss of Rec8 or Rec11 (meiosis-specific fission yeast cohesin) results in aberrant LinE formation (LORENZ *et al.,* 2006; MOLNAR *et al.,* 1995) - the residual levels of LinE formation still observed are attributed to the presence of a Rec8 paralogue, Rad21 (a mitotic cohesin also expressed in meiosis) (LOIDL 2006). Rec10 has been shown to recruit to the chromosomes at low levels in the absence of Rec8 or Rec11 (LORENZ *et al.,* 2004). It has been

proposed that the Rec8-Rec11 meiotic cohesin complex could serve as loading sites for LinE polymerization (MOLNAR *et al.,* 2003). This renders an important role for meiotic cohesins in LinE formation and recombination as well as cohesion.

Although morphologically similar to wild-type LinEs, the temporal quantification of LinE classes observed in *rec12*, *rec14* and *meu13 (HOP2)* mutants (all proteins involved in the formation of meiotic DSBs) differ to that observed in wild-type temporal analyses (MOLNAR *et al.,* 2003). The three mutations caused different changes at different stages of prophase I, indicating a biological significance of the different LinE classes (MOLNAR *et al.,* 2003). From these data it has also been concluded that LinE formation is not DSB-dependent (MOLNAR *et al.,* 2003). *meu13* mutants also exhibit altered LinE formation – differing mostly early on in prophase I (MOLNAR *et al.,* 2003) – suggesting that Meu13 has a role as a base protein required for loading of other LinE-associated proteins (MOLNAR *et al.,* 2003), and that defective chromosome pairing may have an effect of LinE development.

Recent studies also suggest a role for Rad50 (part of the MRN complex) in regulating LinE formation, as *rad50* mutants fail to form LinEs (in *pat1-114* thermally induced meioses*)* (HARTSUIKER *et al.,* 2009).

1.19 Small ubiquitin-related modifier (SUMO)

SUMO-ylation is the reversible post-translational modification of proteins by covalent linkage of SUMO to a lysine residue. The SC can be stained with SUMO-specific antibodies along its entire axis (HOOKER and ROEDER 2006), and has been inferred as having a role in the initiation of SC formation (HOOKER and ROEDER 2006). In *S. cerevisiae*, polymerization of Zip1 along the axial elements of the SC occurs in tandem with the SUMOylation of Red1 via Smt3 (*S. cerevisiae* SUMO precursory protein) (CHENG *et al.,* 2007). Zip1 is essential for wild-type SUMO localization (HOOKER and ROEDER 2006). Like Zip1, SUMO localises to synaptonemal PCs (HOOKER and ROEDER 2006). SUMO has been demonstrated to co-localise with Zip3 (which is involved in initiating the formation, and subsequent elongation of the SC) during early prophase 1, implicating SUMO in the initiation of synapsis (HOOKER and ROEDER 2006). This is confirmed by

analysis of an *ubc9* mutant. Ubc9 is an enzyme required for conjugation of SUMO to its substrates. This mutant is defective in SUMOylation, and also exhibits a delayed SC formation and chromosome synapsis (HOOKER and ROEDER 2006). SUMOylation is therefore essential for normal SC formation (HOOKER and ROEDER 2006).

Red1 is thought to be a likely substrate for SUMOylation within the axial elements (LIN *et al.,* 2010), with the suggestions of synapsis-SUMOylation interdependence (HOOKER and ROEDER 2006). The SUMOylation of the lysine-rich C-terminal tail of Red1, via Zip3, is directly linked to the initiation of SC formation – ensuring timely SC assembly (LIN *et al.,* 2010). It has been proposed that SC elements may be 'sandwiched' together via SUMO chains, which bind with both Red1 and Zip1 (LIN *et al.,* 2010). SUMOylation of Red1 is crucial for normal meiotic progression (LIN *et al.,* 2010).

SUMO localisation to *S. pombe* LinEs is reminiscent of *S. cerevisiae* axial element SUMOylation (SPIREK *et al.,* 2010). However, there is no evidence showing that Rec10 is the target of SUMOylation - other possible targets may be Rec25, Rec27 or other LinE components (SPIREK *et al.,* 2010), and SUMOylation is not a pre-requisite for LinE formation (SPIREK *et al.,* 2010).

1.20 Aims of this study

- → Analysis of the temporal progression of LinE development during a synchronised meiosis.
- → Correlation of temporal development profile of LinEs with the timing of S-phase.
- → Creation of a *rec10* mutant strain, defective in LinE formation but maintaining wild type levels of recombination frequency.
- → Further cytological and genetic analysis on other *rec10* mutants.

Chapter 2

Materials and Methods

2.1 Strains, growth and storage

All *S. pombe* strains used in this study are listed in Table 2.1. Strains were kept in 25% glycerol and put at -80°C for long-term storage. Strains were revived from the freezer by incubation at 30°C (25°C for temperature sensitive strains) for 2-3 days on YEA plates unless stated otherwise. All media used for strain growth is listed in section 2.19.

2.2 Meiotic crosses

All cultures were grown in yeast extract liquid (YEL) to a density of approximately $2x10^7$ cells/ml. 750 μl of each culture were mixed in a 1.5 ml Eppendorf tube, and centrifuged for 30 secs at 10,390 g. The pellets were washed with 1 ml of dH_2O and then resuspended in ~20 μl dH_2O. The suspensions were carefully pippetted on to fully supplemented synthetic sporulation media (SPA) plates and incubated at 30°C (25°C for temperature sensitive strains) for 2-3 days. After incubation, the sporulating cells were scraped off into a 1.5 ml Eppendorf tube containing 1 ml of dH_20 with 0.6% β-glucuronidase (Sigma Aldrich, β-Glucuronidase from *Helix pomatia*, type HP-2, aqueous solution, ≥100,000 units/ml), and incubated for 16 hrs at 25°C. After incubation, 0.5 ml 100% EtOH was added to the solution, and left to incubate for 2 mins at room temperature. The suspensions were then centrifuged, washed with 0.5 ml dH_20 and finally resuspended in 1 ml dH_20.

2.3 Mating type testing

All cultures to be tested were grown in YEL to a density of approximately $2x10^7$ cells/ml; cultures of BP1 (h^-) and BP8 (h^+) were grown alongside these. 750 μl of each culture to be tested was mixed with 750 μl of BP1 and BP8 in separate 1.5 ml Eppendorf tubes and centrifuged for 30 secs at 10,390 g. The pellets were washed with 1 ml of dH_2O and then resuspended in ~20 μl dH_2O. The

suspensions were carefully pippetted on to fully supplemented SPA plates and incubated at 30°C (25°C for temperature sensitive strains) for 2-3 days. The plates were then exposed to iodine vapours, which stained the sporulating cells black, leaving the cells that had not mated unstained.

2.4 Asynchronous meiotic induction.

For meiotic induction of h^+/h^- *ade6-M210/ade6-M216* diploid, cells were streaked onto fresh YEA plates and grown at 30°C for 2-3 days. Single white colonies were taken and inoculated into 5 ml of YEL media and incubated shaking at 30°C for approximately 16 hrs. This culture was used to make 1:100 and a 1:50 dilution in EMM2 media, and incubated shaking at 30°C to a concentration of $5x10^6$ - $1x10^7$ cells per ml. Cells were harvested, washed in equal amount of dH_20 and resuspended (in clean flask) into EMM2-N to induce meiosis. This was recorded as time-point 0 hrs.

2.5 Synchronised temperature sensitive meiotic induction.

For meiotic induction of h^+/h^- - *ade6-M210/ade6-M216 pat1-114/pat1-114* diploid, cells were streaked onto fresh YEA plates and grown at 25°C for 4-5 days. Single white colonies were taken and inoculated into 5 ml of YEL media and incubated shaking at 25°C for approximately 16 hrs. This culture was used to make 1:100 and a 1:50 dilution in EMM2* media, and incubated shaking at 25°C to a concentration of $5x10^6$ - $1x10^7$ cells per ml. Cells were harvested, washed in equal amount of dH_20 and resuspended (in clean flask) into EMM2*-N and incubated shaking for approximately 16 hrs. The culture was warmed to 34°C in a water bath (whilst still shaking) to induce meiosis by heat inactivation of Pat1-114 (time-point 0 hrs), and then incubated at 34°C for remainder of experiment.

2.6 Meiotic induction of *h⁻/h⁻ pat1-114/pat1-114 ade6-M216/ade6-M210 leu1/leu1 lys1::mat-Pc-lys1⁺* mutant.

The strain used in this study was:

h⁻/h⁻ pat1-114/pat1-114 ade6-M216/ade6-M210 leu1/leu1 lys1::mat-Pc-lys1⁺

Strain was streaked onto fresh YEA plate and incubated at 25°C for 4-5 days. A single white colony was taken to inoculate 5 ml YEL, incubated shaking at 25°C to a concentration of 5-6 x10^6 cells/ml. The culture was washed extensively in equal volume of MM-N (1% glucose; 40 mg/l leucine), and then resuspended in MM-N (1% glucose; 40mg/l leucine) to a density of 4x10^6 cells/ml. The culture was incubated shaking at 25°C for 6 hrs and 30 mins to arrest cells at G1. The cell density is expected to be approximately 8x10^6 cells/ml after 6 hrs and 30 mins, with most cells expected to have arrested at G1. Equal volume of fresh MM-N (1% glucose; 40 mg/l leucine) pre-warmed to 34°C, and culture was transferred to shake at 34°C to induce meiosis. This was recorded as time-point 0 hrs.

2.7 Transformation of PCR products into *S. pombe*

All transformations of PCR products into *S. pombe* were done following the protocol in (BÄHLER *et al.,* 1998).

2.8 Chemical transformation of *E. coli*

Aliquot of chemically competent cells was thawed on ice (100 μl per transformation reaction). 1-50 ng of DNA to be transformed was added (≤10 μl) to each aliquot. Mixture was incubated on ice for 10 mins. Mixture was then placed in a water bath at 42°C for 90 secs to heat shock the cells, then returned to ice for a further 2 mins. 900 μl of LB liquid, warmed to 37°C, was added to the mixture, before incubating shaking for 1 hr at 37°C. Mixture was plated out at 1, 1:10, 1:100 dilutions on appropriate antibiotic agar plate, and incubated overnight at 37°C. Transformants would be visible by the next morning.

2.9 Electro-transformation of *E. coli*

Aliquot of electro-competent cells were thawed on ice (100 μl per transformation). Add 1-50 ng of DNA to be transformed (≤10 μl) to each aliquot, and transfer mixture to a pre-chilled electro-cuvette. Pulse the cell mixture once in the electroporator (bio-rad micropulser) on the *E. coli* setting. Transfer mixture to an Eppendorf tube containing 900 μl LB liquid (warmed to 37 °C) and incubate at 37 °C for 1 hr. The mixture was plated out at 1, 1:10, 1:100 dilutions on appropriate antibiotic agar plate, and incubated overnight at 37°C. Transformants would be visible by the next morning.

2.10 Site-directed mutagenesis

Mutations were generated via site-directed mutagenesis, using oligonucleotides that contained the desired mutation to amplify the region to be mutated, thus inserting the mutation. We also utilized the method described by (LIU and NAISMITH 2008).

2.11 Plasmid extraction

All plasmid extractions were done following the protocol for the Qiagen QiaPrep spin miniprep kit.

2.12 DNA extraction

The desired strains were grown in 5 ml YEL to a density of approximately $2x10^7$ cells/ml. They were then centrifuged for 5 mins at 1,789 g. The supernatant was discarded, and the cell pellet washed in 1 ml H_2O and transferred to a 1.5 ml screw-top tube. 200 μl lysis buffer (2% Triton X-100; 1% SDS; 100 mM NaCl; 10 mM TrisHCl; 1 mM EDTA), 100 μl phenol, 100 μl chloroform and 0.3 g glass beads were added to the cell pellet, and the mixture was placed in the fast-prep machine (Bio101 Fastprep fp120) on setting 6.0 for 30 secs to break the cells. The tubes were then centrifuged at 10,390 g for 15 mins. The top aqueous layer was then removed and transferred to a fresh 1.5 ml Eppendorf tube, and 3 volumes of 100% EtOH were added, and the tubes were incubated at -20°C for approximately 16 hrs (or -80°C for approximately 1 hr). The mixture was then

centrifuged at 4°C for 30-60 mins at 14,250 g. The liquid was aspirated off carefully, and the pellet was washed once with 70% EtOH before being left to air-dry. The DNA pellet was then resuspended to the desired volume in either TE or dH_2O.

2.13 DNA purification

Equal volumes of phenol and chloroform were added to the DNA to be purified (so that the volume of phenol + chloroform = volume of DNA to be purified) along with 0.1 M (final concentration) NaCl. The tube was mixed, and then centrifuged for 10 mins at 10,390 g. The top layer was removed and transferred to a clean tube. 3 volumes of 100% EtOH were added, and the tube was placed at -20°C for approximately 8 hrs (or at -80°C for approximately 1 hr). The mixture was then centrifuged at 4°C for 30-60 mins at 14,250 g. The liquid was aspirated off carefully, and the pellet was washed once with 70% EtOH before being left to air-dry. The DNA pellet was then resuspended to the desired volume in either TE or dH_2O.

2.14 Fluorescence Activated Cell Sorting (FACS)

Cell samples were collected and resuspended in 70% EtOH. These could be stored indefinitely at –20°C. For FACS analysis, 0.3 ml of cell sample (~2-3x10^6 cells) was added to 3 ml 50 mM sodium citrate, mixed and centrifuged at 447 g for 5 mins, the supernatant was discarded and the sample pellet was resuspended in 0.5 ml 50 mM sodium citrate containing 0.1 mg/ml RNase; this was left for a minimum of 2 hrs at 37°C. Cells were stained by adding 0.5 ml 50 mM sodium citrate containing 8 μg/ml propidium iodide (PI); giving the sample a final concentration of 4 μg/ml of PI. Cells could be processed immediately or stored for up to 1 week in the dark at 4°C.

2.15 Harvesting Spheroplasts.

Two methods were employed for harvesting spheroplasts.

1. 10 ml samples were taken at time-points wanted, and centrifuged for 5 mins at 447 g. The pellet was resuspended in 2 ml of 0.65 M KCl containing: 40 μl 0.5 M

DTT; 40 μl zymolyase T-100 (10 mg/ml); 40 μl L8757 lysing enzyme (100 mg/ml); 120 μl L1412 lysing enzyme (250 mg/ml); 1 μl 1M PMSF in DMSO, and incubated for 27 mins shaking at 30°C. The suspension was viewed under a light microscope for presence of sufficient levels of spheroplasting. 8 ml of MES buffer (0.1 M 2-(*N*-morpholino) ethane sulfonic acid (MES); 1 mM EDTA; 0.5 mM $MgCl_2$; 1 M sorbitol. pH adjusted to 6.4 with NaOH) was added to the suspension, it was then centrifuged for 4 mins at 447 g. The pellet of spheroplasts was then resuspended in 150 μl MES with 1 μl 1 M PMSF in DMSO. The spheroplast suspension could be spread immediately, or stored on ice for up to 6 hrs before spreading.

2. 5 ml samples were taken at the required time-points, and centrifuges for 5 mins at 447 g. The pellet was resuspended in 1 ml 0.65 M KCl containing: 10 mM DTT (from a 0.5 M stock); 20 μl zymolyase 100-T (10 mg/ml); 20 μl L8757 lysing enzyme (100 mg/ml); 60 μl L1412 lysing enzyme (250 mg/ml); 1 μl 1 M PMSF in DMSO, and incubated for 25-30 mins shaking at 30°C. The suspension was viewed under the light microscope for presence of sufficient levels of spheroplasting. 9 ml of MES buffer was added to the suspension, it was then centrifuged for 4 mins at 447 g. The pellet of spheroplasts was then resuspended in 150 μl MES with 1 μl 1 M PMSF in DMSO. The spheroplast suspension could be spread immediately, or stored on ice for up to 6 hrs before spreading.(LOIDL and LORENZ 2009)

2.16 Nuclear Spreading

20 μl of the spheroplasts suspension was placed onto a slide. 40 μl fixative (3.4% sucrose; 4% paraformaldehyde) and 80 μl lipsol (1% Lipsol detergent in dH_2O) were added, and mixed by carefully tilting the slide. After 30 secs, 80 μl of fixative was added and the mixture was spread over the slide using a glass rod or pipette tip, and left to dry at room temperature overnight. Slides could be stained immediately, or stored at -20°C for later use.

2.16a Making the Fixative

The paraformaldehyde was heated to 80°C in 90 ml distilled water on a magnetic stirrer in a chemical hood. After 20-30 mins the solution should have become clear. If it stayed opaque, 1M NaOH was added until it became clear. After cooling, the sucrose was added to the solution. If NaOH had been added, the solution had to be titrated back to pH8.5 with HCl. The final volume was made up to 100 ml with distilled water. If the fixative was still not completely clear, it could be filtered. The fixative can be stored for several months at 4°C (LOIDL and LORENZ 2009).

2.17 Immunofluorescence

Slides were washed for 3 x 10-15 mins in 1 x phosphate buffered saline (PBS) (1 l of x10 PBS: 80 g NaCl; 2 g KCl; 11.5 g $Na_2HPO_4.7H_20$; 2 g anhydrous KH_2PO_4, pH adjusted to 7.5) containing 0.05% Triton X-100. Excess liquid was shaken off, and slides left to air-dry. Primary antibodies were diluted in 1 x PBS at the following concentrations: rabbit anti-Rec10 1:200; mouse anti-Rad51 1:50; guinea pig anti-Hop1 1:50. 20-25 µl primary antibody was applied, and a cover slip was placed on the slide before it was incubated for 16-24 hrs in a dark humidity chamber at room temperature. The slides were then washed again 3 times in 1 x PBS containing 0.05% Triton X-100, with the excess liquid shaken off, and slides left to air-dry. 20-25 µl secondary antibodies (diluted 1:200 in 1 x PBS) were applied, with a cover slip being placed on the slide before it was incubated again in a dark humidity chamber for 16-24 hrs. The slides were then washed 3 times in 1 x PBS containing 0.05% Triton X-100 for the third time, with excess liquid shaken off and then left to air-dry. An anti-fade solution (Vectashield, Vector Labs) containing 1 mg/ml DAPI (for visualisation of DNA) was applied to each slide (approximately 5 µl), a cover slip was placed on top, and slides kept in the dark. Slides could be viewed instantly or kept for 2-3 weeks at 4°C.

All secondary antibodies were purchased from Invitrogen.

Slides were viewed with a Zeiss Axioskop 2, and pictures were taken using an Axiocam digital camera, and subsequently managed using Axiovision 4.8.

2.18 Determination of intragenic recombination frequency

Intragenic recombination frequency was calculated as total number of prototrophs per 10^6 viable spores. Serial dilutions of spore suspensions were made and 100 μl aliquots were spread onto media specifically supplemented for the particular experiment to determine viable spore numbers. Recombinant numbers were determined by spreading 100 μl aliquots of the spore suspension serial dilutions onto NB agar. Ade+ recombinant numbers were determined by spreading onto YEA guanine plates.

2.19 Determination of intergenic recombination frequency

Intergenic recombination was recorded as genetic distance, which is measured in centimorgans (cM). Genetic distance was calculated using Haldane's equation:

Genetic distance = $-50\ln(1-2R)$

(Where R = the total fraction of prototrophs among all spores analysed).

2.20 Fluorescence *in situ* hybridisation (FISH)

FISH was carried out according to the protocol in (LOIDL and LORENZ 2009). 50 μl of DNase-free RNase (100 μg/ml in 2x SSC) was applied to each immunostained (with Rec10-ab) slide of spread nuclei, covered with a coverslip and incubated for 30 mins at 37°C in a humid chamber. The slides were then incubated in ST buffer [4x SSC (0.6 M NaCl, 60 mM trisodium citrate, pH 7.0), 0.1% Tween-20] at 37°C for 1-3 hrs. Slides were then placed in 70% formamide in 2x SSC, pH 7.0 at 60°C for 2 mins, then immersed immediately in ice-cold 70%, 90% and 96% ethanol for 5 mins each. Slides were then air-dried. 6μl of denatured probe was applied to each slide, covered with a coverslip and sealed with rubber cement. The slides were placed on a heat-block for 10 mins at 80°C, and then put at 37°C for at least 36 hrs. The rubber cement was then peeled off, and coverslip gently rinsed away with 2x SSC. The slides were washed for 5 mins each in: 50% formamide in 2x SSC at 37°C; 2x SSC at 37°C; 1x SSc at room temperature.

2.21 *S. pombe* media

All recipes are for 1 litre of media. For liquid media, agar is omitted. Vitamins, minerals and salts are added after autoclaving. All amino acid supplements were added at a concentration of 200 mg/l unless stated otherwise.

YEA	5 g yeast extract; 30 g glucose; 14 g agar
SPA	10 g glucose; 1 g KH_2PO_4; 30 g agar; 1 ml vitamins (x1000); 200 mg leucine; 200 mg lysine; 200 mg arginine; 200 mg adenine; 200 mg proline; 200 mg histidine; 200 mg uracil
EMM2	3 g potassium hydrogen phthalate; 2.2 g Na_2HPO_4; 5 g NH_4Cl; 20 g glucose *; 14 g agar; 1 ml vitamins (x1000); 20 ml salts (x50); 0.1 ml minerals (x10,000) * - EMM2* = 5 g glucose EMM2-N / EMM2*-N – omit NH_4Cl.
NB	1.7 g nitrogen base; 5 g $(NH_4)_2SO_4$; 5 g glucose; 24 g agar
MM	1 g KH_2PO_4; 0.5 g $MgSO_4.7H_2O$; 0.1 g NaCl; 0.1 g $CaCl_2.2H_2O$; 5 g $(NH_4)_2SO_4$; 10 g glucose; 22 g agar; 1 ml vitamins (x1000); 0.1 ml minerals (x10,000)
VITAMINS (x1000)	1 g pantothenic acid; 10 g nicotinic acid; 10 g inositol; 10 mg biotin
MINERALS (x10,000)	5 g boric acid; 4 g $MnSO_4$; 4 g $ZnSO_4.7H_2O$; 2 g $FeCl_2.6H_20$ 1 g Kl; 0.4 g molybdic acid; 0.4 g $CuSO_4.5H_20$; 10 g citric acid
SALTS (x50)	52.5 g $MgCl_2.6H_20$; 0.735 g $CaCl_2.2H_20$; 50 g KCl; 2 g Na_2SO_4

Table 2.1 Strain list

Name	Genotype	Source
BP4	*h⁺ ade6-M375*	McFarlane collection
BP5	*h⁻ ade6-52*	McFarlane collection
BP12	*h⁺ ade6-M26*	McFarlane collection
BP26	*h⁻ arg3-124*	McFarlane collection
BP29	*h⁺ pro2-1*	McFarlane collection
BP85	*h⁻ lys7-1*	McFarlane collection
BP86	*h⁺ lys7-2*	McFarlane collection
BP404	*h⁻ ura1-61*	McFarlane collection
BP405	*h⁻ ura1-171*	McFarlane collection
BP420	*h⁻ pro1-1*	McFarlane collection
BP444	*h⁻/h⁻ ade6-210/ade6-216 pat1-114/pat1-114*	McFarlane collection
BP451	*h⁺ ade6-3005*	McFarlane collection
BP452	*h⁺ ade6-3006*	McFarlane collection
BP621	*h⁺ ura1-61*	McFarlane collection
BP632	*h⁻ lys7-2*	McFarlane collection
BP633	*h⁺ lys7-1*	McFarlane collection
BP695	*h⁺ ade6-M26-16C*	McFarlane collection
BP735	*h⁺ ade6-3049*	McFarlane collection
BP737	*h⁺ ade6-3009*	McFarlane collection
BP834	*h⁻ ade6-M375*	McFarlane collection
BP888	*h⁺ ade6-52 pro2-1*	McFarlane collection
BP896	*h⁻ ade6-M26 arg3-124*	McFarlane collection
BP950	*h⁻ arg4-55*	McFarlane collection
BP954	*h⁻ arg4-55 leu1-32*	McFarlane collection
BP974	*h⁺ ade8-106*	McFarlane collection
BP980	*h⁺ pro1-1*	McFarlane collection
BP981	*h⁺ pro1-1 leu1-32 rec10-155::LEU2+*	McFarlane collection
BP1027	*h⁺/h⁻ ade6-210/ade6-216*	McFarlane collection
BP1045	*h⁻ ura1-61 rec10-175::KANMX6*	McFarlane collection
BP1046	*h⁺ ura1-171 rec10-175::KANMX6*	McFarlane collection
BP1047	*h⁺ ura1-171*	McFarlane collection
BP1948	*h⁻ ura1-171*	McFarlane collection
BP1101	*h⁻ ura1-171 leu1-32 rec10-155::LEU2+*	McFarlane collection
BP1103	*h⁺/h⁻ ade6-210/ade6-216 rec12Δ/rec12Δ*	McFarlane collection
BP1143	*h⁺ pro2-1 rec10-175::KANMX6*	McFarlane collection
BP1729	*h⁺ lys7-1 rec10-175::KANMX6*	This study
BP1730	*h⁻ lys7-1 rec10-175::KANMX6*	This study

BP1731	*h⁺ ade6-M26 rec10-175::KANMX6*	This study
BP1738	*h⁻ ade6-M375 rec10-Y767F*	This study
BP1739	*h⁻ ade6-52 rec10-175::KANMX6*	This study
BP1767	*h⁺ ade6-M375 rec10-Y767F*	This study
BP1823	*h⁺ ade6-M26 rec10-Y767F*	This study
BP1827	*h⁺ ura1-61 rec10-175::KANMX6*	This study
BP1830	*h⁺ ura1-171 rec10-175::KANMX6*	This study
BP1876	*h⁻ ade6-52 rec10-Y767F*	This study
BP1878	*h⁺ lys7-2 rec10-175::KANMX6*	This study
BP1886	*h⁻ arg4-55 rec10-Y767F*	This study
BP1897	*h⁺ ura1-61 rec10-Y767F*	This study
BP1898	*h⁻ ly7-2 rec10-175::KANMX6*	This study
BP1954	*h⁺ ade8-106 rec10-Y767F*	This study
BP2012	*h⁺/h⁻ ade6-210/ade6-216 rec10-109/rec10-109*	This study
BP2013	*h⁺/h⁻ ade6-210/ade6-216 rec10-144/rec10-144*	This study
BP2033	*h⁺/h⁻ ade6-210/ade6-216 rec27Δ/rec27Δ*	This study
BP2034	*h⁺/h⁻ ade6-210/ade6-216 rec25Δ/rec25Δ*	This study
BP2057	*h⁺ ade8-106 rec10-Y731F*	This study
BP2072	*h⁻ ade6-52 rec10-Y731F*	This study
BP2073	*h⁺ ade6-M375 rec10-K754R*	This study
BP2076	*h⁺ ade6-M26 rec10-K754R*	This study
BP2078	*h⁻ ade6-52 rec10-K754R*	This study
BP2092	*h⁺/h⁻ ade6-210/ade6-216 rec8Δ/rec8Δ*	This study
BP2093	*h⁺/h⁻ ade6-210/ade6-216 leu1-32/leu1-32 rec10-155::LEU2/rec10-155::LEU2*	This study
BP2100	*h⁺ ura1-61 rec10-Y731F*	This study
BP2102	*h⁺ ade6-M26 rec10-2YF*	This study
BP2114	*h⁻ ade6-52 rec10-2YF*	This study
BP2117	*h⁺/h⁻ ade6-210/ade6-216 rec10-Y731F/rec10-Y731F*	This study
BP2119	*h⁻ arg4-55 rec10-2YF*	This study
BP2120	*h⁺ ade6-M375 rec10-2YF*	This study
BP2123	*h⁺ ade6-M26 rec10-2YF*	This study
BP2164	*h⁺ ade6-3049 rec10-2YF*	This study
BP2167	*h⁺ ade6-3049 rec10-Y731F*	This study
BP2172	*h⁺ ade6-3005 rec10-2YF*	This study
BP2174	*h⁺ ade6-M26-16C rec10-2YF*	This study
BP2176	*h⁺ ade6-3005 rec10-Y731F*	This study
BP2179	*h⁺ ade6-M26-16C rec10-Y731F*	This study
BP2181	*h⁺ ade6-3049 rec10-Y767F*	This study
BP2194	*h⁺ ade6-3005 rec10-Y767F*	This study

BP2211	*h⁺ ade6-M26-16C rec10-Y767F*	This study
BP2229	*h⁺ ade6-M26 rec10-K744R*	This study
BP2237	*h⁻ ade6-52 rec10-K744R*	This study
BP2282	*h⁺/h⁻ ade6-210/ade6-216 rec1-Y767F/rec10-Y767F*	This study
BP2284	*h⁺/h⁻ ade6-210/ade6-216 rec10-K744R/rec10-K744R*	This study
BP2310	*h⁺ ade8-106 rec10-2YF*	This study
BP2319	*h⁻ arg4-55 rec10-Y731F*	This study
BP2323	*h⁻ pro1-1 rec10-Y731F*	This study
BP2333	*h⁻ pro1-1 rec10-Y767F*	This study
BP2334	*h⁺ ura1-1 rec10-2YF*	This study
BP2358	*h⁺/h⁻ ade6-210/ade6-216 rec10+/rec10-175*	This study
BP2359	*h⁺/h⁻ ade6-210/ade6-216 rec10-2YF/rec10-2YF*	This study
BP2392	*h⁺ ade6-M26 rec10-K757R*	This study
BP2397	*h⁻ ade6-52 rec10-K757R*	This study
BP2434	*h⁺/h⁻ ade6-210/ade6-216 leu⁺/leu1-32 rec10+/rec10-155::LEU2+*	This study
BP2449	*h⁺ ade6-3006 rec10-Y731F*	This study
BP2450	*h⁺ ade6-3006 rec10-2YF*	This study
BP2454	*h⁺ ade6-M375 rec10-K712R*	This study
BP2456	*h⁺ ade6-M375 rec10-3KR*	This study
BP2458	*h⁺ ade6-M26 rec10-K712R*	This study
BP2460	*h⁻ ade6-52 rec10-3KR*	This study
BP2461	*h⁺ ade6-M26 rec10-3KR*	This study
BP2463	*h⁻ ade6-52 rec10-K712R*	This study
BP2466	*h⁺ ade6-M375 rec10-K744R*	This study
BP2468	*h⁺ ade6-3009 rec10-Y731F*	This study
BP2469	*h⁺ ade6-3009 rec10-2YF*	This study
BP2471	*h⁺ ade6-3006 rec10-Y767F*	This study
BP2478	*h⁺/h⁻ ade6-210/ade6-216 rec10-K757R/rec10-K757R*	This study
BP2487	*h⁺/h⁻ ade6-210/ade6-216 rec10-K712R/rec10-K712R*	This study
BP2491	*h⁺ ade6-3009 rec10-Y767F*	This study
BP2492	*h⁺ ade6-M375 rec10-K757R*	This study
BP2494	*h⁺/h⁻ ade6-210/ade6-216 rec10-3KR/rec10-3KR*	This study
BP2508	*h⁻ pro1-1 rec10-2YF*	This study
BP2510	*h⁻ ade6-M375 rec10-2YF*	This study
BP2511	*h⁺ ade6-M375 rec10-Y731F*	This study
BP2512	*h⁻ ade6-M375 rec10-Y731F*	This study
BP2542	*h⁺ ade6-3049 rec10-3KR*	This study
BP2543	*h⁺ ade6-3005 rec10-3KR*	This study
BP2545	*h⁻ ade6-M375 rec10-K757R*	This study

BP2546	*h⁺ ade6-3049 rec10-K754R*	This study
BP2548	*h⁺ ade6-3049 rec10-K744R*	This study
BP2549	*h⁺ ade6-3005 rec10-K744R*	This study
BP2550	*h⁻ ade6-M375 rec10-K754R*	This study
BP2551	*h⁺ ade6-3049 rec19-K757R*	This study
BP2552	*h⁺ adeg-3005 rec10-K757R*	This study
BP2559	*h⁺ ade6-3049 rec10-K712R*	This study
BP2561	*h⁻ ade6-M375 rec10-K712R*	This study
BP2562	*h⁻ ade6-M375 rec10-3KR*	This study
BP2563	*h⁺ ade6-M26-16C rec10-K757R*	This study
BP2565	*h⁺ ade6-M26-16C rec10-K712R*	This study
BP2566	*h⁺ ade6-M26-16C rec10-3KR*	This study
BP2569	*h⁺ ura1-61 rec10-K712R*	This study
BP2570	*h⁺ ade6-M26-16C rec10-K744R*	This study
BP2572	*h⁺ ura1-61 rec10-3KR*	This study
BP2574	*h⁺ ura1-1 rec10-K744R*	This study
BP2575	*h⁺ ade6-3005 rec10-K712R*	This study
BP2577	*h⁺ ade6-M26-16C rec10-K754R*	This study
BP2578	*h⁻ ade6-M375 rec10-K744R*	This study
BP2579	*h⁺ ade6-3009 rec10-3KR*	This study
BP2580	*h⁺ ade6-3006 rec10-3KR*	This study
BP2581	*h⁺ ade6-3009 rec10-K712R*	This study
BP2582	*h⁺ ade6-3006 rec10-K712R*	This study
BP2583	*h⁺ ade6-3009 rec10-K757R*	This study
BP2584	*h⁺ ade6-3006 rec10-K757R*	This study
BP2585	*h⁺ ade6-3009 rec10-K754R*	This study
BP2586	*h⁺ ade6-3006 rec10-K754R*	This study
BP2587	*h⁺ ade6-3009 rec10-K744R*	This study
BP2588	*h⁺ ade6-3006 rec10-K744R*	This study
BP2591	*h⁺ ade8-106 rec10-3KR*	This study
BP2593	*h⁺ ade8-106 rec10-K712R*	This study
BP2595	*h⁺ ade8-106 rec10-K754R*	This study
BP2596	*h⁺ ade8-106 rec10-K744R*	This study
BP2607	*h⁻ pro1-1 rec10-K744R*	This study
BP2610	*h⁻ pro1-1 rec10-K754R*	This study
BP2611	*h⁻ pro1-1 rec10-K712R*	This study
BP2613	*h⁻ pro1-1 rec10-3KR*	This study
BP2618	*h⁻ arg4-55 rec10-3KR*	This study
BP2619	*h⁻ arg4-55 rec10-K712R*	This study
BP2620	*h⁻ arg4-55 rec10-K757R*	This study
BP2621	*h⁻ arg4-55 rec10-K744R*	This study
BP2622	*h⁺ ura1-61 rec10-K757R*	This study

BP2623	*h^+ ura1-61 rec10-K754R*	This study
BP2632	*h^- arg3-124 rec10-175::KANMX6*	This study
BP2648	*h^- arg4-55 rec10-K754R*	This study
BP2649	*h^+/h^- ade6-210/ade6-216 leu^+/leu1-32 rec10-144/rec10-155::LEU2+*	This study
BP2653	*h^+/h^- ade6-210/ade6-216 rec10-144/rec10-109*	This study
BP2657	*h^+/h^- ade6-210/ade6-216 rec10+/rec10-144*	This study
BP2658	*h^-/h^- pat1-114/pat1-114 lys1::mat-Pc-$lys1^+$*	Tanaka collection
BP2682	*h^+/h^- ade6-210/ade6-216 rec10-144/rec10-175::KANMX6*	This study
BP2685	*h^+ ade6-52 pro2-1 rec10-144*	This study
BP2686	*h^- ade6-M26 arg3-124 rec10-144*	This study
BP2702	*h^+ ade8-106 rec10-144*	This study
BP2707	*h^- pro1-1 rec10-K757R*	This study
BP2711	*h^- arg4-55 rec10-144*	This study
BP2745	*h^+ ade8-106 rec10-K757R*	This study

Table 2.2 Primer list

Primer	Sequence
JSF	GCGCGAATTCCTGCGGTGTGTTCAGTTTC
JSR	CGCGGAATTCCCTGTCTTCTGCATTGATATG
DP1	TAATTGGTCAACGCTTGC
DP2	TTCCAATGTAAGGATGGC
DP3	GTTCCGTCTTTGCTAGC
DP4	GCAAATTGAGGATCTCG
DP5	ATTAGGCGGGCTTGAGC
DP6	GACTCCAGTTCCTGTACCG
DP7	CCGTCACTTATCGATGGC
DP8	CAATATTTGAGCCCGACG
Y731F_FWD	CGTTATACTTCTATGATAGAAATCAAATATTCGAGGGC
Y731F_REV	GCCCTCGAATATTTGATTTCCTATCATAGAAGTATAACG
Y767F_FWD	CGAAAAGACAAACTGCTAGATTTAAGATCATCGAAA
Y767F_REV	GCGCCAATTCCTTTTCGATGATCTTAAATCTAGCAG
K712R_FWD	CCATCTAGCAGATCTGCTACTATTGATGG
K712R_REV	CCATCAATAGTAGCAGATCTGCTAGATGG
K744R_FWD	CGAGAAGGAATTGAGGTCACGTCTTGAGGCTTACC
K744R_REV	GGTAAGCCTCAAGACGTGACCTCAATTCCTTCTCG
K754R_FWD	GCTTGAGGCTTACCACATAAATTGTAACCGAGTGAT
K754R_REV	CGAAAATTCCTTAATCACTCGGTTACAATTTATGTG
K757R_FWD	CACATAAATTGTAACAAAGTGATTCGTGAATTTTCG
K757R_REV	GCAGTTTGTCTTTTCGAAAATTCAGCAATCACTTTG
KR3_FWD	GGAATTGAGGTCAAGGCTTGAGGCTTACCACATAAATTGTAACAG
KR3_REV	CGAAAATTCCCTAATCACTCTGTTACAATTTATGTGGTAAGCCTC
S347A_FWD	GCTATAATTGTTGTCCCTAAATTGACATTAAGGAACCG
S347A_REV	CAATTTAGGAGCAACAATTATAGCTGGTAACAGTTTGTTCATG
S422A_FWD	GTGAAAGATGCTTTATCAGCCGATGACTATGC
S422A_REV	GGCTGATAAAGCATCTTTCACATCTGC
S424A_FWD	GATTCTTTAGCAGCCGATGACTATGCTTATGATAC
S424A_REV	GTCATCGGCTGCTAAAGAATCTTTCACATCTGC
S422AS424A_FWD	GTGAAAGATGCTTTAGCAGCCGATGACTATGCTTATGATAC
S422AS424A_REV	GTCATCGGCTGCTAAAGCATCTTTCACATCTGC
S529A_FWD	GCAATACGCTCCGAAAACCCCCATTTGCAAAATTAACG
S529A_REV	GTTTTCGGAGCGTATTGCAAATTAACATTGG
S356A_FWD	CCTAAATTGACATTAAGGAACCGTGCAATAATTC
S356A_REV	CCTTCTTTTATTTGAATTATTGCACGGTTCC
S513A_FWD	CCTGATACTGAAAATCAAGAAGCTTCGGTG
S513A_REV	GATTTCGCCTTTTTATTTTTCACCGAAGCTTCTTG
S514A_FWD	CCTGATACTGAAAATCAAGAATCTGCGGTG
S514A_REV	GATTTCGCCTTTTTATTTTTCACCGCAGATTCTTG
S513AS514A_FWD	CCTGATACTGAAAATCAAGAAGCTGCGGTG
S513AS514A_REV	GATTTCGCCTTTTTATTTTTCACCGCAGCTTCTTG
K604R_FWD	GTCTTAAAAGCTCCGTATGGAGAGAACTTC
K604R_REV	CCAATGTTTCTCTTTAAGAAGTTCTCTCCATACG
S503A_FWD	CGACAAAAAGAAAAAAACAAAAAGCTTTAAAACC
S503A_REV	GATTTTCAGTATCAGGTTTTAAAGCTTTTTG
KAN_BCL1_FWD	GCATTACCGTGATCACGGATCCCCGGG
KAN_BCL1_REV	CGTAATGGCTGATCAAGGCCACTAGTG

Chapter 3

Temporal Analysis of LinE formation

3.1 Introduction

LinEs develop during early meiotic prophase in fission yeast. They have been classified according to their Rec10-positive immuno-stained morphology (LORENZ *et al.,* 2004). Previous studies have demonstrated a profile of the temporal quantification of LinE classes (see Figure 1. 17 – for images of LinE classes) that infers a distinct profile to the maturation and subsequent degradation of LinEs (LORENZ *et al.,* 2004). This quantification, however, was established by use of an asynchronous meiosis. It is known that Rec10 plays a role during meiotic recombination (ELLERMEIER and SMITH 2005), and that loss of Rec10 function has an effect on chromosome pairing (be that due to the absence of LinEs or decreased levels of recombination) (MOLNAR *et al.,* 2003). However, the relationship between LinE formation and key meiotic events remains fairly poorly understood.

In this chapter we utilise a technique to synchronise meiosis, and aim to: provide a high-resolution profile of the temporal development of LinE formation; correlate LinE formation with the timing of meiotic replication; investigate a link between LinE components and the progression of meiotic replication; quantify the temporal localisation of Rad51 foci onto LinE-containing nuclei; quantify the temporal localisation of Hop1 foci onto LinE-containing nuclei.

3.2 Results

3.2.1 LinE development is aberrant in a *pat1-114/pat1-114* synchronous meiosis

In order to attempt a more precise temporal quantification of LinE appearance and development during meiosis, a synchronous meiosis was utilised. The *S. pombe pat1-114* mutation is a temperature sensitive allele that can be used to induce meiosis by thermal inactivation of the Pat1 kinase (IINO and YAMAMOTO 1985), which is a negative regulator of meiosis in *S. pombe* (YAMAMOTO 1996).

This produces a more synchronous meiosis than that exhibited in wild-type azygotic meiosis (BÄHLER *et al.,* 1991).

Immuno-staining of Rec10 and initial cytological quantification of LinE development in a *pat1-114/pat1-114* thermally induced synchronous meiosis suggested that LinEs do not fully develop in this mutated strain (Figure 3.1A). However, it is important to note that the frequency of nuclei exhibiting LinE structures does not appear to have been affected.

To determine whether the more complex class IIa/IIb structures formed transiently between these time points, the synchronous meiosis was repeated taking additional half hour time points (Figures 3.1B + 3.2). Again, no class II LinEs were observed, suggesting these structures do not form in a *pat1-114* thermally induced meiosis. However, a temporal profile of LinE development and subsequent degradation is still somewhat visible. Class Ia LinEs appear first, at approximately 2 hours after temperature shift, with the appearance of a few class Ib structures by the 2.5 hr time point. Class Ib structures clearly dominate between 3 and 4.5 hrs, before the reappearance of a significantly higher number of class Ia structures than class Ib at 5 hrs – possibly indicative of LinE degradation.

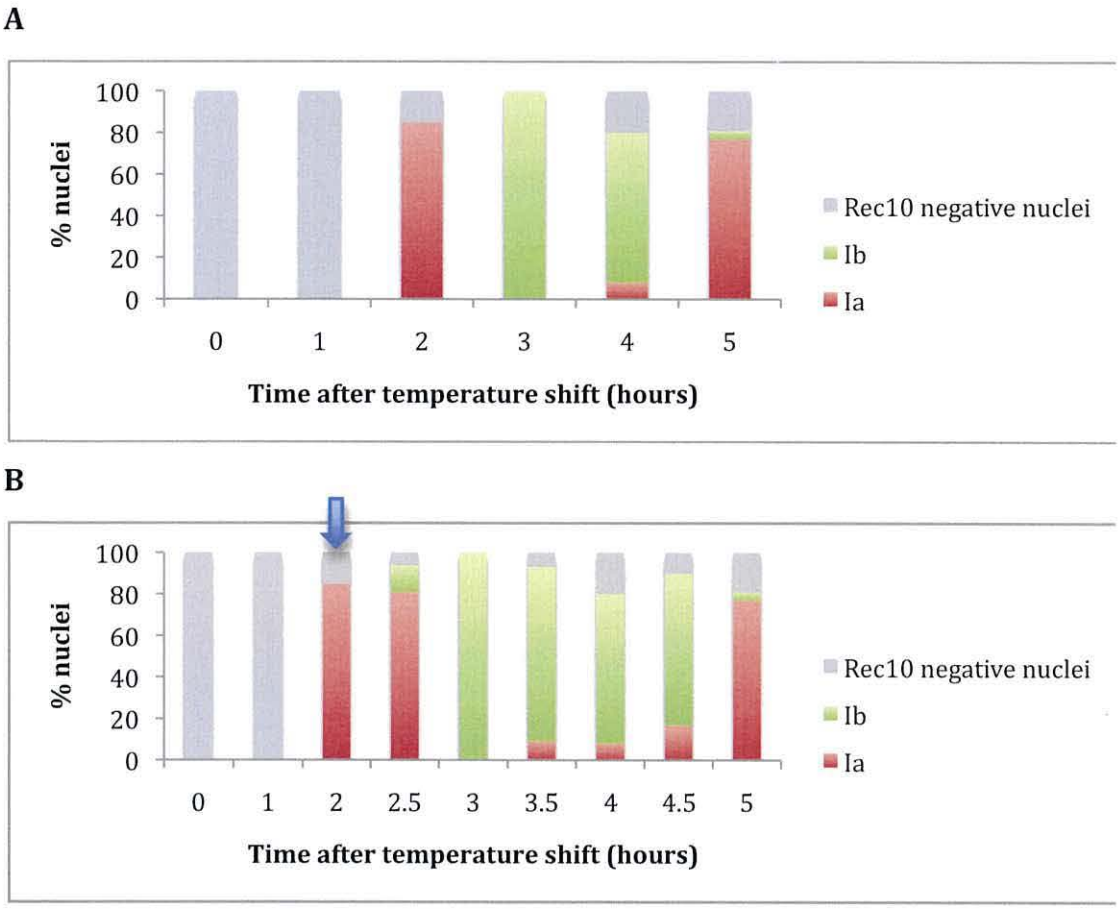

Figure 3.1 Development of LinEs during a temperature-induced *pat1-114/pat1-114* synchronised meiosis. (**A**) Proportions of LinE classes found in samples taken at hourly intervals after transfer of culture to the restrictive temperature. ≥80 nuclei were recorded for each time point. No class II nuclei were observed. (**B**) Proportions of LinE classes found in samples taken at shown intervals after transfer of culture to the restrictive temperature. ≥80 nuclei were recorded for each time point.

Blue arrow indicates the time point where replication is first observed - see Figure 3.3 and text in section 3.2.2

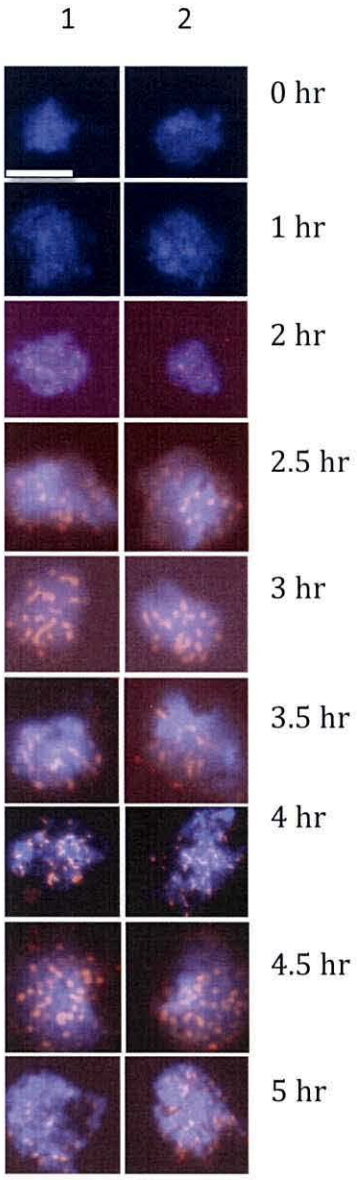

<u>Figure 3.2</u> Examples of LinEs exhibited at time points taken during a *pat1-114/pat1-114* thermally induced synchronous meiosis. LinEs are seen to appear by the 2 hrs time point as class Ia-like structures – seen also at 2.5 hrs. 3 hrs, 3.5 hrs, 4 hrs and 4.5 hrs exhibit a dominance of class Ib-like stuctures. Class Ia-like structures are again visible by the 5 hr time point. 2 examples (columns 1 and 2) are shown for each time point. Scale bar = 5μm.

3.2.2 Appearance of LinEs in relation to S-phase in a *pat1-114/pat1-114* synchronous meiosis

In order to correlate the appearance of LinEs with the timing of replication, a temporal comparison of LinE classification and replication timing [established with a FACS profile (Figure 3.3)] was done on the same *pat1-114/pat1-114* thermally induced synchronous meiosis that was used for immuno-staining of Rec10 (Figures 3.1B + 3.2).

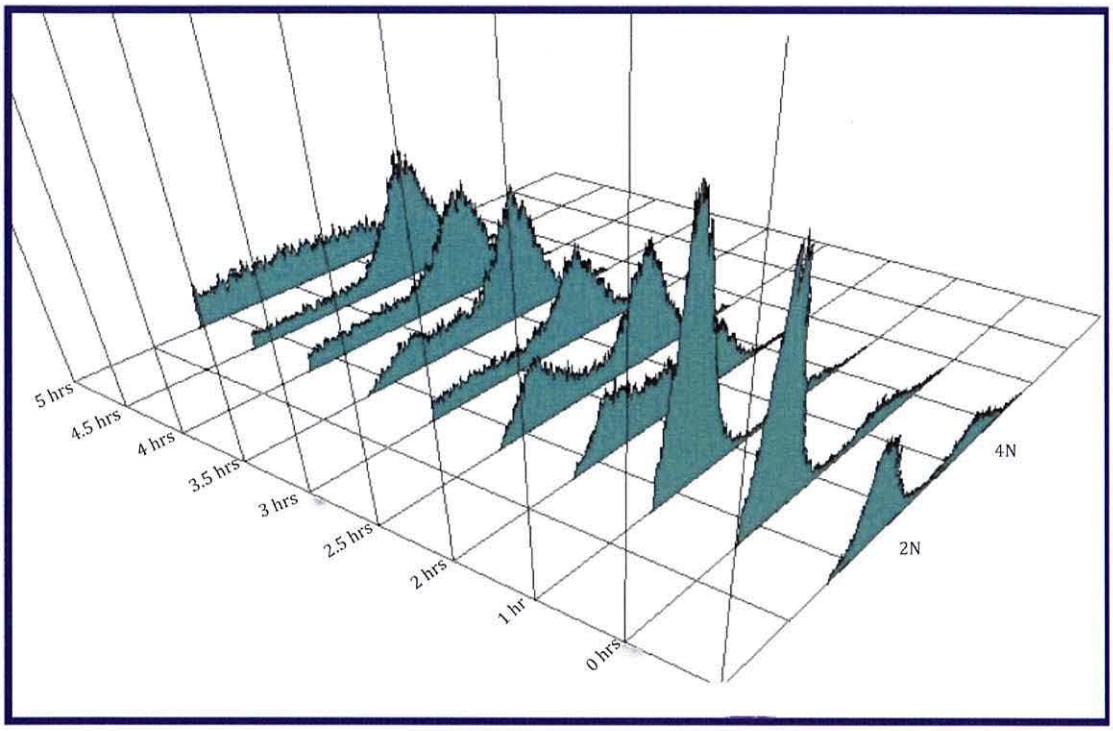

Figure 3.3 FACS profile of *pat1-114/pat1-114* thermally induced synchronous meiosis. 2N and 4N peaks on the control plain indicate the unreplicated (2N) and replicated (4N) DNA.

Figure 3.3 demonstrates that the DNA content begins to shift from the un-replicated state between 1 hr and 2 hrs. By 3 hrs it is shown that the bulk of DNA replication has been completed, as the majority of cells exhibit a 4N DNA content – the DNA content peak has clearly shifted from its original 2N position to the 4N position - indicative of replicated DNA.

Firstly, it is important to note that although LinE formation is aberrant in a *pat1-114/pat1-114* diploid, the strain seems to undergo a complete round of DNA replication.

Visually correlating the temporal classification of LinEs (Figure 3.1B), and the FACS profile (Figure 3.3) of a *pat1-114/pat1-114* synchronous meiosis suggests that LinEs begin to appear around the time that replication is initiated (see blue arrow on Figure 3.1B).

3.2.3 LinEs develop normally in a h^-/h^- *pat1-114/pat1-114 lys1::mat-Pc-lys1*$^+$ thermally induced synchronous meiosis

We have demonstrated that LinEs do not develop normally in a *pat1-114/pat1-114* strain (previous section).

S. pombe is a preferentially haploid organism. The *mat1* (mating type) locus of *S. pombe* has three possible alleles: h^+, h^- and h^{90}. h^{90} is homothallic, meaning it can mate with itself. The heterothallic h^+ and h^- alleles on the other hand, require a partner of the opposite mating type in order to mate. h^- cells produce M (minus) factor, and h^+ cells produce P (plus) factor. A diploid cell requires both M and P factor to initiate meiosis in the absence of a *pat1-114* mutation, with the presence of M and P factors leading to the inactivation of Pat1 kinase.

It has previously been demonstrated that the presence of M and P factors, in addition to inactivation of Pat1 kinase is required for the establishment of monopolar sister-chromatid attachments in fission yeast (YAMAMOTO and HIRAOKA 2003). We obtained a strain, which is a stable diploid (created by fusion of two h^- strains), *pat1-114/pat1-114*, which also carries a *mat1-Pc* allele – allowing it to express P factor, as well as M factor. Having the cell express both P and M factor restores the correct centromere monopolarity to a *pat1-114/pat1-114* diploid, suggesting a meiosis more like that of a wild-type is occurring (Tanaka pers. comm). We used this strain in order to gain a more precise quantification of LinE development during a thermally induced synchronous meiosis, with the hope that known restoration of monopolarity may also indicate restoration of a more normal LinE development.

A

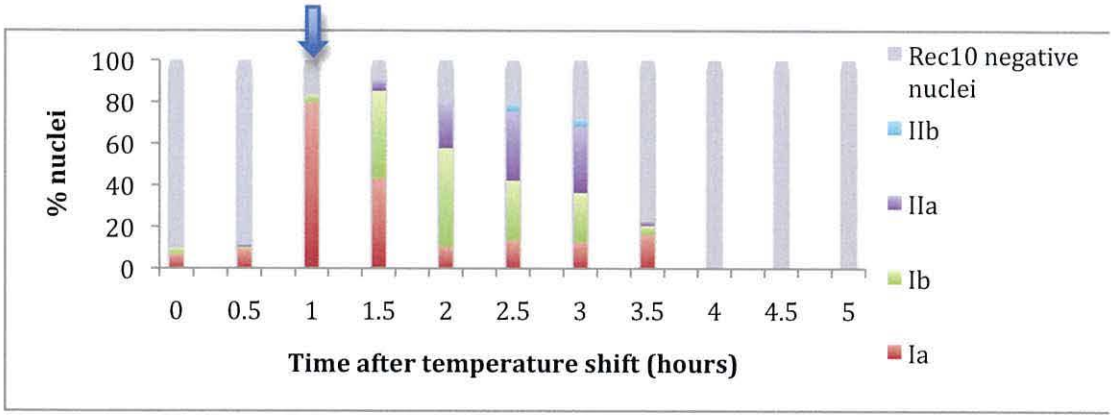

B

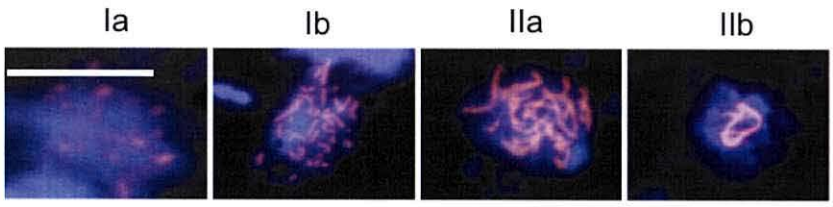

C

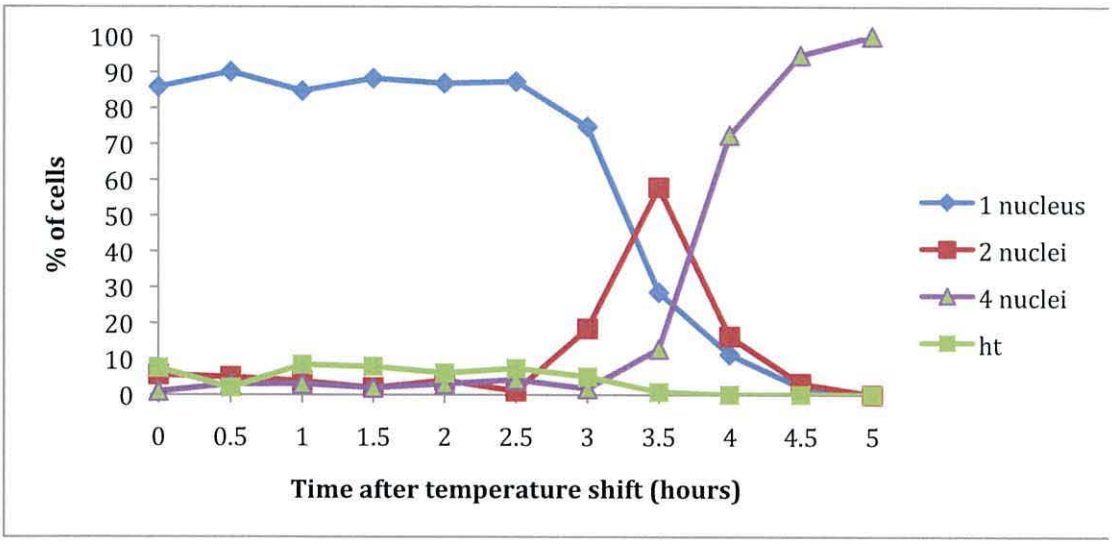

Figure 3.4 Development of LinEs during a *h⁻/h⁻ pat1-114/pat1-114 lys1::mat-Pc-lys1⁺* diploid synchronous meiosis. (**A**) Proportions of LinE classes found in samples taken at hourly intervals after transfer to restrictive temperature. ≥80 nuclei were recorded for each time point. Blue arrow indicates the time point where replication is first observed - see Figure 3.5. (**B**) Examples of Rec10-stained LinE classes. One example is shown for each individual class. Scale bar = 5 μm. (**C**) Analysis of cytological meiotic events in samples taken at hourly intervals after transfer of culture to restrictive temperature. ≥80 nuclei were recorded for each time point. ht – horsetail nuclei

It is shown in Figure 3.4 (A) that all classes of LinEs are exhibited in a *h^-/h^- pat1-114/pat1-114 lys1::mat-Pc-lys1$^+$* thermally induced synchronous meiosis. This synchronous meiosis has revealed a distinct, highly resolved, temporal order of the appearance of different LinE classes, which provides a clear pattern of LinE maturation and subsequent degradation.

It is clear that most LinEs begin to appear at the 1 hr time point, in their most immature class Ia state. Class Ib structures become more prevalent between 1.5 hrs and 2 hrs, with class Ia structures decreasing in frequency. Class IIa structures are first visible at 1.5 hrs, with their frequency increasing by 2 hrs, and again by 2.5 hrs. It is not until 2.5 hrs that class IIb structures are first seen. This defines class IIb structures as clearly developing after class IIa structures, a temporal distinction that has been made possible by the utilisation of this synchronous meiosis that exhibits all classes of LinEs. At 3.5 hrs, the number of nuclei exhibiting positive Rec10 staining has significantly decreased, the most prevalent structures by now being class Ia. This is indicative of the breakdown, or degradation of LinE structures during meiosis. No LinEs are apparent from the 4 hr time point onwards.

Figure 3.4 (B) shows the temporal progression of meiosis by the quantification of the number of nuclei exhibited per cell, and the occurrence of horsetail nuclei. By 3.5 hrs, it is apparent that the majority of cells have completed MI, as they exhibit 2 nuclei per cell. It is only up until 3.5 hrs that LinEs are visible. This indicates that LinEs are present during MI, but not subsequently.

<u>Figure 3.5</u> FACS profile of *h⁻/h⁻ pat1-114/pat1-114 lys1::mat-Pc-lys1⁺* thermally induced synchronous meiosis. The FACS profile in Figure 3.5 shows that DNA replication occurs at approximately the 1 hr time point. This correlates with the bulk-appearance of LinEs (as seen in Figure 3.4A). The FACS profile in Figure 3.5 does not appear to show a full doubling of the DNA content by means of a peak-shift – this is however in accord with previous observations (K. Tanaka pers. comm). However, the appearance of four spore asci with normal spore morphology and equal DNA content indicates that full DNA replication must have occurred.

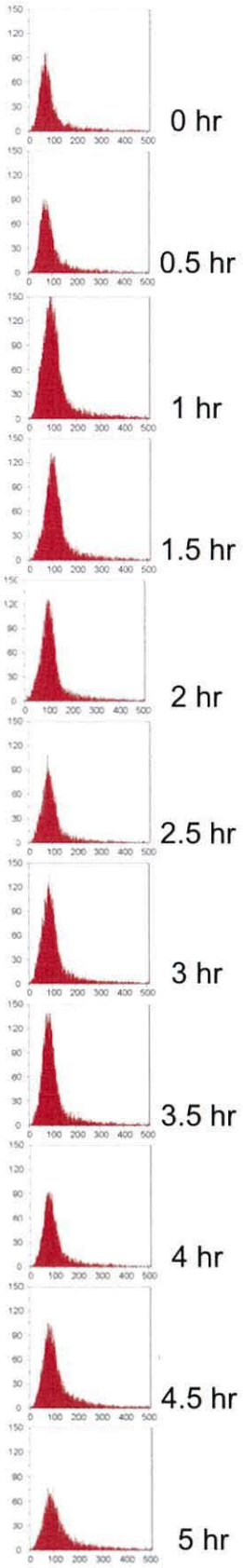

3.2.4 Quantification of Rad51 staining in a *h⁻/h⁻ pat1-114/pat1-114 lys1::mat-Pc-lys1⁺* thermally induced synchronous meiosis

It has been demonstrated that Rad51 binds to DSB sites in *S. pombe* (GRISHCHUK *et al.,* 2004). The presence of Rad51 is indicative of Rad51-dependent recombination events. In order to create a temporal profile of Rad51 localisation, we utilised the *h⁻/h⁻ pat1-114/pat1-114 lys1::mat-Pc-lys1⁺* thermally induced synchronous meiosis.

Rad51 loci do form in a *h⁻/h⁻ pat1-114/pat1-114 lys1::mat-Pc-lys1⁺* thermally induced synchronous meiosis (Figures 3.5 and 3.6). Rad51 foci are seen to co-stain with nuclei exhibiting each different class of LinE (Figures 3.5 and 3.6). Figure 3.6 provides a visualisation of the timing of Rad51 foci appearance. The majority of Rad51 foci appear at the 2.5 hr and 3 hr time points, with a small subset of Rad51 foci appearing earlier, at around the 1 hr time point.

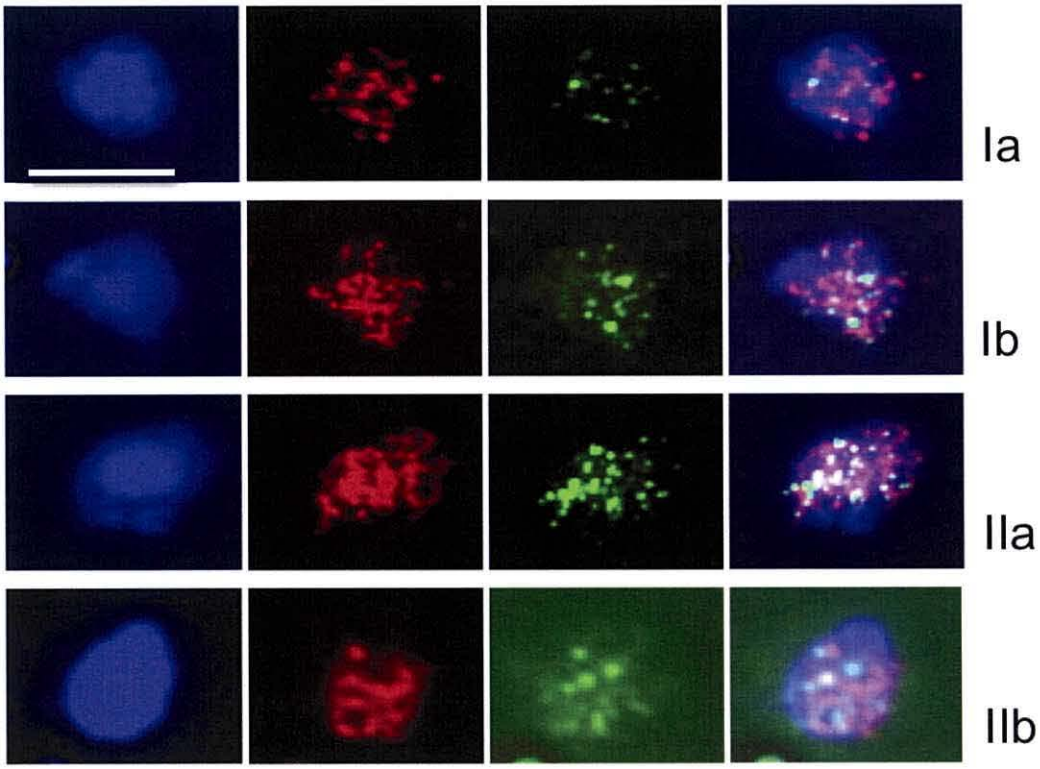

Figure 3.6 Examples of Rad51 and Rec10 co-stained nuclei in a *h⁻/h⁻ pat1-114/pat1-114 lys1::mat-Pc-lys1⁺* thermally induced synchronous meiosis. All nuclei are stained for DNA (blue), Rec10 (red) and Rad51 (green). Co-localisation between Rec10 and Rad51 is shown in yellow. Scale bar = 5 μm.

A

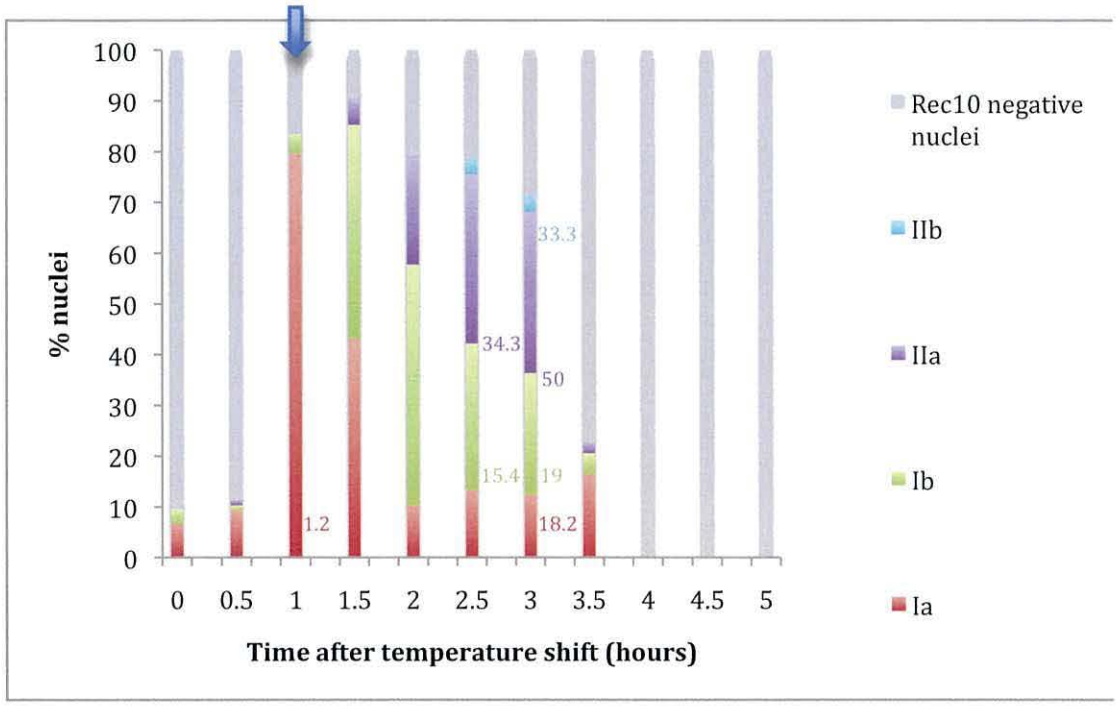

B

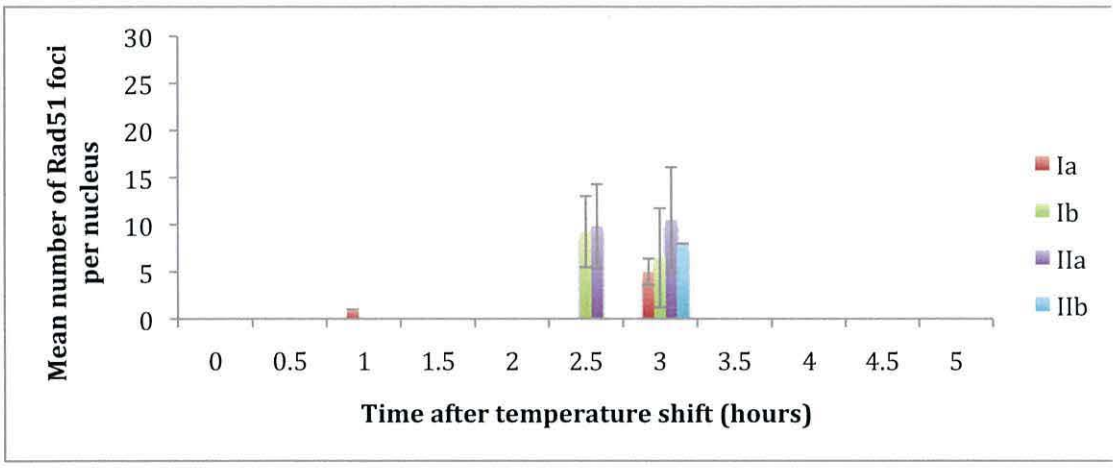

<u>Figure 3.7</u> Quantification of Rad51 staining during a temperature induced synchronous meiosis of a *h⁻/h⁻ pat1-114/pat1-114 lys1::mat-Pc-lys1⁺* synchronous meiosis. (**A**) Proportions of LinE classes found in samples taken at hourly intervals after transfer to restrictive temperature. ≥80 nuclei were recorded for each time point. Numbers adjacent to each column represent the % nuclei scored exhibiting Rad51 and Rec10 co-staining, with the colours representing LinE classes. Absence of a number indicates 0%.
Blue arrow indicates the time point where replication is first observed - see Figure 3.5.
(**B**) Mean number of Rad51 foci scored in each nucleus exhibiting Rec10 and Rad51 co-staining. Error bars represent a 95% confidence interval in all cases.

3.2.5 Quantification of Hop1 staining in a *h⁻/h⁻ pat1-114/pat1-114 lys1::mat-Pc-lys1⁺* thermally induced synchronous meiosis

Previous studies have demonstrated that Hop1 localises to LinEs (LORENZ *et al.*, 2004), with its localisation being Rec10-dependent (LORENZ *et al.*, 2004). Hop1 does not localise along the entire lengths of LinEs (LORENZ *et al.*, 2004). Hop1 was thought to be loaded after LinE nucleation, as the more mature LinE classes virtually all exhibited Hop1 co-staining, whilst class Ia structures often exhibited no Hop1 staining at all (LORENZ *et al.*, 2004).

We utilised the *h⁻/h⁻ pat1-114/pat1-114 lys1::mat-Pc-lys1⁺* thermally induced synchronous meiosis in order to be able to quantify the temporal appearance of Hop1, and its localisation pattern to LinEs. The term co-staining is used to refer to nuclei exhibiting both Hop1 and Rec10 staining, but not necessarily co-localisation of the proteins. The term co-localisation refers to direct co-localisation of Rec10 and Hop1 proteins.

Virtually all nuclei that exhibited Rec10 staining, also exhibited Hop1 staining [Figure 3.8A]. Rec10/Hop1 co-staining only appears to decrease at 3.5 hrs (co-staining of class Ia and IIa LinEs with Hop1 is down to 50%), when the number of Rec10 positively stained nuclei has also dramatically decreased. This infers a contradiction to previously published work, which suggested that Hop1 loads after Rec10 (LORENZ *et al.*, 2004); Figure 3.8A does not suggest that Hop1 appears after Rec10.

Nuclei exhibiting class Ia and class Ib LinE appear to contain some Hop1 foci which do not co-localise to any detectable Rec10 foci – however, this does not dismiss the possibility that the Rec10-stained structures are below detection levels at these early stages of development. Direct Hop1 and Rec10 co-localisation was seen abundantly in later class IIa and IIb structures – consistent with earlier studies (LORENZ *et al.*, 2004); with near perfect co-localisation was demonstrated in many nuclei (see Figure 3.7 class IIb).

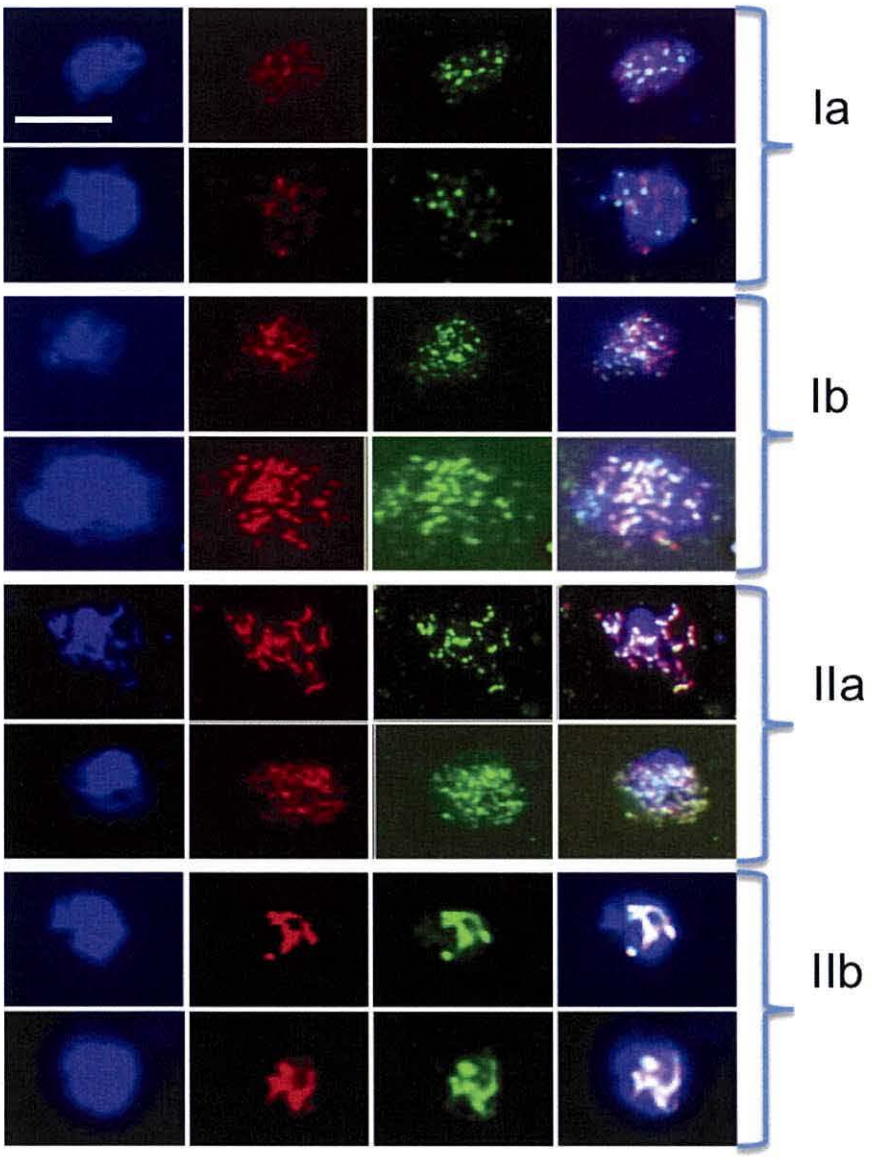

<u>Figure 3.8</u> Examples of Rec10 and Hop1 co-stained nuclei in a *h⁻/h⁻ pat1-114/pat1-114 lys1::mat-Pc-lys1⁺* thermally induced synchronous meiosis. All nuclei are stained for DNA (blue), Rec10 (red) and Hop1 (green). Co-localisation between Rec10 and Hop1 is shown in yellow. Two examples of nuclei are shown for each LinE classification group. Scale bar = 5 μm.

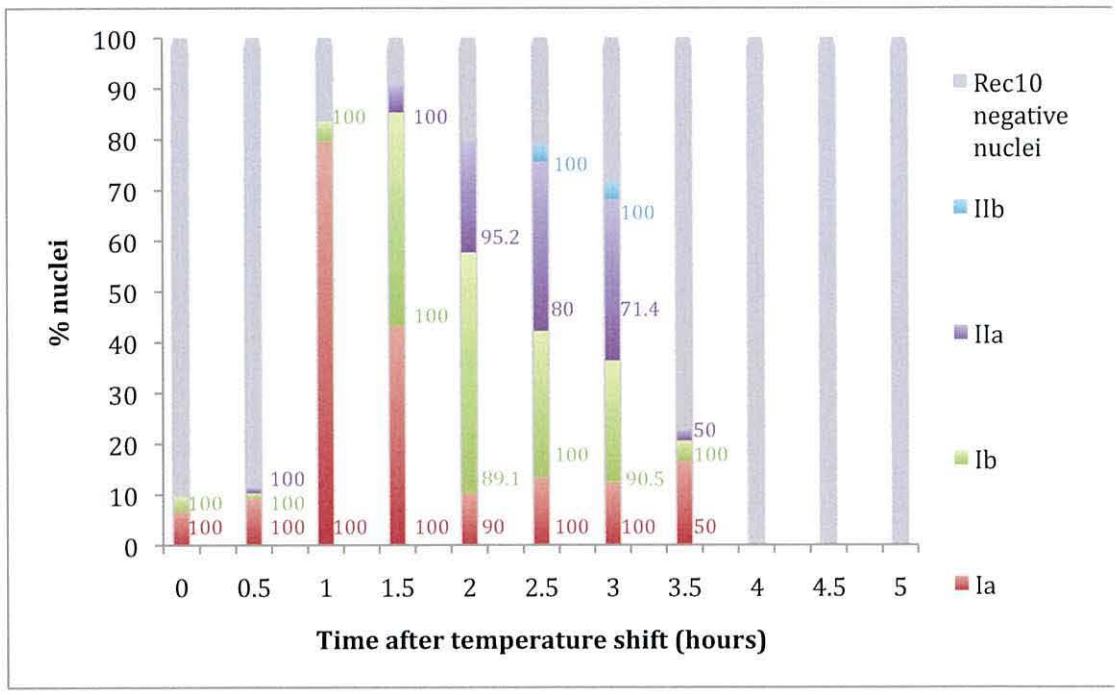

Figure 3.9 Quantification of Hop1 staining of during a h^-/h^- *pat1-114/pat1-114 lys1::mat-Pc-lys1*$^+$ thermally induced synchronous meiosis. Proportions of LinE classes found in samples taken at hourly intervals after transfer to restrictive temperature. ≥80 nuclei were recorded for each time point. Numbers adjacent to each column represent the % nuclei scored exhibiting Hop1 and Rec10 co-staining, with the colours representing LinE classes. Absence of a number indicates 0%.

Whilst analysing the Hop1-Rec10 co-stained nuclei, some unusual Hop1 stained structures became apparent (Figure 3.9). The structures, which were termed 'Hop1 clusters', appear as densely stained Hop1 areas, usually localised to the edge of the intense DAPI stained region. Where a Hop1 cluster was apparent each nucleus exhibited a maximum of one Hop1 cluster structure. The staining patterns appear to show a cluster or bundle of Hop1 heavily stained foci - this possibly indicates the presence of more than one structure within the 'cluster'. Nuclei exhibiting the Hop1 cluster structure also sometimes exhibited Hop1 staining elsewhere in the nucleus (see Figure 3.9 class IIa images), although this is not always the case (see Figure 3.9 class Ia and Ib images). It is noteworthy that Hop1 clusters often appear to correspond to areas of intense DAPI staining (see Figure 3.9). There seems to be an intimate association between DNA and Hop1 clusters. Also, Hop1 clusters seem to be localised to areas that are largely

devoid of Rec10 staining (see Figure 3.9). This suggests that Hop1 clusters are not LinE-associated structures.

The Hop1 cluster structures became visible at the 2.5 hr time point (Figure 3.10). This indicates that Hop1 clusters are not present during pre-meiotic DNA replication (as indicated by the blue arrow in Figure 3.10). Figure 3.10 also provides insight into the distribution of Hop1 cluster structures amongst differing LinE classes. Overall, Hop1 cluster structures appear to be prevalent in all classes except class Ib, at 2.5 hrs. There also seems to be an overall decrease in the frequency of Hop1 cluster structures between 2.5 hrs and 3 hrs, then again between 3 hrs and 3.5 hrs. The exception to this is seen in nuclei exhibiting class Ia LinEs, where there is an increase in Hop1 cluster structure frequency between 3 hrs and 3.5 hrs – interestingly, there is also an increase in frequency of the occurrence of class Ia structures between these two time points.

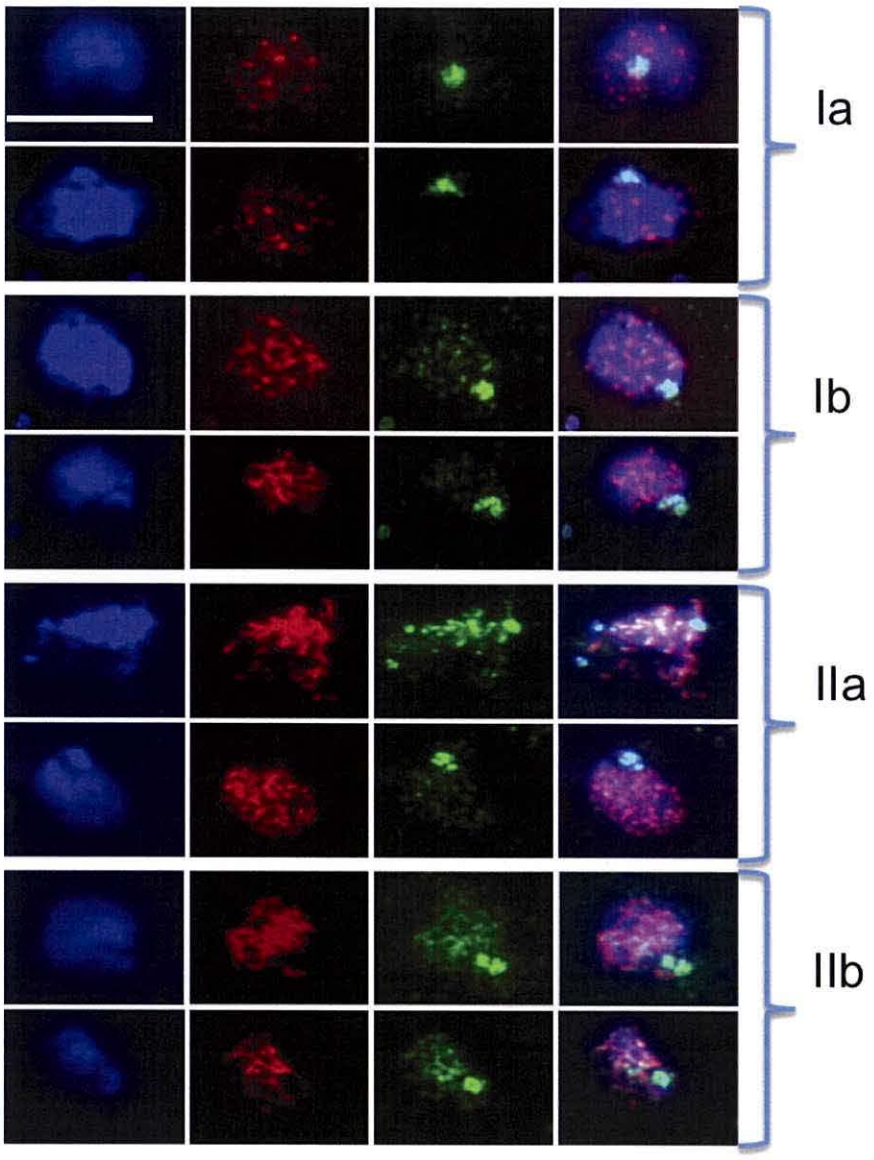

Figure 3.10 Examples of Hop1 cluster structures in a *h⁻/h⁻ pat1-114/pat1-114 lys1::mat-Pc-lys1⁺* thermally induced synchronous meiosis. All nuclei are stained for DNA (blue), Rec10 (red) and Hop1 (green). Co-localisation between Rec10 and Hop1 is shown in yellow. Two examples of nuclei are shown for each LinE classification group. Scale bar = 5 μm.

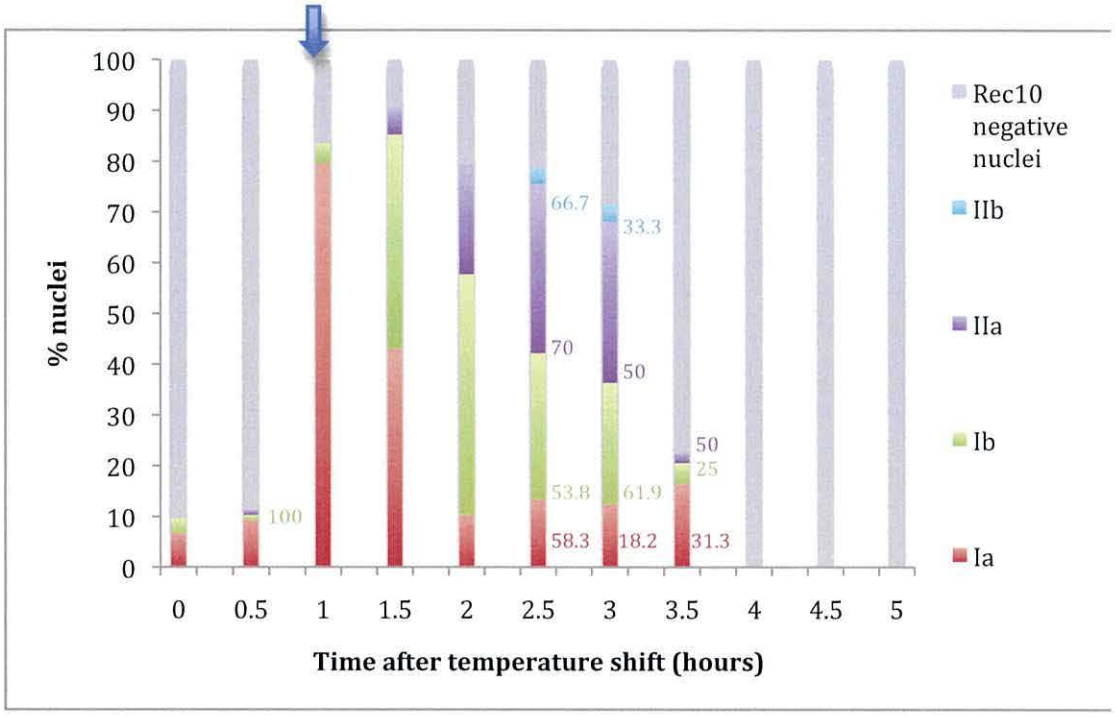

Figure 3.11 Quantification of Hop1 cluster structures during a *h⁻/h⁻ pat1-114/pat1-114 lys1::mat-Pc-lys1⁺* thermally induced synchronous meiosis. Proportions of LinE classes found in samples taken at hourly intervals after transfer to restrictive temperature. ≥80 nuclei were recorded for each time point. Numbers adjacent to each column represent the % nuclei scored exhibiting Hop1 cluster structures, with the colours representing LinE classes. Absence of a number indicates 0%. Blue arrow indicates the time point where replication is first observed (Figure 3.5).

3.2.6 Loss of Rec10 function has no effect on DNA replication timing

Although LinE development is incomplete in the *pat1-114/pat1-114* mutant not expressing both P and M factors, full replication was demonstrated to occur (Figure 3.3). Correlation of FACS data and temporal quantification of LinE development in a *pat1-114* thermally induced meiosis concludes that LinEs begin to appear around the time of replication.

Previous studies have shown that a full deletion of the *rec10* gene results in complete loss of visible LinEs (ELLERMEIER and SMITH 2005). In this current study, the appearance of LinEs correlates well with the timing of DNA replication. Given this, it was important to establish whether DNA replication would progress normally in the absence of Rec10. This was done by comparing the FACS profiles

of two *pat1-114/pat11-4* thermally induced synchronous meioses – one being a *rec10⁺/rec10⁺* strain, the other a *rec10Δ/rec10Δ* strain (Figure 3.12).
Visual correlation of the two FACS profiles seen in Figure 3.12 indicates that full replication still occurs in the absence of *rec10*. There does, however, seem to be a slight delay in the kinetics of DNA replication progression in the absence of *rec10*. In the *rec10⁺* strain, DNA replication appears to begin at approximately 2 hrs 20 mins, whereas in the *rec10Δ* strain, DNA replication appears to begin slightly later at approximately 2 hrs 40 mins.

A

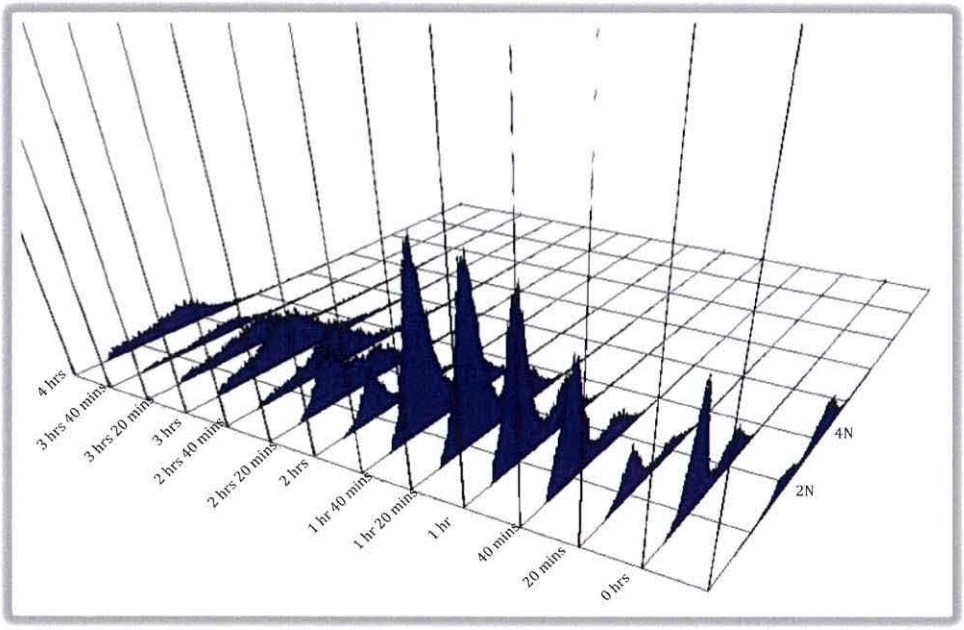

B

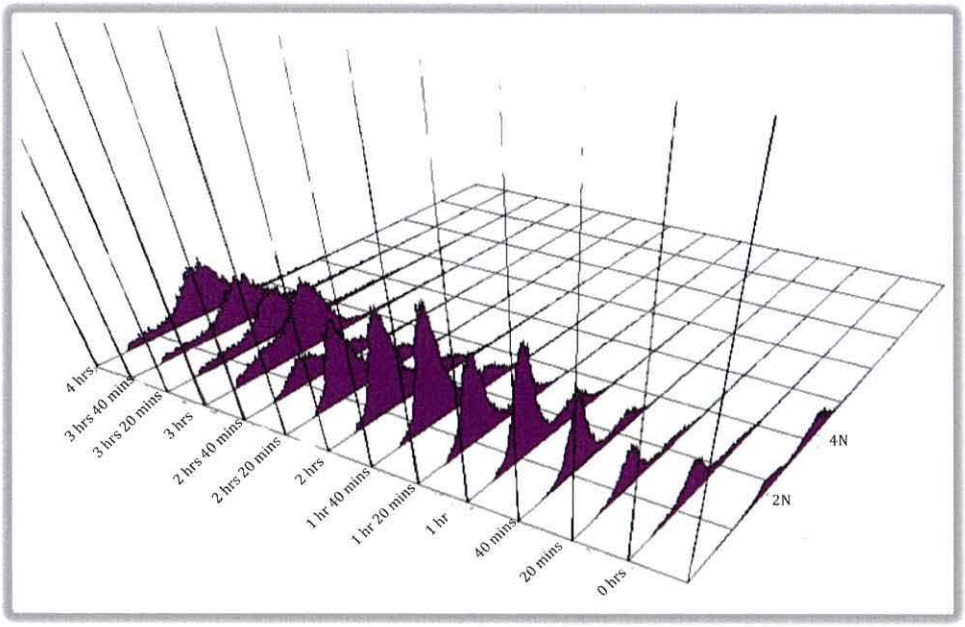

<u>Figure 3.12</u> FACS analysis of *pat1-114/pat1-114* thermally induced meiosis in a *rec10⁺/rec10⁺* and a *rec10Δ/rec10Δ* diploid. (**A**) FACS profile of a *pat1-114/pat1-114* temperature induced synchronous meiosis of a *rec10⁺/ rec10⁺* diploid.

(**B**) FACS profile of a *pat1-114/pat1-114* temperature induced synchronous meiosis of a *rec10Δ/ rec10Δ* diploid.

3.3 Discussion

3.3.1 LinE formation in a *pat1-114* meiosis

Normal meiotic events are not reproduced during a *pat1-114/pat1-114* meiosis that does not express both P and M factor genes. Previous studies have shown that *pat1-114* induction of meiosis exhibits a high percentage (40% in diploid cells) of premature loss of sister chromatid cohesion during MI (YAMAMOTO and HIRAOKA 2003), indicating that monopolar kinetochores are not fully formed in a *pat1-114* mutant strain (CHIKASHIGE *et al.,* 2004). The prominence and frequency of nuclear oscillation (*S. pombe* horsetail stage) is also decreased during a *pat1-114* synchronous meiosis (CHIKASHIGE *et al.,* 2004). *pat1-114* mutants exhibit wild-type telomere clustering to the SPB, although fragmented centromere-SPB associations are still visible in the majority of cells (CHIKASHIGE *et al.,* 2004). This infers that the inactivation of Pat1 via the temperature sensitive *pat1-114* mutation allows entry into meiosis, but is not sufficient for displacing centromere-SPB associations and subsequent movement of centromeres to their meiotic locations within the nucleus (CHIKASHIGE *et al.,* 2004). *pat1-114* meioses also exhibit differences in the temporal order of meiotic events. In a *pat1-114* mutant, telomere clustering occurs after pre-meiotic S-phase; whilst in wild-type cells pre-meiotic S-phase follows telomere clustering (CHIKASHIGE *et al.,* 2004). However, the benefits of the synchronous nature of a *pat1-114* thermally induced meiosis can, at times outweigh the negative aspects of its mutant phenotypes, hence why it is commonly utilised within the meiosis research community.

We have demonstrated here that the mutant phenotypes of *pat1-114* can now also include aberrant LinE development, as only the immature class Ia and class Ib structures become visible in this strain. The fact that the frequency of nuclei exhibiting LinE structures has not decreased suggests that *pat1-114* LinEs simply fail to mature fully, i.e. *pat1-114* does not seem to affect the initiation of LinE formation, only their subsequent maturation. We can therefore conclude that Rec10 still forms initial LinE structures in a *pat1-114* strain.

Previous studies have shown that the presence of P and M factors are required in addition to Pat1 inactivation in order to establish monopolar attachment of sister-chromatids (YAMAMOTO and HIRAOKA 2003). Here we demonstrate the h^-/h^-

pat1-114/pat1-114 lys1::mat-Pc-lys1^{+} thermally induced meiosis demonstrated full LinE development. The presence of both mating factors (P and M) alongside the Pat1 inactivation is therefore essential for inducing a meiosis that forms fully developed LinEs. From these data, we can conclude that the *pat1-114* mutation itself does not inhibit LinE development; it is most likely a side effect of the *pat1-114* inactivation initiation of meiosis. Therefore, Pat1 kinase inactivation can allow entry into meiosis, but it is not sufficient for normal LinE development.

3.3.2 Temporal maturation of LinEs

The restoration of LinE formation in a *h*$^{-}$*/h*$^{-}$ *pat1-114/pat1-114 lys1::mat-Pc-lys1*$^{+}$ thermally induced meiosis made it possible to analyse the temporal appearance of LinEs, as well as quantifying the appearance of the different LinE classes. Changes in the proportions of LinE classes over a time course have been previously observed (LORENZ *et al.,* 2004). These observations however, were made during asynchronous meioses. In this study, a more synchronous meiosis demonstrates a distinct pattern of LinE formation, maturation and degradation in Figure 3.4. A clear distinction between the timing of the appearance of class IIa and class IIb structures has been established – class IIb structures visibly appear after class IIa structures. However, due to the small number of class IIb structures observed and the brief timing of their appearance, it is still unclear whether all nuclei exhibit these structures for a very short period, or merely a subset of nuclei form these late mature structures.

3.3.3 The relationship between LinEs and replication

In this study we demonstrate a positive correlation between the appearance of LinEs and the approximate timing of replication. We also conclude that these are independent events, as loss of LinEs (by deletion of Rec10) has no visible effect on the completion of replication, although a slight delay in the onset of DNA replication may be observed. These data infers that neither the loss of Rec10 nor LinEs effect the full completion of pre-meiotic S-phase.

Previous studies, carried out on an asynchronous meiosis, using a *rec10-155* strain (which carries a truncated C-terminal, and where LinE formation is abolished), exhibited an advancement of approximately 1.5 hrs in the onset of

bulk DNA replication (DOLL *et al.,* 2008). They suggest that Rec10 is involved in regulation of G_1-to-S-phase transition on *S. pombe* (DOLL *et al.,* 2008). It has already been mentioned that a *pat1-114* mutant that does not express both P and M factors exhibits a different temporal order of meiotic events than those seen in a *pat1*$^+$ strain; in a *pat1-114* mutant, telomere clustering occurs after pre-meiotic S-phase; whilst in wild-type cells pre-meiotic S-phase follows telomere clustering (CHIKASHIGE *et al.,* 2004). Correlating this information with the data from this study makes it possible to propose that the change in the temporal order of events exhibited in a *pat1-114* mutant (not expressing P and M factors) could be attributed to the slightly delayed S-phase observed (Figure 3.11). The delay itself could be a *pat1-114* artefact, rather than a side effect of losing *rec10*; this hypothesis fits with previous observations on the effect of the *rec10-155* mutation on timing of replication (DOLL *et al.,* 2008).

Interestingly, DNA replication appears to take place earlier in the *h*$^-$*/h*$^-$ *pat1-114/pat1-114 lys1::mat-Pc-lys1*$^+$ - at around the 1 hr time point (Figure 3.5) – possibly an effect of the expression of both P and M factor in the *pat1-114* thermally induced meiosis.

3.3.4 Temporal analysis of Rad51

A distinct pattern of the appearance of Rad51 foci in nuclei exhibiting LinEs is demonstrated in Figure 3.6. The bulk of Rad51 foci appear between 2.5 and 3 hrs. Previous work has shown that Rec12-mediated DSBs occur just after meiotic DNA replication, and are repaired at around the time of the first meiotic division (CERVANTES *et al.,* 2000). Rad51 is a strand transfer protein, essential for the repair of DSBs (YOUNG *et al.,* 2004). We can positively correlate this information with our own data: Figure 3.4C indicates that the first meiotic division occurs between 2.5 and 4 hrs, and Figure 3.6 indicates that the bulk of Rad51 foci appear between 2.5 and 3 hrs.

The appearance of a minimal number of Rad51 foci at 1 hr (see Figure 3.6) can be attributed to Rad51 being utilised in DNA damage response pathways initiated during DNA replication (see figure 3.5).

3.3.5 Temporal analysis of Hop1

A distinct pattern of the temporal appearance of Hop1 foci in nuclei exhibiting LinEs is demonstrated in Figure 3.10. It has been previously demonstrated that Hop1 localises to LinEs in wild-type meiosis, and that their localisation is Rec10-dependent (MOLNAR *et al.,* 2003). Moreover, Hop1 is not essential for LinE formation (LORENZ *et al.,* 2004). Figure 3.10 demonstrates that Hop1 foci are present in a very high percentage of LinE-containing nuclei, and that no visible Hop1 staining is observed in nuclei exhibiting no Rec10-positive LinE staining. This infers a very strong correlation between the temporal localisation of Rec10 and Hop1. The presence of Hop1 staining on virtually all Rec10-stained nuclei contradicts previous studies, where class Ia structures often exhibited no Hop1 staining (LORENZ *et al.,* 2004). This observation may be an attribute of a *h^-/h^- pat1-114/pat1-114 lys1::mat-Pc-lys1$^+$* thermally induced meiosis - possibly inducing the expression of Hop1 earlier than in wild-type strains.

Hop1 cluster structures were observed and quantified in Figures 3.8 and 3.9(B). These Hop1 cluster structures had not previously been reported in *S. pombe.* This may be due to a number of factors, or a combination of differing ones: the *h^-/h^- pat1-114/pat1-114 lys1::mat-Pc-lys1$^+$* background in the strain used to thermally induce meiosis, this may somehow induce the production of Hop1 clusters – we have already demonstrated that Hop1 foci seem to be abundant sooner than in wild-type (Figure 3.10); the *h^-/h^- pat1-114/pat1-114 lys1::mat-Pc-lys1$^+$* background may influence the spreading procedure carried out on the nuclei, creating an environment where visualisation of the Hop1 cluster structures is possible; indeed a more limited nuclear disruption has been previously observed for *pat1-114* thermally induced meioses (A. Lorenz, Pers. Com.).

The Hop1 cluster structures bear a distinct resemblance to synaptonemal PCs exhibited in other organisms, *S. cerevisiae* for example (Figure 3.12). PCs appear at a significantly higher frequency in yeast mutants (*S. cerevisiae*) that fail to form full SCs (ALANI *et al.,* 1990). Absence of an SC in *S. pombe* would therefore correlate with the presence of PCs.

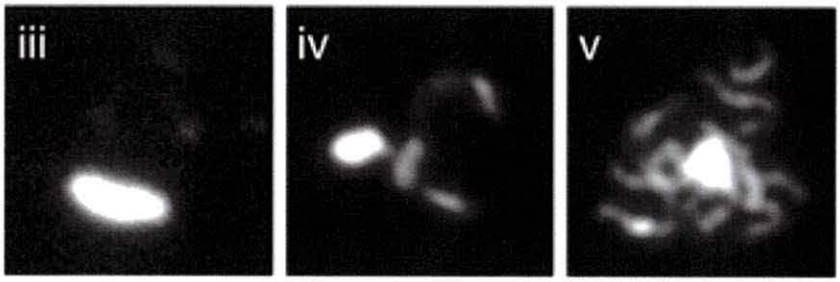

Figure 3.12 Examples of Zip1-stained polycomplexes in *S. cerevisiae*. Zip1 stained PCs are exhibited by the densely stained oval-like structure in each image. iii – Zip1-stained PC in the absence of any other visible Zip1 stained structures in the nucleus. iv – Zip1-stained PC with some Zip1 stained SC structures in the nucleus. v – Zip1-stained PC with extensive Zip1 stained SC networks. Figure adapted from HENDERSON & KEENEY, 2004.

Zip1 is a known component of PCs in *S. cerevisiae* (SYM and ROEDER 1995). Zip1 is a component of the central core of the *S. cerevisiae* SC (SYM *et al.,* 1993). Hop1 however, is thought to be involved in the formation of the SC axial elements in *S. cerevisiae* (HOLLINGSWORTH *et al.,* 1990). Loss of Hop1 has no effect on PC formation (SYM and ROEDER 1995). It has therefore been concluded by previous studies that PCs are composed mainly of unused/disintegrated parts associated with the central core of the SC only (SYM and ROEDER 1995).

If the Hop1 cluster structures observed in this study are indeed PCs, then it infers a difference in the formation and composition of PCs between *S. cerevisiae* and *S. pombe.*

S. pombe Hop1 is known to associate with LinEs - which bear resemblance to the axial elements of the SC. LinEs do not exhibit transverse filaments (LORENZ *et al.,* 2004), therefore no central core region or proteins have been identified in *S. pombe*. We therefore cannot rule out the possibility of Hop1 in having a role in the adjoining of LinEs (if this occurs), as a part of a putative central core region. This would explain its apparent localisation to 'PC' structures.

In *S. pombe*, Hop1 has been implicated in partner choice during meiotic recombination (NIU *et al.,* 2005). Hop1 is thought to transiently inhibit the repair of DSBs until alignment with a homologous chromosome is achieved (LATYPOV *et al.,* 2010) – thus inhibiting inter-sister recombination and promoting inter-homologue recombination. We know that meiotic recombination occurs after

DNA replication (CERVANTES *et al.,* 2000), but prior to the first meiotic division. Figure 3.4C indicates that the first meiotic division occurs between 2.5 hrs and 4 hrs in our *h^-/h^- pat1-114/pat1-114 lys1::mat-Pc-lys1$^+$* thermally induced meiosis. Figure 3.11 indicates that Hop1 clusters appear between 2.5 hrs and 3.5 hrs. These data allow for Hop1 clusters to be implicated in late meiotic recombination events. The location of Hop1 clusters could therefore be regions where it is important that inter-sister recombination events do not occur - hence the presence of Hop1, suppressing inter-sister events. These regions may include:

→ The telomeres, which are important in protecting natural chromosome ends from degradation or inappropriate repair via end-to-end joining or recombination (VERDUN and KARLSEDER 2007). Telomeres contain regions of highly repetitive DNA, making it prone to recombine with itself. Taz1 (telomeric protein) and Trt1 (telomeric reverse transcriptase) are both involved in the inhibition of telomeric recombination. Hop1 suppression of inter-sister recombination may be fundamentally important in telomeric regions. We know that telomeres cluster to the SPB during meiosis; this configuration would correlate well with the appearance of Hop1 clusters if they were telomere-associated structures. Further investigation could include cytological analysis of Taz1 and Trt1 localisation in comparison to Hop1 cluster structures.

→ The centromeres (which also include regions of highly repetitive DNA sequences), where suppression of recombination is imperative for the faithful segregation of homologous chromosomes during meiosis (ELLERMEIER *et al.,* 2010). Failure to establish centromeric suppression in *S. pombe* can lead to occasional meiotic missegregation (HALL *et al.,* 2003). In fission yeast, RNAi and Clr4-Rik1 (histone methyltransferase complex) are both involved in the suppression of centromeric recombination (ELLERMEIER *et al.,* 2010). High-level localisation of Hop1 (as seen in Hop1 cluster structures) to centromeric regions may contribute to the suppression of centromeric recombination.

→ The nucleolus, which contains highly repetitive rDNA sequences – an attractive substrate for recombination events. Unwanted recombination

events may lead to chromosomal deletions/translocations/insertions; repression of meiotic recombination is important in this region (PETES 1980). Hop1 cluster structures could be localising to these regions in order to aid the repression of recombination. In order to test this particular hypothesis, I co-stained a selection of spread nuclei with Hop1 and Nop1 [*S. cerevisiae* homologue of Fibrillarin – a known nucleolus component, which has been used in *S. pombe* (A. Lorenz pers. comm)]. Unfortunately, the Nop1 staining did not work. Further investigation could include optimising the co-staining of Hop1 and Nop1 to analyse their localisation patterns.

The localisation of Hop1 clusters to regions void of Rec10-positive LinE staining may also be an important observation. It has been suggested that LinEs are involved in pairing of homologues (MOLNAR *et al.,* 2003). Taking this into account, elevated levels of Hop1 (as observed in Hop1 clusters) in the absence of LinEs may be present to inhibit inter-sister recombination on a higher level than what is needed in the presence of LinEs. This may be due to lack of pairing giving rise to an elevated probability of inter-sister recombination events.

Chapter 4

Construction and cytological analysis of *rec10* C-terminal mutants

4.1 Introduction

S. pombe exhibits an SC-less meiosis. It does however form structures termed LinEs, which are comparable to axial SC-precursors observed in other organisms. The main component of LinEs is the meiosis-specific protein Rec10 (LORENZ *et al.*, 2004), with inactivation of *rec10* resulting in the complete absence of any detectible LinEs (LORENZ *et al.*, 2004; MOLNAR *et al.*, 2003). Various *rec10* mutations have differing effects on LinE formation and development:

rec10-109 - Two mis-sense point mutations at amino acid positions 176 and 178 result the formation of aberrant LinEs, morphologically comparable with the dot-like class Ia and slightly elongated class Ib LinE stuctures, and also appearing to be fewer in number than seen in a *rec10*$^{+}$ (LORENZ *et al.*, 2004);

rec10-144 - Mis-sense point mutation at amino acid position 727 results in aberrant LinEs, the only structures observed being morphologically comparable to the dot-like class Ia foci, and a slightly fatter, longer structure (PRYCE *et al.*, 2005);

rec10-155 - Truncation of C-terminal 103 amino acids by insertion of *S. cerevisiae LEU2* marker results in the complete absence of any cytologically detectible LinEs (MOLNAR *et al.*, 2003).

rec10-175 Full deletion of the *rec10* open reading frame results in complete absence of LinEs.

Alongside absence of LinEs, the *rec10* deletion (*rec10-175*) results in a genome wide reduction in recombination equivalent to levels observed in a *rec12* (*spo11*) mutant. *rec10-155* (the truncation), on the other hand, whilst void of detectible LinEs (MOLNAR *et al.*, 2003; WELLS *et al.*, 2006), does exhibit intermediate levels of recombination on a genome-wide level. This indicates that LinEs are not completely essential for recombination (MOLNAR *et al.*, 2003; WELLS *et al.*, 2006). The C-terminus of Rec10 shows limited sequence similarity to the C-terminus of *S. cerevisiae* Red1 (LORENZ *et al.*, 2004), a component of the SC axial elements

(ROCKMILL and ROEDER 1988). The C-terminal of *S. cerevisiae* Red1 is proposed to mediate Red1 homo-oligomerization (WOLTERING *et al.,* 2000). It is thought that the C-terminal domain of Rec10 functions in a similar fashion, correlating with the absence of visible LinE formation in the *rec10-155* C-terminal truncation mutant (WELLS *et al.,* 2006).

In this study, specific mutations were made in the *rec10* region encoding the conserved C-terminus; bases were mutated based on conservation patterns exhibited by a multiple sequence alignment (Figure 4.1). The aim of the mutations was to create a 'refined version' of the *rec10-155* mutant, by engineering a *rec10* mutant that was incapable of generating LinEs, yet was able to retain wild type levels of recombination. This would allow us to pinpoint the *rec10* residue(s) directly involved in the formation of LinEs, and also completely separate two distinct functions of *rec10*; LinE formation, and involvement in recombination, which would address the hypothesis that whilst Rec10 is required for meiotic recombination, LinEs are not.

4.2 Results

4.2.1 Introduction of *rec10* C-terminal mutants

4.2.1a Lysine mutants

The C-terminal domains of both Red1 and Rec10 contain lysine-rich regions, predicted to be nuclear targeting sites (Lorenz et al., 2004). This study targeted some of these highly conserved lysine residues for mutation. The residues were mutated from lysine to arginine ($K \rightarrow R$) in the chromosomally encoded rec10 gene. Once created, mutated strains were subjected to DNA sequencing to ensure that no additional mutations were introduced (data not shown). Both lysine and arginine exhibit positively charged side chains. Therefore we are able to rule out the possibility that any mutant phenotypes we observe during our analysis are due to a change of charge in the mutated region, and attribute them directly to the loss of the conserved lysine residue.

Five lysine mutant strains were created (Figure 4.1):

1. A single *K712R* mutation strain (*rec10-K712R*)
2. A single *K744R* mutation strain (*rec10-K744R*)
3. A single *K754R* mutation strain (*rec10-K754R*)
4. A single *K757R* mutation strain (*rec10-K757R*)
5. A strain exhibiting mutations at *K744*, *K754* and *K757* (*rec10-3KR*).

Interestingly, whilst this study was ongoing, K712 and K757 were demonstrated to be ubiquitinated, possibly targeting Rec10 for degradation (SPIREK *et al.,* 2010).

4.2.1b Tyrosine mutants

The other amino acid targeted in this study is tyrosine. Tyrosine can be present in proteins that are part of a signal transduction processes, being a target for phosphorylation via tyrosine protein kinases. The conserved tyrosine residues in the C-terminal oligomerization domain were mutated to phenylalanine (*Y→F*) in the chromosomally encoded *rec10* gene. Once created, the mutant genes were subjected to DNA sequencing to ensure that no additional mutations were introduced (data not shown). Again, both tyrosine and phenylalanine possess similar molecular architecture, both possessing hydrophobic side-chains. This mutation therefore disrupts any nuclear targeting process with minimal alteration to the molecular structure of the mutated region.

Three mutant strains were created (Figure 4.1):

1. A single *Y731F* mutation strain (*rec10-Y731F*)
2. A single *Y767F* mutation strain (*rec10-Y767F*)
3. A strain exhibiting mutations to both tyrosine residues (*rec10-2YF*).

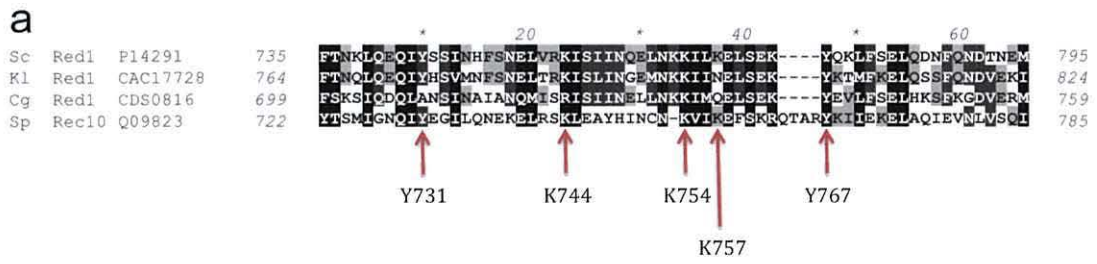

Figure 4.1 Position of *rec10* C-terminal mutations. Multiple sequence alignment of C-terminal region of *S. cerevisiae* (Sc) Red1 and its homologues in *K. lactis* (Kl), *C. glabrata* (Cg) and *S. pombe* (Sp). Sequence conservation is indicated via four different levels of shading, darker shading indicative of more conserved residues. Red arrows indicate positions of tyrosine and lysine residues mutated in this study. An additional lysine residue, not shown in this figure, was also mutated (K712) based on data in SPIREK *et al.*, (2010). Figure adapted from LORENZ *et al.*, (2004).

4.2.2 Cytological profile of meiosis in *rec10*$^+$/*rec10*$^+$ cells

This chapter focuses on the temporal cytological analysis of LinE formation and Rad51 foci in the *rec10* C-terminal mutants created.

4.2.2a Temporal analysis of a *rec10*$^+$/*rec10*$^+$ asynchronous meiosis

The differing morphologies of Rec10-positively stained LinEs have previously been classified (Figure 1.17); however, prior to the cytological analysis of the mutants generated in this study, a full cytological analysis of a wild-type meiosis was conducted to provide a comparison for the subsequent mutants. Figure 4.2 demonstrates the distinction in appearance between LinE classes used throughout this study for their quantification.

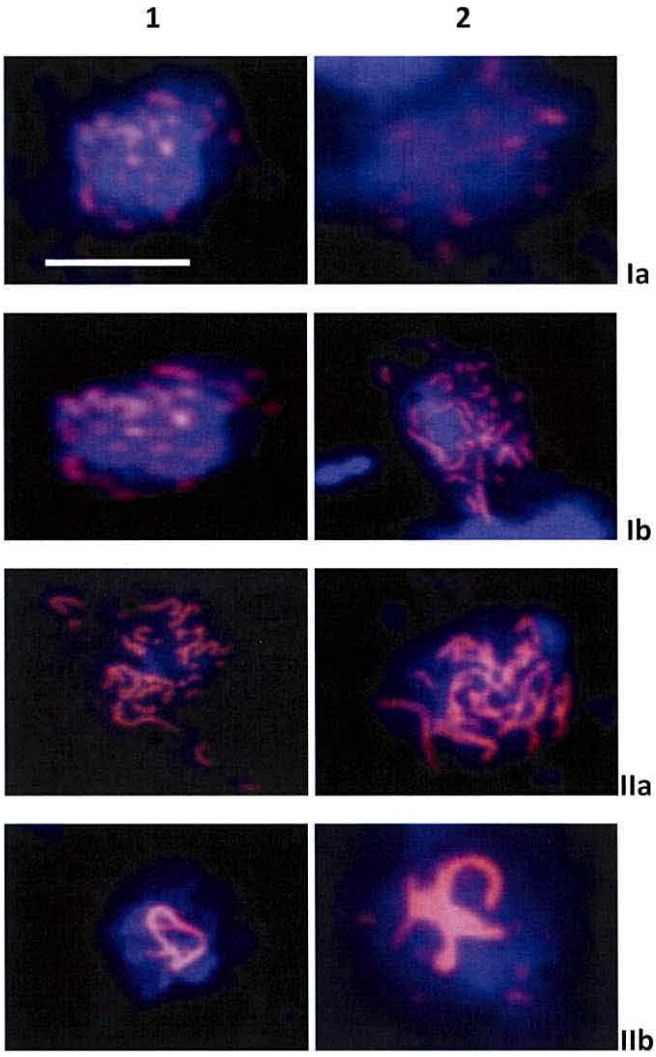

Figure 4.2 Examples of different LinE classes in a *rec10⁺/rec10⁺* diploid. All nuclei are stained for DNA (blue) and Rec10 (red). Two examples of nuclei are shown for each LinE classification group (columns 1+2). Scale bar = 5 μm.

In order to establish a benchmark upon which comparisons could be subsequently made, it was important to analyse a *rec10⁺/rec10⁺* asynchronous meiosis. This included a full temporal profile of LinE formation and development (Figure 4.3A); a temporal profile of the changing morphology of nuclei throughout the time course (Figure 4.3B); a temporal profile of Rad51 foci appearance and frequency (Figure 4.5).

Profiling the temporal changes in nuclear morphology involved the recording the proportionate frequency of mono-nucleate cells, horsetail cells, and cells exhibiting more than 2 nuclei at each time point (at least 80 nuclei were analysed at each time point). This profile allows any effects that the mutations may inflict on the temporal nature of meiotic events to be quantified.

Figure 4.3A establishes a visual pattern of LinE formation and development in a *rec10⁺/rec10⁺* diploid asynchronous meiosis. The data in this figure correlate well with what has previously been published (LORENZ *et al.*, 2004), with minor discrepancies put down to differing laboratory conditions, and possible differences in the visual distinction between LinE classes.

LinEs first appear by the 4 hr time point (predominantly as class Ia structures), although as we did not take a sample at 3 hrs, we cannot rule out the possibility that LinEs were present at 3 hrs. There is a definite shift in the proportions of LinE classes as the time course proceeds. Class Ia structures are predominant at 4 hrs and 5 hrs. Class Ib structures are the most frequently observed at 6 hrs. Class IIa structures become visibly more frequent by 7 hrs. Although class IIb structures have been observed throughout, an increase in their frequency is seen between 7-9 hrs. After 7 hrs, the frequency of nuclei exhibiting any LinEs begins to decrease.

4.2.2b Temporal profile of nuclear morphology during a *rec10⁺/rec10⁺* asynchronous meiosis

Figure 4.3B demonstrates the temporal pattern of meiosis by following nuclear morphology. The last mitotic division is signified by the brief reduction in cells with 1 nucleus, alongside the increase in cells exhibiting ≥2 nuclei – seen in Figure 4.3C at the 1 hr time point. The horsetail stage occurs between time points 4 hrs and 9 hrs. The first meiotic division is seen to begin at around the 9 hr time point, with meiosis being completed by the 24 hr time point.

A

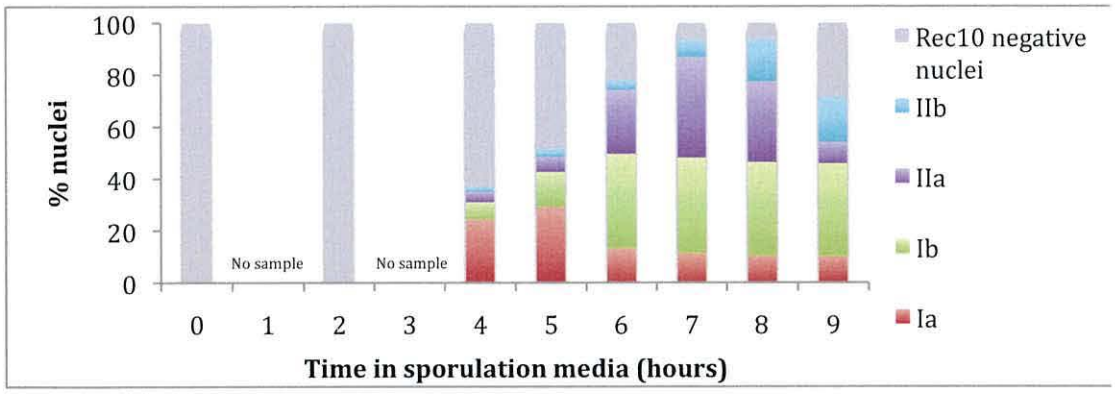

B

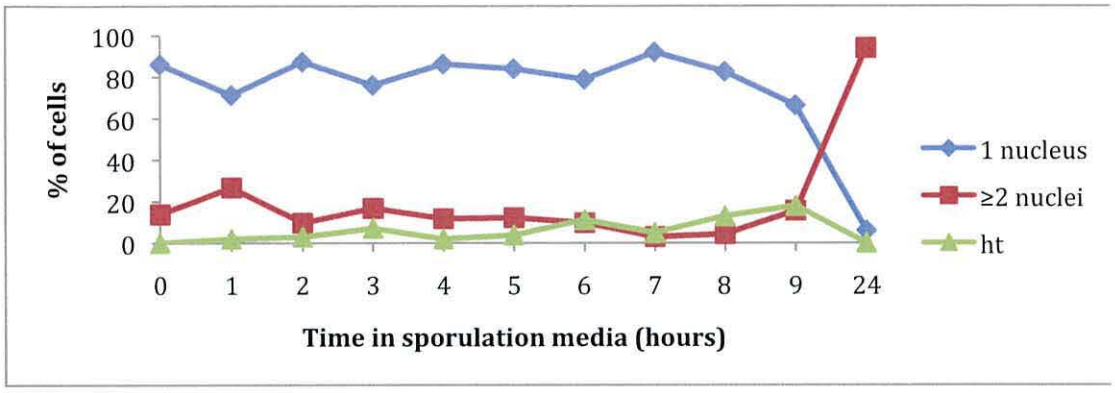

Figure 4.3 Development of LinEs during an asynchronous meiosis of a *rec10⁺/rec10⁺* diploid. (**A**) Proportions of LinE classes found in samples taken at hourly intervals after transfer of culture to sporulation media. ≥80 nuclei were scored for each time point*. (* - No data was collected for time points 1 and 3 hours). (**B**) Analysis of cytological meiotic events in samples taken at hourly intervals after transfer of culture to sporulation media. ≥80 nuclei were scored for each time point. ht – horsetail nuclei.

4.2.1c Temporal quantification of Rad51 staining

Rad51 is a strand invasion protein that binds to DSB sites in *S. pombe* (GRISHCHUK *et al.*, 2004). It has been proposed that Rad51 associates with LinEs (LOIDL 2006). Rad51 foci do not form in a *rec10Δ* strain (LORENZ *et al.*, 2006), where DSB lesions are not detected (ELLERMEIER and SMITH 2005). The failure in formation of DSBs and Rad51 foci localisation in the *rec10Δ* strain suggests that recombination is not initiated in the absence of *rec10*, and explains the low levels of recombination exhibited in a *rec10Δ* strain (ELLERMEIER and SMITH 2005). The *rec10-155* C-terminal truncation mutant, which fails to form any visible LinEs,

does however exhibit a high frequency of Rad51 foci (concurrent with the mutant exhibiting intermediate levels of recombination) (WELLS *et al.,* 2006). In order to have a benchmark to which the temporal analysis of Rad51 foci in *rec10* C-terminal mutants can be compared, cytological quantification of Rad51 foci was performed for a *rec10⁺/rec10⁺* asynchronous meiosis. Figure 4.4 shows examples of Rec10/Rad51 co-stained nuclei in a *rec10⁺/rec10⁺* asynchronous meiosis.

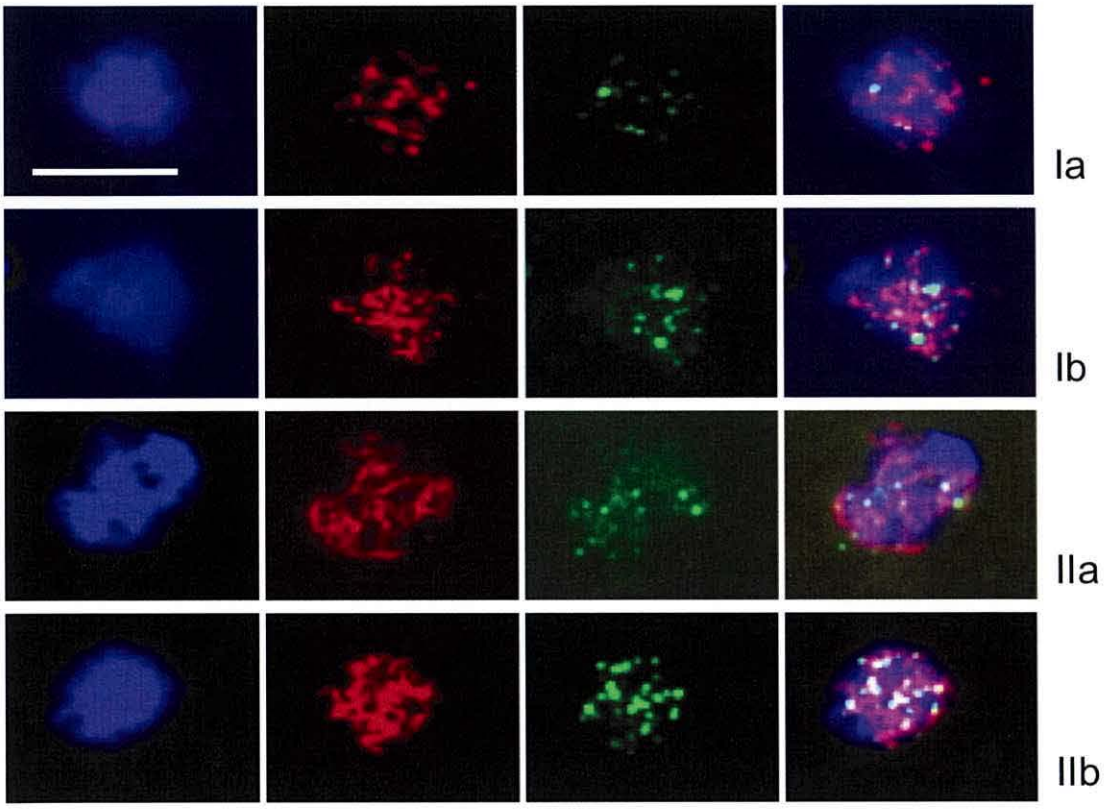

Figure 4.4 Examples of Rec10/Rad51 co-stained nuclei. Nuclei are stained for DNA (blue), Rec10 (red) and Rad51 (green). Rec10/Rad51 co-localisation is indicated in yellow. One example is shown for each LinE class. Scale bar = 5 μm.

4.2.1d Temporal quantification of Rad51 staining during a *rec10⁺/rec10⁺* asynchronous meiosis

Figure 4.5A demonstrates that Rad51 foci appear concomitantly with Rec10-positively stained LinEs. Nuclei containing all classes of LinEs exhibit Rad51 foci co-staining (Figure 4.5A). As a rule, nuclei exhibiting the more mature classes of LinEs seem to display a higher proportion of Rad51 co-stained nuclei (4.5A).

There does not seem to be a significant increase or decrease in the proportion of Rad51/Rec10 co-stained nuclei throughout the time course.

Figure 4.5B appears to show that nuclei exhibiting class IIa and class IIb LinE structures are observed to contain more Rad51 foci than nuclei exhibiting class Ia and Ib structures.

A

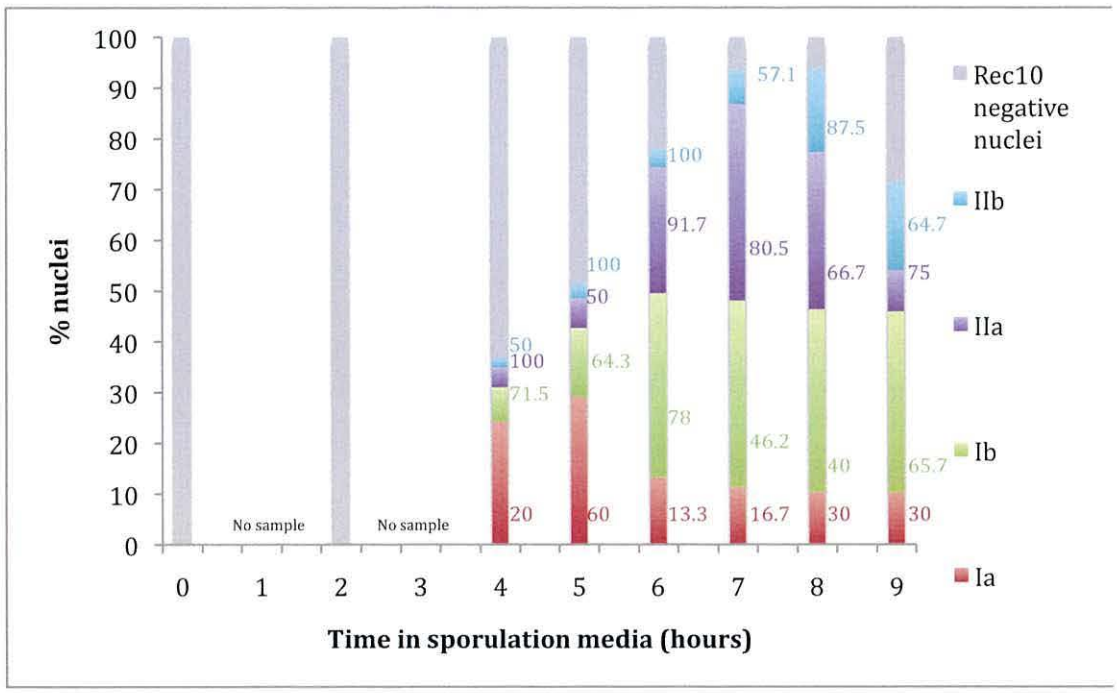

B

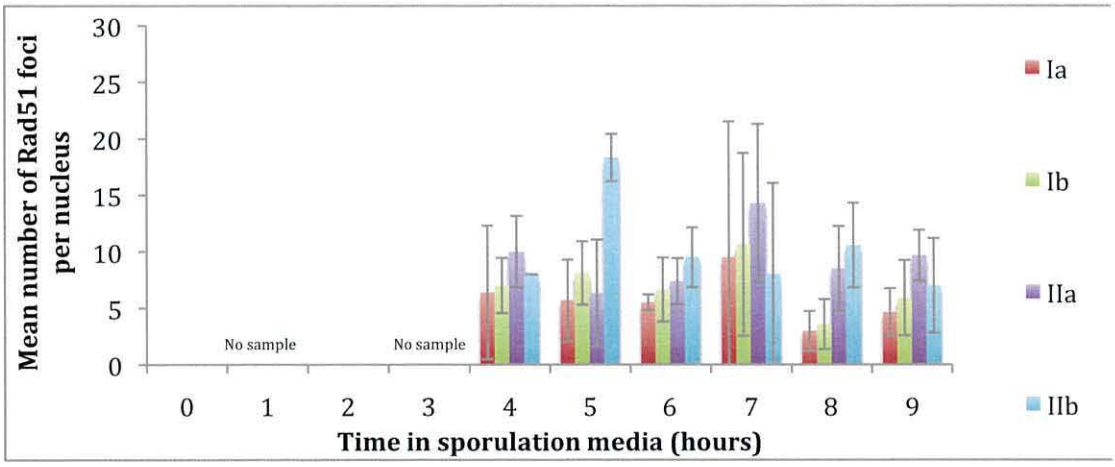

<u>Figure 4.5</u> Quantification of Rad51 staining during an asynchronous meiosis of a *rec10⁺/rec10⁺* diploid. (**A**) Proportions of LinE classes found in samples taken at hourly intervals after transfer to sporulation media. ≥80 nuclei were recorded for each time point. Numbers adjacent to each column represent the % nuclei scored exhibiting Rad51 and Rec10 co-staining, with the colours representing LinE classes. Absence of a number indicates 0%. (**B**) Mean number of Rad51 foci scored in each nucleus exhibiting Rec10 and Rad51 co-staining. Error bars represent a 95% confidence interval in all cases.

4.2.3 Cytological analysis of LinE formation and development in *rec10* C-terminal *K→R* mutants

4.2.3a Analysis of LinE formation during a *rec10-K712R/rec10-K712R* diploid asynchronous meiosis

Figure 4.6B demonstrates that Rec10-positively stained LinEs are first visible by the 4 hr time point in a *rec10-K712R/rec10-K712R* asynchronous meiosis; class Ia and Ib structures are observed at 4 hrs. By the 5 hr time point, there is no real increase in the frequency of nuclei exhibiting Rec10-positively stained LinEs, but all four classes of LinE structures are now observed. There is a slight increase in the frequency of nuclei exhibiting Rec10-positively stained LinEs at the 6 hr time point, with the ratio of each LinE class being fairly proportionate to that observed at the 5 hr time point; class Ia and Ib LinEs appearing slightly more prevalent than class IIa, with only a few class IIb structures recorded. At the 7 hr time point, there is a dramatic reduction in the frequency of Rec10-positively stained nuclei (~20%); virtually no class Ia structures were observed, and only a small number of class Ib, IIa and IIb structures were recorded. By the 8 hr time point, however, the frequency of Rec10-positively stained structures has increased to approximately 80%; class Ia and Ib structures appearing equally prevalent, followed by class IIa structures, and a small number of class IIb LinEs. LinE quantification at the 9 hr time point is fairly similar to that observed at 8 hrs – the only visible difference is the decrease in the frequency of class IIa LinEs. In comparison with a *rec10⁺/rec10⁺* asynchronous meiosis (Figure 4.6A), the temporal quantification of LinEs during a *rec10-K712R/rec10-K712R* (Figure 4.6B) demonstrates:

- → A lower frequency of nuclei exhibiting class Ib and class IIa LinEs during time points 6 hrs and 7 hrs.
- → An increased frequency of nuclei exhibiting class Ia LinEs at time points 8 hrs and 9 hrs.
- → A dramatically (~4 fold) lower frequency of Rec10-positively stained nuclei at time point 7 hrs.
- → A lower frequency of class IIb LinE structures during time points 8 hrs and 9 hrs.

4.2.3b Analysis of meiotic progression during a *rec10-K712R/rec10-K712R* diploid asynchronous meiosis

Figure 4.6C, shows that the last mitotic division is observed to occur at the 1 hr time point after switching the cells to sporulating media. The horsetail stage appears to take place between the 3 hr and 8 hr time points, peaking at approximately 6 hrs. The first meiotic division appears o begin at approximately the 6 hr time point, with nearly half the recorded cells exhibiting ≥2 nuclei by the 9 hr time point. Meiosis is complete by the 24 hr time point.

In comparison with a *rec10⁺/rec10⁺* asynchronous meiosis (Figure 4.3B), the temporal profile of meiotic nuclei during a *rec10-K712R/rec10K712R* (Figure 4.6C) demonstrates:

→ A possible advancement (up to 2-3 hrs) in the first meiotic division during a *rec10-K712R/rec10K712R* asynchronous meiosis.

A

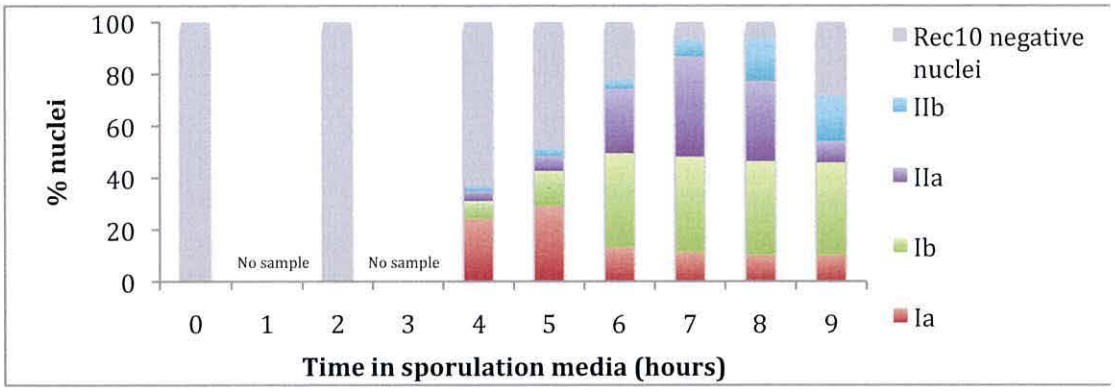

B

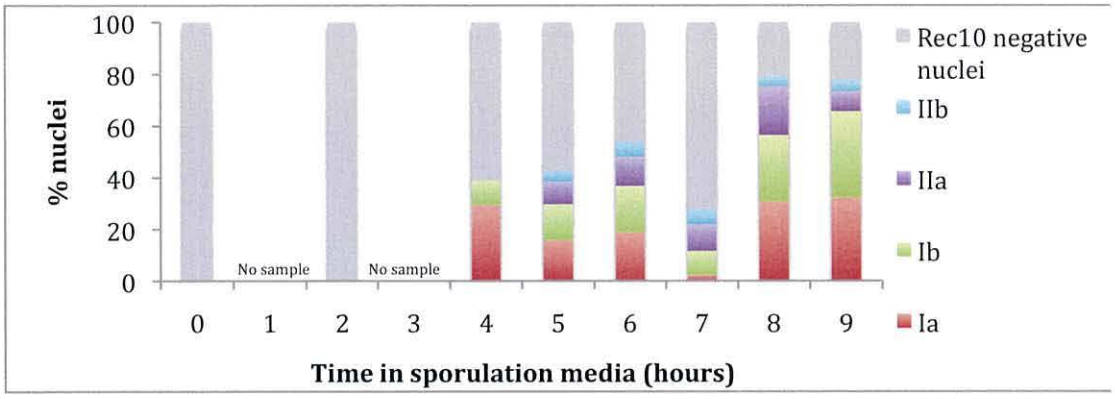

C

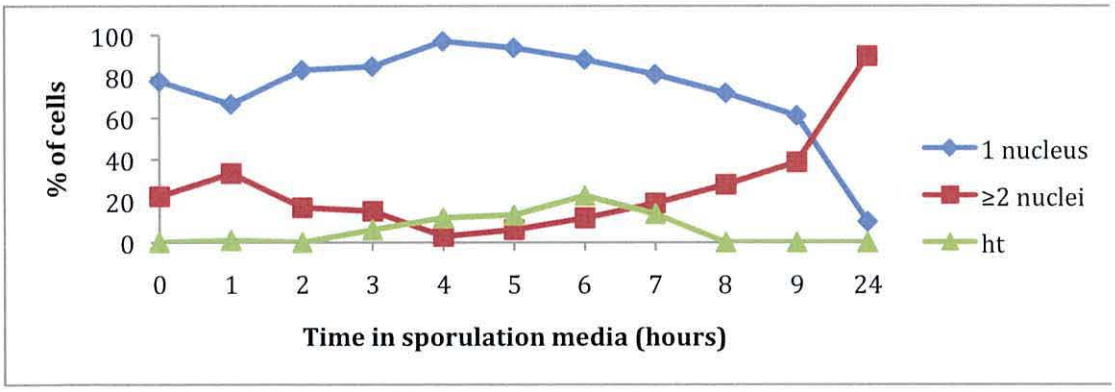

Figure 4.6 Development of LinEs during an asynchronous meiosis of a *rec10-K712R/rec10-K712R* diploid. (**A**) Proportions of LinE classes scored in *rec10⁺/rec10⁺* diploid asynchronous meiosis* **. (**B**) Proportions of LinE classes found in samples taken at hourly intervals after transfer of *rec10-K712R/rec10-K712R* culture to sporulation media. ≥80 nuclei were scored for each time point*. (* - No data was collected for time points 1 and 3 hours; ** These data are a duplication of Figure 4.3A and are represented for case of comparison). (**C**) Analysis of cytological meiotic events in samples taken at hourly intervals after transfer of *rec10-K712R/rec10-K712R* culture to sporulation media. ≥80 nuclei were scored for each time point. ht – horsetail nuclei.

4.2.3c Analysis of LinE formation during a *rec10-K744R/rec10-K744R* diploid asynchronous meiosis

Figure 4.7B shows that LinEs first appear at 4 hrs after the switch to sporulating medium, where they are predominantly class Ia structure, with some class Ib LinEs also present. Time points 5 hrs, 6 hrs, 7 hrs, 8 hrs and 9 hrs all appear to exhibit a similar pattern in the frequency and proportion of nuclei containing the different LinE classes; class Ib being most prevalent throughout, then classes IIa and Ia, and a small number of class Ib structures are observed during this period. In comparison with a *rec10⁺/rec10⁺* asynchronous meiosis (Figure 4.7A), the temporal quantification of LinEs during a *rec10-K744R/rec10-K744R* (Figure 4.7B) demonstrates:

→ Class IIa and IIb structures are first observed approximately 1 hour later during a *rec10-K744R/rec10-K744R* asynchronous meiosis.

→ The frequency of nuclei exhibiting Rec10-postive staining remains fairly constant from the 5 hr time point to the last (9 hr) time point, indicative of possible lack of LinE degradation during a *rec10-K744R/rec10-K744R* asynchronous meiosis.

→ The frequency of nuclei exhibiting class IIb LinEs is lower at time points 7 hrs, 8 hrs and 9 hrs during a *rec10-K744R/rec10-K744R* asynchronous meiosis.

4.2.3d Analysis of meiotic progression during a *rec10-K744R/rec10-K744R* diploid asynchronous meiosis

Figure 4.7C shows that the horsetail stage appears to take place between time points 3 hrs and 9 hrs, peaking at time point 5 hrs. The first meiotic division is seen to begin at approximately 7 hrs, with at least 40% of the nuclei exhibiting ≥2 nuclei by the 9 hr time point. By the 24 hr time point, it appears as though meiosis has been completed.

In comparison with a *rec10⁺/rec10⁺* asynchronous meiosis (Figure 4.3B), the temporal profile of meiotic nuclei during a *rec10-K744R/rec10K744R* (Figure 4.7C) demonstrates:

→ A possible advancement (up to 2 hrs) in the initiation of the first meiotic division, with more cells (more than 2 fold) exhibiting ≥2 nuclei by the 9 hr time point.

A

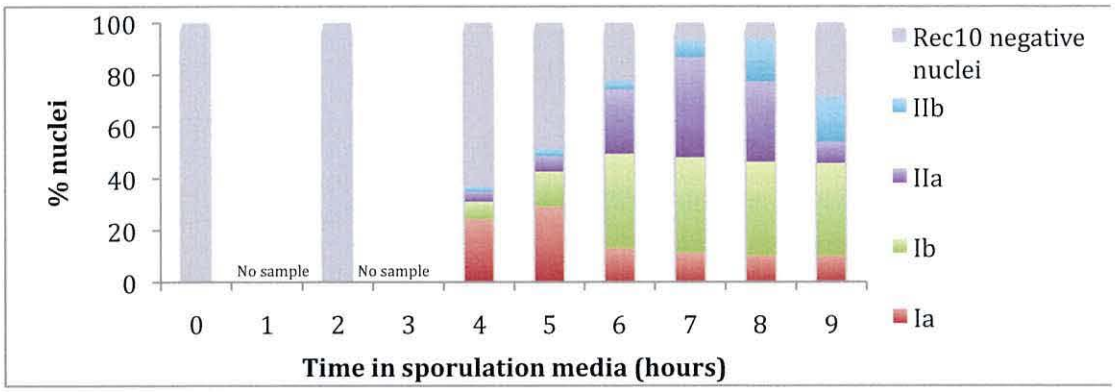

B

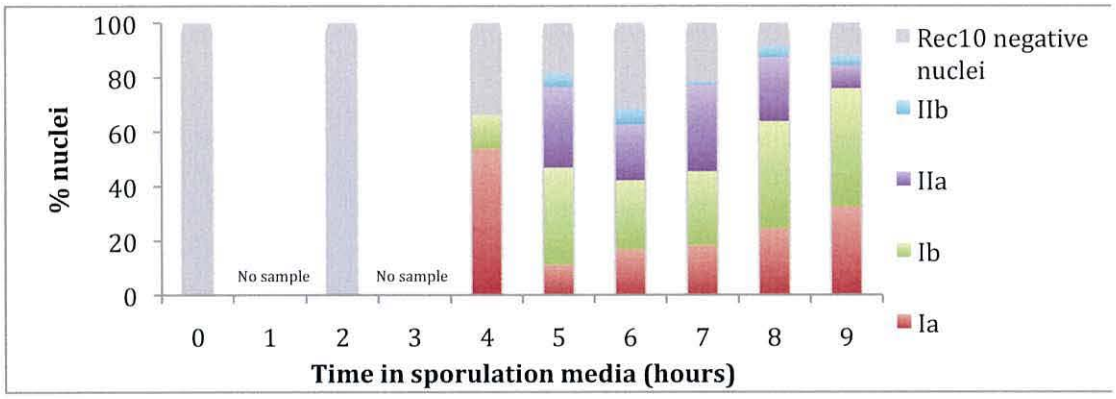

C

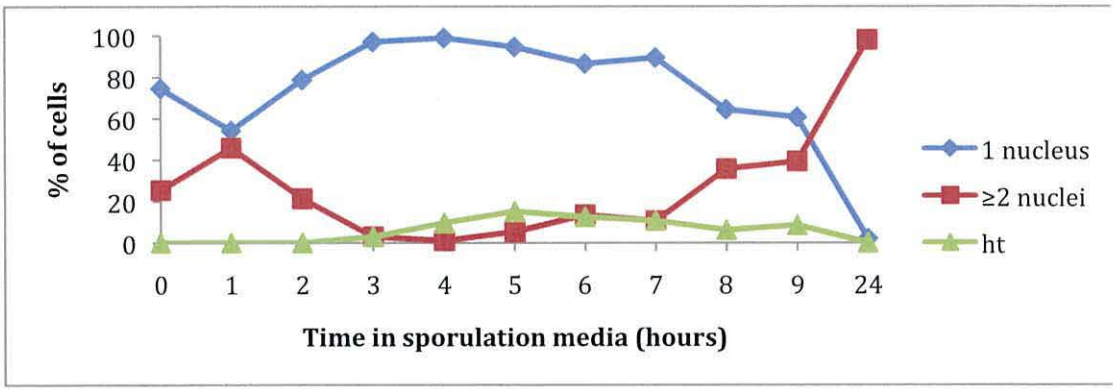

Figure 4.7 Development of LinEs during an asynchronous meiosis of a *rec10-K744R/rec10-K744R* diploid. (**A**) Proportions of LinE classes scored in *rec10⁺/rec10⁺* diploid asynchronous meiosis* **. (**B**) Proportions of LinE classes found in samples taken at hourly intervals after transfer of *rec10-K744R/rec10-K744R* culture to sporulation media. ≥80 nuclei were scored for each time point*. (* - No data was collected for time points 1 and 3 hours; ** These data are a duplication of Figure 4.3A and are represented for case of comparison). (**C**) Analysis of cytological meiotic events in samples taken at hourly intervals after transfer of *rec10-K744R/rec10-K744R* culture to sporulation media. ≥80 nuclei were scored for each time point. ht – horsetail nuclei.

4.2.3e Analysis of LinE formation during a *rec10-K754R/rec10-K754R* diploid asynchronous meiosis

Figure 4.8B shows that LinEs first appear at the 4 hr time point following the switch to sporulating medium; all classes are present, with class Ia being most frequently recorded, followed by class Ib, and a small number of both class IIa and IIb structures. The frequency of nuclei exhibiting Rec10-positive LinE staining increases between 4 hrs and 5 hrs (with only a small number of class IIa and IIb LinEs present again at the 5 hr time point), and again between the 5 hr time point and 6 hrs, with an increase in he number of class IIa LinEs by the 6 hr time point also apparent. The number of Rec10-positively stained nuclei decreases by the 7 hr and 8 hr time points – with the proportion of classes appearing similar at both time points. At the 8 hr time point, we observe a dramatic decrease in the number of Rec10-positively stained nuclei (down to approximately 10% of all recorded nuclei) – however all classes are still present. In comparison with a *rec10⁺/rec10⁺* asynchronous meiosis (Figure 4.8A), the temporal quantification of LinEs during a *rec10-K754R/rec10-K754R* (Figure 4.8B) demonstrates:

→ A decrease in the number of Rec10-positively stained nuclei earlier (approximately 2 hrs) during a *rec10-K754R/rec10-K754R* asynchronous meiosis – possibly indicative of an advancement in LinE degradation, or that LinEs are not fully formed.

→ Fewer nuclei exhibiting class IIb LinEs at time points 7 hrs, 8 hrs and 9 hrs during a *rec10-K754R/rec10-K754R* asynchronous meiosis.

→ A dramatically lower number of nuclei exhibiting Rec10-positive staining at the 9 hr time point during a *rec10-K754R/rec10-K754R* asynchronous meiosis – possibly indicative of an advancement in LinE degradation.

4.2.3f Analysis of meiotic progression during a *rec10-K754R/rec10-K754R* diploid asynchronous meiosis

Figure 4.8C shows that the horsetail stage appears to begin to take place at 5 hrs after the switch to sporulating medium and has still not finished by 9 hrs. The first meiotic division appears to begin at 7 hrs. There does not appear to be any significantly visible differences on comparison of the temporal profile of meiotic nuclei in a *rec10*$^{+}$/*rec10*$^{+}$ (Figure 4.3B) asynchronous meiosis, and a *rec10-K754R/rec10-K754* asynchronous meiosis (Figure 4.8C).

A

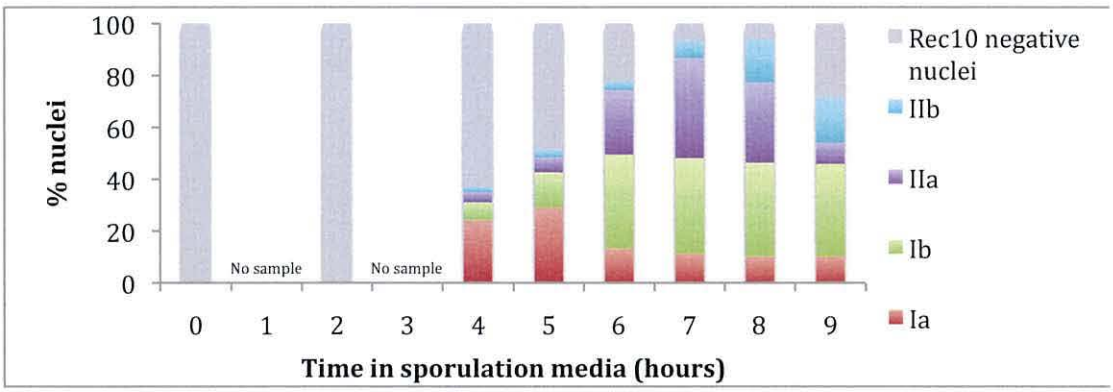

B

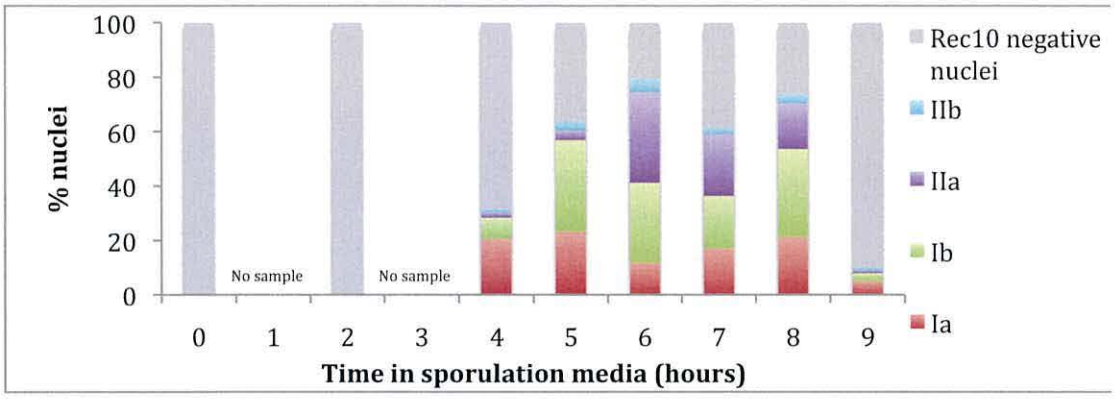

C

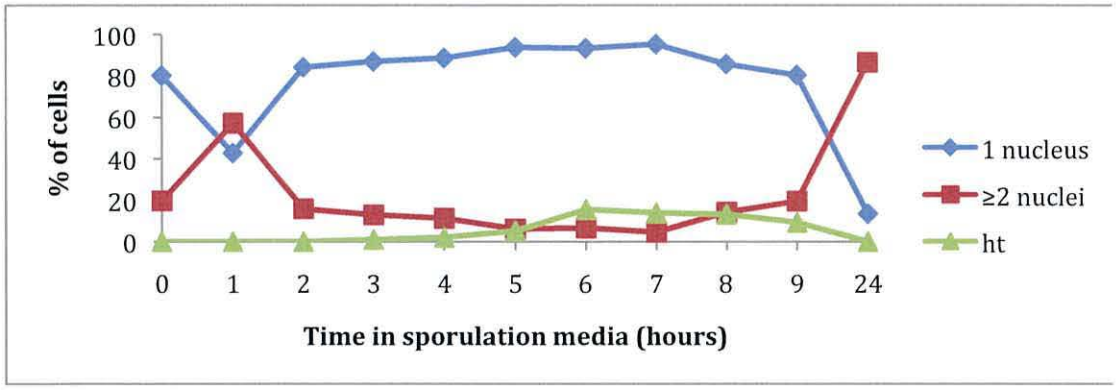

<u>Figure 4.8</u> Development of LinEs during an asynchronous meiosis of a *rec10-K754R/rec10-K754R* diploid. (**A**) Proportions of LinE classes scored in *rec10⁺/rec10⁺* diploid asynchronous meiosis* **. (**B**) Proportions of LinE classes found in samples taken at hourly intervals after transfer of *rec10-K754R/rec10-K754R* culture to sporulation media. ≥80 nuclei were scored for each time point*. (* - No data was collected for time points 1 and 3 hours; ** These data are a duplication of Figure 4.3A and are represented for case of comparison). (**C**) Analysis of cytological meiotic events in samples taken at hourly intervals after transfer of *rec10-K754R/rec10-K754R* culture to sporulation media. ≥80 nuclei were scored for each time point. ht – horsetail nuclei.

4.2.3g Analysis of LinE formation during a *rec10-K757R/rec10-K757R* diploid asynchronous meiosis

Figure 4.9B shows that LinEs first become visible by 4 hrs after transfer to sporulating medium during a *rec10-K757R/rec10-K757R* asynchronous meiosis, with class Ia, class Ib and class Ia LinEs present. An increase in the frequency of nuclei exhibiting Rec10-positively stained structures is apparent between time points 4 hrs and 5 hrs, with an increase in the frequency of class IIa LinEs and the appearance of class IIb LinEs by 5 hrs. The number of Rec10-positively stained nuclei remains fairly constant from 5 hrs until 9 hrs; during this period no increase in the frequency of class IIb LinEs is observed. The frequency of nuclei exhibiting class Ib structures become more numerous and nuclei with class Ia structure decrease in number, until they are virtually non-existent by 9 hrs.
In comparison with a *rec10⁺/rec10⁺* asynchronous meiosis (Figure 4.9A), the temporal quantification of LinEs during a *rec10-K757R/rec10-K757R* (Figure 4.9B) demonstrates:

→ Class IIb LinEs appear later during a *rec10-K757R/rec10-K757R* asynchronous meiosis.

→ The number of nuclei exhibiting class IIb LinEs is lower throughout the whole time course during a *rec10-K757R/rec10-K757R* asynchronous meiosis.

→ The highest frequency of nuclei exhibiting Rec10-positive staining is approximately 75%, lower than observed in wild type, during a *rec10-K757R/rec10-K757R* asynchronous meiosis.

4.2.3h Analysis of meiotic progression during a *rec10-K757R/rec10-K757R* diploid asynchronous meiosis

Figure 4.9C shows that the horsetail stage appears to occur between 4 hrs and 9 meiotic division appears to begin at approximately 6 hrs, however by 24 hrs, not all the nuclei seem to have completed meiosis (approximately 70%).

In comparison with a *rec10⁺/rec10⁺* asynchronous meiosis (Figure 4.3B), the temporal profile of meiotic nuclei during a *rec10-K757R/rec10-K757R* (Figure 4.9C) demonstrates:

→ A possible delay in the completion of meiosis during a *rec10-K757R/rec10-K757R* asynchronous meiosis.

A

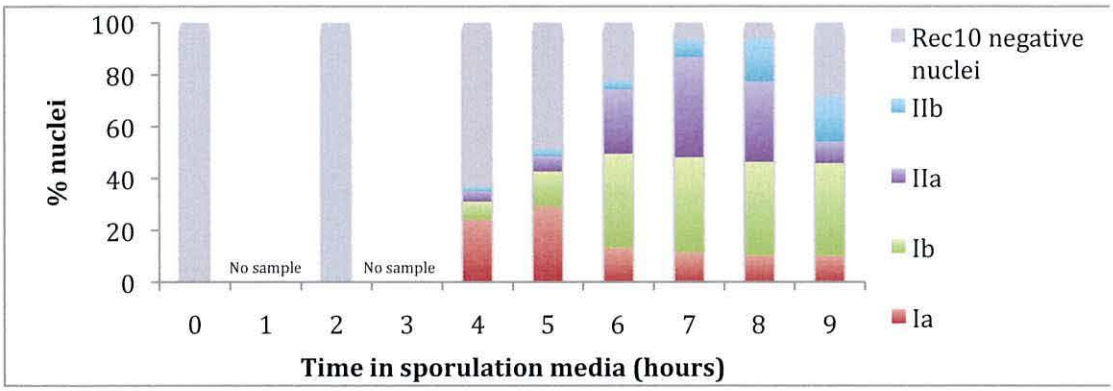

B

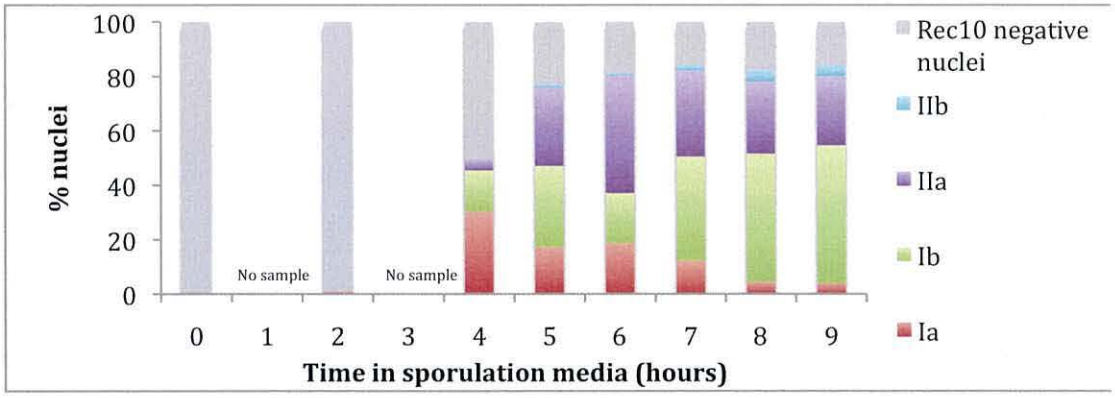

C

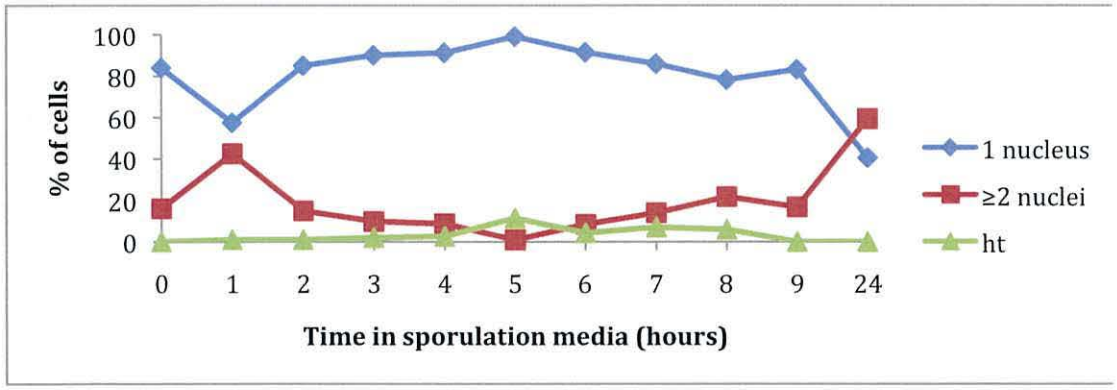

<u>Figure 4.9</u> Development of LinEs during an asynchronous meiosis of a *rec10-K757R/rec10-K757R* diploid. (**A**) Proportions of LinE classes scored in *rec10⁺/rec10⁺* diploid asynchronous meiosis* **. (**B**) Proportions of LinE classes found in samples taken at hourly intervals after transfer of *rec10-K757R/rec10-K757R* culture to sporulation media. ≥80 nuclei were scored for each time point*. (* - No data was collected for time points 1 and 3 hours; ** These data are a duplication of Figure 4.3A and are represented for case of comparison). (**C**) Analysis of cytological meiotic events in samples taken at hourly intervals after transfer of *rec10-K757R/rec10-K757R* culture to sporulation media. ≥80 nuclei were scored for each time point. ht – horsetail nuclei.

4.2.3i Analysis of LinE formation during a *rec10-3KR/rec10-3KR* diploid asynchronous meiosis

Figure 4.10B demonstrates that LinEs first appear by 4 hrs after transferring the cells to sporulating medium, during a *rec10-3KR/rec10-3KR* asynchronous meiosis, where approximately 70% of nuclei recorded exhibit Rec10-positive staining, and classes Ia, Ib and IIa LinEs present. The number of Rec10-positive nuclei fluctuates between approximately 70% and 90% between time points 4 hrs and 8 hrs. From the 5 hr time point to the 8 hr time point, nuclei exhibiting class IIa LinEs are most frequent, we also observe class IIb structures present in small numbers. Ar 9 hrs there is a dramatic decrease in the frequency of Rec10-positively stained nuclei (falling to approximately 15-20%), however all classes are still present.

In comparison with a *rec10⁺/rec10⁺* asynchronous meiosis (Figure 4.10A), the temporal quantification of LinEs during a *rec10-3KR/rec10-3KR* (Figure 4.10B) demonstrates:

- → A higher frequency of nuclei exhibiting Rec10-positively stained LinEs at 4 hrs and 5 hrs during the *rec10-3KR/rec10-3KR* asynchronous meiosis.
- → A higher frequency of class IIa LinEs in the period between 5 hrs and 8 hrs during the *rec10-3KR/rec10-3KR* asynchronous meiosis.
- → A lower number of nuclei exhibiting class IIb LinEs at 7 hrs, 8 hrs and 9 hrs.
- → A dramatically lower number of nuclei exhibiting Rec10-positive LinE staining at 9 hrs.

4.2.3j Analysis of meiotic progression during a *rec10-3KR/rec10-3KR* diploid asynchronous meiosis

Figure 4.10C shows that the horsetail stage occurs between 2 hrs and 8 hrs during a *rec10-3KR/rec10-3KR* asynchronous meiosis. The first meiotic division begins at approximately 5 hrs, with more than 50% of recorded nuclei exhibiting ≥2 nuclei by 9 hrs. Meiosis appears to have been completed by 24 hrs.

In comparison with a *rec10⁺/rec10⁺* asynchronous meiosis (Figure 4.3B), the temporal profile of meiotic nuclei during a *rec10-3KR/rec103KR* (Figure 4.10C) demonstrates:

→ A possible advancement in the timing of the horsetail stage during the *rec10-3KR/rec103KR* asynchronous meiosis.

→ A possible advancement (up to 3 hrs) in the first meiotic division during the *rec10-3KR/rec103KR* asynchronous meiosis.

→ A higher number of cells (up to 3-fold) exhibiting ≥2 nuclei by 9 hrs during the *rec10-3KR/rec103KR* asynchronous meiosis.

A

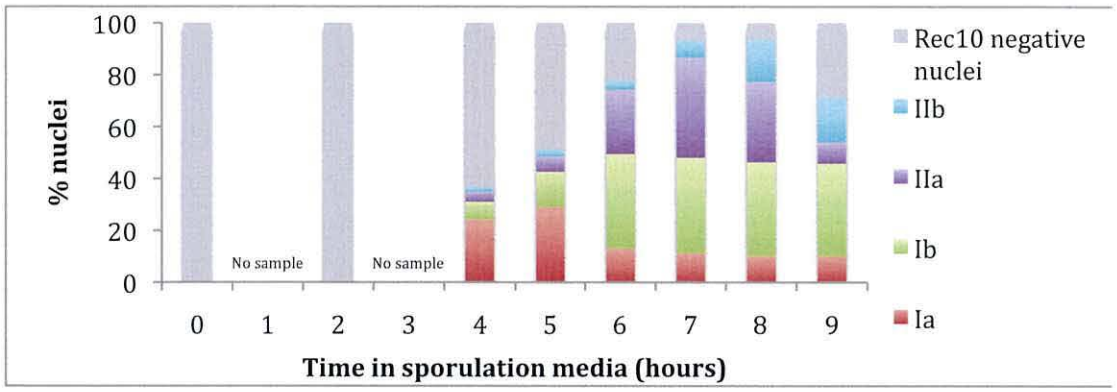

B

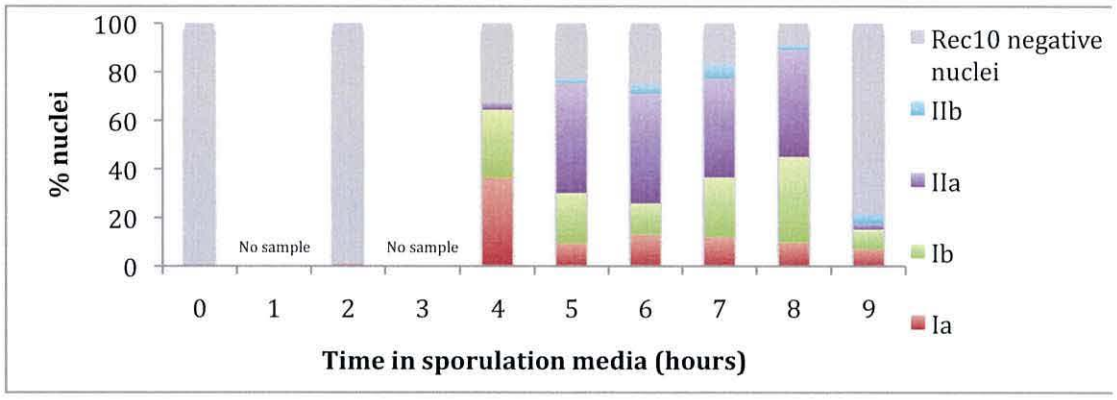

C

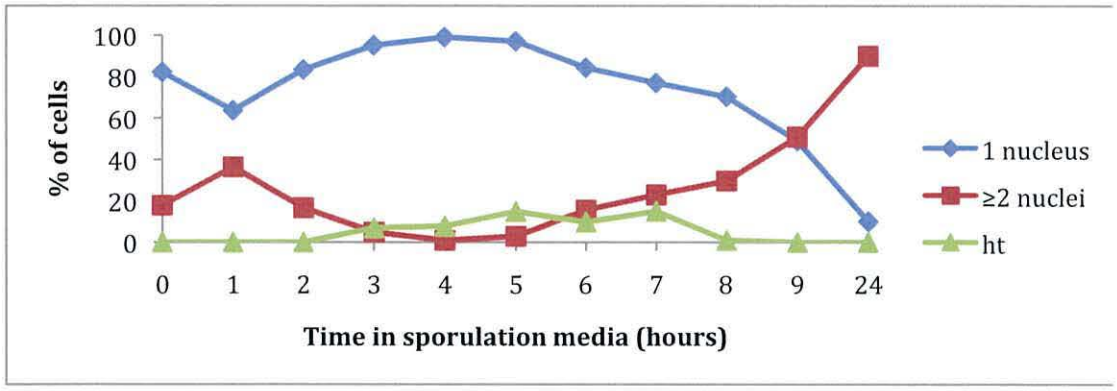

Figure 4.10 Development of LinEs during an asynchronous meiosis of a *rec10-3KR/rec10-3KR* diploid. (**A**) Proportions of LinE classes scored in *rec10⁺/rec10⁺* diploid asynchronous meiosis* **. (**B**) Proportions of LinE classes found in samples taken at hourly intervals after transfer of *rec10-3KR/rec10-3KR* culture to sporulation media. ≥80 nuclei were scored for each time point*. (* - No data was collected for time points 1 and 3 hours; ** These data are a duplication of Figure 4.3A and are represented for case of comparison). (**C**) Analysis of cytological meiotic events in samples taken at hourly intervals after transfer of *rec10-3KR/rec10-3KR* culture to sporulation media. ≥80 nuclei were scored for each time point. ht – horsetail nuclei.

4.2.4 Cytological analysis of LinE formation and development in *rec10* C-terminal *Y→F* mutants

4.2.4a Analysis of LinE formation during a *rec10-Y731F/rec10-Y731F* diploid asynchronous meiosis

Figure 4.11B shows that class Ia LinEs are first observed at 2 hrs during a *rec10-Y731F/rec10-Y731F* asynchronous meiosis. The 4, 5, 6, and 7 hr time points seem to exhibit a similar number (~50%) of Rec10 positively stained LinE structures. The proportions of class Ia, Ib and IIa structures appear to be fairly comparable between 4 – 6 hrs, with class IIa only become slightly more prevalent by 7 hrs. Class IIb structures are present in small (≤5) numbers from 4 – 8 hrs. At 8 hrs, there is a significant increase in the number of Rec10 positively stained LinE structure observed (close to 100% of the nuclei recorded). Class Ib structures are the prominent structures at 8 hrs. At 9 hrs there is a decrease in the number of Rec10 positively stained structures recorded, but an increase in the number of class IIb structures exhibited (~20 nuclei).

In comparison with a *rec10⁺/rec10⁺* asynchronous meiosis (Figure 4.11A), the temporal quantification of LinEs during a *rec10-Y731F/rec10-Y731F* (Figure 4.11B) demonstrates:

- → LinE formation is possibly slightly advanced during the *rec10-Y731F/rec10-Y731F* asynchronous meiosis.
- → The frequency of class IIa LinEs at the earlier (4 hr and 5 hr) time points is much higher during the *rec10-Y731F/rec10-Y731F* asynchronous meiosis.
- → The frequency of class Ib LinEs at 6 hrs and 7 hrs is lower during the *rec10-Y731F/rec10-Y731F* asynchronous meiosis.
- → The frequency of nuclei exhibiting Rec10-posisitve staining is lower at 6 hrs and 7 hrs, during the *rec10-Y731F/rec10-Y731F* asynchronous meiosis.

4.2.4b Analysis of meiotic progression during a *rec10-Y731F/rec10-Y731F* diploid asynchronous meiosis

The last mitotic division is indicated in Figure 4.11C at 1 hrs, with the brief dipping in the number of cells exhibiting only 1 nucleus concomitantly with the increase in cells exhibiting ≥2 nuclei. Figure 4.5C demonstrates that the horsetail stage occurs between 3 – 8 hrs during the *rec10-Y731/rec10-Y731* asynchronous meiosis; peaking at around 5 hrs. Figure 4.11C shows that the first meiotic division begins to occur at around 7 hrs, with meiosis being completed by 24 hrs. In comparison with a *rec10⁺/rec10⁺* asynchronous meiosis (Figure 4.3B), the temporal profile of meiotic nuclei during the *rec10-Y731F/rec10-Y731F* (Figure 4.11C) demonstrates:

→ A possible advancement of the horsetail stage (by around 1 hr), peaking at approximately 5 hrs during the *rec10-Y731F/rec10-Y731F* asynchronous meiosis.

→ A possible advancement (up to 1-2 hrs) in the first meiotic division with cells appearing to begin to divide at approximately 7 hrs during the *rec10-Y731F/rec10-Y731F* asynchronous meiosis.

A

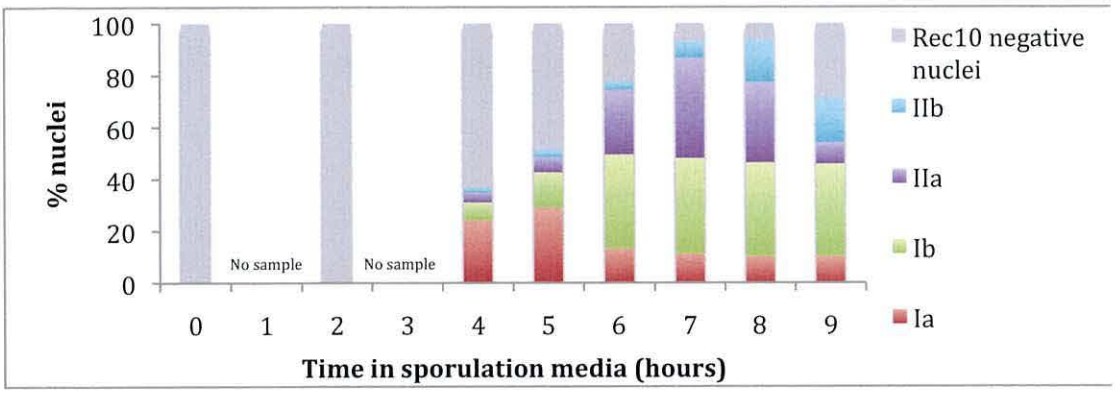

B

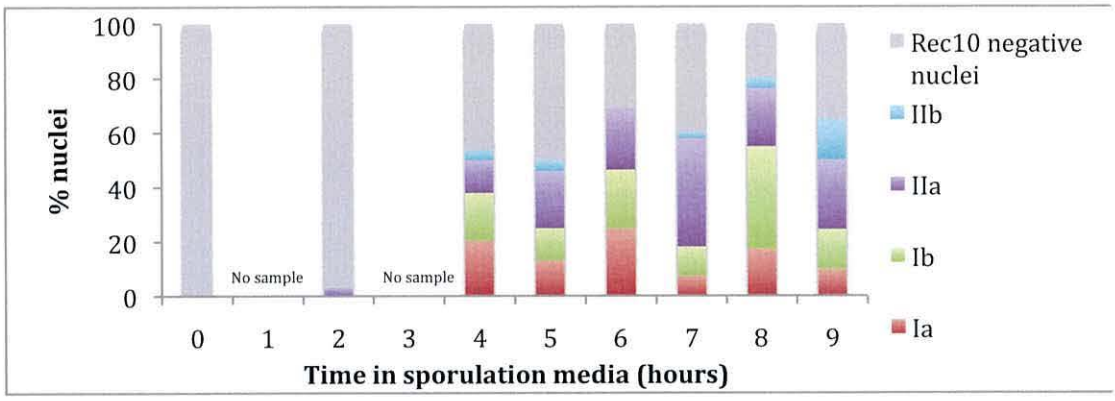

C

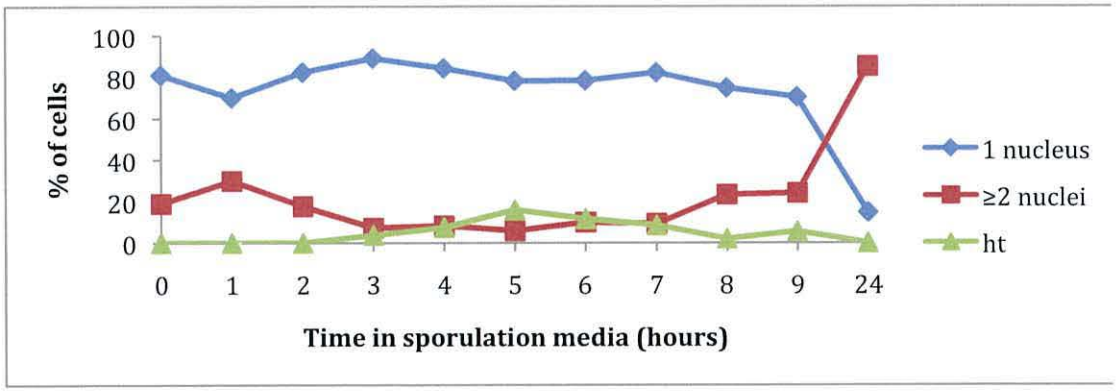

Figure 4.11 Development of LinEs during an asynchronous meiosis of a *rec10-Y731F/rec10-Y731F* diploid. (**A**) Proportions of LinE classes scored in *rec10⁺/rec10⁺* diploid asynchronous meiosis* **. (**B**) Proportions of LinE classes found in samples taken at hourly intervals after transfer of *rec10-Y731F/rec10-Y731F* culture to sporulation media. ≥80 nuclei were scored for each time point*. (* - No data was collected for time points 1 and 3 hours; ** These data are a duplication of Figure 4.3A and are represented for case of comparison). (**C**) Analysis of cytological meiotic events in samples taken at hourly intervals after transfer of *rec10-Y731F/rec10-Y731F* culture to sporulation media. ≥80 nuclei were scored for each time point. ht – horsetail nuclei.

4.2.4c Analysis of LinE formation during a *rec10-Y767F/rec10-Y767F* diploid asynchronous meiosis

Figure 4.12B shows that LinEs are first observed at 2 hrs after transferring the cells to sporulating medium during a *rec10-Y767F/rec10-Y767F* asynchronous meiosis – with a few nuclei exhibiting class IIa and IIb structures. There is an increase in the number of Rec10-positively stained nuclei by 4 hrs, where class Ia, Ib and IIa structures are visible. At 5 hrs, an increase in the number of Rec10-positively stained nuclei is observed; numbers of class Ia and Ib structures have increased, and class IIb structures are exhibited for the first time. The frequency of Rec10-positively stained nuclei increases again at 6 hrs; class Ia is the dominant class here, followed by classes Ib, IIa and IIb respectively. At 7 hrs, 8 hrs and 9 hrs, virtually all recorded nuclei exhibit Rec10-positive staining. Class Ia structures are virtually non-exisitent, and there is a marked increase in the frequency of class Ib and IIa structures – class Ib structures possessing the largest proportion of recorded nuclei. The frequency of class IIb structures remains fairly constant between 5 hrs and 9 hrs.

In comparison with a *rec10⁺/rec10⁺* asynchronous meiosis (Figure 4.12A), the temporal quantification of LinEs during the *rec10-Y767F/rec10-Y767F* (Figure 4.12B) demonstrates:

→ A possible advancement in the formation of LinEs during a *rec10-Y767F/rec10-Y671F* asynchronous meiosis.

→ No decrease in the frequency of Rec10-positively stained nuclei at the later (8 hr and 9 hr) time points, possibly indicative of lack of LinE degradation during a *rec10-Y767F/rec10-Y671F* asynchronous meiosis.

4.2.4d Analysis of meiotic progression during a *rec10-Y767F/rec10-Y767F* diploid asynchronous meiosis

Figure 4.12C shows a peak in horsetail nuclei numbers at approximately 6 hrs (horsetail nuclei being visible between 5 hrs and 7 hrs). The first meiotic division appears to begin at around 7-8 hrs, and meiosis is seen to be complete by 24 hrs. The last mitotic division is indicated at 1 hrs by the reduction of cells exhibiting 1 nucleus, and the increase in cells exhibiting ≥2 nuclei.

In comparison with a *rec10⁺/rec10⁺* asynchronous meiosis (Figure 4.3B), the temporal profile of meiotic nuclei during the *rec10-Y767F/rec10-Y767F* (Figure 4.12C) demonstrates:

→ Possibly a more compact horsetail stage during a *rec10-Y767F/rec10-Y767F* asynchronous meiosis – peaking at 6 hrs, but only visible between 5 hrs and 7 hrs.

→ A possible advancement in the first meiotic division, with cells appearing to begin to divide by 7 hrs, and with approximately 40% (as opposed to ~15% observed in wild-type) of cells exhibiting ≥2 nuclei by 9 hrs.

A

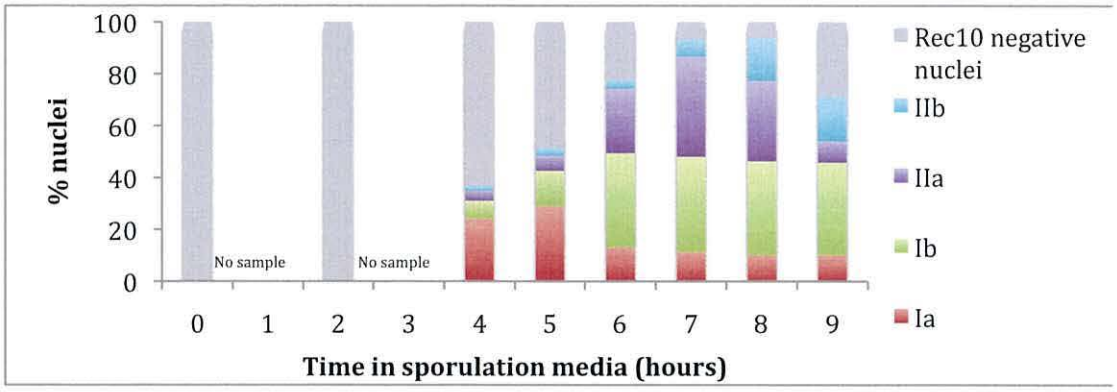

B

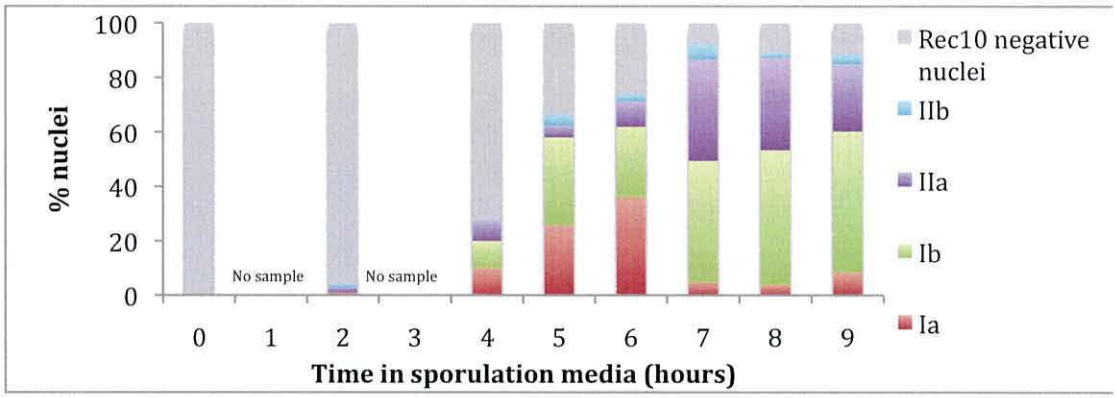

C

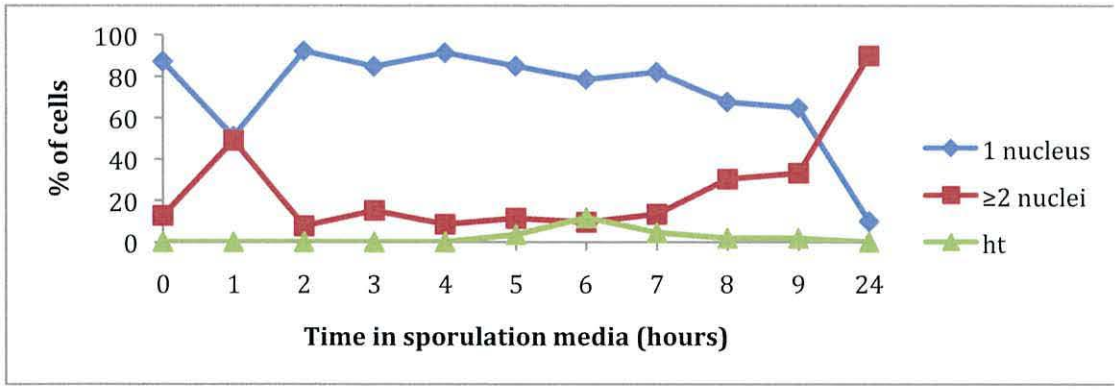

Figure 4.12 Development of LinEs during an asynchronous meiosis of a *rec10-Y767F/rec10-Y767F* diploid. (**A**) Proportions of LinE classes scored in *rec10⁺/rec10⁺* diploid asynchronous meiosis* **. (**B**) Proportions of LinE classes found in samples taken at hourly intervals after transfer of *rec10-Y767F/rec10-Y767F* culture to sporulation media. ≥80 nuclei were scored for each time point*. (* - No data was collected for time points 1 and 3 hours; ** These data are a duplication of Figure 4.3A and are represented for case of comparison). (**C**) Analysis of cytological meiotic events in samples taken at hourly intervals after transfer of *rec10-Y767F/rec10-Y767F* culture to sporulation media. ≥80 nuclei were scored for each time point. ht – horsetail nuclei.

4.2.4e Analysis of LinE formation during a *rec10-2YF/rec10-2YF* diploid asynchronous meiosis

Figure 4.13B shows LinE development during a *rec10-2YF/rec10-2YF* asynchronous meiosis. It shows classes Ia, Ib and IIa LinEs first appearing at 2 hrs. Class IIb structures appear by 4 hrs, where classes Ia, Ib and IIa seem to have a fairly equal proportion of the Rec10-positively stained nuclei recorded (~15 each). The number of Rec10-positively stained nuclei remains fairly constant between 4 hrs and 5 hrs, although no class IIb structures are observed at 5 hrs. At 6 hrs, class IIb structures reappear, alongside an increase in the frequency of Rec10-positively stained nuclei recorded. Rec10-positively stained nuclei account for virtually all nuclei recorded at 7 hrs and 8 hrs. There are very few class Ia and class IIb structures observed at either time point, and a prevalence of class IIa structures is very apparent. The frequency of Rec10-positively stained nuclei has decreased somewhat by 9 hrs; no class IIb structures were recorded, and class Ib structures appear to be most prominent.

In comparison with a *rec10⁺/rec10⁺* asynchronous meiosis (Figure 4.13A), the temporal quantification of LinEs during a *rec10-2YF/rec10-2YF* (Figure 4.13B) demonstrates:

- → A possible advancement in the formation of LinEs during a *rec10-2YF/rec10-2YF* asynchronous meiosis.
- → A virtual absence (7 hrs and 8 hrs) and complete absence (9 hrs) of nuclei exhibiting class IIb LinEs.
- → An increased frequency of nuclei exhibiting class IIa LinEs at 7 hrs and 8 hrs.

4.2.4f Analysis of meiotic progression during a *rec10-2YF/rec10-2YF* diploid asynchronous meiosis

Figure 4.13C shows that the horsetail stage takes place between 2 hrs and 6 hrs – peaking at approximately 3-4 hrs. The last mitotic division is signified at 1 hr. The first meiotic division appears to begin at approximately 8 hrs, however by 24 hrs, meiosis does not seem to have been completed in all nuclei.

In comparison with a *rec10⁺/rec10⁺* asynchronous meiosis (Figure 4.3B), the temporal profile of meiotic nuclei during a *rec10-2YF/rec10-2YF* (Figure 4.13C) demonstrates:

→ A possible advancement (2-3 hrs) in the horsetail stage during a *rec10-2YF/rec10-2YF* asynchronous meiosis.

→ A possible advancement (approximately 1 hr) of the first meiotic division during a *rec10-2YF/rec10-2YF* asynchronous meiosis.

A

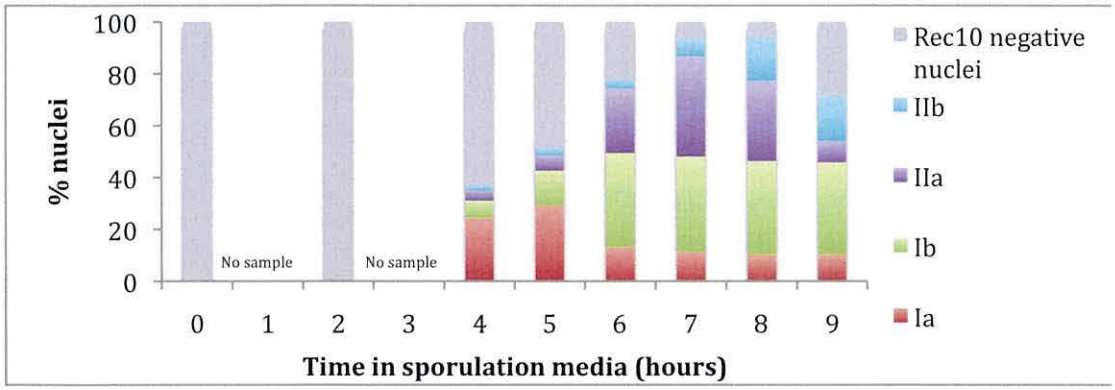

B

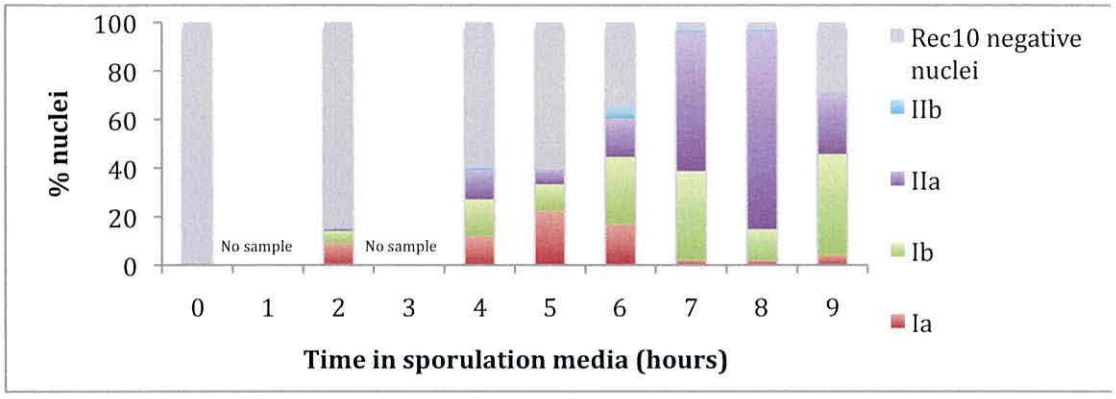

C

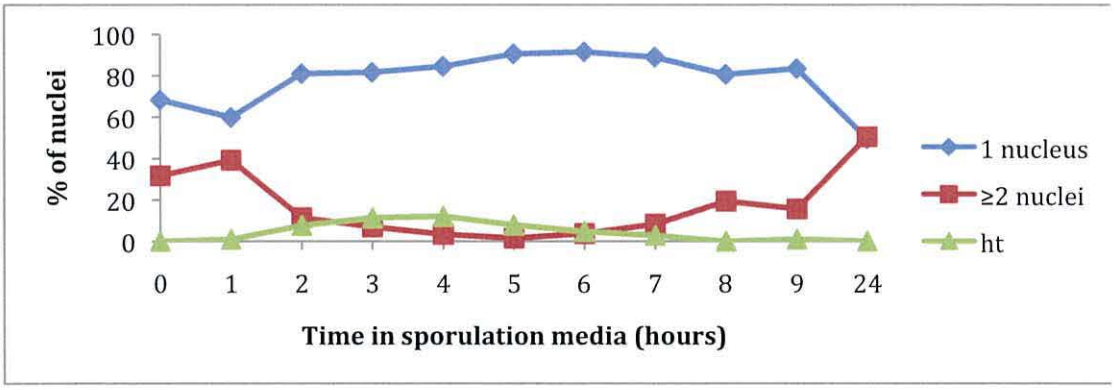

Figure 4.13 Development of LinEs during an asynchronous meiosis of a *rec10-2YF/rec10-2YF* diploid. (**A**) Proportions of LinE classes scored in *rec10⁺/rec10⁺* diploid asynchronous meiosis* **. (**B**) Proportions of LinE classes found in samples taken at hourly intervals after transfer of *rec10-2YF/rec10-2YF* culture to sporulation media. ≥80 nuclei were scored for each time point*. (* - No data was collected for time points 1 and 3 hours; ** These data are a duplication of Figure 4.3A and are represented for case of comparison). (**C**) Analysis of cytological meiotic events in samples taken at hourly intervals after transfer of *rec10-2YF/rec10-2YF* culture to sporulation media. ≥80 nuclei were scored for each time point. ht – horsetail nuclei.

4.2.5 Cytological quantification of Rad51 foci in *rec10* C-terminal *K→R* mutants

Quantifying Rad51 staining in *rec10* C-terminal mutants involves comparing their temporal profiles against that of a *rec10+* profile. In this study the temporal profiles of Rad51 staining were composed on a temporal profile of LinE development. The mutants studied have differing basic LinE temporal profiles, as does the *rec10⁺* strain – this complicates the process of comparing their respective quantifications. Therefore, in this study we aim to visually compare the general trend of Rad51 foci quantification seen in *rec10* C-terminal mutants *vs.* the *rec10⁺* profile, outlining any significant fluctuations observed.

We define co-staining of Rec10 and Rad51 as nuclei exhibiting both Rec10 and Rad51 staining. Co-staining does not signify co-localisation of the immuno-fluoresced foci.

4.2.5a Temporal quantification of Rad51 foci during a *rec10-K712R/rec10-K712R* diploid asynchronous meiosis

Figure 4.14A demonstrates that Rad51 foci are first observed concomitantly with Rec10-positively stained structures at 4 hrs. Nuclei containing all classes of Rec10-positively stained LinEs exhibit some degree of Rad51 co-staining at each time point. Nuclei exhibiting class IIa and IIb LinEs exhibit the highest percentage of Rad51 co-staining at all time points.

In comparison with a *rec10⁺/rec10⁺* asynchronous meiosis (Figure 4.5A), the temporal quantification of Rad51 foci during a *rec10-K712R/rec10-K712R* (Figure 4.14A) demonstrates:

→ A much higher frequency of Rad51 co-staining in nuclei exhibiting class Ia LinEs at 4 hrs, 6 hrs and 7 hrs.

A

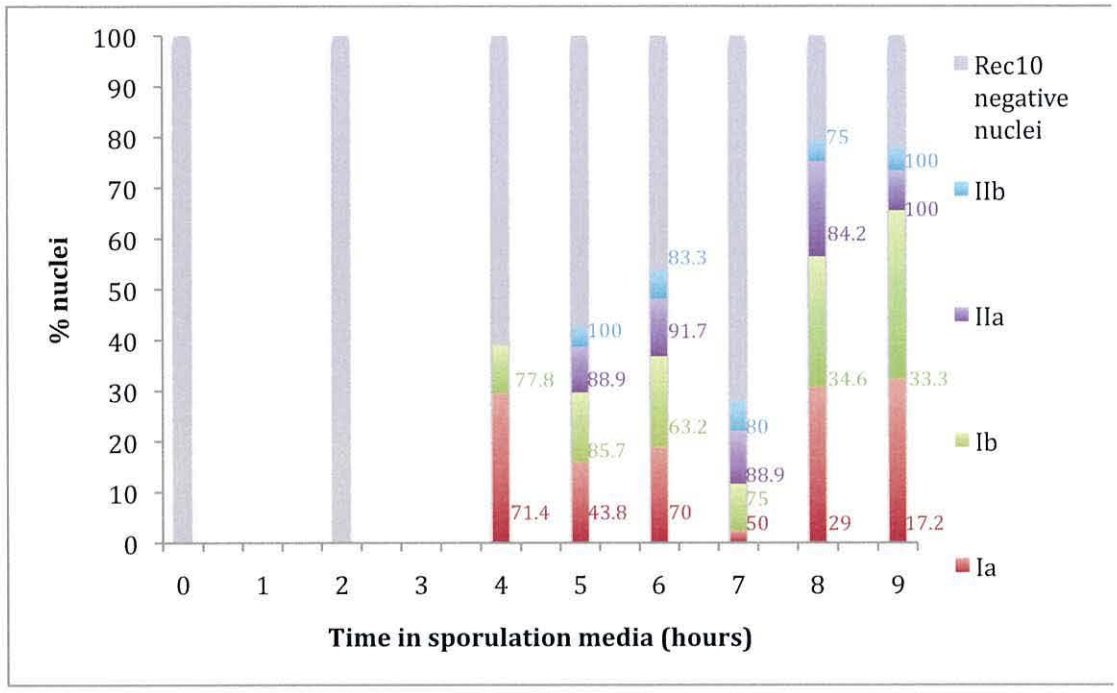

B

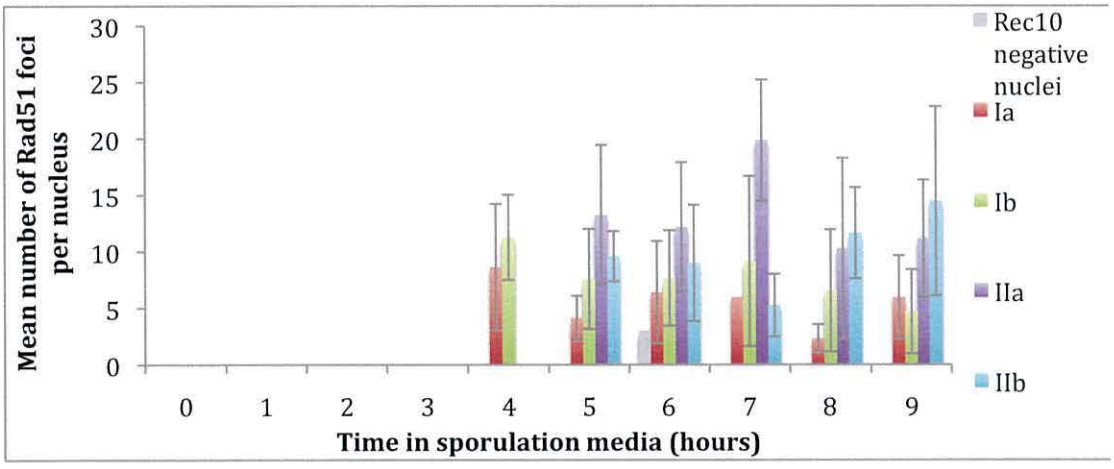

Figure 4.14 Quantification of Rad51 staining during an asynchronous meiosis of a *rec10-K712R/rec10-K712R* diploid. (**A**) Proportions of LinE classes found in samples taken at hourly intervals after transfer to sporulation media. ≥80 nuclei were recorded for each time point. Numbers adjacent to each column represent the % nuclei scored exhibiting Rad51 and Rec10 co-staining, with the colours representing LinE classes. Absence of a number indicates 0%. (**B**) Mean number of Rad51 foci scored in each nucleus exhibiting Rec10 and Rad51 co-staining. Error bars represent a 95% confidence interval in all cases.

4.2.5b Temporal quantification of Rad51 foci during a *rec10-K744R/rec10-K744R* diploid asynchronous meiosis

Figure 4.15A shows that Rad51 foci appear concomitantly with Rec10-positively stained LinE structures, at 4 hrs. There is a low percentage of Rad51 staining observed in Rec10 negative nuclei at 4 hrs (3.7%). Rad51 staining is absent in nuclei exhibiting class IIb LinEs at 7 hrs and 9 hrs, and in class Ia LinE nuclei at 9 hrs. Nuclei containing class Ib structures appear to exhibit a steady decrease in the frequency of Rad51 co-stained nuclei from 6 hrs onwards, similar to nuclei containing class IIa LinEs.

In comparison with a *rec10⁺/rec10⁺* asynchronous meiosis (Figure 4.5A), the temporal quantification of Rad51 foci during a *rec10-K744R/rec10-K744R* (Figure 4.15A) demonstrates:

→ Lack of Rad51 foci in nuclei exhibiting class IIb structures at 7 hrs and 9 hrs, as well as in nuclei containing class Ia structures at 9 hrs.

→ A lower frequency of Rad51 staining in class IIb structures at 5 hrs and 6 hrs.

→ A reduction in the frequency of Rad51 co-staining in nuclei exhibiting each class of LinEs by 9 hrs – possibly indicative of earlier Rad51 degradation/dissociation.

→ In general, a lower frequency of Rad51/Rec10 co-stained nuclei.

A

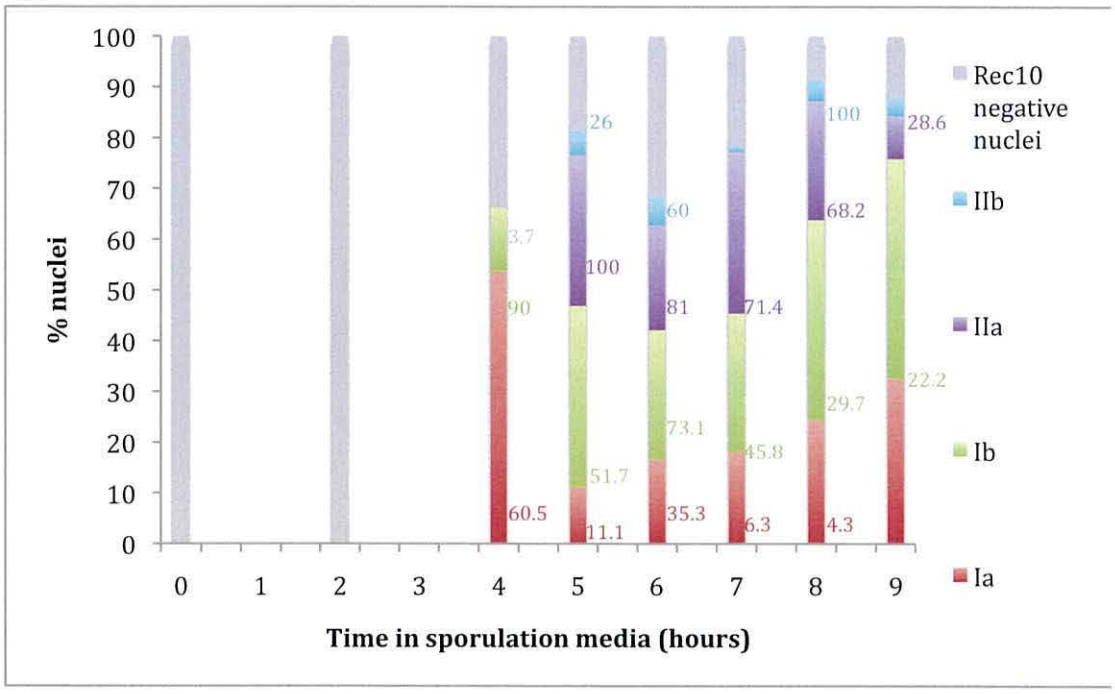

B

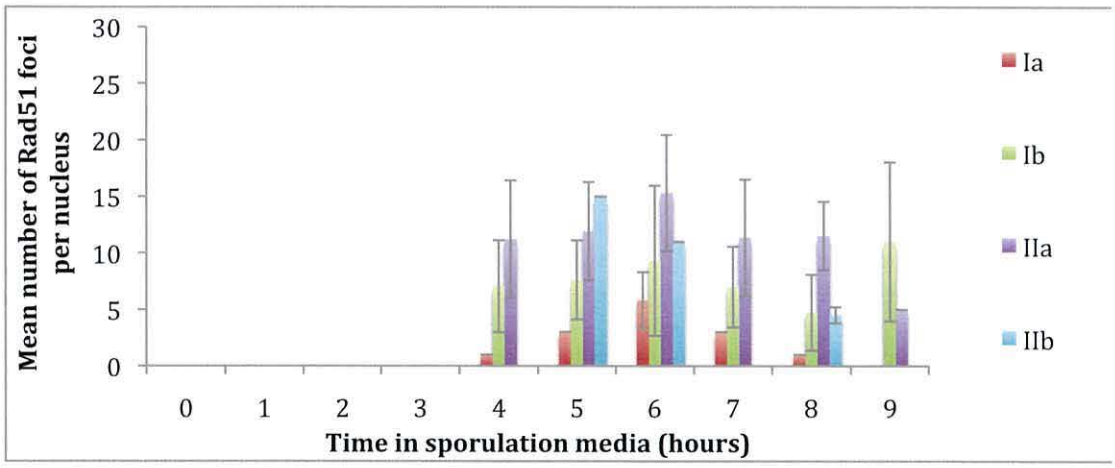

<u>Figure 4.15</u> Quantification of Rad51 staining during an asynchronous meiosis of a *rec10-K744R/rec10-K744R* diploid. (**A**) Proportions of LinE classes found in samples taken at hourly intervals after transfer to sporulation media. ≥80 nuclei were recorded for each time point. Numbers adjacent to each column represent the % nuclei scored exhibiting Rad51 and Rec10 co-staining, with the colours representing LinE classes. Absence of a number indicates 0%. (**B**) Mean number of Rad51 foci scored in each nucleus exhibiting Rec10 and Rad51 co-staining. Error bars represent a 95% confidence interval in all cases.

4.2.5c Temporal quantification of Rad51 foci during a *rec10-K754R/rec10-K754R* diploid asynchronous meiosis

Figure 4.16 shows that Rad51 foci appear at the same time Rec10-positively stained structures are first visible, 4hrs. Rad51 foci are observed in nuclei exhibiting each class of LinE at every time point. The general trend of Rad51 staining appears to be a reduction in Rad51 co-stained nuclei between 4 hrs and 6 hrs, then between the 6 hrs and 9 hrs the frequency of Rad51/Rec10 co-stained nuclei appears to increase once more.

In comparison with a *rec10⁺/rec10⁺* asynchronous meiosis (Figure 4.5A), the temporal quantification of Rad51 foci during a *rec10-K754R/rec10-K754R* (Figure 4.16A) demonstrates:

→ A higher frequency of Rad51/Rec10 co-stained nuclei observed at 4 hrs during a *rec10-K754R/rec10-K754R* asynchronous meiosis.

→ A reduced frequency of Rad51/Rec10 co-stained nuclei at 6 hr in comparison with a *rec10⁺/rec10⁺*.

A

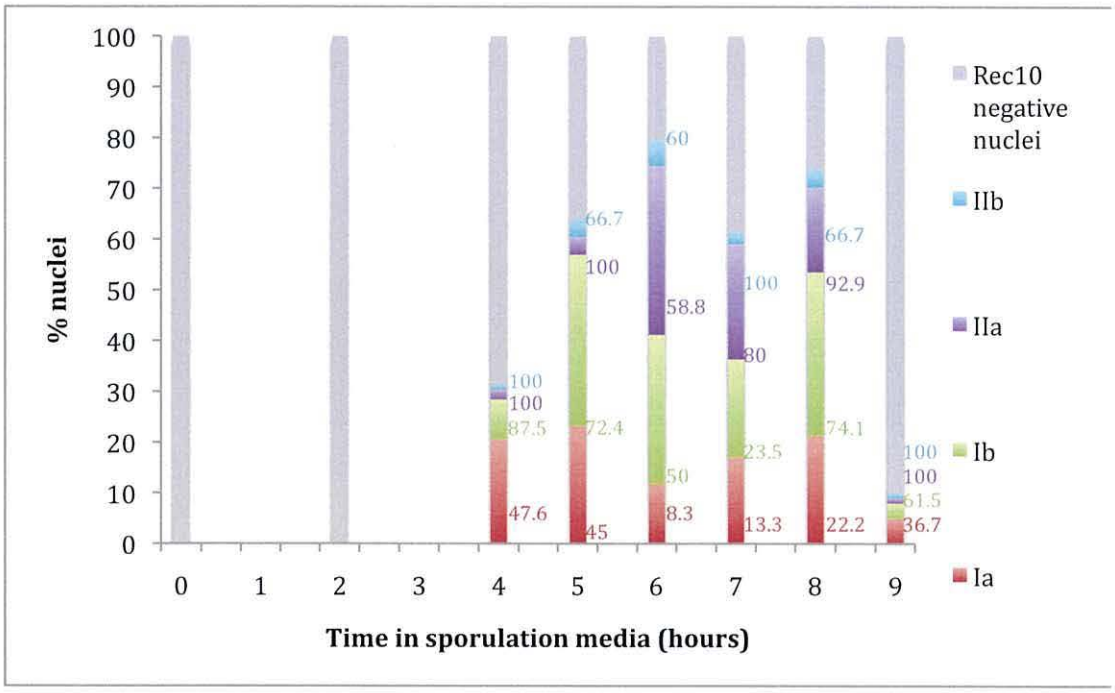

B

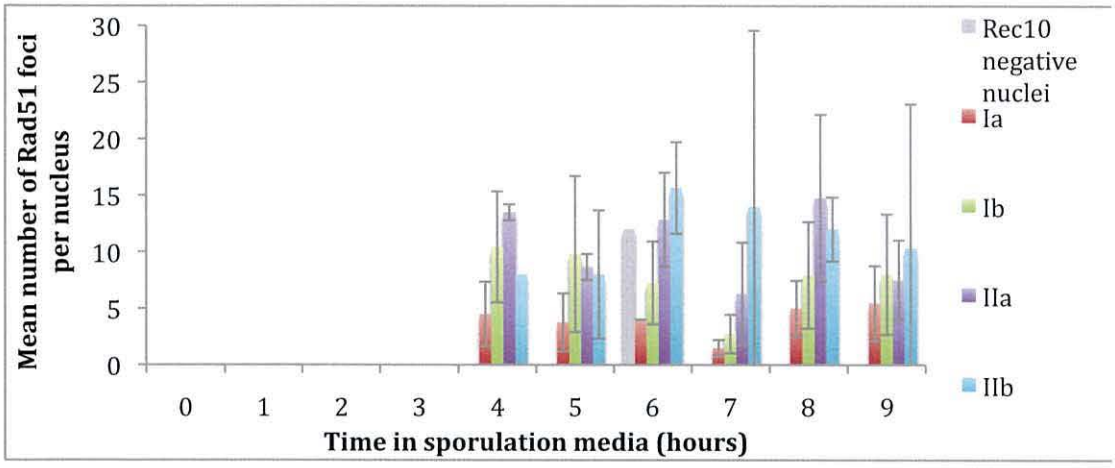

<u>Figure 4.16</u> Quantification of Rad51 staining during an asynchronous meiosis of a *rec10-K754R/rec10-K754R* diploid. (**A**) Proportions of LinE classes found in samples taken at hourly intervals after transfer to sporulation media. ≥80 nuclei were recorded for each time point. Numbers adjacent to each column represent the % nuclei scored exhibiting Rad51 and Rec10 co-staining, with the colours representing LinE classes. Absence of a number indicates 0%. (**B**) Mean number of Rad51 foci scored in each nucleus exhibiting Rec10 and Rad51 co-staining. Error bars represent a 95% confidence interval in all cases

4.2.5d Temporal quantification of Rad51 foci during a *rec10-K757R/rec10-K757R* diploid asynchronous meiosis

Figure 4.17 demonstrates the appearance of Rad51 foci at 2 hr in the *rec10-K757R/rec10-K757R* mutant, concomitant with the first appearance of Rec10 positively stained structures. Rad51 staining is not observed in nuclei exhibiting class IIb LinEs at 5 hrs. Nuclei containing class Ia LinEs exhibit the lowest frequency of Rad51 co-staining throughout the time course, with the exception of 8 hrs. The frequency of Rad51 co-stained nuclei remains fairly constant in nuclei exhibiting class Ib structures, and in nuclei exhibiting class IIa LinEs.

In comparison with a *rec10⁺/rec10⁺* asynchronous meiosis (Figure 4.5A), the temporal quantification of Rad51 foci during a *rec10-K757R/rec10-K757R* (Figure 4.17A) demonstrates:

→ Rad51 foci appear earlier, at 2 hrs, during a *rec10-K757R/rec10-K757R* asynchronous meiosis – although Rec10 positively stained structures are also observed at 2 hr in this mutant.

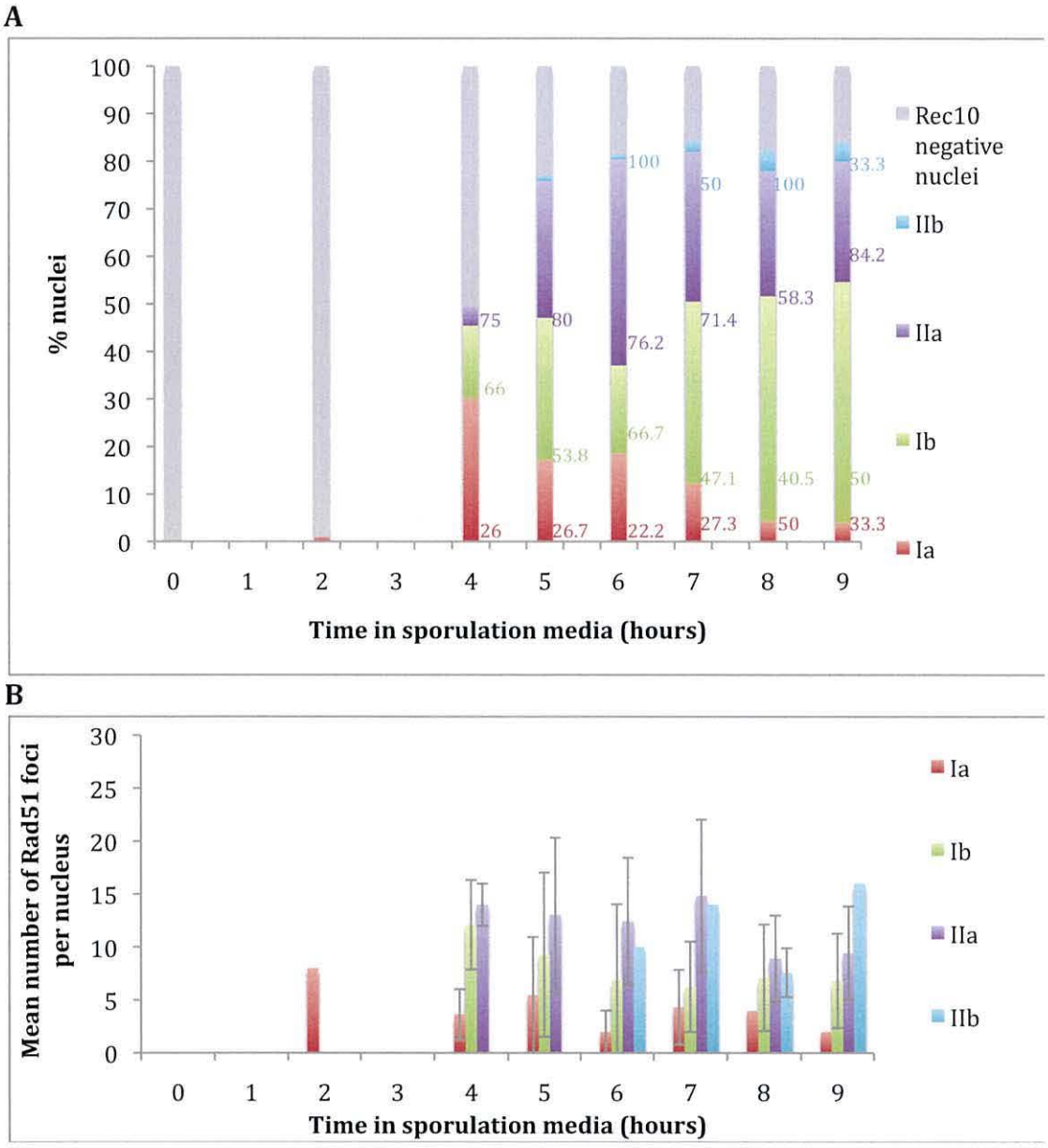

Figure 4.17 Quantification of Rad51 staining during an asynchronous meiosis of a *rec10-K757R/rec10-K757R* diploid. (**A**) Proportions of LinE classes found in samples taken at hourly intervals after transfer to sporulation media. ≥80 nuclei were recorded for each time point. Numbers adjacent to each column represent the % nuclei scored exhibiting Rad51 and Rec10 co-staining, with the colours representing LinE classes. Absence of a number indicates 0%. (**B**) Mean number of Rad51 foci scored in each nucleus exhibiting Rec10 and Rad51 co-staining. Error bars represent a 95% confidence interval in all cases.

4.2.5e Temporal quantification of Rad51 foci during a *rec10-3KR/rec10-3KR* diploid asynchronous meiosis

Figure 4.18 demonstrates that Rad51 foci appear at 4 hrs, although Rec10-positively stained structures were recorded earlier at 2 hrs. Rad51 staining is not observed in nuclei containing class Ia LinEs at 8 hrs.

In comparison with a *rec10⁺/rec10⁺* asynchronous meiosis (Figure 4.5A), the temporal quantification of Rad51 foci during a *rec10-3KR/rec10-3KR* (Figure 4.18A) demonstrates:

→ Rad51 foci appear later than Rec10-positively stained structures during a *rec10-3KR/rec10-3KR* asynchronous meiosis.

A

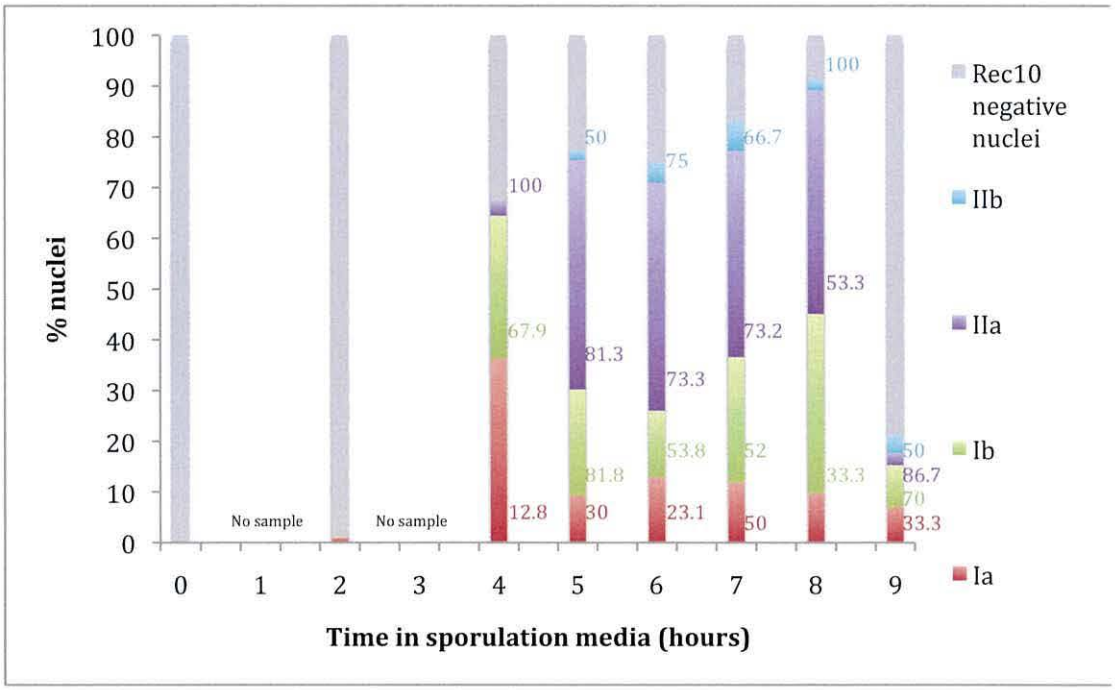

B

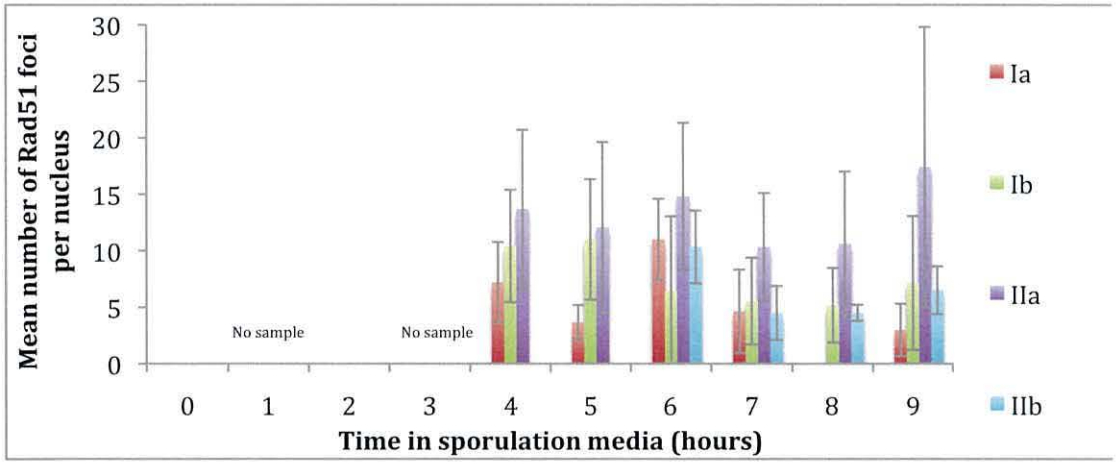

<u>Figure 4.18</u> Quantification of Rad51 staining during an asynchronous meiosis of a *rec10-3KR/rec10-3KR* diploid. (**A**) Proportions of LinE classes found in samples taken at hourly intervals after transfer to sporulation media. ≥80 nuclei were recorded for each time point. Numbers adjacent to each column represent the % nuclei scored exhibiting Rad51 and Rec10 co-staining, with the colours representing LinE classes. Absence of a number indicates 0%. (**B**) Mean number of Rad51 foci scored in each nucleus exhibiting Rec10 and Rad51 co-staining. Error bars represent a 95% confidence interval in all cases.

4.2.6 Cytological quantification of Rad51 foci in *rec10* C-terminal *Y→F* mutants

4.2.6a Temporal quantification of Rad51 foci during a *rec10-Y731F/rec10-Y731F* asynchronous meiosis

Figure 4.19A indicates that the Rad51 foci do not appear until 4 hrs after transfer of cells into sporulating medium, whilst Rec10-positively stained nuclei are present at the 2 hr time point. Nuclei exhibiting class Ia LinEs are observed to have the lowest proportion of Rad51 co-staining out of all the classes, apart from at 9 hrs. Nuclei exhibiting class Ib, IIa and IIb LinEs appear to have a fairly consistent, high proportion of Rad51 co-staining the exceptions to this being class Ib nuclei at 6 hrs and 9 hrs and class IIa nuclei at 7 hrs – both exhibiting slightly lower Rad51/Rec10 co-stained nuclei than at other time points. At 8 hrs, a decrease in the proportion of Rad51/Rec10 co-stained nuclei is seen in nuclei exhibiting all classes of LinEs. 10% of the nuclei exhibiting Rec10-negative staining appear to have Rad51 staining at 5 hrs.

In comparison with a *rec10⁺/rec10⁺* asynchronous meiosis (Figure 4.5A), the temporal quantification of Rad51 foci during a *rec10-Y731F/rec10-Y731F* (Figure 4.19A) demonstrates:

- → That there are higher numbers of class Ia LinE-containing-nuclei exhibiting both Rec10 and Rad51 staining at early (4 hrs and 5 hrs) and late (9hr) time points during the *rec10-Y731F/rec10-Y731F* asynchronous meiosis.
- → That there is a lack of Rad51 staining in nuclei exhibiting class IIb LinEs at 4 hrs during the *rec10-Y731F/rec10-Y731F* asynchronous meiosis.
- → That a small number (10%) of Rec10-negatively stained nuclei exhibiting Rad51 co-staining at 5 hr during the *rec10-Y731F/rec10-Y731F* asynchronous meiosis.
- → That we first observe Rad51 foci appears at the 4 hr time point (although they may be present at 3 hrs), even though Rec10-staining is observed at the 2 hr time point during the *rec10-Y731F/rec10-Y731F* asynchronous meiosis. This infers a separation of timing for Rec10/Rad51 localisation.

Figure 4.19B appears to demonstrate that nuclei exhibiting class Ib and IIa LinEs have the highest number of Rad51 foci at 4-6 hrs. At 7-9 hrs more mature class IIa and IIb LinEs contain the highest number of Rad51 foci. Nuclei exhibiting class Ia structures consistently contain the least number of Rad51 foci out of all classes.

A

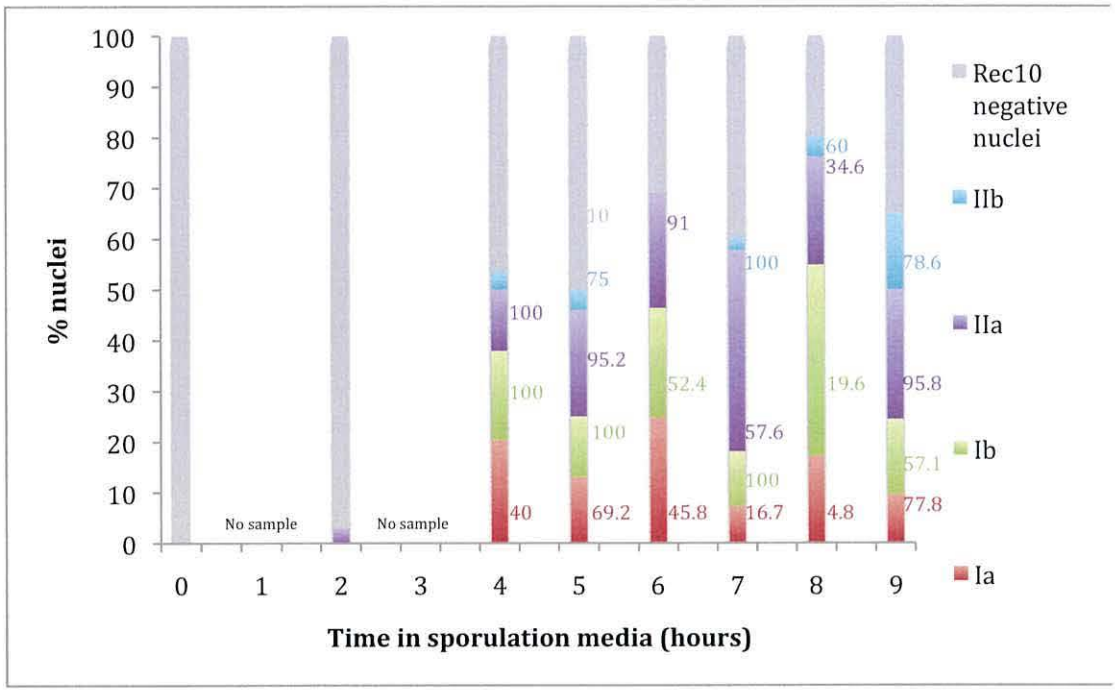

B

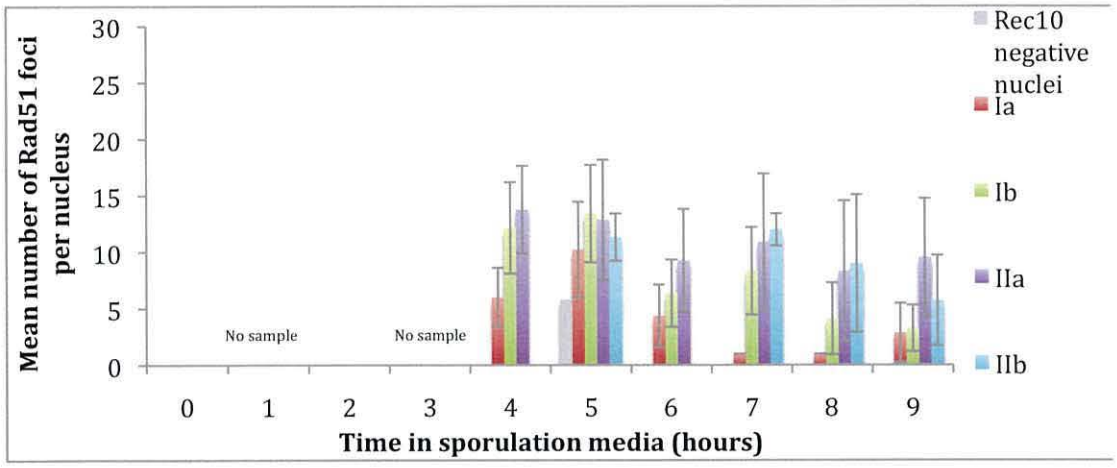

<u>Figure 4.19</u> Quantification of Rad51 staining during an asynchronous meiosis of a *rec10-Y731F/rec10-Y731F* diploid. (**A**) Proportions of LinE classes found in samples taken at hourly intervals after transfer to sporulation media. ≥80 nuclei were recorded for each time point. Numbers adjacent to each column represent the % nuclei scored exhibiting Rad51 and Rec10 co-staining, with the colours representing LinE classes. Absence of a number indicates 0%. (**B**) Mean number of Rad51 foci scored in each nucleus exhibiting Rec10 and Rad51 co-staining. Error bars represent a 95% confidence interval in all cases.

4.2.6b Temporal quantification of Rad51 foci during a *rec10-Y767F/rec10-Y767F* asynchronous meiosis

The temporal quantification of the appearance of Rad51 foci during a *rec10-Y767F/rec10-Y767F* asynchronous meiosis (Figure 4.20A) demonstrates that nuclei exhibiting Rec10-positive staining appear earlier (2 hrs) than nuclei exhibiting Rad51 staining (by 4 hrs). From 4 hrs onwards Rad51 staining is observed at each time point to some degree in nuclei exhibiting all classes of LinEs. When present, nuclei exhibiting class IIb LinEs observe the highest frequency of Rad51 co-staining with the exception of 5 hrs, where nuclei exhibiting class Ia LinEs have the lowest proportion of Rad51 co-staining (Figure 4.20A).

In comparison with a *rec10⁺/rec10⁺* asynchronous meiosis (Figure 4.5A), the temporal quantification of Rad51 foci during a *rec10-Y767F/rec10-Y767F* (Figure 4.20A) demonstrates:

→ That there is a higher number of class Ia LinE-containing-nuclei exhibiting both Rec10 and Rad51 staining at early (4 hrs and 5 hrs) and late (9hr) time points during the *rec10-Y767F/rec10-Y767F* asynchronous meiosis.

→ That a small number (14.3%) of Rec10-negatively stained nuclei exhibit Rad51 co-staining at 5 hrs during the *rec10-Y767F/rec10-Y767F* asynchronous meiosis.

→ That no Rad51 co-staining is apparent in nuclei exhibiting class IIb LinEs at 6 hrs during the *rec10-Y767F/rec10-Y767F* asynchronous meiosis.

→ The first appearance of Rad51 foci is observed to be at 4 hrs (they may be present at 3 hrs), even though LinEs are observed at the 2 hr time point during the *rec10-Y767F/rec10-Y767F* asynchronous meiosis. This demonstrates a difference in the timing of Rec10 and Rad51 localisation.

Figure 4.20B appears to demonstrate that nuclei exhibiting class Ib and IIa LinEs have the highest number of Rad51 foci at 4-6 hrs. At 7-9 hrs more mature class IIa and IIb LinEs contain the highest number of Rad51 foci. Nuclei exhibiting class Ia structures consistently contain the lowest number of Rad51 foci.

A

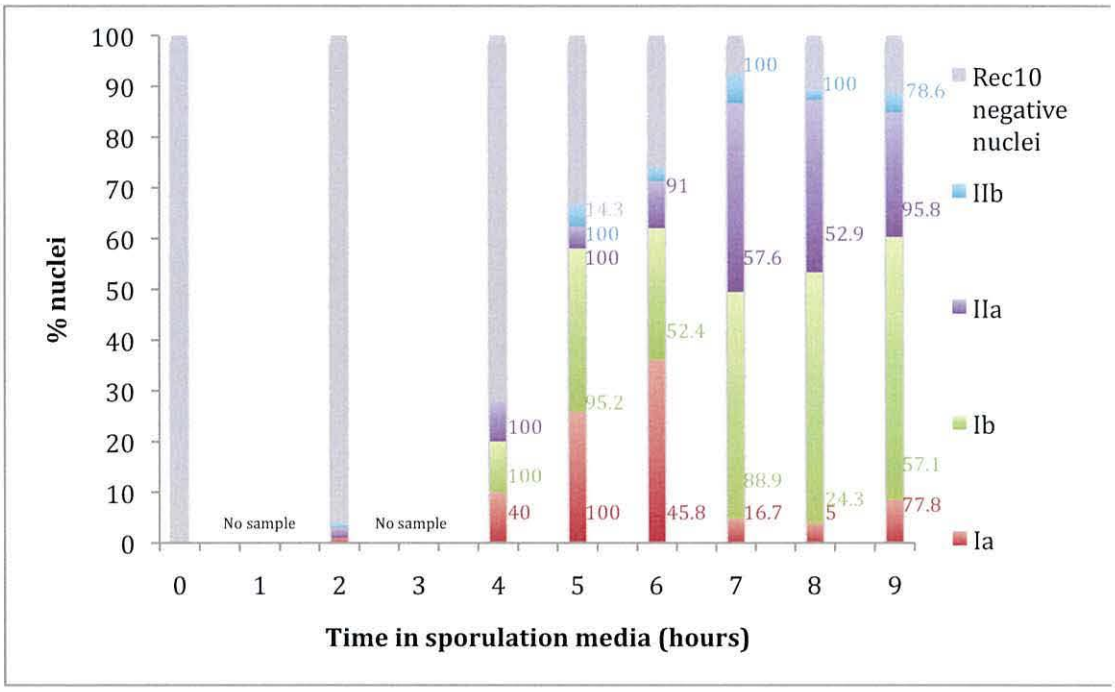

B

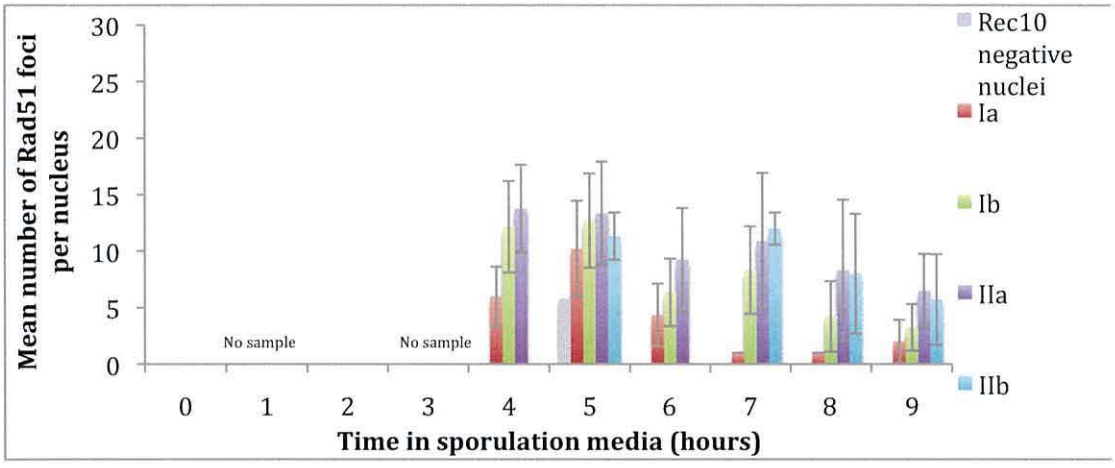

Figure 4.20 Quantification of Rad51 staining during an asynchronous meiosis of a *rec10-Y767F/rec10-Y767F* diploid. (**A**) Proportions of LinE classes found in samples taken at hourly intervals after transfer to sporulation media. ≥80 nuclei were recorded for each time point. Numbers adjacent to each column represent the % nuclei scored exhibiting Rad51 and Rec10 co-staining, with the colours representing LinE classes. Absence of a number indicates 0%. (**B**) Mean number of Rad51 foci scored in each nucleus exhibiting Rec10 and Rad51 co-staining. Error bars represent a 95% confidence interval in all cases.

4.2.6c Temporal quantification of Rad51 foci during a *rec10-2YF/rec10-2YF* asynchronous meiosis

Figure 4.21A demonstrates that Rad51 foci appear at 4 hrs, whilst Rec10-positively stained LinE structures appear earlier at 2 hrs during a *rec10-Y731F/rec10-Y731F* asynchronous meiosis. The highest proportion of nuclei exhibiting both Rad51 and Rec10 staining appear at 4 hrs and 5 hrs, with virtually all Rec10-postitively stained nuclei also exhibiting Rad51 staining (4.21A). Nuclei exhibiting class Ia LinEs appear to have no Rad51 co-staining from 7 hrs onwards (Figure 4.21A).

In comparison with a *rec10⁺/rec10⁺* asynchronous meiosis (Figure 4.5A), the temporal quantification of Rad51 foci during a *rec10-2YF/rec10-2YF* (Figure 4.21A) demonstrates:

- → That no Rad51 co-staining in nuclei exhibiting class Ia LinEs at 7-9 hrs during the *rec10-2YF/rec10-2YF* asynchronous meiosis.
- → That no Rad51 co-staining in nuclei exhibiting class IIb LinEs at 4 hrs during the *rec10-2YF/rec10-2YF* asynchronous meiosis.
- → That the first Rad51 foci are observed at 4 hrs (not ruling out the possibility that Rad51 foci may be present at 3 hrs), even though LinEs are observed at 2 hrs during the *rec10-Y767F/rec10-Y767F* asynchronous meiosis. This points towards a difference in the timing of Rec10 and Rad51 localisation.
- → A higher frequency of Rad51 staining is apparent in nuclei exhibiting class Ia and Ib LinEs at 4 hrs and 5 hr during the *rec10-2YF/rec10-2YF* asynchronous meiosis.

Figure 4.21B shows that nuclei exhibiting class Ia, Ib and IIa LinEs appear to contain a similar number of Rad51 foci at 4 hrs and 5 hrs. The highest number of Rad51 foci is observed in nuclei containing class IIa and IIb LinEs at 6 hrs and 8 hrs.

A

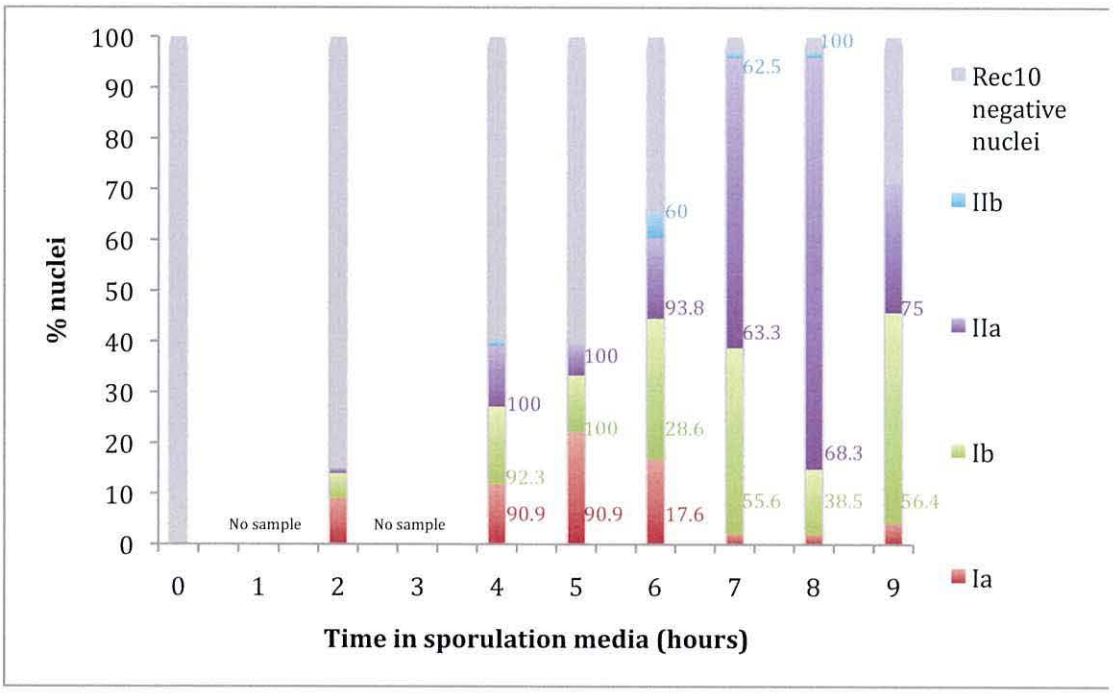

B

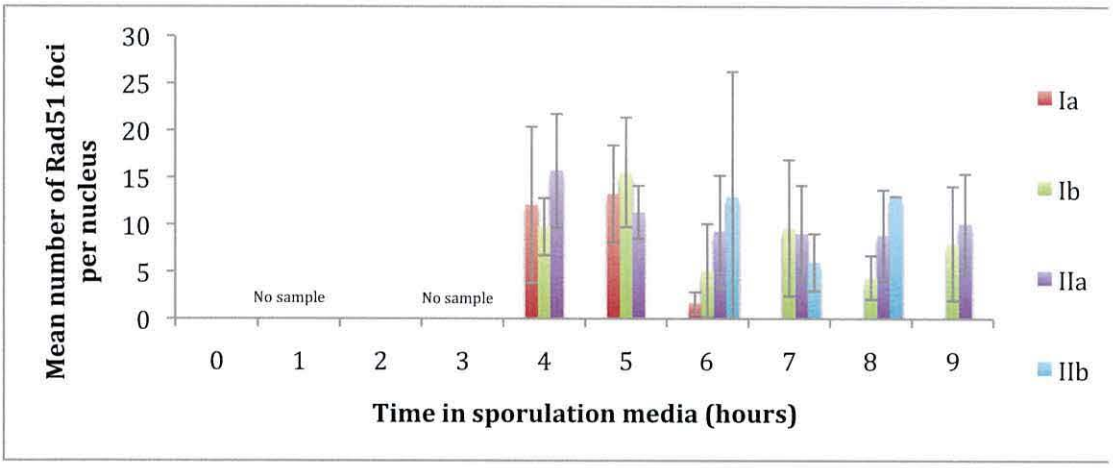

<u>Figure 4.21</u> Quantification of Rad51 staining during an asynchronous meiosis of a *rec10-2YF/rec10-2YF* diploid. (**A**) Proportions of LinE classes found in samples taken at hourly intervals after transfer to sporulation media. ≥80 nuclei were recorded for each time point. Numbers adjacent to each column represent the % nuclei scored exhibiting Rad51 and Rec10 co-staining, with the colours representing LinE classes. Absence of a number indicates 0%. (**B**) Mean number of Rad51 foci scored in each nucleus exhibiting Rec10 and Rad51 co-staining. Error bars represent a 95% confidence interval in all cases.

4.3 Discussion

A summary of *rec10* C-terminal LinE profiles can be seen in Table 5.9.

4.3.1 Effect of *rec10* C-terminal mutants on the temporal development and formation of LinEs

Altered temporal profiles of LinE formation and development are exhibited for all *rec10* C-terminal mutants studied in this chapter compared to a *rec10*$^{+}$ temporal LinE profile.

4.3.2 Analysis of LinE formation in *rec10* C-terminal *Y→F* mutants

All three *rec10* C-terminal *Y→F* mutants studied in this chapter exhibit subtle differences (to varying extents) in the temporal profile of LinE formation and development during an asynchronous meiosis relative to a *rec10*$^{+}$ profile.
Class Ia, Ib, IIa and IIb LinEs are all exhibited in each mutant, with their respective morphologies being comparative to that seen in *rec10*$^{+}$ nuclei.
The temporal nature of LinE formation and subsequent development, and the frequency of the different LinE classes at each time point, both appear to be affected during an asynchronous meiosis of any of the three *rec10* C-terminal Y→F mutants, albeit to a limited extent.
LinEs first appear earlier in all three mutants (at the 2 hr time point) as compared to *rec10*$^{+}$ where LinEs first appear at 4 hrs.

4.3.2a Timing of LinE appearance in *rec10* C-terminal Y→F mutants

Three of the *rec10* C-terminal mutants studied in this chapter exhibit advancement in the appearance of LinEs when compared to *rec10*$^{+}$: *rec10-Y31F*, *rec10-Y767F* and *rec10-2YF*. LinEs are first apparent at 2 hrs in all three of these mutants, in comparison with LinE appearance first visualised at 4 hrs in *rec10*$^{+}$ (although it should be noted that samples were not taken at 3 hrs). The *rec10-Y731F* mutant exhibits <5 class IIa LinEs at 2 hrs; whilst the *rec10-Y767F* mutant exhibits <5 nuclei containing class IIa or IIb LinEs. The *rec10-2YF* mutant exhibits class Ia, Ib and IIa LinEs at 2 hrs, with approximately15-20% of cells exhibiting

Rec10 positive staining. These data suggest that the *rec10-2YF* tyrosine double mutant has a more profound effect on the timing of the appearance of LinEs than either of the single tyrosine mutants – possibly indicative of an accumulative effect on losing both tyrosine residues.

Therefore, *rec10* C-terminal tyrosine mutants all exhibit advancements in the formation of LinEs, whilst *rec10* C-terminal lysine mutants do not exhibit any advancement using the resolution employed in this study. These data infer that the tyrosine residues mutated play a role in the timing of LinE formation.

It is known that tyrosine is a possible target for nuclear post-translational modification, being a known substrate for phosphorylation – an important pathway within eukaryotic cells regulating many cellular events. One example of this in *S. pombe* is Wee1 inhibition of Cdc2, which is a key regulator various cell cycle checkpoints (COLEMAN and DUNPHY 1994). Cdc2 is Wee1 inhibits Cdc2 by phosphorylating it on two different sites – Tyrosine 15 and Threonine 14 (DEN HAESE *et al.,* 1995).

Therefore, mutating tyrosine residues in the C-terminal region of Rec10 may disrupt a phosphorylation pathway responsible for regulating the timing of LinE formation.

It would be interesting to conduct a more refined analysis of the first 4 hrs of an asynchronous meiosis in each of these tyrosine mutants; taking time point samples at smaller intervals in order to better visualise the timing of LinE formation in these mutants. One may argue that it would also be beneficial to do the same with the lysine mutants as a more refined analysis could reveal previously overlooked details.

4.3.3 Temporal development of LinEs in *rec10* C-terminal Y→F mutants

As previously mentioned, the different classes of LinEs exhibited during meiosis are thought to reflect different stages of LinE maturation (MOLNAR *et al.,* 2003), and the data in Chapter 3 strongly infers a distinct temporal progression of LinE maturation. Various differences are exhibited in the temporal development of LinEs in the *rec10* C-terminal mutants studied in this chapter.

4.3.3a Mutants exhibiting delays in the timing of LinE maturation

Class IIb LinEs are first observed at 4 hrs during a *rec10⁺/rec10⁺* asynchronous meiosis (Figure 4.4A), and are continuously exhibited with increased frequency throughout the remainder of the time course – having a peak frequency of approximately 20% by 9 hrs.

The following *rec10* C-terminal mutants do not exhibit class IIb structures until 5 hrs during their respective time courses: *rec10-K712R*, *rec10-K744R*, *rec10-K757R* and *rec10-3KR*. These data suggest that lysines 712, 744 and 757 may have a role in the maturation of LinEs, possibly via homo-oligomerization; mutating the lysines appears to cause a delay in LinE development. The *rec10-3KR* mutant (which exhibits mutations in K744, K754 and K757) does not appear to exhibit a greater delay in the appearance of class IIb structures, inferring that the presence of multiple mutated lysines does not have an accumulative increased effect on LinE maturation.

4.3.3b Mutants exhibiting reduced frequencies of the more mature class IIb LinEs

All of the *rec10* C-terminal mutants analysed during this chapter, bar one (*rec10-Y731F*), exhibits a reduced frequency of nuclei exhibiting class IIb LinEs.

These data infer that loss of any of the mutated residues (with the exception of Y731) affects the maturation of LinEs into class IIb structures. *rec10-3KR* does not appear to exhibit a more pronounced reduction of class IIb structures, therefore we can ascertain that the presence of more than one mutated lysine does not amplify the mutant phenotype.

The *rec10-2YF* mutant displays very few class IIb LinEs throughout the time course (peaking at ~5% at 6 hrs), and no class IIb LinEs at all by 9 hrs. The *rec10-2YF* mutant also exhibits a much higher frequency of class IIa LinEs at 7 hrs and 8 hrs. These data suggest that class IIa structures appear to accumulate in a *rec10-2YF* mutant, possibly indicative of a failure to mature into class IIb LinEs.

Although the *rec10-Y731F* does not exhibit a reduction in the frequency of class IIb LinEs, these data does suggest that the tyrosine double mutant (*rec10-2YF*) exhibits a greater reduction in visible class IIb LinEs that either of the single

tyrosine mutant – inferring that mutating both tyrosine residues has an accumulative negative effect on the maturation of LinEs into class IIb structures.

4.3.4 Temporal dissociation of LinEs

The temporal analysis of LinE formation and development in a *rec10⁺/rec10⁺* asynchronous meiosis shows an increase in the frequency of nuclei exhibiting Rec10 positively stained structures from 4 hrs to 7 hrs; it also demonstrates a reduction in the frequency of Rec10 positively stained structures from 7 hrs onwards. This infers the dissociation or degradation of LinEs subsequent to their potential utilisation during meiosis.

4.3.4a Delayed dissociation of LinEs

The *rec10-Y767F* mutant does not show a reduction in the number of Rec10 positively stained nuclei recorded between 7 hrs and 9 hrs (Figure 4.12B), suggesting that LinEs have not yet began to dissociate/degrade by 9 hrs in this mutant. These data suggest that the Y767 residue of Rec10 has a role in regulating the dissociation/degradation of LinEs.

The same phenotype, however, is not observed in the *rec10-2YF* mutant, which exhibits an *Y731F* mutation alongside the *Y767F* mutation. In this case, the *Y731F* mutation may somehow mask the effect of the *Y67F* mutation.

To further investigate LinE degradation in the *rec10-Y767F* mutant; it would be interesting to analyse samples at time points subsequent to 9 hrs in order to establish when, (if at all), LinEs begin to degrade/dissociate in a *rec10-Y767F* mutant, and therefore better understand the extent of the effect that a *Y767* mutation has on LinE degradation/dissociation.

4.3.4b Advanced degradation/dissociation of LinEs

The *rec10-K712R* mutant exhibits a much lower frequency of Rec10 positively stained nuclei at 7 hrs, although the frequency increases again by 8 hrs. This may be indicative of unstable LinEs, or a premature onset of degradation, which is subsequently rescued by some other factor.

rec10-K754R and *rec10-3KR* mutants exhibit a drastic decrease in the frequency of nuclei exhibiting Rec10 positive staining between 8 hrs and 9 hrs (decreasing

from ~60%→<20% in *rec10-K754R*, and from ~90%→<20% in *rec10-3KR*). These data show that the *rec10-K754R* mutation exhibits a much faster dissociation/degradation of LinEs than observed in *rec10⁺*. This implies that lysine 754 may be involved in the stabilisation of LinEs, or alternatively play a role in regulating their dissociation/degradation.

4.3.5 Effect of *rec10* C-terminal mutants on temporal progression of meiosis

Previous studies have demonstrated that a *rec10-155* mutant exhibits advancements in meiotic progression (DOLL *et al.*, 2008). They proposed that Rec10, alongside other meiotic proteins, regulate the transition between G^1→S-phase, thus explaining why a mutation in one of these regulatory proteins (e.g., Rec10) leads to an advancement of meiotic events.

4.3.5a Mutants exhibiting advancement in the onset of the horsetail stage

rec10-K712R, *rec10-K744R*, *rec10-3KR* and *rec10-Y731F* all appear to exhibit an advancement in the onset of the horsetail stage during their respective asynchronous meiosis, in comparison to *rec10⁺*. This implicates the K712, K744 and Y731 residues in regulating the G^1→S-phase transition, if agreement is to be found with the hypothesis of (DOLL *et al.*, 2008).

4.3.5b Mutants exhibiting advancement in the onset of the first meiotic division

We define the onset of the first meiotic division as the time point where we observe an increased frequency of cells exhibiting ≥2 nuclei. During a *rec10⁺/rec10⁺* meiosis, the frequency of cells exhibiting ≥2 nuclei increased from ~0% to ~20% between 8hrs and 9 hrs (Figure 4.3B).

rec10-K712R exhibits an increased frequency of cells with ≥2 nuclei at the 5-6 hr time point – up to 3 hrs earlier than seen in *rec10⁺*; by 9 hrs ~50% of cells exhibit ≥2 nuclei.

In *rec10-K744R*, an increased frequency of cells exhibiting ≥2 nuclei is observed at the 5-6 hr time point – up to 3 hrs prior to that reported in *rec10⁺* cells; by 9 hrs ~50% of cells are recorded to exhibit ≥2 nuclei.

The *rec10-3KR* mutant exhibits an increase in the cells containing ≥2 nuclei at 6 hrs –up to 3 hrs sooner than exhibited in *rec10*$^{+}$ cells; and by 9 hrs ~60% of cells exhibit ≥2 nuclei.

In the *rec10-Y731F* and *rec10-Y767F* mutants, increased frequency of cells containing ≥2 nuclei is observed at 7-8 hrs, an advancement of up to 2 hrs. ~30% of cells exhibit ≥2 nuclei by 9 hrs in the *rec10-Y731F* mutant, and ~40% in the *rec10-Y767F* mutant.

From these data, we can infer that residues K712, K744, Y731 and Y767 have some role to play in regulating the timing meiotic events.

The *rec10-3KR* mutant shows a higher frequency of cells exhibiting ≥2 nuclei at 9 hrs than either of the two single lysine mutants; suggesting an accumulative effect on mutating the two lysine residues.

Although we see that the single Y731F and Y767F mutants display altered timing in the start of the first meiotic division, this phenotype is not seen in the *rec10-2YF* mutant. The *rec10-2YF* mutant does not, however, exhibit 100% cells with ≥2 nuclei by 24 hrs, possibly indicative of an incomplete meiosis. Therefore the altered timing observed during an asynchronous meiosis of the single tyrosine mutants may culminate in a failure to complete meiosis when both residues are mutated (*rec10-2YF*).

rec10-K757R also exhibits <100% cells containing ≥2 nuclei by the 24 hr time point. This phenotype is not seen in the *rec10-3KR* mutant – this may suggest that loss of the other two lysines (K754 and K744) have a dominant effect over the loss of merely K757.

4.3.6 Observations on the temporal appearance of Rad51 foci and their Rec10 co-staining pattern in a *rec10*$^{+}$/*rec10*$^{+}$ asynchronous meiosis

4.3.6a Effect of *rec10* C-terminal mutants on timing of Rad51 foci appearance

Rad51 foci appear concomitantly with Rec10 positively stained structures during a *rec10*$^{+}$/*rec10*$^{+}$ asynchronous meiosis, at 4 hrs (Figure 4.5A)

LinEs appear earlier (2 hrs) in *rec10-Y731F*, *rec10-Y767F* and *rec10-2YF* mutants than in rec10+ (4 hrs). However, the first Rad51 foci are not observed until 4 hrs

in these three tyrosine mutants. These data suggest that the timing of the localisation of Rad51 foci is not dependent upon the timing of LinE formation.

4.3.6b Effect of *rec10* C-terminal mutants on Rad51 foci numbers

I do not believe that any of the *rec10* C-terminal mutants studied analysed during this chapter exhibit a significantly different profile of Rad51 foci numbers than that seen in the *rec10*$^{+}$.

4.3.7 Conclusions

- → None of the mutants generated in this study exhibited a complete lack of LinEs. The absence of LinEs in the *rec10* C-terminal truncation mutant (*rec10-155*) must be due to loss of a combination of the residues analysed in this study, or loss of another as yet unidentified residue.
- → Tyrosine residues in the C-terminal region of Rec10 may play a role in a phosphorylation pathway responsible for regulating the timing of LinE formation.
- → Lysines 712, 744 and 757 may have a role in the maturation of LinEs.
- → Y767 residue may have a role in regulating the dissociation/degradation of LinEs.
- → Lysine 754 may be involved in the stabilisation of LinEs, or alternatively play a role in regulating their dissociation/degradation.
- → K712, K744 and Y731 residues may regulate the G^1→S-phase transition, if agreement is to be found with the hypothesis of Doll *et al.*, (2008).
- → The timing of the localisation of Rad51 foci may not be dependent upon the timing of LinE formation.

(note: The cytological observations in *rec10* C-terminal mutants in this chapter are subtle therefore we take care as to not over-state any of our observations).

Chapter 5

Genetic analysis of *rec10* C-terminal mutants

5.1 Introduction

Meiotic homologous recombination plays an essential role in the correct segregation of meiotic homologous chromosomes during MI as well as driving genetic diversity within populations. In *S. pombe*, many proteins are known to be involved in meiotic recombination, including Rec6, Rec7, Rec10, Rec12, Rec14, Rec15, Rec24, Rec25, Rec27 and Mde2 (CERVANTES *et al.,* 2000; MARTIN-CASTELLANOS *et al.,* 2005; ELLERMEIER and SMITH 2005) (See Section 1.7b for more details).

Rec10 has been demonstrated to influence meiotic recombination on a genome-wide basis (WELLS *et al.,* 2006). Several *rec10* mutants defective in LinEs formation display altered recombination frequencies compared to *rec10*$^{+}$. *rec10-109* and *rec10-144*, which both form aberrant LinEs, exhibit regional specificity in recombination proficiency (PRYCE *et al.,* 2005; DEVEAUX and SMITH 1994). Complete deletion of *rec10* results in failure to form any visible LinEs and a genome wide reduction in recombination (LORENZ *et al.,* 2004; ELLERMEIER and SMITH 2005).

The *rec10-155* (C-terminal 103 amino acid truncation) mutant does not form LinEs, but does however maintain intermediate levels of recombination (WELLS *et al.,* 2006), inferring the possibility of two distinct functions for Rec10 - LinE development and a role in meiotic recombination; it remains unknown if these two functions are mutually exclusive.

Meiotic recombination occurs preferentially at sites termed recombination hotspots. The *ade6-M26* hotspot of *S. pombe* is created by a single base pair (G→T) nonsense mutation, generating a heptameric sequence (5'-ATGACGT-3' – mutated residue highlighted in red) that exhibits a ~13-fold increase in recombination relative to a non-hotspot control (*ade6-M375*) (GUTZ 1971). Several *M26*-containing hotspots have been introduced into the *ade6* open reading frame, at different positions, and in different orientations (FOX *et al.,* 2000). *M26*-hotspot activation is dependent upon its chromatin context (STEINER

and SMITH 2005), the binding of the heterodimeric transcription factor Atf1-Pcr1 alongside the kinase pathway required for its activation (KON *et al.,* 1997; MIZUNO *et al.,* 2001; FOX 2001; KON *et al.,* 1998). Atf1-Pcr1 is essential for the chromatin transition and hyperacetylation of histones H3 and H4 at *M26*-containing hotspots (YAMADA *et al.,* 2004).

Previous studies have reported that Rec10 is implicated in the full activation of some, but not all, *M26*-containing hotspots, in a temperature-dependent manner (PRYCE *et al.,* 2005). As previously mentioned the chromatin transition is absolutely required for hotspot activation at the *ade6-M26* hotspot. These findings lead to generation of a model (Figure 5.1) by which Rec10 has an unknown function in chromatin alteration at some hotspots.

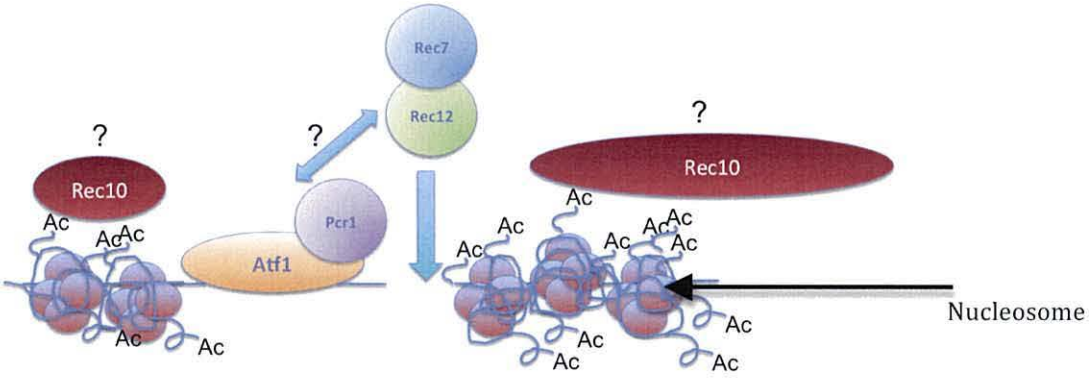

Figure 5.1 Model for activation of *ade6-M26* recombination hotspot. On entry to meiosis, hotspot-associated chromatin becomes hyper-acetylated, and the nucleosomes are re-modelled in an Atf1-Pcr1-dependent fashion (refer to text for more details), allowing for DSB formation via Rec12 and associated proteins. It has been proposed that Rec10 influences the chromatin transition, although details of Rec10 interactions remain unclear. Question marks are indicative of interactions that are currently hypothetical. Figure adapted from PRYCE & MACFARLANE, (2009).

In this study, several *rec10* C-terminal mutants were created (described in Chapter 4). The aim of generating these mutants was to attempt to create a *rec10* mutant strain that exhibited wild-type levels of recombination whilst being void of any visible LinEs, thus completely separating LinE and recombination functions of Rec10. Cytological and genetic analysis on all mutants was carried

out concomitantly. In this chapter, the results of the genetic analysis of the *rec10* C-terminal mutations are presented.

Analysing the effect that specific *rec10* C-terminal mutations (described in Chapter 4) have on meiotic recombination could facilitate the pinpointing of residues directly involved in meiotic recombination, alongside residues possibly involved in chromatin remodelling at hotspot sites.

5.2 Results

Meiotic recombination frequencies at four distinct *M26*-containing hotspots in the *ade6* gene were analysed and compared to their respective non-hotspot counterparts. The approximate positions and the orientations of these four hotspot alleles are shown in Figure 5.2.

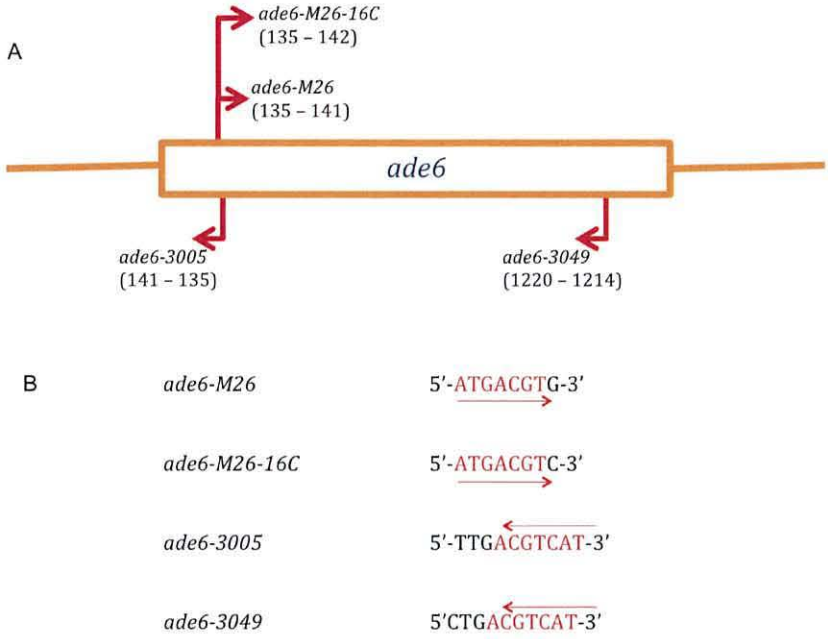

Figure 5.2 Positions of the four *M26*-containing hotspots within the *ade6* open reading frame. (**A**) Position and orientation of *M26* heptamers introduced into the *ade6* open reading frame. The numbers in the parentheses indicate the nucleotide positions of the heptamers, nucleotide 1 being the A of the ATG start codon of the *ade6* open reading frame. (**B**) Sequences and orientations of 4 *M26* containing hotspots in the *ade6* open reading frame. Figure is not to scale. Adapted from PRYCE *et al.*, (2005).

5.2.1 Rec10 C-terminal lysine mutants: influence on recombination

In order to establish whether the *rec10* C-terminal conserved lysine residues analysed during this study had an effect on the activation of the *ade6-M26* hotspot, we utilised two factor crosses to establish the intergenic recombination frequency at the *ade6* locus in *rec10* C-terminal lysine mutants.
(note: the hotspot allele is *ade6-M26*, whilst the non-hotspot allele is *ade6-M375*).

Table 5.1 shows that the *rec10-K712R* mutant exhibits a dramatic reduction in recombination frequency in two-factor crosses using the *ade6-M26* hotspot allele at 30°C, resulting in the hotspot value being decreased to <0.01. At 30°C both *rec10-K744R* and *rec10-K754R* exhibit a ~2-fold increase in their hotspot values due to a reduction in recombination frequency of the non-hotspot allele (*ade6-M375*) in both cases. No significant deviations from *rec10*$^{+}$ recombination frequencies are observed at the elevated temperature of 33°C.

Table 5.1 Intragenic meiotic recombination and hotspot activation for *rec10 K→R* mutants at the *ade6-M26* locus.

Temp.	*rec10* allele	*ade6* allele [e]	mean rf [a, b, c]	% of *rec10⁺* rf [d]	hv	% of *rec10⁺* hv
30°C	*wt*	*ade6-M26*	3595 +/- 846	-	10.4	-
		ade6-M375	345 +/- 43	-		
	K712R	*ade6-M26*	0.4 +/- 0.89	0.01 ***	<0.01	<0.01
		ade6-M375	271 +/- 119	78.6		
	K744R	*ade6-M26*	3507 +/- 2156	97.6	19.3	184.8
		ade6-M375	182 +/- 63	52.8 **		
	K754R	*ade6-M26*	2778 +/- 449	77.3	19.7	189.4
		ade6-M375	141 +/- 40	40.9 ***		
	K757R	*ade6-M26*	3570 +/- 901	99.3	9.3	89.4
		ade6-M375	383 +/- 140	111.0		
	3KR	*ade6-M26*	4151 +/- 1110	115.5	14.0	134.5
		ade6-M375	296 +/- 77	85.8		
33°C	*wt*	*ade6-M26*	3471 +/- 697	-	15.9	-
		ade6-M375	218 +/- 43	-		
	K712R	*ade6-M26*	4400 +/- 892	126.8	30.4	191.2
		ade6-M375	145 +/- 83	66.5		
	K744R	*ade6-M26*	4241 +/- 1300	122.2	17.4	109.6
		ade6-M375	243 +/- 105	111.5		
	K754R	*ade6-M26*	3600 +/- 702	103.7	20.0	125.6
		ade6-M375	180 +/- 50	82.6		
	K757R	*ade6-M26*	2539 +/- 695	73.1	7.7	48.6
		ade6-M375	329 +/- 154	150.9		
	3KR	*ade6-M26*	3436 +/- 552	99.0	25.9	162.9
		ade6-M375	133 +/- 91	61.0		

rf – recombination frequency
hv – hotspot value
a – recombination frequency calculated by counting number of adenine prototrophs per 10^6 viable spores
b - n≥3 in all cases
c - +/- indicates 95% confidence interval
d – Student's *t*-test *P*-values of two tailed comparisons of *rec10* mutant *vs. rec10⁺* (*P<0.05; **P<0.01; ***P<0.005)
e – test allele is *ade6-52* in all cases

5.2.1b Rec10 C-terminal tyrosine mutants: influence on recombination

To establish the effect of *rec10* C-terminal tyrosine mutants on the activation of the *ade6-M26* hotspot, intergenic recombination frequencies at the *ade6* locus were determined via two-factor crosses of *rec10* C-terminal tyrosine mutants. A significant increase in the hotspot value of *ade6-M26* is observed in a *rec10-2YF* mutant at both 30°C (~7-8-fold increase, $P<0.005$) and 33°C (~4-5-fold increase, $P<0.01$) (Table 5.2). In both cases, the increase in hotspot value is due to a decreased recombination frequency in the non-hotspot allele (*ade6-M375*) rather than an increased recombination frequency at the hotspot allele (*ade6-M26*). Significant differences in meiotic recombination are also observed in: the *rec10-Y731F* mutant, exhibiting a decreased recombination frequency at the non-hotspot allele at 30°C resulting in a ~2.5-fold increase in hotspot value; the *rec10-Y767F* mutant, exhibiting an increased recombination frequency at the hotspot allele at 30°C resulting in a ~2-fold increase in hotspot value, and a decrease in the recombination frequency at the non-hotspot allele at 33°C resulting in a ~2.5-fold increase in hotspot value.

Table 5.2 Intragenic meiotic recombination and hotspot activation for *rec10* C-terminal *Y→F* mutants at the *ade6-M26* locus

Temp.	*rec10* allele	*ade6* allele [e]	mean rf [a, b, c]	% of *rec10*⁺ rf [d]	hv	% of *rec10*⁺ hv
30°C	*wt*	*ade6-M26*	3288 +/- 769	-	7.6	-
		ade6-M375	431 +/- 102	-	-	-
	Y731F	*ade6-M26*	4244 +/- 866	129.0	19.5	256.2
		ade6-M375	217 +/- 28	50 *	-	-
	Y767F	*ade6-M26*	5565 +/- 1559	169 *	15.4	201.7
		ade6-M375	361 +/- 49	83.9	-	-
	2YF	*ade6-M26*	3712 +/- 276	112.9	59.1	774.7
		ade6-M375	62 +/- 24	14 ***	-	-
33°C	*wt*	*ade6-M26*	4363 +/- 762	-	10.5	-
		ade6-M375	417 +/- 113	-	-	-
	Y731F	*ade6-M26*	5749 +/- 2303	131.8	19.5	186.5
		ade6-M375	294 +/- 94	70.6	-	-
	Y767F	*ade6-M26*	4742 +/- 962	108.7	25.7	245.6
		ade6-M375	184 +/- 115	44 *	-	-
	2YF	*ade6-M26*	4414 +/- 836	101.2	47.2	450.9
		ade6-M375	93 +/- 41	22 **	-	-

rf – recombination frequency
hv – hotspot value
a – recombination frequency calculated by counting number of adenine prototrophs per 10^6 viable spores
b - n≥3 in all cases
c - +/- indicates 95% confidence interval
d – Student's *t*-test *P*-values of two tailed comparisons of *rec10* mutant *vs. rec10*⁺ (*P<0.05; **P<0.01; ***P<0.005)
e – test allele is *ade6-52* in all cases

5.2.2a The analysis of the *ade6-3005* hotspot

The *ade6-3005* hotspot is located at the same position as the *ade6-M26* hotspot, but the *M26* heptamer is in the opposite orientation, providing us with an analytical tool to measure the effect of heptamer orientation on hotspot activation in *rec10* C-terminal mutants.
(note: the hotspot allele is *ade6-3005*, whilst the non-hotspot allele is *ade6-3006*).

5.2.2a(i) Lysine mutants

In Table 5.3, it can be seen that the *rec10-K744R* mutant exhibits a ~5-fold increase in the hotspot value at 30°C due to a dramatic increase in recombination frequency of the hotspot allele (~10-fold) alongside a slight reduction in recombination frequency in crosses using the non-hotspot allele. This result is also apparent at 33°C, with an elevated recombination frequency of the hotspot allele resulting in a ~3-fold increase in hotspot value.
The *rec10-K754R* mutant exhibits a ~5-fold decrease in hotspot value at 30°C due to a dramatically lower recombination frequency of the hotspot and non-hotspot alleles; a result also seen at 33°C in the hotspot allele, but no data was obtained for the non-hotspot allele.
The data obtained at 30°C also shows that the *rec10-3KR* mutant exhibits a higher (~5-fold) hotspot value than observed in *rec10*$^{+}$, due to a highly significant increased recombination frequency at the hotspot allele, alongside a slight decrease in recombination frequency of the non-hotspot allele.

Table 5.3 Activation of the *ade6-3005* meiotic recombination hotspot in *rec10* *K→R* mutants.

Temp.	*rec10* allele	*ade6* allele [e]	mean rf [a, b, c]	% of *rec10⁺* rf [d]	hv	% of *rec10⁺* hv
30°C	*wt*	*ade6-3005*	8034 +/- 1113	-	23.0	-
		ade6-3006	349 +/- 71	-		
	K712R	*ade6-3005*	7714 +/- 1204	96.0	21.3	92.6
		ade6-3006	362 +/- 186	103.7		
	K744R	*ade6-3005*	20278 +/- 6678	252.4 **	124.8	542.7
		ade6-3006	163 +/- 107	46.7 *		
	K754R	*ade6-3005*	301 +/- 314	3.7 ***	4.4	19.2
		ade6-3006	68 +/- 57	19.5 ***		
	K757R	*ade6-3005*	5121 +/- 2067	63.7 *	7.1	30.7
		ade6-3006	725 +/- 869	207.7		
	3KR	*ade6-3005*	20840 +/- 6596	259.4 ***	124.9	543.3
		ade6-3006	167 +/- 48	47.9 **		
33°C	*wt*	*ade6-3005*	9140 +/- 1062	-	33.9	-
		ade6-3006	269 +/- 98	-		
	K712R	*ade6-3005*	5578 +/- 3683	61.0	17.9	52.8
		ade6-3006	311 +/- 137	115.6		
	K744R	*ade6-3005*	39794 +/- 7046	435.4 ***	111.4	328.3
		ade6-3006	357 +/- 55	132.7		
	K754R	*ade6-3005*	51.04 +/- 60.92	0.006 ***	-	-
		ade6-3006	no data	no data		
	K757R	*ade6-3005*	6063 +/- 3204	66.3	29.4	86.6
		ade6-3006	206 +/- 245	76.6		
	3KR	*ade6-3005*	13655 +/- 5908	149.4	53.7	158.5
		ade6-3006	254 +/- 73	94.4		

rf – recombination frequency
hv – hotspot value
a – recombination frequency was calculated by counting the number of adenine prototrophs per 10^6 viable spores.
b - n≥3 in all cases
c - +/- indicates 95% confidence interval
d – Student's t-test P-values of two tailed comparisons of *rec10* mutant *vs. rec10⁺* (*P<0.05; **P<0.01; ***P<0.005).
e – test allele was *ade6-52* in all cases.

5.2.2a(ii) Tyrosine mutants

No significant differences are observed in the activation of the *ade6-3005* hotspot in *rec10* C-terminal Y→F mutants at 30°C (Table 5.4). At the elevated temperature of 33°C, however, a highly significant ($P<0.005$) decrease in recombination frequencies at the *ade6-3005* hotspot allele is observed for all three mutant strains, resulting in a ~2-3-fold decrease in hotspot value compared to the *rec10*$^{+}$ value in all cases.

Table 5.4 Activation of the *ade6-3005* meiotic recombination hotspot in *rec10* C-terminal *Y→F* mutants

Temp.	*rec10* allele	*ade6* allele [e]	mean rf [a, b, c]	% of *rec10*⁺ rf [d]	hv	% of *rec10*⁺ hv
30°C	*wt*	*ade6-3005*	8034 +/- 1113		23.0	-
		ade6-3006	349 +/- 71			
	Y731F	*ade6-3005*	6711 +/- 724	83.5	18.9	82.2
		ade6-3006	355 +/- 78	101.7		
	Y767F	*ade6-3005*	6498 +/- 2858	80.9	15.9	69.0
		ade6-3006	410 +/- 167	117.5		
	2YF	*ade6-3005*	7727 +- 1527	96.2	18.4	80.1
		ade6-3006	419 +/- 121	120.1		
33°C	*wt*	*ade6-3005*	9140 +/- 1062	-	33.9	-
		ade6-3006	262 +/- 61	-		-
	Y731F	*ade6-3005*	3833 +/- 1258	41.9 ***	19.2	56.5
		ade6-3006	383 +/- 145	146.2		
	Y767F	*ade6-3005*	5215 +/- 680	57.1 ***	10.3	30.5
		ade6-3006	496 +/- 275	189.3		
	2YF	*ade6-3005*	4780 +/- 606	52.3 ***	10.4	30.8
		ade6-3006	462 +/- 367	176.3		

rf – recombination frequency
hv – hotspot value
a – recombination frequency was calculated by counting the number of adenine prototrophs per 10^6 viable spores.
b - n≥3 in all cases
c - +/- indicates 95% confidence interval
d – Student's *t*-test *P*-values of two tailed comparisons of *rec10* mutant *vs. rec10*⁺ (*P<0.05; **P<0.01; ***P<0.005).
e – test allele was *ade6-52* in all cases.

5.2.2b The analysis of the *ade6-3049* hotspot

The *ade6-3049* hotspot exhibits very high recombination frequencies (PRYCE *et al.,* 2005) – therefore more subtle changes in hotspot activation are more easily recorded.

(note: the hotspot allele is *ade6-3049*, whilst the non-hotspot allele is *ade6-3009*).

5.2.2b(i) Lysine mutants

The results in Table 5.5 show that at 33°C, *rec10-K712R*, *rec10-K744R*, *rec10-K757R* and *rec10-3KR* exhibit increased hotspot values due to decreased recombination frequencies (of varying extents) of the non-hotspot allele. However, the *rec10-K754R* mutant exhibits abolition of hotspot activity due to a complete loss of recombination at the hotspot allele, alongside a drastically reduced recombination frequency at the non-hotspot allele.

At 30°C, we see that the hotspot value of the *rec10-K754R* mutant is drastically decreased, due to reductions in recombination frequencies at both hotspot and non-hotspot alleles. The *rec10-K712R* mutant displays a ~4.8-fold increase in hotspot value due to a ~2-fold increase in recombination frequency at the hotspot allele.

Table 5.5 Activation of the *ade6-3049* meiotic recombination hotspot in *rec10* *K→R* mutants.

Temp.	*rec10* allele	*ade6* allele [e]	mean rf [a, b, c]	% of *rec10*⁺ rf [d]	hv	% of *rec10*⁺ hv
30°C	*wt*	*ade6-3049*	9043 +/- 5057	-	79.4	-
		ade6-3009	114 +/- 66	-		
	K712R	*ade6-3049*	20103 +/- 5057	222.3 *	385.7	485.9
		ade6-3009	52 +/- 12	45.6		
	K744R	*ade6-3049*	14001 +/- 4786	155.0	216.2	272.3
		ade6-3009	65 +/- 15	57.0		
	K754R	*ade6-3049*	7 +/- 5	0.007 **	0.3	0.3
		ade6-3009	26 +/- 6	22.8 *		
	K757R	*ade6-3049*	7929 +/- 3706	87.8	43.2	54.5
		ade6-3009	183 +/- 194	160.5		
	3KR	*ade6-3049*	15425 +/- 4104	170.7	236.3	297.7
		ade6-3009	65 +/- 37	57.0		
33°C	*wt*	*ade6-3049*	11333 +/- 2309	-	40.2	-
		ade6-3009	282 +/- 62	-		
	K712R	*ade6-3049*	18878 +/- 6484	166.6	322.0	801.2
		ade6-3009	59 +/- 9	20.9 ***		
	K744R	*ade6-3049*	21786 +/- 7576	192.2	400.8	997.2
		ade6-3009	54 +/- 62	19.1 *		
	K754R	*ade6-3049*	0	0***	0	0
		ade6-3009	39.87 +/- 36.58	0.14***		
	K757R	*ade6-3049*	12458 +/- 2644	109.9	103.2	256.8
		ade6-3009	121 +/- 92	42.9 *		
	3KR	*ade6-3049*	8422 +/- 4026	74.3	178.4	443.9
		ade6-3009	47 +/- 31	16.7 ***		

rf – recombination frequency
hv – hotspot value
a – recombination frequency was calculated by counting the number of adenine prototrophs per 10^6 viable spores.
b - n≥3 in all cases
c - +/- indicates 95% confidence interval
d – Student's *t*-test *P*-values of two tailed comparisons of *rec10* mutant *vs. rec10*⁺ (*P<0.05; **P<0.01; ***P<0.005).
e – test allele was *ade6-M375* in all cases.

5.2.2b(ii) Tyrosine mutants

Table 5.6 indicates that there is a slightly significant decrease in recombination frequency of the non-hotspot allele in *rec10-Y731F* and *rec10-Y767F* mutants at 30°C, resulting in a ~2- and ~4-fold reduction in their hotspot values, respectively. However, at 33°C, a very significant increase in recombination frequency for the hotspot allele alongside a significantly lower recombination frequency for the non-hotspot allele yields a ~4-fold increase in the comparative hotspot value of the *rec10-Y731F* mutant; there is a highly significant decrease in the levels of recombination frequency at both hotspot and non-hotspot alleles in the *rec10-Y767F* mutant, which results in a 2-fold increase in hotspot value; there is a slight, yet significantly lower level of recombination in the non-hotspot allele in the *rec10-2YF* mutant, which results in a ~3-fold reduction in hotspot value.

Table 5.6 Activation of the *ade6-3049* meiotic recombination hotspot in *rec10* C-terminal *Y→F* mutants

Temp.	*rec10* allele	*ade6* allele [e]	mean rf [a, b, c]	% of *rec10⁺* rf [d]	hv	% of *rec10⁺* hv
30°C	*wt*	*ade6-3049*	9043 +/- 5057	-	79.4	-
		ade6-3009	114 +/- 66	-		
	Y731F	*ade6-3049*	12000 +/-4943	132.7	40.1	50.5
		ade6-3009	300 +/- 92	263.2 *		
	Y767F	*ade6-3049*	23330 +/- 14567	258.2	18.9	23.8
		ade6-3009	1234 +/- 553	1082.5 *		
	2YF	*ade6-3049*	12198 +/- 3761	135.0	81.1	102.1
		ade6-3009	150 +/- 23	131.6		
33°C	*wt*	*ade6-3049*	11333 +/- 2309	-	40.2	-
		ade6-3009	282 +/- 62	-		-
	Y731F	*ade6-3049*	23025 +/- 1393	203.2 ***	177.3	441.2
		ade6-3009	130 +/- 46	46.1 *		
	Y767F	*ade6-3049*	26575 +/- 2708	234.5 ***	79.7	198.3
		ade6-3009	2190 +/- 438	776.6 ***		
	2YF	*ade6-3049*	6515 +/- 2624	57.5	12.1	30.2
		ade6-3009	82 +/- 55	29.1 *		

rf – recombination frequency
hv – hotspot value
a – recombination frequency was calculated by counting the number of adenine prototrophs per 10^6 viable spores.
b - n≥3 in all cases
c - +/- indicates 95% confidence interval
d – Student's *t*-test *P*-values of two tailed comparisons of *rec10* mutant *vs. rec10⁺* (*P<0.05; **P<0.01; ***P<0.005).
e – test allele was *ade6-M375* in all cases.

5.2.2c The analysis of the *ade6-M26-16c* hotspot

The *ade6-M26-16C* hotspot has a G→C change in the 3' nucleotide immediately following the *M26* heptamer compared to the *ade6-M26* hotspot; a change that appears to restore the hotspot activity of *M26*, lost in *rec10-144* mutants (PRYCE *et al.,* 2005). The *ade6-M26-16c* hotspot has been demonstrated to exhibit a more restricted chromatin transition than that seen in the *ade6-M26* hotspot (MIZUNO *et al.,* 1997)

(note: the hotspot allele is *ade6-M26-16c*, whilst the non-hotspot allele is *ade6-M375*).

5.2.2c(i) Lysine mutants

The data in Table 5.7 indicate that the *rec10-K712R* mutant exhibits a reduced hotspot value at 30°C, due to a reduction in recombination frequency for the hotspot allele; however, at 33°C, the same mutant exhibits an elevated hotspot value due to a decreased recombination frequency for the non-hotspot allele. The *rec10-K744R* mutants exhibits a ~2-fold reduction in recombination frequency for both hotspot and non-hotspot alleles at 30°C, which does not appear to have a drastic effect on the hotspot value in the mutant. Both *rec10-K754R* and *rec10-K757R* mutants exhibit strikingly lower hotspot values at 30°C; the *rec10-K754R* mutants having a dramatically reduced recombination frequency for both hotspot and non-hotspot alleles (a result also apparent at 33°C), and the *rec10-K757R* mutant showing a significant reduction in the recombination frequency exhibited for the hotspot allele. The *rec10-3KR* mutant only shows a statistically significant difference at the elevated temperature of 33°C, as it exhibits a ~6.4-fold increase in hotspot value due to a combination of increased recombination frequency for the hotspot allele (~2-fold) alongside a reduction in recombination frequency for the non-hotspot allele (~3-fold).

Table 5.7 Activation of the *ade6-M26-16c* meiotic recombination hotspot in *rec10* *K→R* mutants.

Temp.	*rec10* allele	*ade6* allele	mean rf	% of *rec10*⁺ rf	hv	% of *rec10*⁺ hv
30°C	*wt*	*ade6-M2616c*	5498 +/- 1582	-	12.76	-
		ade6-M375	431 +/- 102	-		
	K712R	*ade6-M2616c*	2276 +/- 827	41.4 *	8.39	65.79
		ade6-M375	271 +/- 119	62.88		
	K744R	*ade6-M2616c*	3088 +/- 681	56.17 *	16.96	132.95
		ade6-M375	182 +/- 63	42.23 ***		
	K754R	*ade6-M2616c*	3 +/- 2	0.06 ***	0.02	0.19
		ade6-M375	141 +/- 40	32.72 ***		
	K757R	*ade6-M2616c*	269 +/- 285	4.893 **	0.70	5.50
		ade6-M375	383 +/- 140	88.86		
	3KR	*ade6-M2616c*	4253 +/- 592	77.36	14.37	112.66
		ade6-M375	296 +/- 77	68.68		
33°C	*wt*	*ade6-M2616c*	4374 +/- 1465	-	10.49	-
		ade6-M375	417 +/- 113	-		
	K712R	*ade6-M2616c*	4943 +/- 2267	113	34.16	325.66
		ade6-M375	145 +/- 83	34.77 **		
	K744R	*ade6-M2616c*	4231 +/- 1243	96.73	17.38	165.73
		ade6-M375	243 +/- 105	58.27		
	K754R	*ade6-M2616c*	505 +/- 572	11.55 ***	2.80	26.7
		ade6-M375	180 +/- 50	43.17 **		
	K757R	*ade6-M2616c*	2118 +/- 3363	48.42	6.44	61.44
		ade6-M375	329 +/- 154	78.9		
	3KR	*ade6-M2616c*	8963 +/- 1701	204.92 **	67.58	644.36
		ade6-M375	133 +/- 91	31.9 **		

rf – recombination frequency
hv – hotspot value
a – recombination frequency was calculated by counting the number of adenine prototrophs per 10^6 viable spores.
b - n≥3 in all cases
c - +/- indicates 95% confidence interval
d – Student's *t*-test *P*-values of two tailed comparisons of *rec10* mutant *vs. rec10*⁺ (*P<0.05; **P<0.01; ***P<0.005).
e – test allele was *ade6-52* in all cases.

5.2.2c(ii) Tyrosine mutants

The data in Table 5.8 show that the *rec10-Y731F* mutant exhibits a significantly lower recombination frequency at the non-hotspot allele at both temperatures, resulting in a ~9-fold increase in hotspot value at 30°C, and a ~3-fold increase in hotspot value at 33°C. There is a slight, yet significant decrease in the recombination frequency of the non-hotspot allele in the *rec10-Y767F* mutant at 30°C, this does not have an effect on its relative hotspot value. A lower recombination frequency for both hotspot and non-hotspot alleles in the *rec10-2YF* mutant results in a ~6-7-fold increase in hotspot value.

Table 5.8 Activation of the *ade6-M26-16c* meiotic recombination hotspot in *rec10* C-terminal *Y→F* mutants

Temp.	*rec10* allele	*ade6* allele [e]	mean rf [a, b, c]	% of *rec10⁺* rf [d]	hv	% of *rec10⁺* hv
30°C	*wt*	*ade6-M2616c*	5497 +/- 1582	-	12.8	-
		ade6-M375	431 +/- 102	-		
	Y731F	*ade6-M2616c*	7490 +/- 3439	136.7	119.2	934.8
		ade6-M375	63 +/- 24	14.6 ***		
	Y767F	*ade6-M2616c*	4238+/- 2093	77.1	19.5	101.8
		ade6-M375	217 +/- 28	50.3 *		
	2YF	*ade6-M2616c*	6163 +/- 1644	112.1	17.0	133.6
		ade6-M375	362 +/- 49	84.0		
33°C	*wt*	*ade6-M2616c*	4374 +/- 1465	-	10.5	-
		ade6-M375	417 +/- 113	-		-
	Y731F	*ade6-M2616c*	6061 +/- 377	139.4	32.8	313.2
		ade6-M375	185 +/- 115	44.4 *		
	Y767F	*ade6-M2616c*	5102 +/- 2117	116.6	12.2	116.6
		ade6-M375	295 +/- 94	70.7		
	2YF	*ade6-M2616c*	6347 +/- 1172	145.1 *	67.8	646.6
		ade6-M375	94 +/- 42	22.5 **		

rf – recombination frequency
hv – hotspot value
a – recombination frequency was calculated by counting the number of adenine prototrophs per 10^6 viable spores.
b - n≥3 in all cases
c - +/- indicates 95% confidence interval
d – Student's *t*-test *P*-values of two tailed comparisons of *rec10* mutant *vs. rec10⁺* (*P<0.05; **P<0.01; ***P<0.005).
e – test allele was *ade6-52* in all cases.

5.2.3 Intergenic recombination in *rec10* C-terminal mutants

Meiotic recombination can result in the production of non-crossover (gene conversions) or crossover products. Previous studies have reported that crossover frequencies appear reduced in *rec10-144* and *rec10-155* mutants (WELLS *et al.,* 2006). Therefore, we wanted to see if our specific *rec10* C-terminal mutations had an effect on crossover frequencies, in order to pin-point residues that may play a role in regulating crossovers in *S. pombe.*

Intergenic recombination was measured at two intervals (*ade8-arg4* and *ura1-pro1*) in all mutants.

5.2.3a Lysine mutants

Figure 5.3 demonstrates that there are no significant differences in crossover frequencies at either interval in any of the *rec10* C-terminal lysine mutants.

5.2.3b Tyrosine mutants

Figure 5.4 demonstrates that the *rec10-2YF* mutant shows a reduced crossover frequency at both tested intervals – although a greater reduction at the *ade8-arg4* interval than at *ura1-pro1* (as indicated by statistical testing). The *rec10-Y731F* mutant is also shown to have a statistically significantly reduced crossover frequency at the *ade8-arg4* interval.

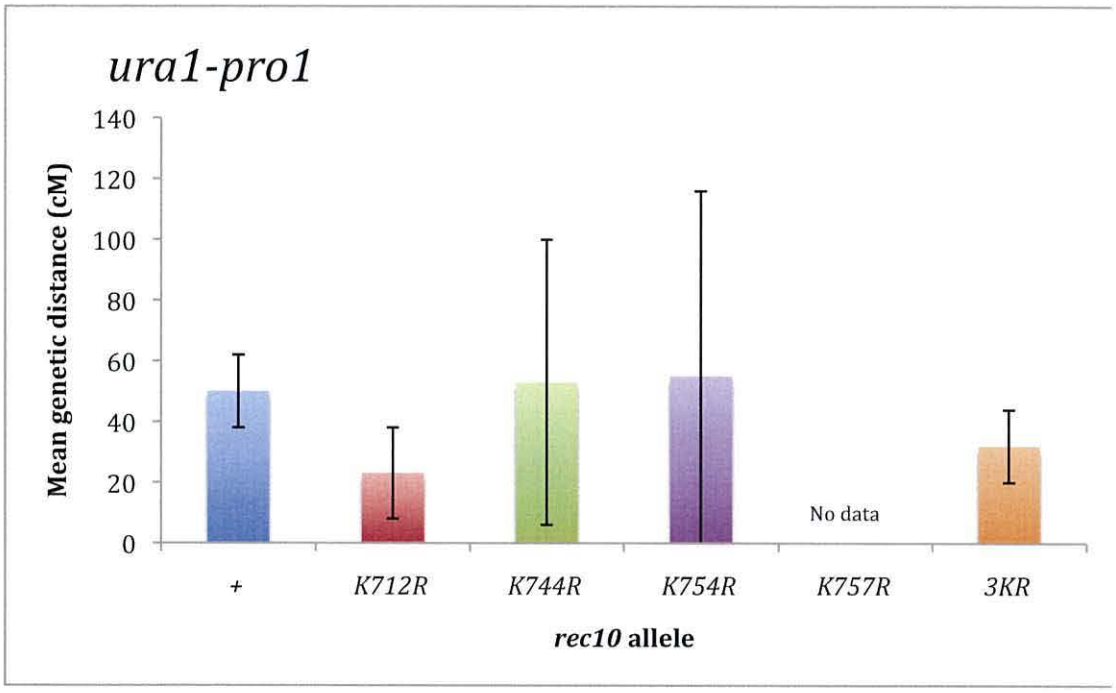

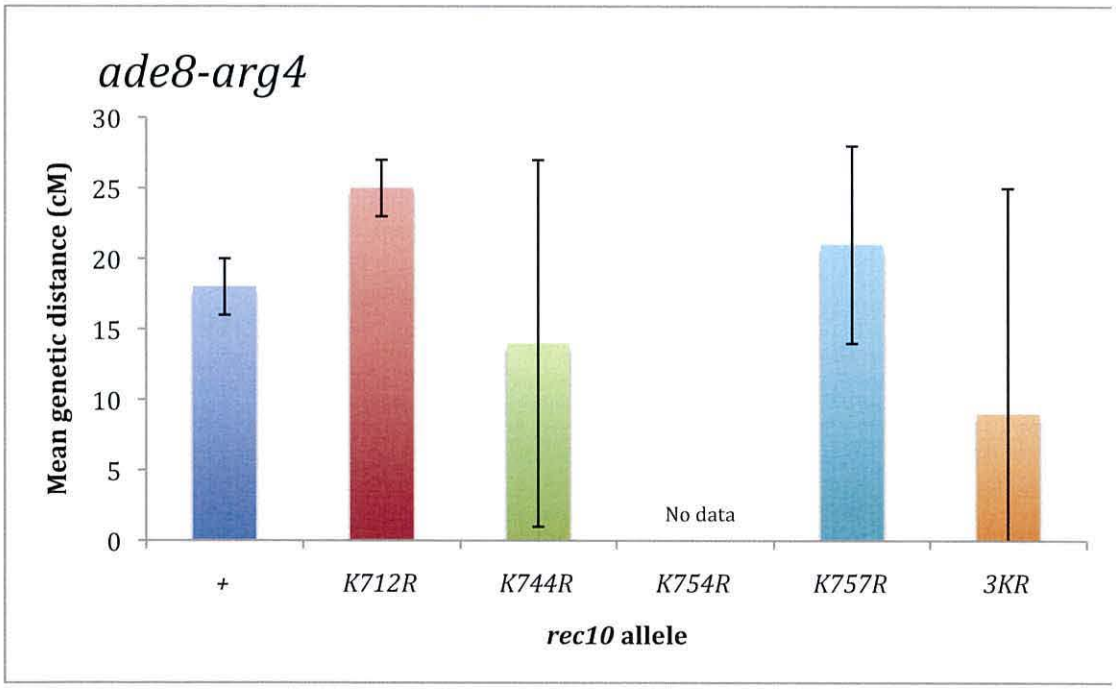

Figure 5.3 Intergenic recombination of *rec10 K→R* mutants at the *ura1-pro1* and *ade8-arg4* intervals. cM distances are calculated using Haldane's formula: cM=-50ln(1-2R), where R is the total number of recombinants out of number of spores analysed. n≥3 in all cases. Error bars indicate 95% confidence interval in all cases. Student's *t*-test *P*-values of two tailed comparisons of *rec10* mutants *vs. rec10⁺* (*P<0.05; **P<0.01; ***P<0.005).

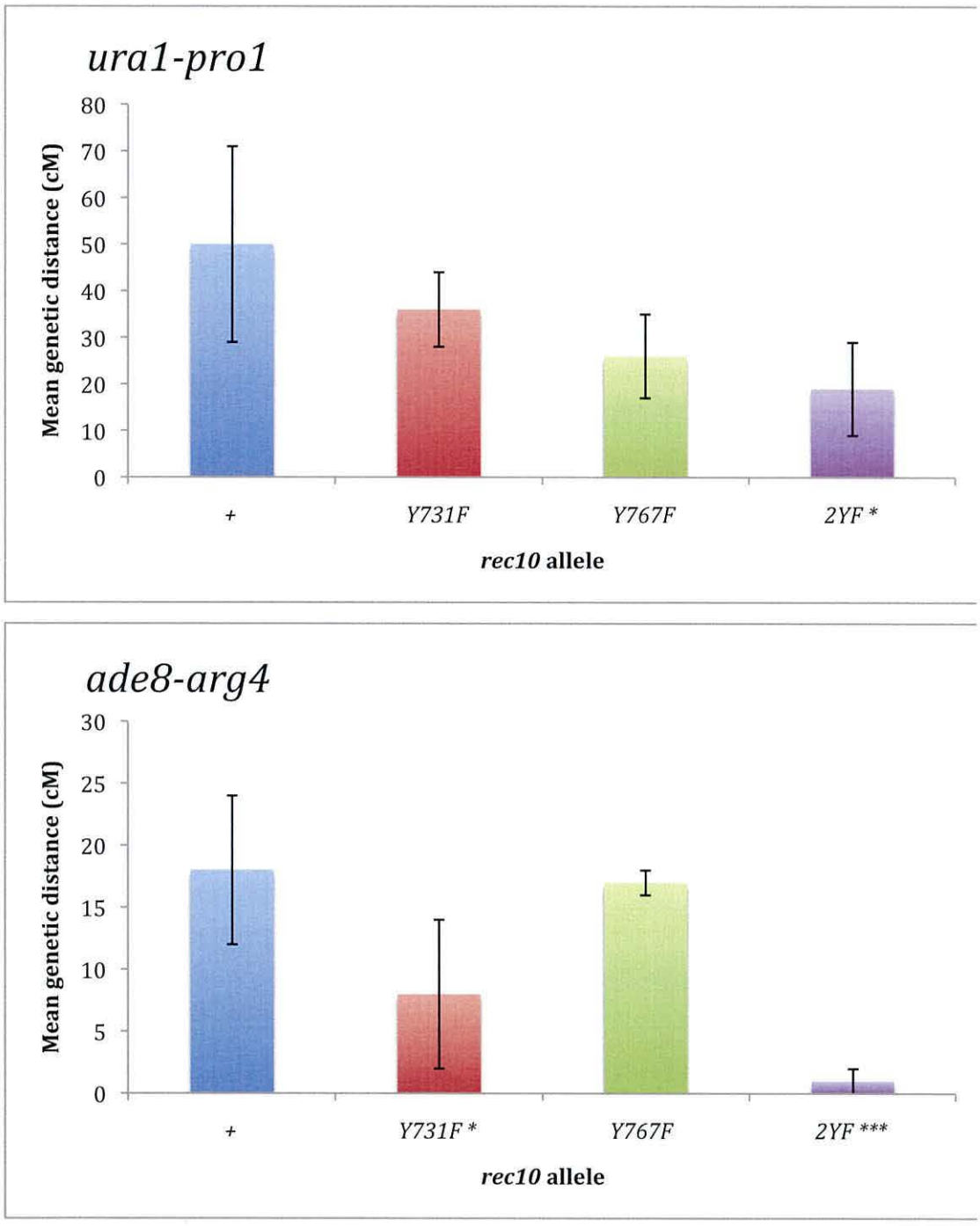

Figure 5.4 Intergenic recombination of *rec10 Y→F* mutants at the *ura1-pro1* and *ade8-arg4* intervals. cM distances are calculated using Haldane's formula; cM=-50ln(1-2R), where R is the total number of recombinants out of number of spores analysed. n≥3 in all cases. Error bars indicate 95% confidence interval in all cases. Student's *t*-test *P*-values of two tailed comparisons of *rec10* mutants *vs. rec10⁺* (*P<0.05; **P<0.01; ***P<0.005).

5.3 Discussion

Table 5.9 Summary of *rec10* C-terminal mutant's LinE profiles and intragenic recombination data

rec10 allele	LinEs	RF [a]	HA [b] ([c])	RF [a]	HA [b] ([c])
		30° C		33°C	
rec10⁺	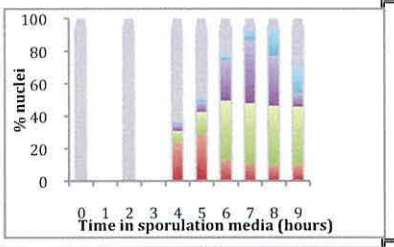	*M26* - 3595 ± 846 *M26-16c* - 5497 ± 1582 *M375* - 345 ± 43 *3005* - 8034 ± 1113 *3006* - 349 ± 71 *3049* - 9034 ± 5057 *3009* - 114 ± 66	7.6 (~) 12.8 (~) 23.0 (~) 79.4 (~_)	*M26* - 3471 ± 697 *M26-16c* -4347±1465 *M375* - 218 ± 43 *3005* - 9140 ± 1062 *3006* - 262 ± 61 *3049* - 11333 ± 2309 *3009* - 282 ± 62	10.5 (~) 10.5 (~) 33.9 (~) 40.2 (~)
rec10-Y731F	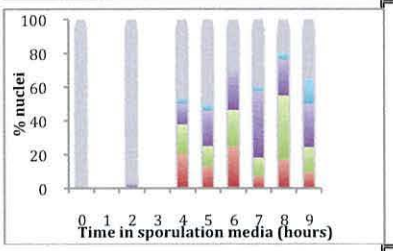	*M26* - 4244 ± 866 *M26-16c* - 7490 ± 3439 *M375* - 217 ± 28 *3005* - 6711 ± 724 *3006* - 355 ± 78 *3049* - 12000 ± 4943 *3009* - 300±92	19.5 (2.56) 119.2 (9.34) 18.9 (0.82) 40.1 (0.51	*M26* - 5749 ± 2303 *M26-16c* - 6061± 377 *M375* - 294 ± 94 *3005* - 3833 ± 1258 *3006* - 383 ± 145 *3049* - 23025 ± 1393 *3009* 130 ± 46	19.5(1.9) 32.8 (3.13) 19.2 (0.56) 177.3 (4.4)
rec10-Y767F	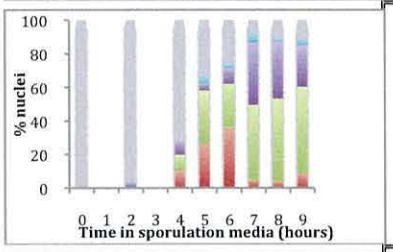	*M26* - 5565 ± 1559 *M26-16c* - 4238 ± 2093 *M375* - 361 ± 49 *3005* - 6498 ± 2858 *3006* - 410 ± 167 *3049* - 23330 ± 14567 *3009* - 1234 ± 553	15.4 (2.0) 19.5 (1.02) 15.9 (0.69) 18.9 (0.24)	*M26* - 4742 ± 962 *M26-16c* -5102±2117 *M375* - 184 ± 115 *3005* - 5215 ± 680 *3006* - 496 ± 275 *3049* - 26575 ± 1393 *3009* - 2190 ± 438	25.7 (2.5) 12.2 (1.17) 10.3 (0.3) 79.7 (1.98)
rec10-2YF	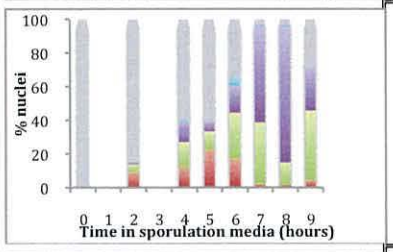	*M26* - 3712 ± 276 *M26-16c* - 6163 ± 1644 *M375* - 62 ± 24 *3005* - 7727 ± 1527 *3006* - 419 ± 121 *3049* - 12198 ± 3761 *3009* - 150 ± 23	59.1(7.7) 17 (1.34) 18.4 (0.8) 81.1 (1.02)	*M26* - 4414 ± 836 *M26-16c* -6347±1172 *M375* - 93 ± 41 *3005* - 4780 ± 606 *3006* - 462 ± 367 *3049* - 6515 ± 2624 *3009* - 82 ± 55	47.2 (4.5) 67.8 (6.47) 10.4 (0.3) 12.1 (0.3)
rec10-K712R	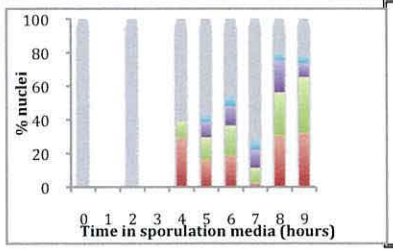	*M26* - 0.4 ± 0.89 *M26-16c* - 2276 ± 827 *M375* - 271 ± 119 *3005* - 7714 ± 1204 *3006*- 362 ± 186 *3049* - 20103 ± 5057 *3009* - 52 ± 12	<0.01(<0.01) 8.39 (0.66) 21.3 (0.93) 385.7 (4.86)	*M26* - 4400 ± 892 *M26-16c* -4943±2267 *M375* - 145 ± 83 *3005* - 5578 ± 3683 *3006* - 311 ± 137 *3049* - 18878 ± 6484 *3009* - 59 ± 9	30.4 (1.9) 34.2 (3.26) 17.9 (0.52) 322.0 (8.0)

rec10-K744R 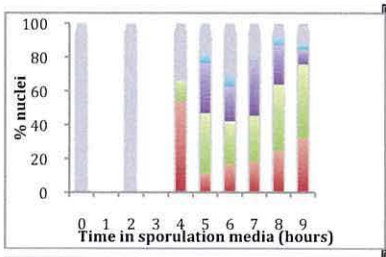	*M26* - 3507 ± 2156 *M26-16c* - 3088 ± 681 *M375* - 182 ± 63 *3005* - 20278 ± 6678 *3006* - 163 ± 107 *3049* - 14001 ± 4786 *3009* - 65 ± 15	19.3 (1.8) 16.96 (1.32) 124.8 (5.43) 216.2 (2.7)	*M26* - 4241 ± 1300 *M26-16c* -4231±1243 *M375* - 243 ± 105 *3005* - 39794 ± 7046 *3006* - 357 ± 55 *3049* - 21786 ± 7576 *3009* - 54 ± 62	17.4 (1.1) 17.4 (1.65) 111.4 (3.2) 400.8 (9.9)
rec10-K754R 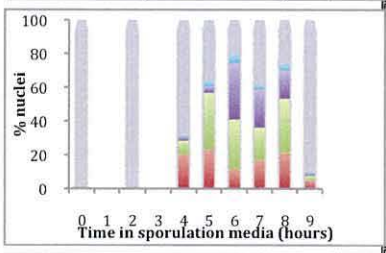	*M26* - 2778 ± 449 *M26-16c* - 3 ± 2 *M375* - 141 ± 40 *3005* - 301 ± 314 *3006* - 68 ± 57 *3049* - 7 ± 5 *3009* - 26 ± 6	19.7 (1.9) 0.02 (0.002) 4.4 (0.19) 0.3 (0.003)	*M26* - 3600 ± 702 *M26-16c* - 505 ± 572 *M375* - 180 ± 50 *3005* - 51.04 ± 60.92 *3006* - no data *3049* - 0 *3009* - 39.87 ± 36.58	20.0 (1.26) 2.8 (0.26) ~ 0 (0)
rec10-K757R 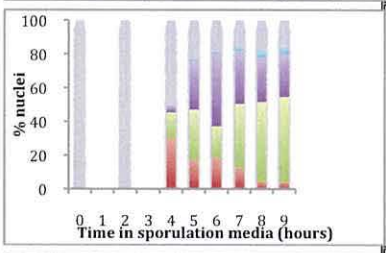	*M26* - 3570 ± 901 *M26-16c* - 269 ± 285 *M375* - 383 ± 140 *3005* - 5121 ± 2067 *3006* - 725 ± 869 *3049* - 7929 ± 3706 *3009* - 183 ± 194	9.3 (0.89) 0.7 (0.05) 7.1 (0.31) 43.2 (0.55)	*M26* - 2539 ± 695 *M26-16c* -2118±3363 *M375* - 329 ± 154 *3005* - 6063 ± 3204 *3006* - 206 ± 245 *3049* - 12458 ± 2644 *3009* - 121 ± 92	7.7 (0.49) 6.44 (0.61) 29.4 (0.87) 103 (2.57)
rec10-3KR 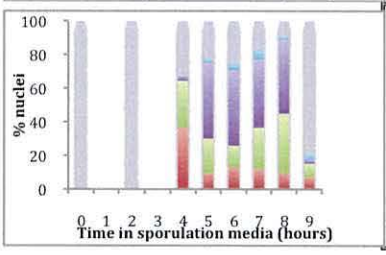	*M26* - 4151 ± 1110 *M26-16c* - 4253 ± 592 *M375* - 296 ± 77 *3005* - 20840 ± 6596 *3006* - 167 ± 48 *3049* - 15425 ± 4104 *3009* - 65 ± 37	14.0 (1.35) 14.4 (1.13) 124.9 (5.4) 236.3 (2.97)	*M26* - 3436 ± 552 *M26-16c* -8963±1701 *M375* - 133 ± 91 *3005* - 13655 ± 5908 *3006* - 254 ± 73 *3049* - 8422 ± 4026 *3009* - 47 ± 31	25.9 (1.63) 67.6 (6.44) 53.7 (1.59) 178.4 (4.4)

[a] - Recombination frequency (Ade$^+$ recombinants/10^6 viable spores)
[b] - Hotspot value
[c] - Hotspot value relative to *rec10*$^+$

5.3.1 Intragenic recombination at the *ade6-M26* hotspot in *rec10* C-terminal mutants

The only *rec10* C-terminal mutant to exhibit a statistically significant difference in recombination frequency at the *ade6-M26* hotspot allele, at either test temperature, was *rec10-K712R*. The *rec10-K712R* mutant exhibits a dramatically reduced recombination frequency at the hotspot allele of *ade6-M26* at 30°C, resulting in a hotspot value of <0.01 (Table 5.1) – this is not reflected in the data obtained at 33°C.

These data allow us to suggest that the *rec10-K712* residue specifically, is essential for *ade6-M26* hotspot activation at 30°C, and that this dependence is lost at the elevated temperature of 33°C.

This statement however, is contrary to previous proposals made based on the analysis of the *rec10-144* mutant, in which greater reductions in hotspot activity are observed at elevated temperatures; data which lead to the suggestion that some function of Rec10 is required for *ade6-M26* hotspot activation (PRYCE *et al.*, 2005). In fact, the data reported in this study suggest the complete opposite - that some function of Rec10, relating specifically to the role of the K712 residue, is a requirement for *ade6-M26* hotspot activation at 30°C, but not at the elevated temperature of 33°C. The *rec10-K712* residue does not however, seem to be required for hotspot activation at any of the other 3 hotspots analysed here. Further investigation could include analysing *ade6-M26* hotspot activation in *rec10-K712R* mutants at temperatures lower than 30°C.

Previous studies have implicated Rec10 as being required for chromatin modification at the *M26* hotspot (PRYCE *et al.*, 2005). The activation of the *M26* hotspot is dependent on the context of its surrounding chromatin (PONTICELLI and SMITH 1992; VIRGIN *et al.*, 1995). The chromatin surrounding the *ade6-M26* hotspot is re-modelled during early meiosis, becoming more sensitive to micrococcal nucleases (MNase) (MIZUNO *et al.*, 1997). This chromatin alteration is vital for the activation of recombination at the *ade6-M26* hotspot (HIROTA *et al.*, 2008). Therefore, it is possible to suggest a direct role for the *rec10-K712* residue in the modification of chromatin at the *ade6-M26* hotspot at 30°C, a role that may be regulated by some other mechanisms at elevated temperatures.

Chromatin remodelling around the *M26* hotspot is strictly dependent on the Atf1-Pcr1 stress-response transcription factor heterodimer (Figure 5.5) (YAMADA *et al.*, 2004).

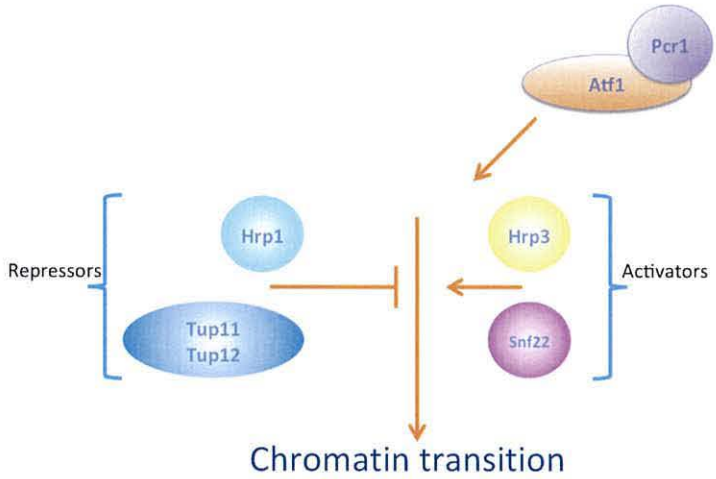

Figure 5.5 Atf1-Pcr1-dependent chromatin transition pathway

However, in the absence of Atf1-Pcr1, basal levels of recombination are still observed for the *M26* allele (KON *et al.,* 1997; WAHLS and SMITH 1994). Loss of Snf22 and/or Hrp3 also results in complete abolition of hotspot activity, but has little or no effect on non-hotspot recombination frequencies (YAMADA *et al.,* 2004).

The level of recombination observed in the *rec10-K712R* mutant at the hotspot allele however, is far lower than the basal recombination frequencies (non-hotspot allele recombination frequencies) (Table 5.1). Therefore, it would be fair to suggest that although we cannot rule out possibility that the *rec10-K712R* mutation may possibly inhibit Atf1-Pcr1 function, or the function of Snf22/Hrp3, it must exert an effect on some other key process of hotspot activation at the *ade6-M26* hotspot allele at 30°C. In fact, loss of the K712 residue must be inhibitory to recombination at the *ade6-M26* allele.

As previously mentioned, an open chromatin structure is essential for hotspot activation of the *ade6-M26* hotspot, but it is not in itself enough to activate the hotspot, as localisation of the DSB-initiating protein Rec12 is also essential (STEINER *et al.,* 2002). Open chromatin is essential for high-frequency cleavage of DNA via Rec12 at the *M26* hotspot. Rec12 loading is dependent on Rec7 (LORENZ *et al.,* 2006), and Rec7 aggregation is dependent on Rec10 (LORENZ *et al.,* 2006). Therefore, it would be fair to suggest that the *rec10-K712R* mutation may somehow disrupt the localisation of Rec12 to the open chromatin (either

directly, or indirectly via disruption of Rec7 function) at the *ade6-M26* hotspot at 30°C, resulting in the failure to form any DSBs, but not at elevated temperatures. In the *rec10* C-terminal tyrosine mutants, several disparities from wild type recombination frequencies are observed for the *ade6-M26* hotspot (Table 5.2). The *rec10-2YF* mutant displays elevated hotspot values at both 30°C (~7-fold) and 33°C (~4.5-fold). In both cases this is due to a reduced recombination frequency at the *ade6-M375* (non-hotspot) allele. Neither single mutant exhibits such a reduction in recombination frequency at the non-hotspot allele at either temperature. (This is also exhibited in Table 5.8, with the exception of the data at 30°C). The data suggests that the loss of both tyrosine residues in the *rec10-2YF* mutant infers a greater effect on recombination frequency at *ade6-M375* than the loss of either of the single tyrosine residues. This may suggest that both tyrosine residues act in pathways that are somewhat distinct from each other, loss of both pathways resulting in a greater accumulative reduction in recombination frequency, with neither residue playing a role in the regulation of recombination at the hotspot allele.

Previous data demonstrated that the basal recombination frequency at the *ade6-M375* allele is reduced by ~250-fold in a *rec10-155* mutant (WELLS *et al.,* 2006). None of the *rec10* C-terminal mutants analysed in this chapter exhibit such a large reduction in recombination frequency for the *ade6-M375* allele. Therefore it can be presumed that the reduction seen in the *rec10-155* mutant is due to losing a combination of the residues analysed in this study, or due to the loss of another as yet unidentified residue within the C-terminal of *rec10*.

5.3.2 Hotspot activation of *ade6-3005*, *ade6-3049* and *ade6-M26-16C* in *rec10* C-terminal mutants

5.3.2a *rec10-K754R*

The data in Tables 5.3, 5.5 and 5.7 demonstrate a most striking reduction in hotspot activation at three distinct hotspots in the *rec10-K754R* mutant. The recombination frequency for the *ade6-3005*, *ade6-3049* and *ade6-M26-16C* hotspot alleles is reduced to 3.7% (~30-fold), 0.007% (~10, 000-fold) and 0.055% (~3000-fold) of the *rec10*$^{+}$ recombination frequency respectively (at

30°C); with the hotspot values reduced to ~19% (~5-fold), 0.3% (~300-fold) and 0.185% (~500-fold) respectively. These reductions are also seen at 33°C, with recombination frequencies reduced to 0.006%, 0% and 11.56% at the *ade6-3005*, *ade6-3049* and *ade6-M26-16C* hotspot alleles, respectively, resulting in complete and ~4-fold reductions in hotspot values for the *ade6-3049* and *ade6-M26-16C* hotspots (as no data was obtained for the *ade6-3005* hotspot value at 33°C).

For all three hotspots, the most prominent reduction in recombination frequency is observed for the hotspot allele, although there remains a marked reduction in recombination frequency at the non-hotspot allele in each case.

Previous studies analysing the *rec10-144* mutation reported; ~18-fold, ~8-fold and ~0.6-fold reductions in meiotic recombination at the *ade6-3005*, *ade6-3049* and *ade6-M26-16C* hotspot alleles at 30°C; and ~29-fold (*ade6-3005*) and ~15-fold (*ade6-M26-16C*) reductions in meiotic recombination at 33°C (PRYCE *et al.,* 2005). This study demonstrated a temperature sensitivity in hotspot activation – increased reductions seen at increased temperatures in the *rec10-144* mutant (PRYCE *et al.,* 2005).

The reductions reported here in the *rec10-K754R* mutant are significantly greater than seen in the *rec10-144* mutant; although they seem to adhere to the same temperature sensitivity seen in the *rec10-144* mutant, with the exception of the *ade6-M26-16C* allele, which appears to have a lower recombination frequency at 30°C. These data indicate that Rec10, and specifically the K754 residue is essential for hotspot activation at three of the hotspots tested during this study.

Furthermore, whilst a reduction in hotspot activity was reported for some *ade6* alleles in the *rec10-144* mutant (PRYCE *et al.,* 2005), the hotspots were never reported to have turned 'cold'. The data reported here analysing hotspot activation in the *rec10-K754R* mutant appears to demonstrate that the *ade6-3005*, *ade6-3049* and *ade6-M26-16C* hotspot alleles have in fact turned to 'cold-spots'. This is a most striking observation, as it suggests that these hotspot alleles are specifically aborting from recombination events. What we observe in these data is not merely a failure to activate the recombination hotspot, but a mutant

(*rec10-K754R*) that in fact does significant harm to recombination levels in a hotspot-specific manner.

Similarly to the data for *rec10-K712R* at the *ade6-M26* hotspot allele, the recombination frequency at the *ade6-3005*, *ade6-3049* and *ade6-M26-16C* hotspot alleles is reduced far lower than basal recombination frequencies in all cases in the *rec10-K754R* mutant (see Tables 5.3, 5.5 and 5.7), alongside a substantial reduction in recombination frequencies at the non-hotspot alleles in all cases. As basal recombination levels are not retained at hotspot nor non-hotspot alleles, these data (again not ruling out the possibility of defective Atf1-Pcr1 binding or Snf2/Hrp3 function), point towards a defect in another key regulator of meiotic recombination at these three hotspots in a *rec10-K754R* mutant. We can therefore again suggest that the *rec10-K754R* mutant may be somehow affecting the localisation of Rec12 to the hotspot sites, either directly, or by way of defective Rec7 behaviour.

Interestingly, the *rec10-K754R* mutant only exhibits reductions in hotspot activation at the *ade6-3005*, *ade6-3049* and *ade6-M26-16C* allele, whilst the *rec10-K712R* mutant only exhibits reduction in hotspot activation at the *ade6-M26* allele. These data infer that the *ade6-M26* hotspot is activated/regulated in a pathway that is somehow distinct from the *ade6-3005*, *ade6-3049* and *ade6-M26-16C* hotspots. There must therefore be a distinction between the hotspots themselves. All four hotspots in question contain the *M26*-heptamer (as demonstrated in Figure 5.3B). However, previous studies have noted that generation of the *ade6-3005* inverted *M26*-heptamer and the *ade6-3049* hotspot allele, also resulted in the creation of an additional CRE sequence, which is in the same orientation as *ade6-M26* (Fox *et al.*, 1997; Pryce *et al.*, 2005), the same being exhibited by the additional G→C mutation observed in the *ade-M26-16C* allele (Figure 5.7). Atf1-Pcr1 has been demonstrated to bind to CRE sequences, which themselves can serve as meiotic recombination hotspots (Steiner and Smith 2005). It is possible that the differential regulation of hotspot activity observed in the four hotspots analysed in this chapter may be attributed to the presence of this additional CRE sequence. Therefore, we can suggest that the *rec10-K712* residue may have a regulatory role in the activation of *M26-*

containing hotspots, and the K754 residue of *rec10* may play a role in the regulation of hotspot activity at CRE-containing hotspot alleles. The reduction in recombination frequency observed at the CRE-containing hotspots of *ade6-3005*, *ade6-3049* and *ade6-M26-16C* may be due to the loss of the *rec10-K754* residue; this reduction may mask the true result for the activation of the *ade6-M26* heptamer. We are therefore suggesting that although Atf1-Pcr1 binds to both *M26*- and CRE- containing hotspots, there are distinctions in the activation of hotspot activity between both sequences. Further investigation could include analysing hotspot activation at CRE-containing hotspots that do not exhibit the *M26* heptamer in the *rec10-K754R* mutant.

ade6-M26	5'-ATGACGTG-3'
ade6-M26-16C	5'-ATGACGTC-3'
ade6-3005	5'-TTGACGTC AT-3'
ade6-3049	5'-CTGACGTC AT-3'
CRE consensus	5'-NTGACGT(C/A)-3'

Figure 5.6 Additional CRE consensus sequences in three *M26*-containing hotspots.

The *M26*-heptamer is highlighted in red. The CRE consensus sequence is highlighted by the blue boxes.

5.3.2b *rec10-3KR*

The *rec10-3KR* mutant does not exhibit the same reduction in recombination frequencies and hotspot values in the three hotspots tested as observed in the *rec10-K754R* mutant (Tables 5.3, 5.5 and 5.7). In fact, the *rec10-3KR* mutation exhibits increased hotspot values (of varying extents) at all three hotspots at both 30°C and 33°C - mainly due to varying increments in recombination frequencies at the hotspot alleles alongside reductions in recombination

frequencies at the non-hotspot alleles. This suggests that the other two lysine mutations (*rec10-K744R* and *rec10-K757R*) exhibited by *rec10-3KR* somehow mask, dull, or rescue the effect of the *rec10-K754R* mutant on meiotic recombination (seen to dramatically reduce recombination frequencies at all three hotspots).

5.3.2c Tyrosine mutants

5.3.2c(i) *ade6-3005*

Y→F mutants, all exhibit decreased *ade6-3005* hotspot values due to reduction in recombination frequency of the hotspot allele at 33°C - no statistical change is seen at 30°C, although all mutants show a slight (but statistically insignificant) reduction of recombination frequency at the hotspot allele. From these data it can be proposed that the *rec10* Y731 and Y767 residues are both required to regulate hotspot activation at the *ade6-3005* hotspot at elevated temperatures (33°C).

The recombination frequencies of the *rec10-2YF* mutant do not appear to exhibit an accumulative effect of losing both tyrosine residues; therefore we can suggest that both tyrosine residues act in a similar pathway in regulating *ade6-3005* hotspot activation at elevated temperatures (33°C) – both being required for full activation.

The reduced recombination frequencies observed at the hotspot allele at 33°C are not reduced as low as the basal recombination level. This suggests that the reduction we see is not due to a complete loss of Atf1-Pcr1 binding (which reduces hotspot activity to basal recombination level), or loss of Snf22/Hrp3 (which result in complete loss of hotspot activation), but alternatively a possible irregularity in the function of Atf1-Pcr1, or Snf22/Hrp3 activators.

5.3.2c(ii) *ade6-3049*

A most striking observation at the *ade6-3049* hotspot allele is the highly elevated recombination frequencies observed at the non-hotspot allele (*ade6-3009*) in the *rec10-Y767F* mutant, at both temperatures; ~10-fold at 30°C, and ~8-fold at

33°C (Table 5.6). A statistically significant increase in recombination frequency is not observed at any other non-hotspot allele for any of the *rec10* C-terminal mutants analysed during this work (with the exception of a ~2-fold increase at the *ade6-3009* allele in the *rec10-Y731F* mutant at 30°C).

So, mutating the *rec10*-Y767 residue results in an increase of up to ~10-fold in the frequency of basal recombination at the *ade6-3009* non-hotspot allele. Therefore, although the *rec10-Y767F* mutant may not instigate an effect on hotspot activation at the *ade6-3049 allele*, it does seem to trigger a higher basal recombination frequency at the *ade6-3009* allele.

It may be that the *rec10-Y767F* mutant results in the generation of more open areas of chromatin across the genome, resulting in higher basal recombination levels.

At 33°C, the behaviour of the *rec10* C-terminal tyrosine mutants gives very interesting results at the *ade6-3049* hotspot allele.

Both single mutants exhibit a ~2-fold increase in their recombination frequencies at the hotspot allele, the double mutant however exhibits a ~2-fold decrease. The single mutants exhibit a ~2-fold decrease (Y731F) and a ~7-fold increase (Y767F) in their recombination frequencies at the non-hotspot allele, whilst the double mutant exhibits a ~3-4-fold decrease.

These data tell us that mutating both tyrosine residues results in a recombinogenic phenotype different to that seen in either single mutation, and does not appear to be the result of the accumulative effects of mutating each single tyrosine residue.

5.3.3 Effect of *rec10* C-terminal mutants on intergenic recombination

In Figure 5.3, it is observed that the *rec10* C-terminal lysine mutations bear no effect on crossover frequency at the two intervals tested. We can therefore presume that these conserved lysine residues play no specific role in regulating meiotic crossover events.

Figure 5.4 demonstrates that *rec10-2YF* exhibits a reduced crossover frequency at both tested intervals, and *rec10-Y731F* exhibits a reduced crossover frequency at the *ade8-arg4* interval. From these data we can gather that;

→ The Rec10 Y767 residue is not required for wild-type levels of crossing over at the intervals tested.

→ The Rec10 Y731 residue is required for wild-type levels of crossing over on regionally specific basis

→ Loss of both tyrosine residues results in reduced crossover frequencies at both intervals tested.

As loss of both tyrosine residues appears to have a greater effect on crossover frequency at both intervals tested than the loss of merely one residue. We can therefore presume that the Rec10 Y731F residue is not essential for crossing over, but it may perform to enhance the frequency of crossing over at certain intervals.

5.3.4 Summary of main findings

→ *rec10* K712 residue appears to play a key role in hotspot activation at the *ade6-M26* hotspot at 30°C.

→ *rec10* K754 residue may regulate the hotspot activation at Cre-containing alleles..

→ The *rec10-K744R* and *rec10-K757R* mutations also present in *rec10-3KR* seem to mask/dull/compensate for the reduction in recombination frequency caused by the *rec10-K754R* mutation in the *rec10-3KR* mutant.

→ Reduction of basal recombination to the extent seen in *rec10-155* must be due to a combination of our *rec10* C-terminal mutations, or due to another as yet unidentified residue.

→ The *rec10* Y731 and Y767 residues are both required to regulate hotspot activation at the *ade6-3005* hotspot at elevated temperatures (33°C).

→ The *rec10* Y731 residue is required for wild type levels of crossing over on regionally specific basis

→ Loss of both tyrosine residues results in a greater reduction in crossover frequencies at both intervals tested, as compared to loss of either single residue.

Chapter 6

Cytological analysis of other *rec10* mutants, and mutants of other LinE-associated proteins

6.1 Introduction

LinE formation has been analysed in several well-known *rec10* mutants. We have previously mentioned that homozygous *rec10* deletion strains (*rec10-175*), or a 103 amino acid C-terminal truncation of *rec10* (*rec10-155*) results in the complete absence of visible LinEs (LORENZ *et al.,* 2004; MOLNAR *et al.,* 2003; WELLS *et al.,* 2006) .The *rec10-144* mutation (previously known as *rec20-144*) was first identified as a mutant defective in intragenic recombination at the *ade6* locus (DE VEAUX *et al.,* 1992), then as an allele involved in LinE and hotspot regulation (PRYCE *et al.,* 2005). *rec10-144* homozygous mutants are defective in LinE formation, exhibiting only small dot-like (similar to wild type class Ia LinEs), or short fat LinE structures (PRYCE *et al.,* 2005). *rec10-109* was first identified as a region-specific activator of meiotic recombination (DEVEAUX and SMITH 1994). The *rec10-109* mutation exhibits small dot like foci similar to class Ia LinEs (LORENZ *et al.,* 2004). We are also aware of several other proteins, which if mutated, have a detrimental effect on LinE formation and/or development. These proteins include:

- → Cohesin component Rec8; rudimentary LinE structures are still formed in the absence of Rec8, with only structures similar to class IIb LinEs being exhibited (LORENZ *et al.,* 2004)
- → DSB initiating protein Rec12; forming all classes of LinEs, but their frequency and temporal distribution differing from that seen in wild type (MOLNAR *et al.,* 2003; LORENZ *et al.,* 2004)
- → LinE components Rec25 and Rec27; forming no visible LinEs in a *pat1-114* temperature-induced synchronous meiosis (DAVIS *et al.* ,2008)

In this chapter, we aim to clarify the temporal order of LinE formation and development in these mutants, alongside analysing the temporal progression in each case.

6.2 Results

6.2.1 Temporal analysis of LinE formation and development in *rec10* mutants previously reported to exhibit aberrant LinEs

Previous studies have already revealed the aberrant nature of LinE structures in *rec10-109* (LORENZ *et al.,* 2004) and *rec10-144* (PRYCE *et al.,* 2005). In this study, we performed an asynchronous time course experiment to gain a temporal profile of LinE formation and development in these two mutants.

6.2.1a(i) LinE formation and development during a *rec10-109/rec10-109* asynchronous meiosis

Whilst analysing LinE formation in the *rec10-109/rec10-109* mutant, we observed only two different LinE morphologies; nuclei containing "class Ia-like" dot-like foci, and nuclei containing slightly elongated foci, which we have termed "class Ib-like" in this study (Figure 6.1).

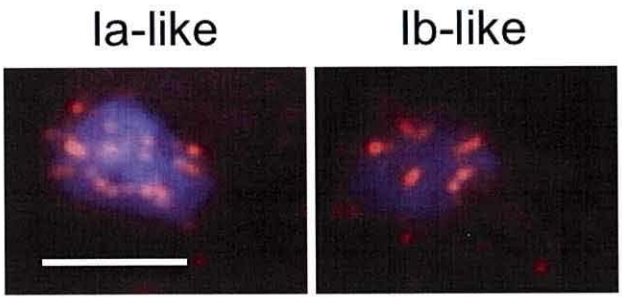

Figure 6.1 Examples of Rec10-positively stained nuclei in a *rec10-109/rec10-109* asynchronous meiosis. All nuclei are stained for DNA (blue) and Rec10 (red). One example is shown for each class of LinE observed in this mutant, which were termed "class Ia-like" and "class Ib-like" structures. Scale bar = 5 μm.

In Figure 6.2B, we first observe LinEs at 2 hrs after transferring the cells to sporulation media, with over 80% of nuclei recorded exhibiting Rec10-positive staining. At 2 hrs, both class Ia-like and class Ib-like nuclei are visible, class Ia-like structures being clearly dominant. At 4 hrs, Rec10-positive staining is only exhibited in approximately 5% of recorded nuclei – with only class Ib-like

structures present. Class Ia-like structures re-appear by 5 hrs, but only in small quantities, with the frequency of Rec10-positively stained nuclei staying below 20%. No Rec10-positively stained structures are visible at 6 hrs. At 7 hrs, there is a brief re-appearance of class Ia-like LinEs (accounting for approximately 10% of recorded nuclei); no LinEs are visible at 8 hrs and 9 hrs.

In comparison with a *rec10⁺/rec10⁺* asynchronous meiosis (Figure 6.2A), the temporal quantification of LinEs during a *rec10-109/rec10-109* (Figure 6.2B) demonstrates:

→ Only class Ia-like and class Ib-like LinEs are observed during a *rec10-109/rec10-109* asynchronous meiosis.

→ LinEs first appear at 2 hrs (up to 2 hrs earlier than seen in wild type) during a *rec10-109/rec10-109* asynchronous meiosis.

→ The number of Rec10-positively stained nuclei at 2 hrs during a *rec10-109/rec10-109* asynchronous meiosis is similar to that seen at 6-7 hrs during a wild type asynchronous meiosis.

→ The number of Rec10-positively stained nuclei from 4-9 hrs is dramatically lower (if there at all) during a *rec10-109/rec10-109* asynchronous meiosis.

6.2.1a(ii) Meiotic progression during a *rec10-109/rec10-109* asynchronous meiosis

Figure 6.2C shows that the horsetail stage occurs between approximately 2 hr and 8 hrs, peaking at 5 hrs. We observe that cells appear to begin the first meiotic division at approximately 7 hrs.

In comparison with a *rec10⁺/rec10⁺* asynchronous meiosis (Figure 4.3B), the temporal profile of meiotic nuclei during a *rec10-109/rec10-109* (Figure 6.2C) demonstrates no obvious differences.

A

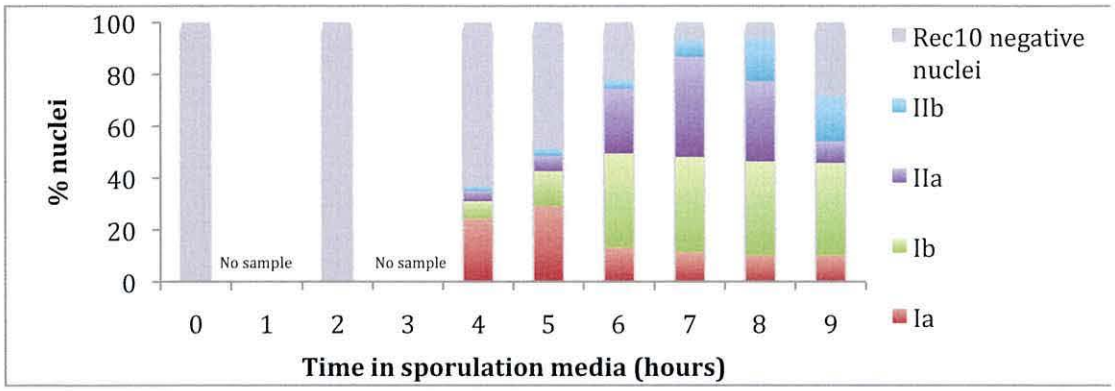

B

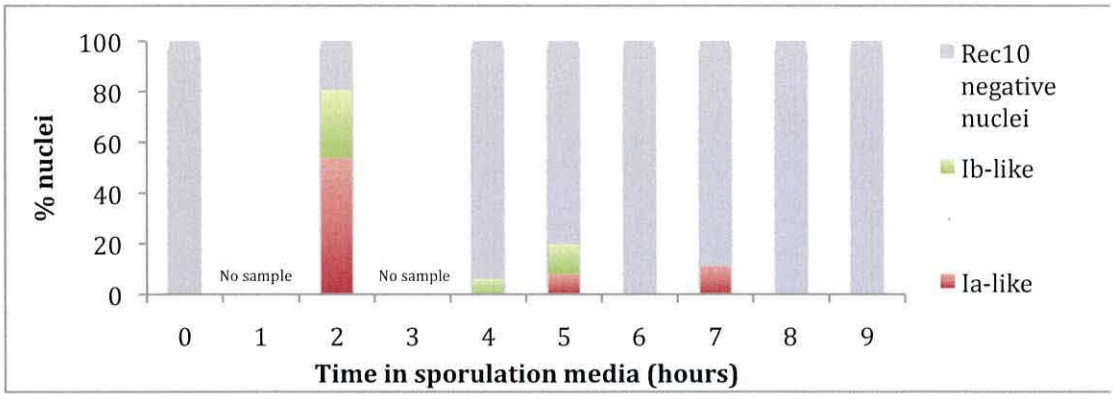

C

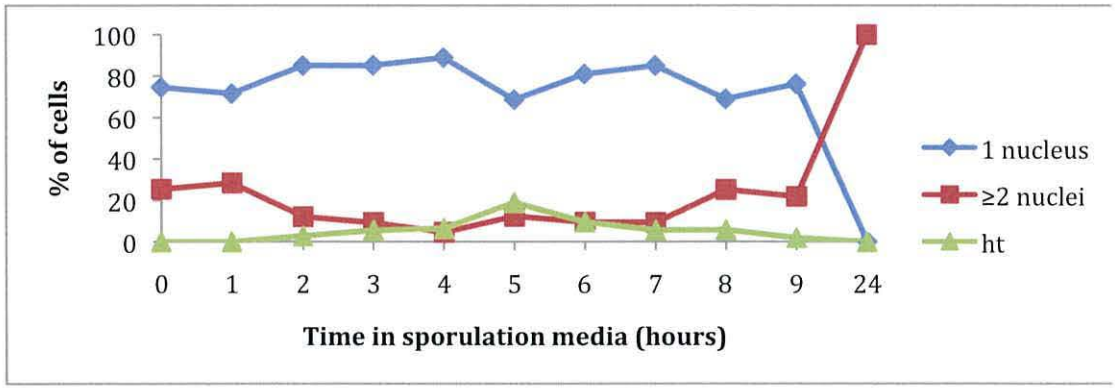

Figure 6.2 Development of LinEs during an asynchronous meiosis of a *rec10-109/rec10-109* diploid. (**A**) Proportions of LinE classes scored in *rec10⁺/rec10⁺* diploid asynchronous meiosis*. (**B**) Proportions of LinE classes found in samples taken at hourly intervals after transfer of *rec10-109/rec10-109* culture to sporulation media. ≥80 nuclei were scored for each time point* **. (* - No data was collected for time points 1 and 3 hours; ** These data are a duplication of Figure 4.3A and are represented for case of comparison)). (**C**) Analysis of cytological meiotic events in samples taken at hourly intervals after transfer of *rec10-109/rec10-109* culture to sporulation media. ≥80 nuclei were scored for each time point. ht – horsetail nuclei.

6.2.1b(i) LinE formation and development during a *rec10-144/rec10-144* asynchronous meiosis

Whilst analysing LinE formation in a *rec10-144/rec10-144* asynchronous meiosis, only two different types of LinE structures were observed; nuclei containing small dot-like class Ia-like foci, and nuclei containing slightly more elongated class Ib-like foci.

Figure 6.3B demonstrates that LinEs first appear 5 hrs after transferring the cells to sporulation media, during a *rec10-144/rec10-144* asynchronous meiosis, where approximately 50% of nuclei recorded exhibit Rec10-positive staining (~40% class Ia-like; ~10% class Ib-like). The number of Rec10-positively stained nuclei decreases by approximately half by 6 hrs and 7 hrs, with class Ia –like structures remaining dominant at 6 hrs, whilst class Ib-like structures dominate the 7 hrs. By 8 hrs, only ~5% of recorded nuclei exhibit Rec10-positive staining. No LinEs are visible by 9 hrs.

In comparison with a *rec10⁺/rec10⁺* asynchronous meiosis (Figure 6.3A), the temporal quantification of LinEs during a *rec10-144/rec10-144* (Figure 6.3B) demonstrates:

- → LinEs appear later (by ~1 hr) during a *rec10-144/rec10-144* asynchronous meiosis.
- → Only class Ia-like and class Ib-like LinE structures are observed during a *rec10-144/rec10-144* asynchronous meiosis.
- → LinEs 'disappear' earlier (by 1 hr or more) during a *rec10-144/rec10-144* asynchronous meiosis.

6.2.1b(ii) Meiotic progression during a *rec10-144/rec10-144* asynchronous meiosis

In Figure 6.3C, we see that the horsetail stage occurs between 4-9 hrs – peaking at approximately 5-6 hrs. Cells appear to begin the first meiotic division at approximately 5 hrs, with ~40% of cells exhibiting ≥2 nuclei by 9 hrs, and meiosis appearing to have completed by 24 hrs.

In comparison with a *rec10⁺/rec10⁺* asynchronous meiosis (Figure 4.3B), the temporal profile of meiotic nuclei during a *rec10-144/rec10-144* asynchronous meiosis (Figure 6.3C) demonstrates:

→ A slight advancement in the timing of the onset of the horsetail stage during a *rec10-144/rec10-144* asynchronous meiosis.

→ Advancement in cells starting the first meiotic division during a *rec10-144/rec10-144* asynchronous meiosis.

A

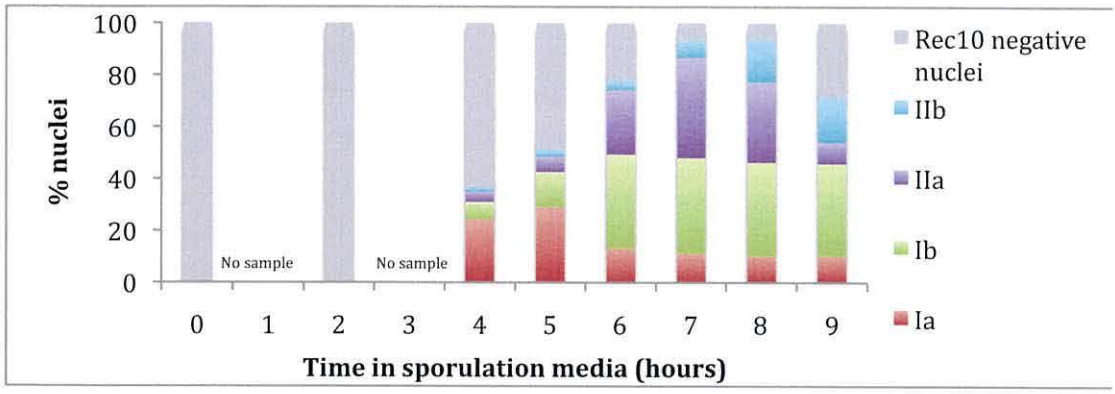

B

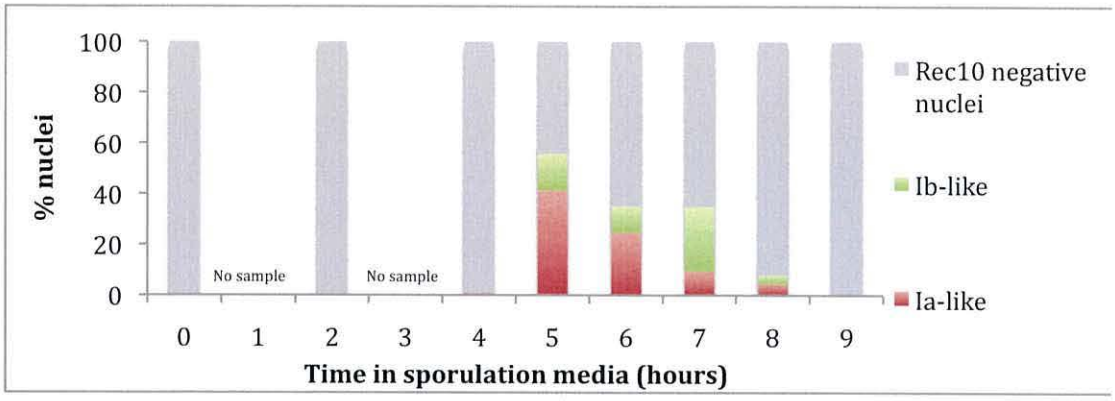

C

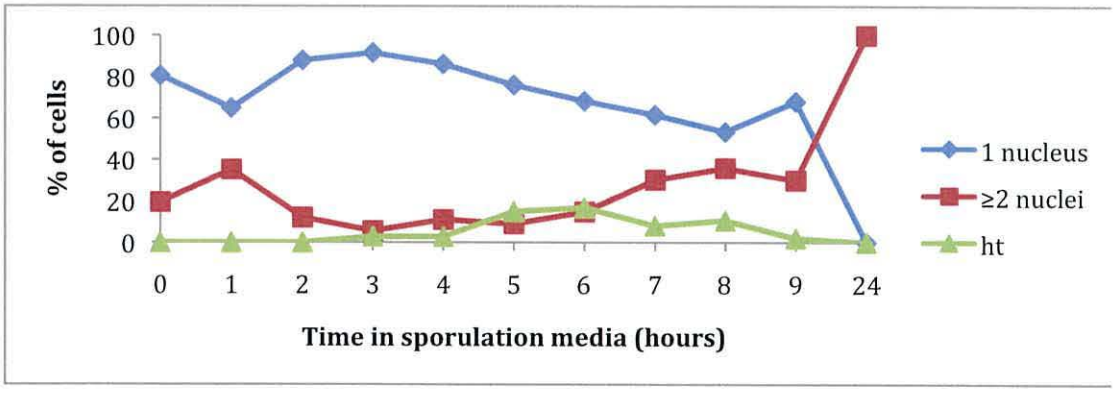

Figure 6.3 Development of LinEs during an asynchronous meiosis of a *rec10-144/rec10-144* diploid. (**A**) Proportions of LinE classes scored in *rec10⁺/rec10⁺* diploid asynchronous meiosis*. (**B**) Proportions of LinE classes found in samples taken at hourly intervals after transfer of *rec10-144/rec10-144* culture to sporulation media. ≥80 nuclei were scored for each time point* **. (* - No data was collected for time points 1 and 3 hours; ** These data are a duplication of Figure 4.3A and are represented for case of comparison). (**C**) Analysis of cytological meiotic events in samples taken at hourly intervals after transfer of *rec10-144/rec10-144* culture to sporulation media. ≥80 nuclei were scored for each time point. ht – horsetail nuclei.

6.2.2 Analysis of LinE formation and development, and meiotic progression in mutants of LinE-associated proteins

As previously mentioned, LinE formation is aberrant in a *rec8* mutant (MOLNAR *et al.,* 2003; LORENZ *et al.,* 2004) they exhibit temporal differences in a *rec12* mutant (MOLNAR *et al.,* 2003; LORENZ *et al.,* 2004) and LinEs are absent in both *rec25* and *rec27* mutants (DAVIS *et al.,* 2008).

6.2.2a *rec8*

In *S. pombe* loss of Rec8 results in aberrant LinE formation (LORENZ *et al.,* 2006; MOLNAR *et al.,* 1995), although Rec10 has been shown to recruit to the chromosomes at low levels in the absence of Rec8 (LORENZ *et al.,* 2004). The residual levels of LinE formation still observed are attributed to the presence of a Rec8 paralogue, Rad21 (a mitotic cohesin also expressed in meiosis) (LOIDL 2006).

6.2.2a(i) LinE formation and development during a *rec8Δ/rec8Δ* asynchronous meiosis

Whilst analysing LinE formation in a *rec8Δ/rec8Δ* asynchronous meiosis, we grouped the aberrantly formed LinE structures visualised into two distinct classes; nuclei containing two or more short (reminiscent of class Ib LinEs) Rec10-positively stained foci were categorised as 'A' nuclei, and nuclei containing longer (reminiscent of class IIa/IIb LinEs) Rec10-positively stained structures were categorised as 'B' nuclei (see Figure 6.4).

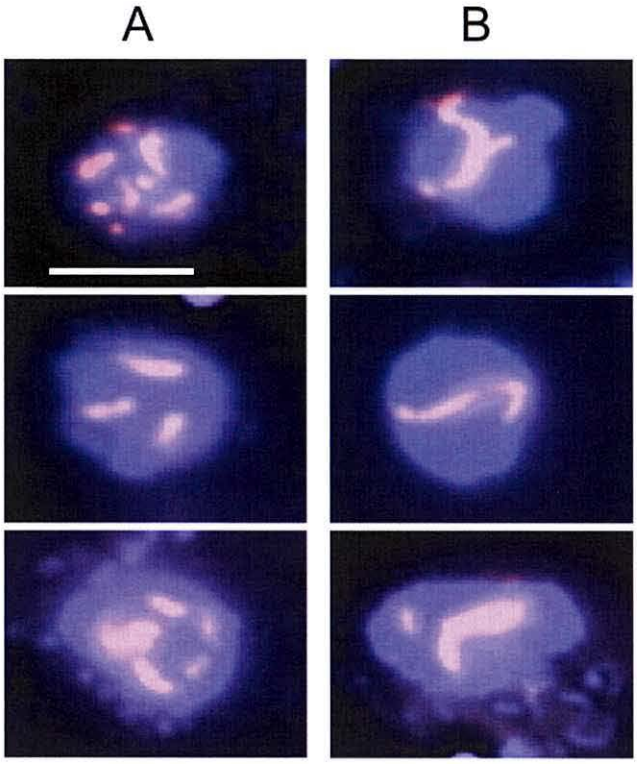

Figure 6.4 Examples of Rec10-positively stained nuclei in a *rec8Δ/rec8Δ* asynchronous meiosis. All nuclei are stained for DNA (blue) and Rec10 (red). Three examples are shown for each category (A and B). Scale bar = 5 μm.

In Figure 6.5B LinEs are first observed at 4 hr after transfer of the cells to sporulation medium, with 'A' and 'B' structures present in a fairly equal proportion, totalling ~60% of all recorded nuclei. The number of Rec10-positively stained nuclei decreases by 5 hrs to ~30%, both 'A' and 'B' structures are still observed. The frequency of LinE-containing nuclei drops again by 6 hrs, and again by 7 and 8 hrs. No LinEs were recorded at all at 9 hrs.
In comparison with a *rec10⁺/rec10⁺* asynchronous meiosis (Figure 6.5A), the temporal quantification of LinEs during a *rec8Δ/rec8Δ* asynchronous meiosis (Figures 6.5B) demonstrates:

→ Only aberrantly formed LinEs, which we have categorised into class 'A' and class 'B' structures are formed during a *rec8Δ/rec8Δ* asynchronous meiosis.

→ A dramatically reduced frequency of Rec10 positively stained nuclei from 5 hrs onwards during a *rec8Δ/rec8Δ* asynchronous meiosis.

→ Complete lack of visible LinEs at 9 hrs during a *rec8Δ/rec8Δ* asynchronous meiosis.

6.2.2a(ii) Meiotic progression during a *rec8Δ/rec8Δ* asynchronous meiosis

In Figure 6.5C, the horsetail stage is demonstrated to occur between 1-5 hrs, peaking at approximately 4 hrs. Cells begin the first meiotic division at approximately 2 hrs, with ~100% of cells exhibiting ≥2 nuclei by 5 hrs.

In comparison with a *rec10⁺/rec10⁺* asynchronous meiosis (Figure 4.3B), the temporal profile of meiotic nuclei during a *rec8Δ/rec8Δ* asynchronous meiosis (Figure 6.5C) demonstrates:

→ Advancement of up to 4 hrs in the timing of the onset of the horsetail stage during a *rec8Δ/rec8Δ* asynchronous meiosis.

→ Advancement of up to 7 hrs in the onset of the first meiotic division during a *rec8Δ/rec8Δ* asynchronous meiosis.

→ No visible profiling of the last mitotic division during a *rec8Δ/rec8Δ* asynchronous meiosis.

A

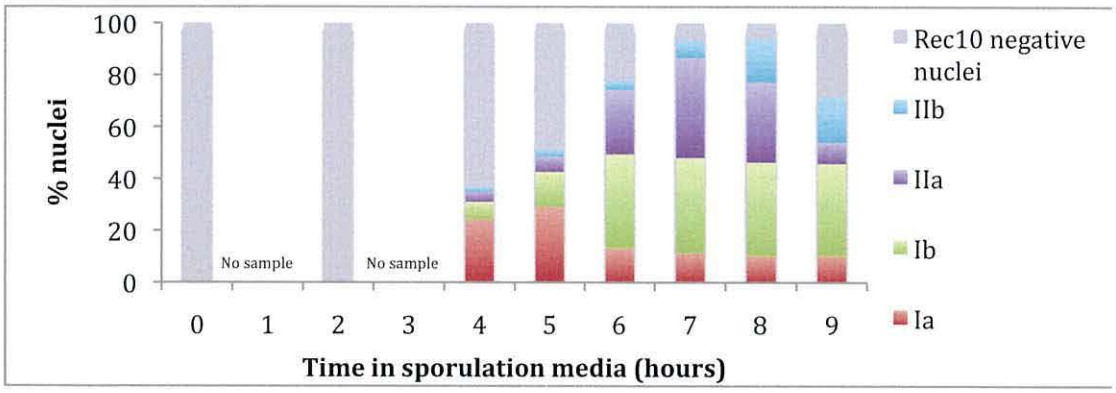

B

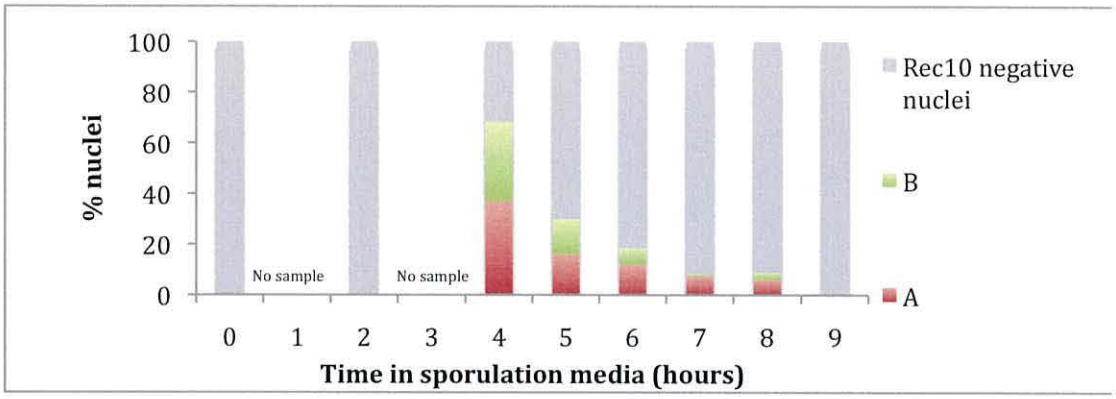

C

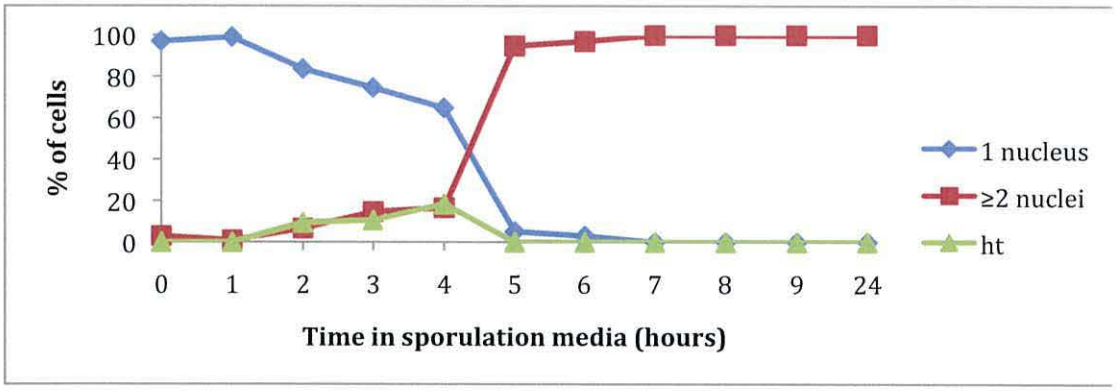

Figure 6.5 Development of LinEs during an asynchronous meiosis of a *rec8Δ/rec8Δ* diploid. (**A**) Proportions of LinE classes scored in *rec10⁺/rec10⁺* diploid asynchronous meiosis. * (**B**) Proportions of LinE classes found in samples taken at hourly intervals after transfer of *rec8Δ/rec8Δ* culture to sporulation media. ≥80 nuclei were scored for each time point* **. (* - No data was collected for time points 1 and 3 hours; ** These data are a duplication of Figure 4.3A and are represented for case of comparison). (**C**) Analysis of cytological meiotic events in samples taken at hourly intervals after transfer of *rec8Δ/rec8Δ* culture to sporulation media. ≥80 nuclei were scored for each time point. ht – horsetail nuclei.

6.2.2b *rec12*

Previous studies have analysed the temporal development of LinEs in a *rec12-152* mutant (MOLNAR *et al.,* 2003). However, these analyses were performed on silver stained nuclei visualised with an electron microscope, and also used a different classification system to what is currently widely used an accepted (described in Chapter 1). We therefore utilised Rec10-positive staining of LinEs in a *rec12Δ/rec12Δ* strain in order to enhance previous studies on LinE formation and development in the absence of Rec12.

6.2.2b(i) LinE formation and development during a *rec12Δ/rec12Δ* asynchronous meiosis

Whilst analysing LinE development in a *rec12Δ/rec12Δ* asynchronous meiosis, we observed all classes of LinEs found in a wild-type meiosis (Figure 6.6).

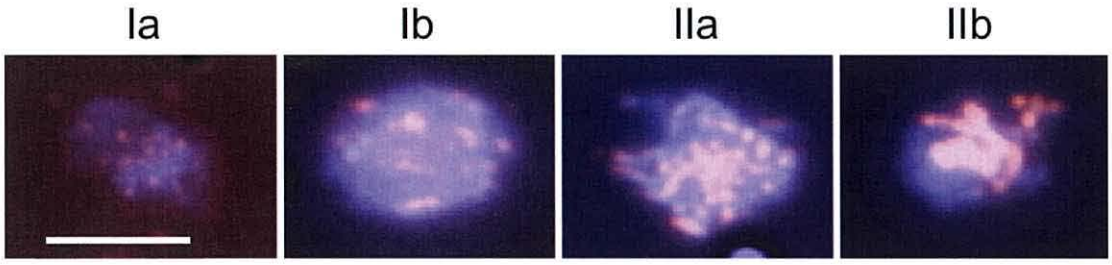

Figure 6.6 Examples of Rec10-stained nuclei in a *rec12Δ/rec12Δ* mutant. Nuclei are stained for DNA (blue) and Rec10 (red). One example is shown for each LinE class. Scale bar = 5 μm.

Figure 6.7B demonstrates the first appearance of LinEs occurs at 4 hrs after cells were transferred to sporulation medium, with class Ia (~35%), class Ib (~5%) and class IIa (~1%) structures visible. Class Ia LinEs continue to be the most frequently recorded structures from 4-7 hrs. Class IIb LinEs are present in small numbers (<5%) at 5 -7 hrs. The frequency of Rec10-postively stained structures remains fairly constant at ~30-35% between 5-7 hrs. At 7 hrs, the frequency of Rec10-positively stained nuclei falls to <10%, and by 9 hrs, no LinEs are visible.

In comparison with a *rec10⁺/rec10⁺* asynchronous meiosis (Figure 6.7A), the temporal quantification of LinEs during a *rec12Δ/rec12Δ* asynchronous meiosis (Figures 6.7B) demonstrates:

→ Reduced frequency of Rec10-positively stained structures from 5 hrs onwards during a *rec12Δ/rec12Δ* asynchronous meiosis.

→ No LinEs visible at 9 hrs during a *rec12Δ/rec12Δ* asynchronous meiosis.

→ Reduction in the frequency of class Ib, IIa and IIb structures throughout the time course during a *rec12Δ/rec12Δ* asynchronous meiosis.

6.2.2b(ii) Meiotic progression during a *rec12Δ/rec12Δ* asynchronous meiosis

Figure 6.7C demonstrates that the horsetail stage appears to occur between 3-6 hrs, peaking at 4 hrs. Cells start the first meiotic division at 5 hrs, with all cells exhibiting ≥2 nuclei by 6 hrs.

In comparison with a *rec10⁺/rec10⁺* asynchronous meiosis (Figure 4.3B), the temporal profile of meiotic nuclei during a *rec12Δ/rec12Δ* asynchronous meiosis (Figure 6.7C) demonstrates:

→ Advancement in the onset of the horsetail stage during a *rec12Δ/rec12Δ* asynchronous meiosis.

→ Advancement in starting the first meiotic division during a *rec12Δ/rec12Δ* asynchronous meiosis.

→ Appearance of a more rapid meiotic division in a *rec12Δ/rec12Δ* asynchronous meiosis.

A

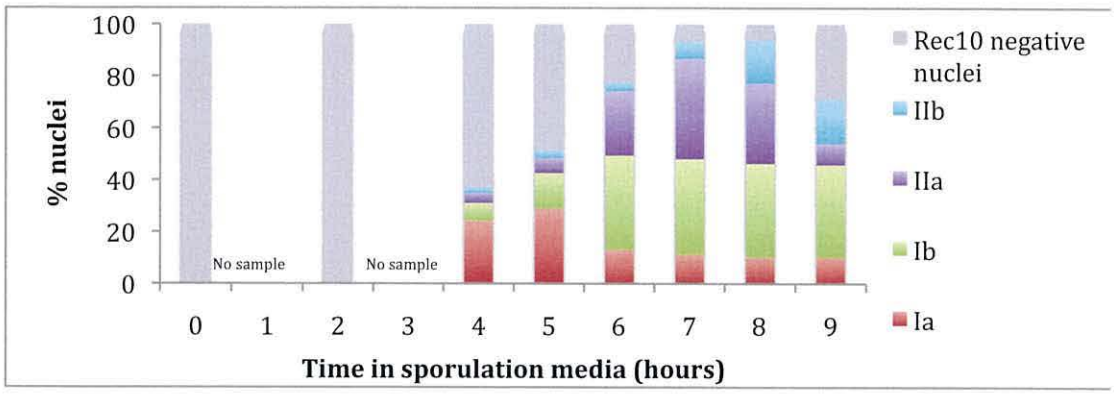

B

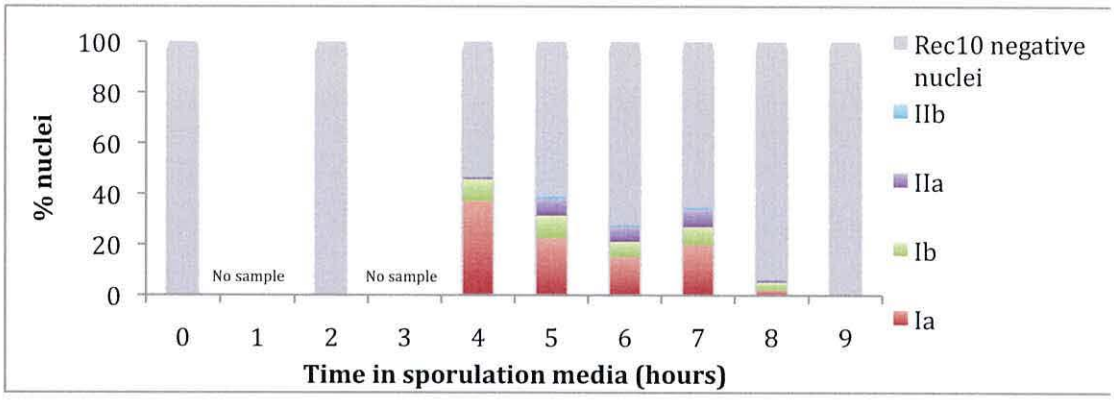

C

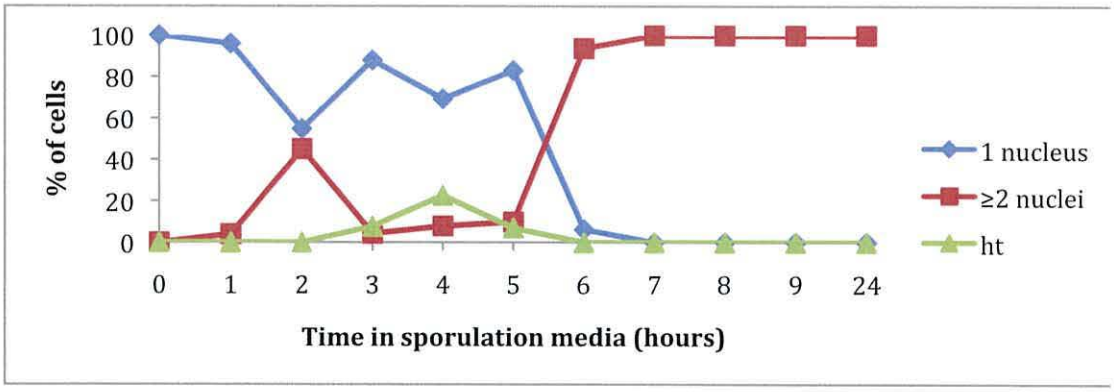

Figure 6.7 Development of LinEs during an asynchronous meiosis of a *rec12Δ/rec12Δ* diploid. (**A**) Proportions of LinE classes scored in *rec10⁺/rec10⁺* diploid asynchronous meiosis*. (**B**) Proportions of LinE classes found in samples taken at hourly intervals after transfer of *rec12Δ/rec12Δ* culture to sporulation media. ≥80 nuclei were scored for each time point* **. (* - No data was collected for time points 1 and 3 hours; ** These data are a duplication of Figure 4.3A and are represented for case of comparison). (**C**) Analysis of cytological meiotic events in samples taken at hourly intervals after transfer of *rec12Δ/rec12Δ* culture to sporulation media. ≥80 nuclei were scored for each time point. ht – horsetail nuclei.

6.2.2c *rec27*

Previous studies reported that both Rec25 and Rec27 are components of LinEs, and are required for localization of Rec10 to LinEs; no Rec10-positively stained LinEs being observed by cytological analysis of *rec25Δ* and *rec27Δ* (DAVIS *et al.*, 2008).They proposed that Rec10, Rec25 and Rec27 may act as a complex (due to their co-localisation patterns), and that Rec10 and Rec25 act together to promote the majority of meiotic recombination (DAVIS *et al.*, 2008).

Previous cytological analysis of LinE formation and development in *rec25Δ* and *rec27Δ* meioses were performed during a *pat1-114* temperature induced synchronous meiosis (DAVIS *et al.*, 2008). Our analysis of LinE formation and development in a *pat1-114* background revealed that LinEs do not form normally during a *pat1-114* temperature induced synchronous meiosis (data in Chapter 3). Therefore, we analysed the temporal profile of LinE formation and development during an asynchronous *pat1*$^+$ meioses for both *rec25Δ* and *rec27Δ* mutants.

We did not observe any Rec10-positively stained structures whilst analysing spread nuclei from a *rec25Δ/rec25Δ* asynchronous meiosis.

6.2.2c(i) LinE formation and development during a *rec27Δ/rec27Δ* asynchronous meiosis

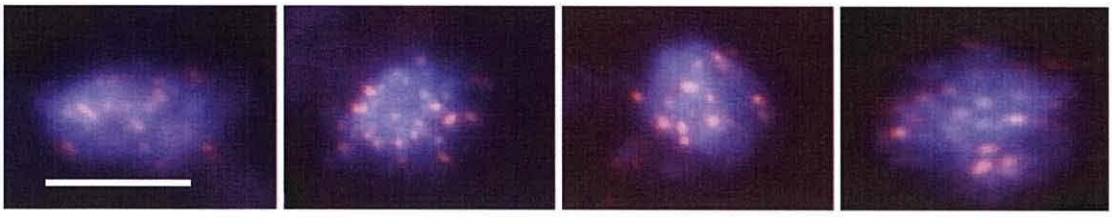

Figure 6.8 Examples of Rec10 positively stained nuclei in a *rec27Δ/rec27Δ* asynchronous meiosis. Nuclei are stained for DNA (blue) and Rec10 (red). Four examples are shown. Scale bar = 5 μm.

In Figure 6.9A, class Ia LinEs (Figure 6.8) are demonstrated to appear at 4 hrs after cells were transferred to sporulation medium, representing ~50-60% of all recorded nuclei - no other Rec10-positive structures are observed at any other

time point. Following the brief appearance of LinEs, as visualised in Figure 6.9A, the time course experiment was repeated, and additional samples were taken, as seen in Figure 6.9B. The data in Figure 6.9B shows that class Ia LinEs appear at 4 hrs after cells were transferred to sporulation medium (~50% of all nuclei recorded), and are still visible at 4.5 hrs, at a reduced frequency of ~10%. No LinEs are observed after 4.5 hrs.

In comparison with a *rec10⁺/rec10⁺* asynchronous meiosis, the temporal quantification of LinEs during a *rec27Δ/rec27Δ* asynchronous meiosis (Figures 6.9A + 6.9B) demonstrates:

→ Only class Ia LinEs are exhibited during a *rec27Δ/rec27Δ* asynchronous meiosis.

→ Rec10-positively stained LinEs are only observed at 4 hrs and 4.5 hrs during a *rec27Δ/rec27Δ* asynchronous meiosis.

6.2.2c(ii) Meiotic progression during a *rec27Δ/rec27Δ* asynchronous meiosis

In Figure 6.9C, we observe that the horsetail stage occurs between 2-6 hrs, peaking at 3 hrs. The first cells appear to begin the first meiotic division at approximately 4 hrs, with 100% of cells exhibiting ≥2 nuclei by 8 hrs.

In comparison with a *rec10⁺/rec10⁺* asynchronous meiosis (Figure 4.3B), the temporal profile of meiotic nuclei during a *rec27Δ/rec27Δ* asynchronous meiosis (Figure 6.9C) demonstrates:

→ Advancement of the timing (~4 hrs) of the onset of the horsetail stage during a *rec27Δ/rec27Δ* asynchronous meiosis.

→ Advancement of ~5 hrs in cells beginning the first meiotic division during a *rec27Δ/rec27Δ* asynchronous meiosis.

→ All cells exhibiting ≥2 nuclei by 8 hrs during a *rec27Δ/rec27Δ* asynchronous meiosis.

A

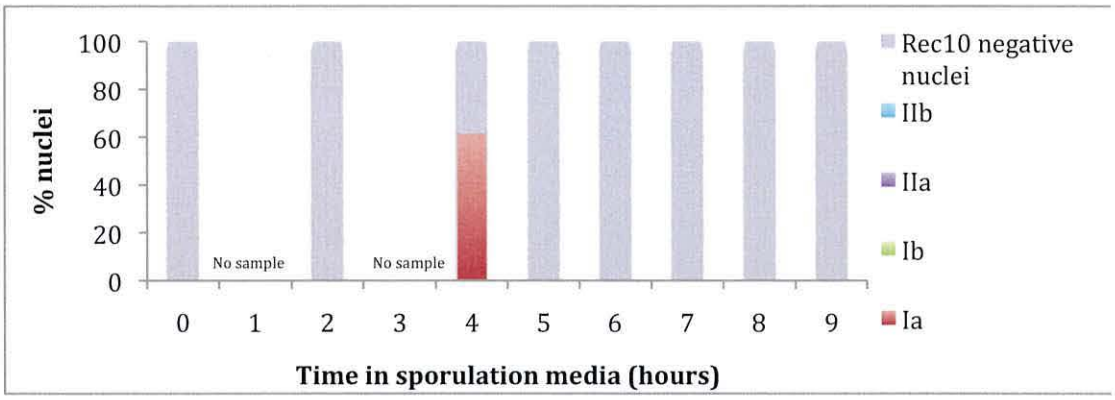

B

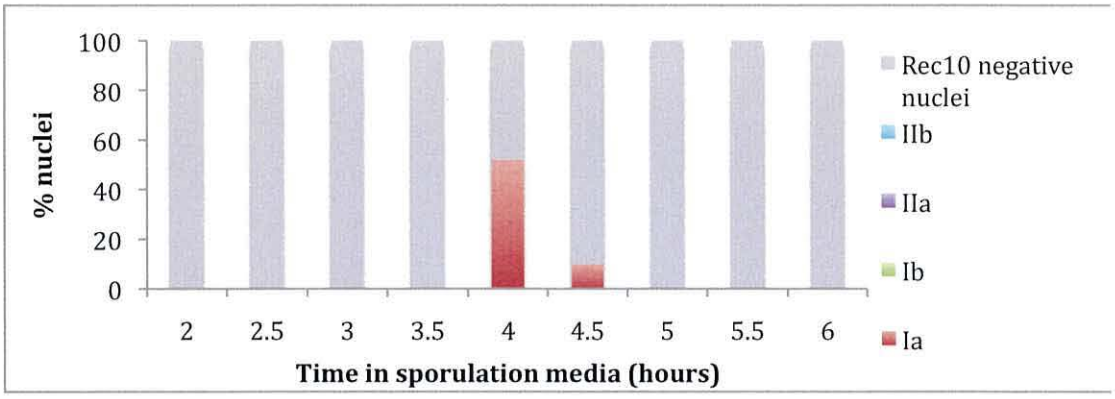

C

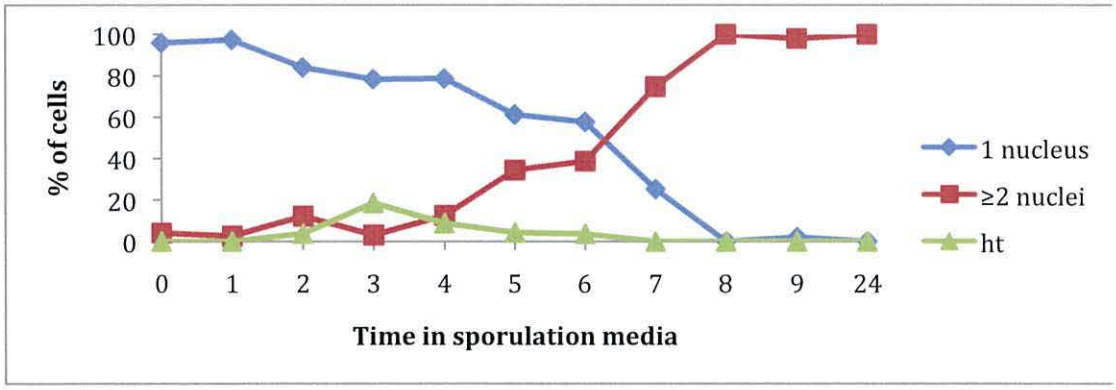

Figure 6.9 Development of LinEs during an asynchronous meiosis of a *rec27Δ/rec27Δ* diploid. (**A**) Proportions of LinE classes found in samples taken at hourly intervals after transfer of culture to sporulation media. ≥80 nuclei were scored for each time point*. (**B**) Proportions of LinE classes found in samples taken at half hourly intervals after transfer of *rec27Δ/rec27Δ* culture to sporulation media. ≥80 nuclei were scored for each time point*. (* - No data was collected for time points 1 and 3 hours). (**C**) Analysis of cytological meiotic events in samples taken at hourly intervals after transfer of *rec27Δ/rec27Δ* culture to sporulation media. ≥80 nuclei were scored for each time point. ht – horsetail nuclei.

6.3 Discussion

6.3.1 Observations on the temporal profile of LinE formation and development in *rec10-109* and *rec10-144* mutants

6.3.1a *rec10-109*

Previous studies reported that *rec10-109* mutants exhibited only dot-like or short-lines of Rec10-positive staining (LORENZ *et al.,* 2004); the data in Figure 6.2 is in agreement with this.

The observations reported here highlight the high frequency of Rec10-positively stained structures exhibited at 2 hrs in Figure 6.2. This observation makes it possible for us to suggest that the *rec10-109* mutation has an effect on the timing of LinE appearance, inferring that the amino acids mutated in this strain (176 and 178) play a role in the temporal regulation of LinE formation as well as maturation. Subsequent to 2 hrs, the maximum number of Rec10-positively stained nuclei throughout the time course is ~20% at 5 hrs. This suggests that the *rec10-109* mutant fails to maintain stable LinE structures.

6.3.1b *rec10-144*

During a *rec10-144/rec10-144* asynchronous meiosis, Figure 6.2 demonstrates that LinEs first appear at a later time point (5 hrs) than observed in wild-type. This delay in LinE formation may be due to a defect in initiation LinE formation caused by the *rec10-144* mutation. Alongside delayed formation, the *rec10-144/rec10-144* mutant displays only class Ia-like and class Ib-like structures; this is in agreement with previous studies that observed a lack of more mature structures (PRYCE *et al.*, 2005).

The *rec10-144* mutant exhibits a mis-sense point mutation at amino acid position 727, which is located in the C-terminal domain of Rec10 – a region thought to be involved in the homo-oligomerisation of Rec10, resulting in LinE development and maturation. The presence of this point mutation in the proposed homo-oligomerisation domain of Rec10, may explain the failure of LinEs to mature in a *rec10-144* mutant.

6.3.2 Observations on the temporal profile of LinE formation and development in four LinE-associated proteins

6.3.2a *rec8*

It has previously been reported than LinE formation is aberrant in a *rec8Δ* meiosis (LORENZ *et al.,* 2004; MOLNAR *et al.,* 2003). Silver-staining of *rec8* mutant spread nuclei revealed a prevalence of what was then termed class III nuclei (similar to our class 'B' designation) throughout the time course – proposed to be unspecific aggregates of LinE forming compounds rather than mature LinE structures (MOLNAR *et al.,* 1995). The data reported here, using Rec10-postitive staining of LinEs is in agreement with these previous studies. The advancement in meiotic progression observed in Figure 6.5C is in agreement with previous findings, made in a *rec8* mutant exhibiting a point mutation (MOLNAR *et al.,* 1995).

6.4.3b *rec12*

Previous studies on silver-stained nuclei of a *rec12* mutant revealed a prevalence of what they classed as 'class III' LinEs (which resemble our distinction of class IIb structures) throughout their time course (MOLNAR *et al.,* 2003). Later studies confirmed that the LinEs observed in *rec12* mutants were Rec10-positively stained structures, although a temporal profile of Rec10-positively stained structures was never obtained (LORENZ *et al.,* 2004).

The data obtained here (Figure 6.7B), utilises Rec10-positive staining to follow the temporal progression of LinE formation and development in the absence of *rec12*. These data demonstrate a highly reduced frequency of the more mature class Ib, IIa and IIb LinEs throughout the time course. This is not in agreement with previous studies, which reported a prevalence of more mature LinE structures throughout (MOLNAR *et al.,* 2003). In fact, the observations made in this study show a prevalence of class Ia structures throughout (Figure 6.4B). This indicates that although LinE formation appears to be initiated normally, LinEs fail to fully develop in the absence of *rec12*. Consequently, this study supports the conclusion that the formation of LinEs is not dependent on the formation of DSBs (MOLNAR *et al.,* 2003), but their subsequent development and maturation may be dependent upon a process initiated by DSB formation.

The observation made in this study, that meiotic divisions appear to initiate sooner in the absence of Rec12 is in agreement with previous studies (MOLNAR *et al.,* 2003). However, we report the appearance of a more rapid meiotic division in a *rec12Δ/rec12Δ* asynchronous meiosis, which is not in agreement with previous findings (MOLNAR *et al.,* 2003).

6.4.3c *rec27*

Our cytological analysis of a *rec25Δ/rec25Δ* asynchronous meiosis, revealed no Rec10-positively stained LinE structures (data not shown), in agreement with previous findings. However, Figure 6.9A + 6.9B demonstrates that LinEs are formed, albeit in a compromised manner, during a *rec27Δ/rec27Δ* asynchronous meiosis.

These data indicate that LinE formation can be initiated, without subsequent maturation in the absence of Rec27, and that the complete absence of Rec10-positively stained LinEs in a *rec27Δ/rec27Δ* asynchronous meiosis previously reported may bean artefact caused by the use of the *pat1-114* synchronisation method.

These data suggest that Rec27, although not fully essential for Rec10 loading as previously reported, is required for wild-type levels of LinE formation and development, as Rec10-positively stained structures are observed at a dramatically reduced frequency during a *rec27Δ/rec27Δ* asynchronous meiosis. Previous studies have suggested that Rec10, Rec25 and Rec27 are not loaded in a step-wise manner, as their loading was proposed to be inter-dependent (DAVIS *et al.,* 2008). However, our data indicate that Rec10 loading is not Rec27-dependent.

Chapter 7

Analysis of potential regions of crossover preference governed by linear elements

7.1 Introduction

Rec10 is the main component of *S. pombe* LinEs (LORENZ *et al.,* 2004). It has also been demonstrated to function in recombination, regulation of hotspot activation and pairing of homologous chromosomes (ELLERMEIER and SMITH 2005; LORENZ *et al.,* 2006; MOLNAR *et al.,* 2003; PRYCE and MCFARLANE 2009; WELLS *et al.,* 2006). Studies on meioses that are heterozygous for *rec10* alleles that result in varying degrees of defective LinE formation, have also demonstrated a region-specific loss of crossover function; these data inferring a role for LinEs in mediating crossing over (WELLS *et al.,* 201X).

A model has been proposed, in which LinEs define regions of crossover preference (RCP) across the genome (WELLS *et al.,* 201X). The model suggests that crossing over preferentially occurs in regions associated with LinEs. Therefore, in cases where LinE formation is defective (aberrant in LinE maturation) such as in a *rec10⁺/rec10-155* heterozygous meiosis (WELLS *et al.,* 201X), the shorter LinE structures associate with specific regions of the genome, ensuring crossover proficiency in these regions.

This chapter, the work described aims to study the recombination frequencies of *rec10* heterozygote crosses, analysing the apparent semi-dominant nature of some *rec10* mutant alleles. We also aim to further test the hypothesis of RCP in several *rec10* mutants. Alongside this, we look at the effect of *rec10* heterozygosity on the formation and development of LinEs.

7.2 Results

7.2.1 *rec10⁺/rec10-175*

7.2.1a Analysis of intragenic recombination in *rec10-175* hetero- and homo- zygous crosses

Previous studies on *rec10+/rec10-155* and *rec10+/rec10-144* heterozygote crosses have shown that they exhibit a ~2-fold reduction in intragenic recombination frequency compared to *rec10⁺/rec10⁺*; data that lead to the proposal of semi-dominance for the *rec10-144* and *rec10-155* mutant alleles (PRYCE *et al.* 2005).

Here, two factor crosses were employed to analyse the effect of *rec10-175* heterozygosity on intragenic recombination frequency at three distinct loci in the *S. pombe* genome. In Table 7.1, firstly looking at the data for the *ade6-M26* hotspot allele, we observe that both *rec10-175* heterozygous and homozygous crosses result in a highly significant reduction in recombination frequency in comparison to the wild type frequency. There is a greater reduction in recombination frequency in the *rec10-175* homozygous mutant (~100-fold) than observed in either heterozygote (which exhibit fairly similar frequencies to each other: ~4-fold).

At the *ura1*and *lys7* loci, (with the exception of one result) we observe than only the *rec10-175* homozygous mutants exhibit a significant reduction in recombination frequency, again ~100-fold.

Table 7.1 **Intragenic recombination in *rec10⁺/rec10-175* heterozygous and *rec10-175/rec10-175* homozygous diploids at the *ade6*, *ura1* and *lys7* loci**

	rec10 alleles	Test alleles h^+	Test alleles h^-	Mean rf [a, b, d]	% of *rec10⁺* rf [c]
ade6	*wt x wt*	*M26*	*52*	3778 ± 574	-
	wt x 175	*M26*	*52*	807 ± 318	21.4 ***
	175 x wt	*M26*	*52*	953 ± 624	25.2 ***
	175 x 175	*M26*	*52*	7 ± 13	0.9 ***
ura1	*wt x wt*	*171*	*61*	180 ± 13	-
	wt x wt	*61*	*171*	308 ± 94	-
	wt x 175	*61*	*171*	171 ± 121	55.5
	175 x wt	*171*	*61*	110 ± 32	61.1 *
	wt x 175	*171*	*61*	254 ± 58	141.1
	175 x wt	*61*	*171*	220 ± 220	71.4
	175 x 175	*61*	*171*	3 ± 2	0.97 ***
	175 x 175	*171*	*61*	2 ± 2	1.1 ***
lys1	*wt x wt*	*2*	*1*	63 ± 96	-
	wt x wt	*1*	*2*	133 ± 97	-
	wt x 175	*2*	*1*	34 ± 34	54.0
	175 x wt	*1*	*2*	158 ± 154	118.8
	wt x 175	*2*	*1*	53 ± 73	84.1
	175 x wt	*1*	*2*	89 ± 119	66.9
	175 x 175	*2*	*1*	0.0	0.0 ***
	175 x 175	*1*	*2*	3 ± 9	2.3 ***

rf – recombination frequency

a – n≥3 in all cases.

b – recombination frequency calculated by counting number of prototrophs per 10^6 viable spores.

c – Student's *t*-test *P*-values for two tailed comparisons of *rec10* mutant data *vs. rec10⁺* (*P<0.05; **P<0.01; ***P<0.005)

d - +/- indicate 95% confidence interval.

7.2.1b LinE formation and development during a *rec10⁺/rec10-175* asynchronous meiosis

Previous studies have reported a complete absence of LinEs in a *rec10-175* homozygous mutant. We analysed LinE formation and development during a *rec10⁺/rec10-175* asynchronous meiosis. All four classes of LinEs, as shown in Figure 7.1, were observed.

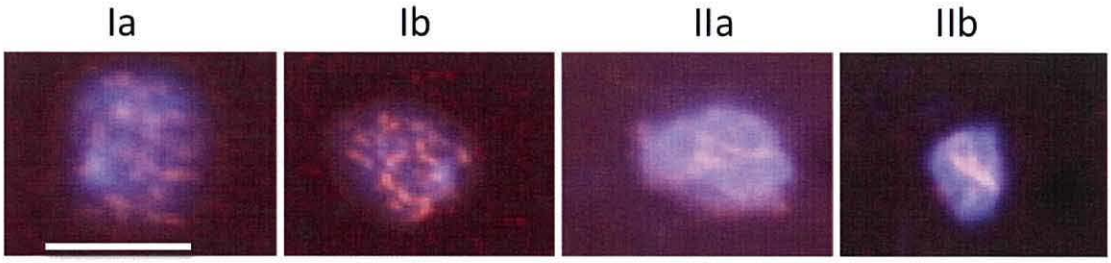

Figure 7.1 Examples of Rec10-positively stained nuclei in a *rec10⁺/rec10-175* asynchronous meiosis. All nuclei are stained for DNA (blue) and Rec10 (red). One example is shown for each LinE class. Scale bar = 5 μm.

Class Ia LinEs become visible at 2 hrs after transfer of cells into sporulation medium (Figure 7.2B). Class Ia, Ib and IIb LinEs are visible by 4 hrs, accounting for ~40% of all recorded nuclei. The frequency of Rec10-positively stained nuclei remains fairly constant between 4-6 hrs, as do the frequency of class Ia (~25%) and class Ib (~15%) LinEs. At 7 hrs the highest frequency of Rec10-positively stained nuclei is observed (~80%) – consisting mainly of class Ib LinEs (~50%), followed by ~20% class IIa LinEs. Class Ib LinEs remain to be most frequently observed at 8 hrs and 9 hrs, with both time points exhibiting ~60% Rec10-positively stained nuclei.

In comparison with a *rec10⁺/rec10⁺* asynchronous meiosis (Figure 7.2A), the temporal quantification of LinEs during a *rec10⁺/rec10-175* asynchronous meiosis (Figures 7.2B) demonstrates:

→ LinEs first appear at 2 hrs during a *rec10⁺/rec10-175* asynchronous meiosis.

→ A reduced frequency of class IIa and IIb LinEs throughout a *rec10⁺/rec10-175* asynchronous meiosis.

→ A reduced frequency of Rec10-positively stained nuclei during a *rec10⁺/rec10-175* asynchronous meiosis

7.2.1c Meiotic progression during a *rec10⁺/rec10-175* asynchronous meiosis

Figure 7.2C demonstrates that the horsetail stage appears to occur between the 3 hr and 7-8 hr time points, peaking between 3 hrs and 4 hrs. Progression to the first meiotic division begins at around 6 hrs, with all cells exhibiting ≥2 nuclei by the 24 hrs.

In comparison with a *rec10⁺/rec10⁺* asynchronous meiosis (Figure 4.3B), the temporal profile of meiotic nuclei during a *rec10⁺/rec10-175* asynchronous meiosis (Figure 7.2C) demonstrates:

→ Advancement in the onset of the horsetail stage during a *rec10⁺/rec10-175* asynchronous meiosis.

→ Advancement in the onset of the first meiotic division during a *rec10⁺/rec10-175* asynchronous meiosis.

A

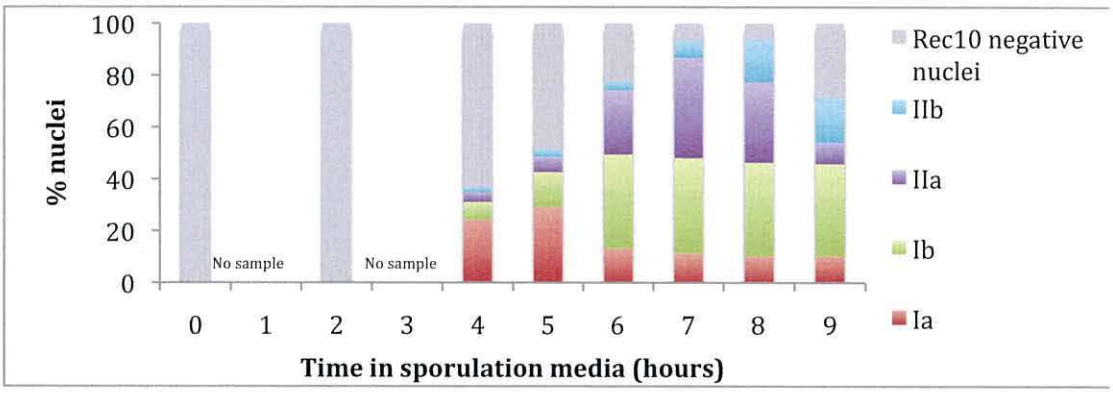

B

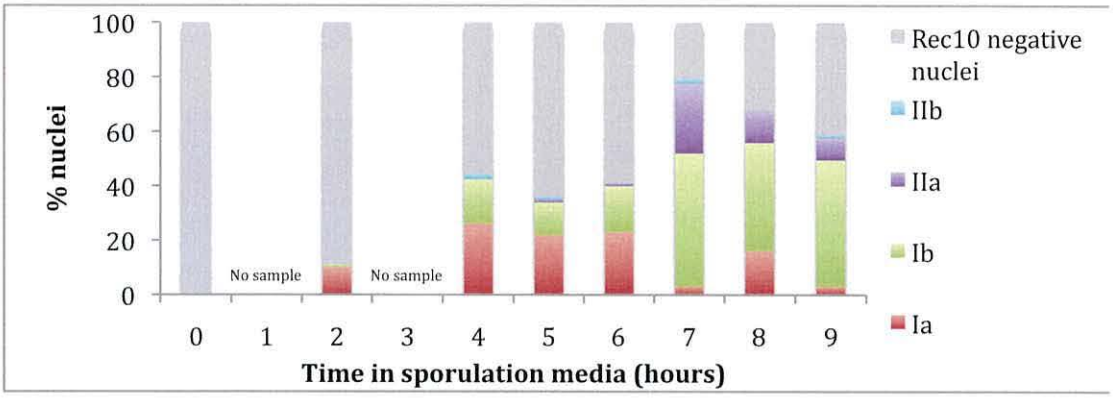

C

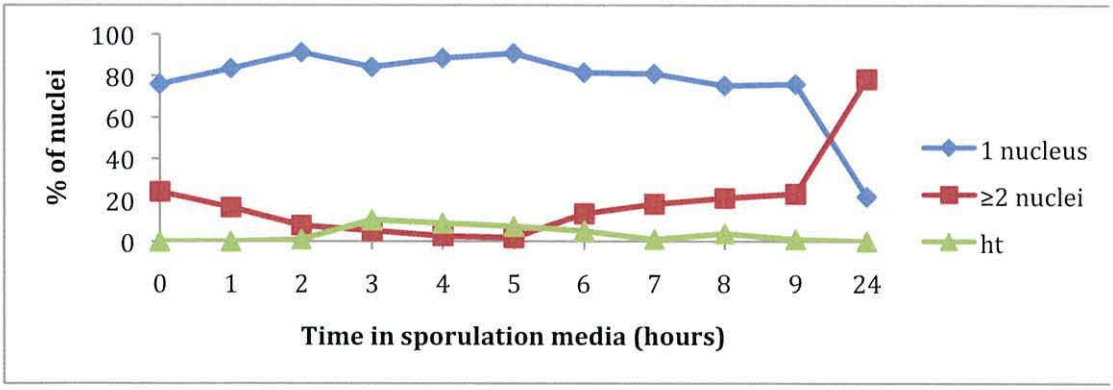

Figure 7.2 Development of LinEs during wild an asynchronous meiosis of a *rec10+/rec10-175* heterozygous diploid. (**A**) Proportions of LinE classes scored in *rec10⁺/rec10⁺* diploid asynchronous meiosis*. (**B**) Proportions of LinE classes found in samples taken at hourly intervals after transfer of *rec10+/rec10-175* culture to sporulation media. ≥80 nuclei were scored for each time point* **. (* - No data was collected for time points 1 and 3 hours; ** These data are a duplication of Figure 4.3A and are represented for case of comparison). (**C**) Analysis of cytological meiotic events in samples taken at hourly intervals after transfer of *rec10+/rec10-175* culture to sporulation media. ≥80 nuclei were scored for each time point. ht – horsetail nuclei.

7.2.2 *rec10⁺/rec10-155*

7.2.2a Intergenic recombination

Previous studies have reported that *rec10-155* homozygous mutant crosses exhibit significant reductions in intergenic recombination at the *ura1-pro1, pro2-arg3, lys4-his4, ade8-arg3* and *ade6-tps16* intervals (WELLS *et al.,* 2006). *rec10-155* heterozygous crosses (with *rec10⁺*) exhibit regional specificity in crossover proficiency – leading to the generation of the RCP model (WELLS PH.D., WELLS *et al.*, 201X). Studies have shown that at the *his4-lys4* and *pro2-arg3* intervals, the *rec10-155* heterozygous crosses exhibit a crossover frequency similar to that of *rec10-155* homozygous crosses, whilst at the *ade6-tps16* and *ade8-arg4* intervals, *rec10*-heterozyous crosses exhibit crossover proficiency similar to that of *rec10+* homozygous crosses (WELLS PH.D., WELLS *et al.*, 201X).

In this study we analyse the crossover frequency of *rec10-155* heterozygote crosses in comparison with *rec10⁺* and *rec10-155* homozygote crosses in order to further investigate the regional specificity of crossover proficiency reported in *rec10-155* heterozygote crosses. All intervals tested are shown in Figure 7.3.

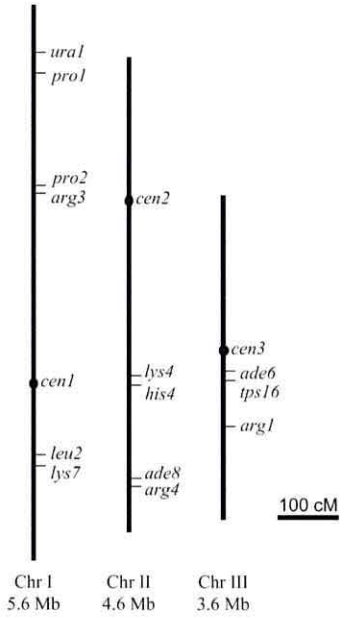

<u>Figure 7.3</u> Chromosomal positions of intergenic recombination intervals analysed in this study. Figure adapted from WELLS *et al.*, 2006.

Figure 7.4 demonstrates that at the *ade8-arg4* interval, the *rec10-155* homozygote exhibits a highly significant reduction in crossover frequency; the *rec10-155* heterozygote however does not exhibit a significant reduction in crossover frequency, and exhibit a frequency visibly comparable to that of the wild-type. At the *ura1-pro1* interval on the other hand, the *rec10-155* homozygous and heterozygous crosses all exhibit significant reductions in crossover frequencies.

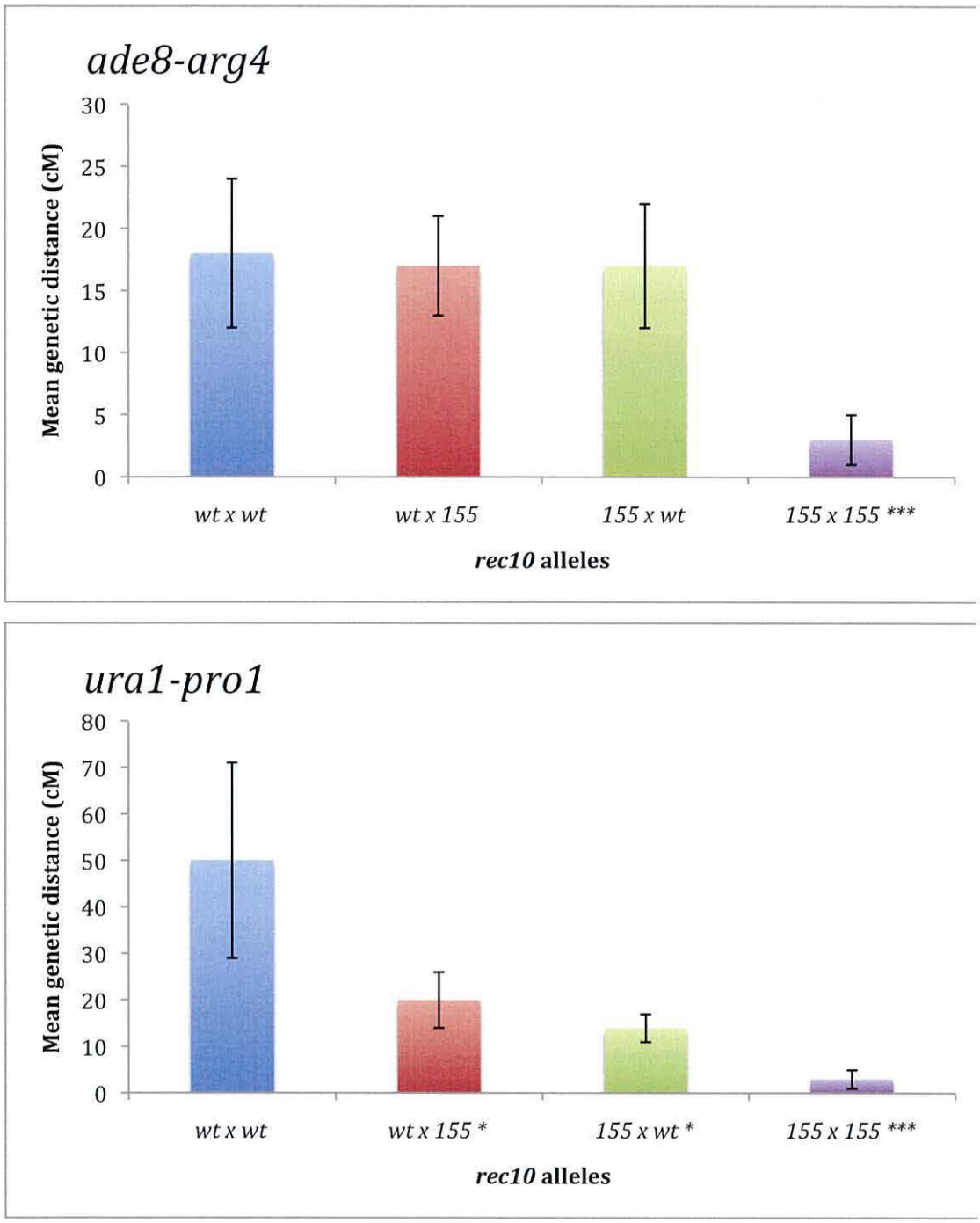

Figure 7.4 Intergenic recombination of *rec10⁺/rec10-155* heterozygous diploids and *rec10-155/rec10-155* homozygous diploids at the *ade8-arg4* and *ura1-pro1* intervals. cM distances are calculated using Haldane's formula; cM=-50ln(1-2R), where R is the total number of recombinants out of number of spores analysed. n≥3 in all cases. Error bars indicate 95% confidence interval in all cases. Student's *t*-test *P*-values of two tailed comparisons of *rec10* mutants *vs. rec10⁺* (*P<0.05; **P<0.01; ***P<0.005).

7.2.2b LinE formation and development during a *rec10⁺/rec10-155* asynchronous meiosis

LinEs do not form in *rec10-155* homozygous mutants. Therefore, we analysed LinE formation and development in a *rec10-155* heterozygous meiosis in order to establish whether the semi-dominance observed in analysing recombination frequencies in *rec10-155* heterozygotes spills over to effect LinE formation. Whilst analysing LinE formation in the *rec10-155* heterozygote, we observed all four classes of LinEs, as shown in Figure 7.5.

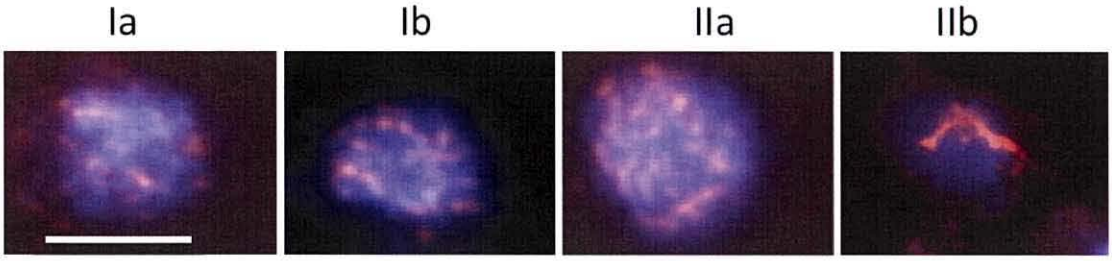

Figure 7.5 Examples of Rec10-stained nuclei in a *rec10⁺/rec10-155* asynchronous meiosis. All nuclei are stained for DNA (blue) and Rec10 (red). One example is shown for each LinE class. Scale bar = 5 μm.

In Figure 7.6B, class Ia LinEs first appear, in small numbers, at 2 hrs after transferring the cells to sporulation medium. All four classes of LinEs are visible by 4 hrs, with ~30% class Ia, ~30% class Ib and <5% class IIa and IIb LinEs. At 5 hrs only ~15% of all recorded nuclei contain Rec10-positively stained structures, this increases to ~30% by 6 hrs due to an increase frequency of class Ia LinEs. By 7 hrs, ~50% of all recorded nuclei contain Rec10-positively stained structures, consisting mainly of class Ib structures, although all 4 classes are present. The frequency of Rec10-positively stained nuclei is reduced by 8 hrs to ~20%, and by 9 hrs, no LinEs are recorded.

In comparison with a *rec10⁺/rec10⁺* asynchronous meiosis (Figure 7.6A), the temporal quantification of LinEs during a *rec10⁺/rec10-155* asynchronous meiosis (Figures 7.6B) demonstrates:

→ LinEs appear earlier (at 2 hrs) during a *rec10⁺/rec10-155* asynchronous meiosis.

→ A reduced frequency of class IIa and IIb LinEs throughout a *rec10⁺/rec10-155* asynchronous meiosis.

→ A reduced frequency of class Ib LinEs from 6 hrs onwards during a *rec10⁺/rec10-155* asynchronous meiosis.

→ A reduced frequency of Rec10-positively stained nuclei from 5 hrs onwards during a *rec10⁺/rec10-155* asynchronous meiosis.

→ No LinEs are present at all at 9 hrs during a *rec10⁺/rec10-155* asynchronous meiosis.

7.2.2c Meiotic progression during a *rec10⁺/rec10-155* asynchronous meiosis

Figure 7.6C shows the horsetail stage appearing to occur between 3-9 hrs, peaking at approximately 5 hrs. Cells begin the first meiotic division at about 6-7 hrs, with ~80% of cells exhibiting ≥2 nuclei by 9 hrs, and all cells appearing to exhibit ≥2 nuclei by 24 hrs.

In comparison with a *rec10⁺/rec10⁺* asynchronous meiosis (Figure 4.3B), the temporal profile of meiotic nuclei during a *rec10⁺/rec10-155* asynchronous meiosis (Figure 7.6C) demonstrates:

→ Advancement in the first meiotic division, of up to 3 hrs is seen during a *rec10⁺/rec10-155* asynchronous meiosis.

A

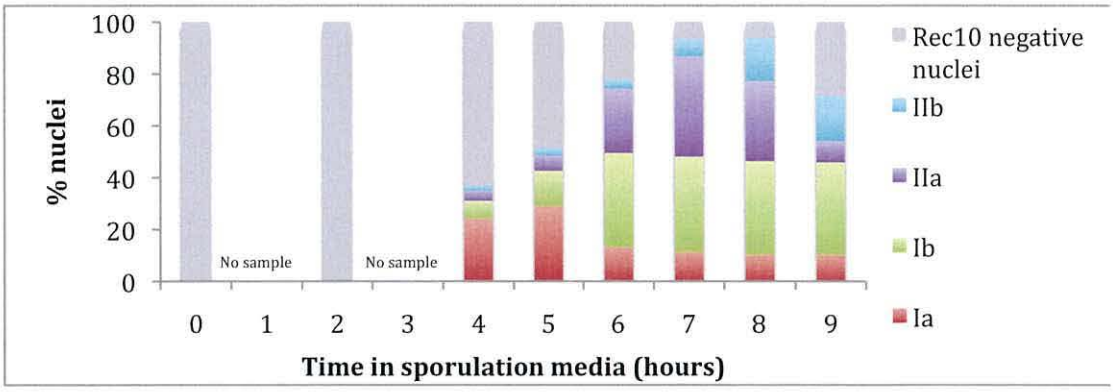

B

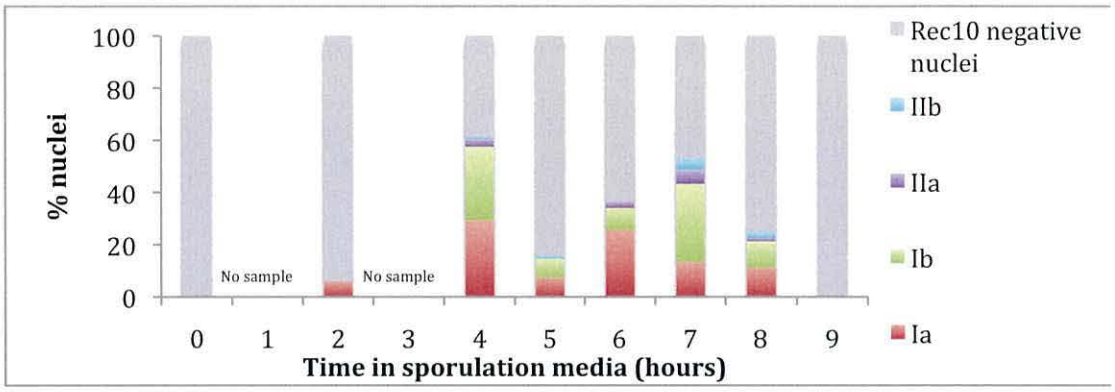

C

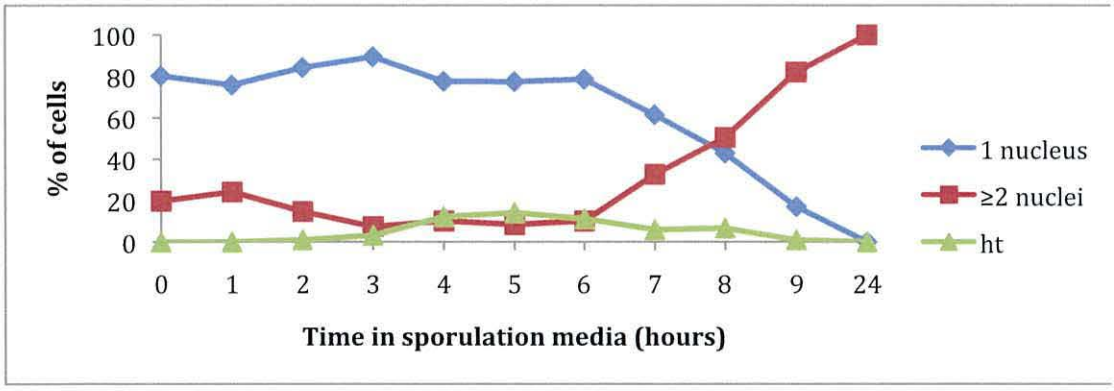

Figure 7.6 Development of LinEs during an asynchronous meiosis of a *rec10⁺* /*rec10-155* heterozygous diploid. (**A**) Proportions of LinE classes scored in *rec10⁺/rec10⁺* diploid asynchronous meiosis*. (**B**) Proportions of LinE classes found in samples taken at hourly intervals after transfer of *rec10⁺ /rec10-155* culture to sporulation media. ≥80 nuclei were scored for each time point* **. (* - No data was collected for time points 1 and 3 hours; ** These data are a duplication of Figure 4.3A and are represented for case of comparison). (**C**) Analysis of cytological meiotic events in samples taken at hourly intervals after transfer of *rec10⁺ /rec10-155* culture to sporulation media. ≥80 nuclei were scored for each time point. ht – horsetail nuclei.

7.2.3 *rec10⁺/rec10-144*

7.2.3a Analysis of intergenic recombination in *rec10-144* homozygous and heterozygous crosses

Previous studies have reported that *rec10-144/rec10-144* homozygous mutant crosses exhibit significant reductions in intergenic recombination at the *leu2-lys7*, *lys4-his4* and *ade6-tps16* intervals (WELLS *et al.*, 2006).

A *rec10+/rec10-144* heterozygote cross, exhibits levels of crossing over similar to that seen in a homozygous wild-type diploid at the *ade6-tps16* interval (WELLS *et al.*, 201X) however, at the *leu2-lys7* interval, a *rec10+/rec10-144* heterozygous cross exhibits a crossover frequency similar to that exhibited by a *rec10-144* homozygous cross (WELLS *et al.*, 201X).

In this study, we analysed the crossover frequency of a *rec10-144* heterozygous mutant at two further intervals to further investigate the regional specificity of crossover reductions observed in *rec10-144* heterozygotes.

Figure 7.7 shows that there is a highly statistically significant reduction in crossover frequency at both intervals in *rec10-144* homozygous mutant crosses. The crossover frequencies for the *rec10-144* heterozygous crosses at the *ade8-arg4* interval are visibly similar to that of the wild-type cross. At the *pro2-arg3* interval however, we observed than one *rec10-144* heterozygote cross bears crossover frequencies similar to that of the wild-type cross, and the other heterozygous cross exhibits a complete loss of crossovers, as does the *rec10-144* homozygous cross. The result observed at the *pro2-arg3* interval is highly unusual, and may be due to an unknown/unrecorded auxotrophy in one of the *rec10-144* mutant strains. This auxotrophy was not tested, and I believe the experiment needs to be repeated using newly constructed strains.

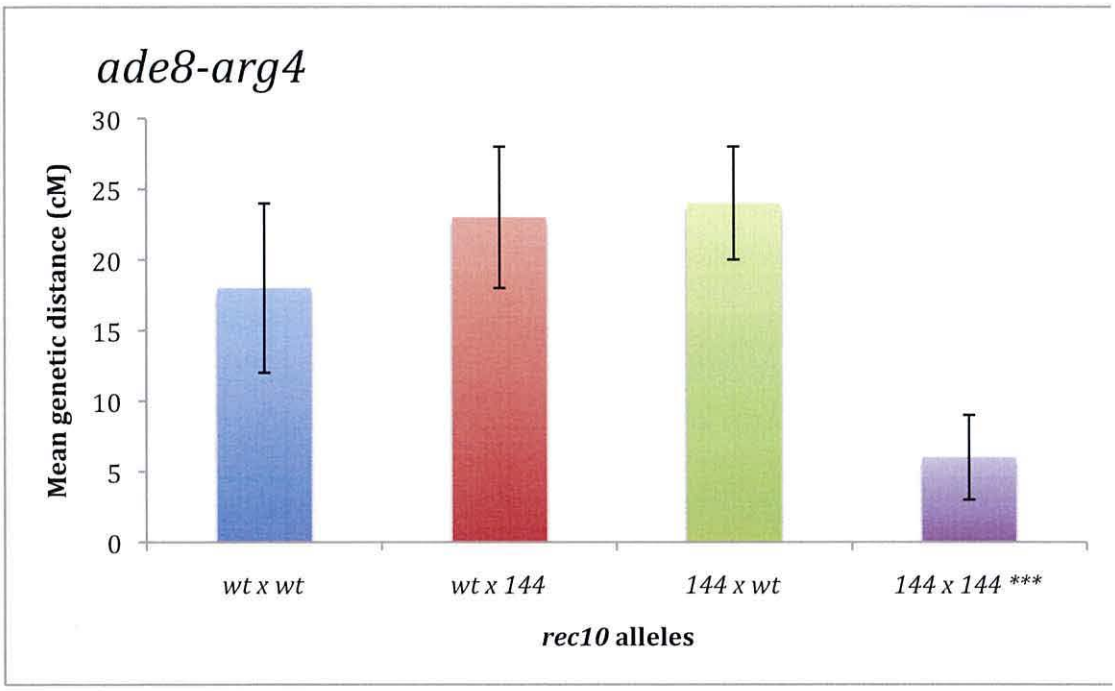

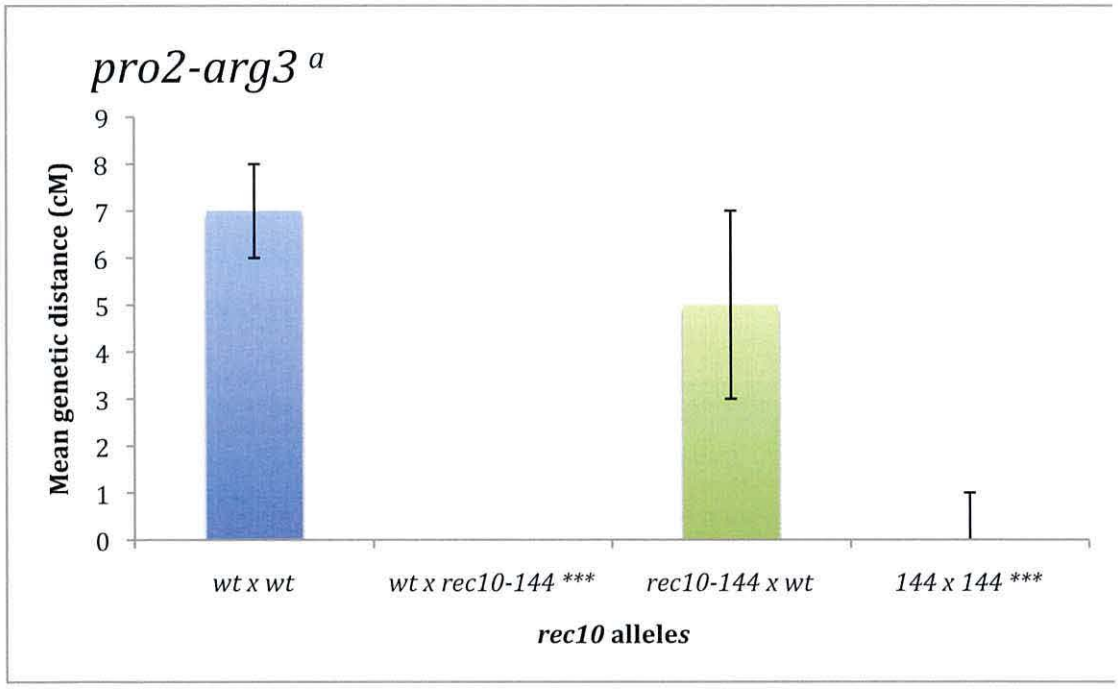

Figure 7.7 Intergenic recombination of *rec10+/rec10-144* heterozygous diploids and *rec10-144/rec10-144* homozygous diploids at the *ade8-arg4* and *pro3-arg2* intervals. cM distances are calculated using Haldane's formula; cM=-50ln(1-2R), where R is the total number of recombinants out of number of spores analysed. n≥3 in all cases. Error bars indicate 95% confidence interval in all cases. Student's *t*-test *P*-values of two tailed comparisons of *rec10* mutants vs. *rec10*$^{+}$ (*P<0.05; **P<0.01; ***P<0.005).

a – These crosses were performed in strains exhibiting an *ade6* mutant background.

7.2.4 Temporal analysis of LinE formation and development in various *rec10-144* heterozygous diploids

The aberrant nature of LinE formation and development in a *rec10-144/rec10-144* homozygous diploid mutant has already been mentioned (Chapter 6). We have also mentioned the regional specificity in crossover proficiency exhibited by *rec10-144* heterozygotes (WELLS *et al.*, 201X; this study), and the semi-dominant nature of the *rec10-144* allele in recombination proficiency (PRYCE *et al.* 2005).

We therefore wanted to look at the formation and development of LinEs in various *rec10-144* heterozygotes, to further analyse the apparent dominance of *rec10* mutant alleles.

7.2.4a LinE formation and development during a *rec10⁺/rec10-144* asynchronous meiosis

Whilst analysing LinE formation in a *rec10⁺/rec10-144* asynchronous meiosis, we observed all four classes of LinEs, as shown in Figure 7.8.

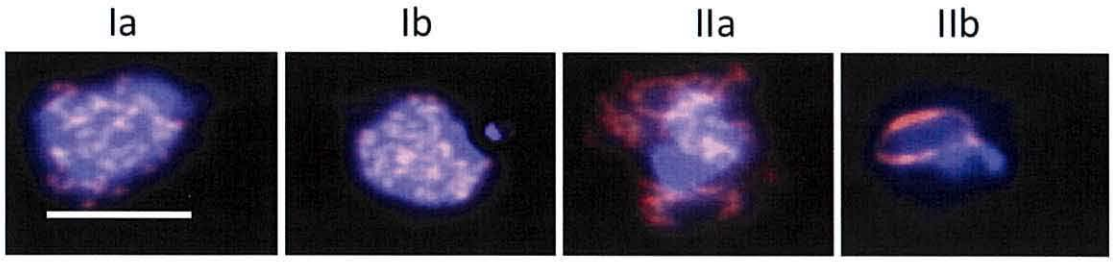

Figure 7.8 Examples of Rec10 positively stained nuclei in a *rec10⁺/rec10-144* asynchronous meiosis. One example is shown for each class of LinE. All nuclei are stained for DNA (blue) and Rec10 (red). Scale bar = 5 μm.

Figure 7.9B shows that LinEs first appear at 4 hrs after transferring the cells to sporulation media (although no sample was taken at 3 hrs, therefore we cannot rule out the possibility that LinEs were present at 3hrs), all classes visible, totalling ~70% of all recorded nuclei. The frequency of Rec10-positively stained nuclei remains fairly constant between 4-7 hrs, with an increase in the presence of class IIa LinEs seen at 7 hrs and 8 hrs. The LinEs recorded at 8 hrs are almost

exclusively class Ia structures with the exception of a few class Ib. By 9 hrs, all four classes of LinEs are again visible; class Ia's remaining the predominant majority.

In comparison with a *rec10⁺/rec10⁺* asynchronous meiosis (Figure 7.9A), the temporal quantification of LinEs during a *rec10⁺/rec10-144* asynchronous meiosis (Figures 7.9B) demonstrates:

→ An increased frequency of Rec10-positively stained nuclei is observed at 4 hrs and 5 hrs during a *rec10⁺/rec10-144* asynchronous meiosis.

→ A reduced frequency of class Ib LinEs is between 6-9 hrs during a *rec10⁺/rec10-144* asynchronous meiosis.

→ An increased frequency of class Ia LinEs at 7-9 hrs during a *rec10⁺/rec10-144* asynchronous meiosis.

→ A reduction in the frequency of class IIa and IIb LinEs at 8 hrs and 9 hrs during a *rec10⁺/rec10-144* asynchronous meiosis.

7.2.4b Meiotic progression during a *rec10⁺/rec10-144* asynchronous meiosis

In figure 7.9C, the horsetail stage appears to occur between 4-9 hrs, peaking at approximately 7 hrs. Progression into the first meiotic division occurs at approximately 8 hrs, with all cells exhibiting ≥2 nuclei by 24 hrs.

In comparison with a *rec10⁺/rec10⁺* asynchronous meiosis (Figure 4.3B), the temporal profile of meiotic nuclei during a *rec10⁺/rec10-144* asynchronous meiosis (Figure 7.9C) demonstrates no significant difference.

A

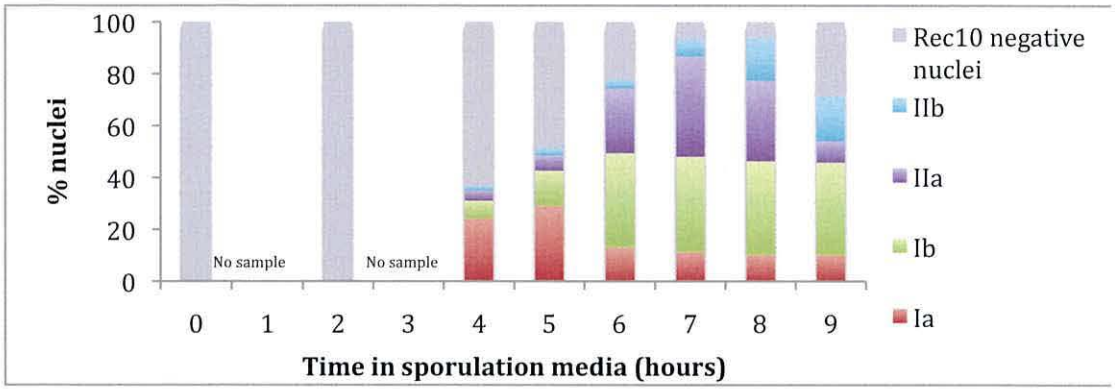

B

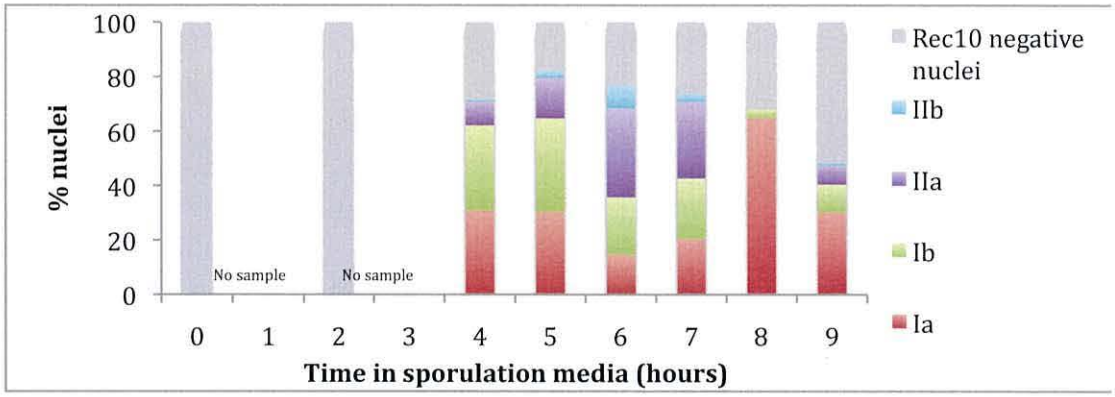

C

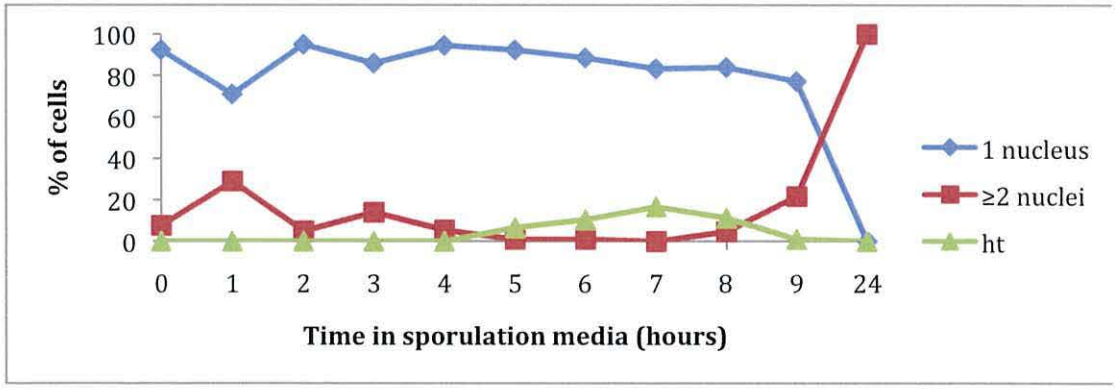

Figure 7.9 Development of LinEs during an asynchronous meiosis of a *rec10⁺/rec10-144* heterozygous diploid. (**A**) Proportions of LinE classes scored in *rec10⁺/rec10⁺* diploid asynchronous meiosis*. (**B**) Proportions of LinE classes found in samples taken at hourly intervals after transfer of *rec10⁺/rec10-144* culture to sporulation media. ≥80 nuclei were scored for each time point* **. (* - No data was collected for time points 1 and 3 hours; ** These data are a duplication of Figure 4.3A and are represented for case of comparison). (**C**) Analysis of cytological meiotic events in samples taken at hourly intervals after transfer of *rec10⁺/rec10-144* culture to sporulation media. ≥80 nuclei were scored for each time point. ht – horsetail nuclei.

7.2.4c LinE formation and development during a *rec10-144/rec10-109* asynchronous meiosis

It has been previously demonstrated that the *rec10-144* and *rec10-109* alleles exhibit partial complementation (PRYCE *et al.* 2005).

We have already mentioned the aberrant nature of LinE formation in both *rec10-144* and *rec10-109* homozygous mutants. Whilst analysing LinE formation in a *rec10-144/rec10-109* mutant, all four classes were observed, albeit with a slightly different morphology to that seen in wild type nuclei (Figure 7.10).

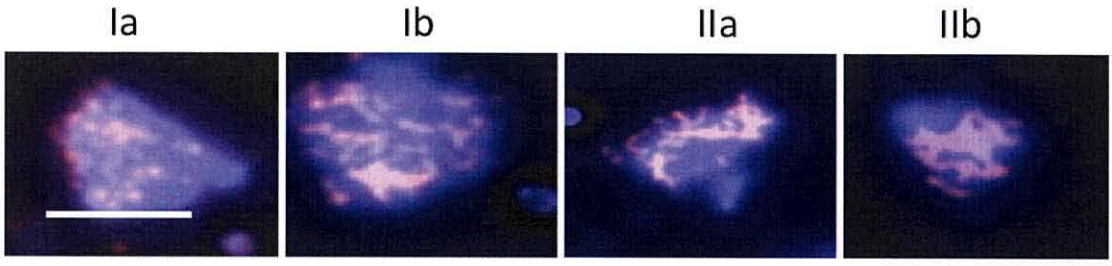

Figure 7.10 Examples of Rec10-positively stained nuclei in a *rec10-144/rec10-109* asynchronous meiosis. All nuclei are stained for DNA (blue) and Rec10 (red). One example is shown for each LinE class. Scale bar = 5 μm.

In figure 7.11B, class Ia, Ib and IIa LinEs are first visible at 2 hrs after the transfer of cells to sporulation media, their combined total accounting for ~5% of all recorded nuclei. All four classes of LinEs are visible by 4 hrs, all together accounting for ~70% of all recorded nuclei. By 5 hrs, the frequency of Rec10-positively stained nuclei has increased to ~95%, consisting mainly of class Ia LinEs (~80%), although the other three classes remain present. There is a reduction in the frequency of Rec10-positively stained nuclei by 6 hrs– down to ~50%, with all classes still present. A further reduction is seen by 7 hrs alongside absence of class IIb LinEs. Nuclei exhibiting class Ia LinEs account for the majority of Rec10-positively stained nuclei at 8 hrs, with a few class Ib LinEs also recorded. Class IIb LinEs are again recorded at 9 hrs, albeit in very small numbers.

In comparison with a *rec10⁺/rec10⁺* asynchronous meiosis (Figure 7.11A), the temporal quantification of LinEs during a *rec10-144/rec10-109* asynchronous meiosis (Figures 7.11B) demonstrates:

→ Advancement in the appearance of LinEs during a *rec10-144/rec10-109* asynchronous meiosis.

→ Increased frequency of class Ia LinEs at 5 hrs during a *rec10-144/rec10-109* asynchronous meiosis.

→ Reduced frequency of Rec10-postitively stained nuclei from 6 hrs onwards during a *rec10-144/rec10-109* asynchronous meiosis.

→ Marked reduction in the frequency of class IIa and IIb LinEs throughout a *rec10-144/rec10-109* asynchronous meiosis.

7.2.4d Meiotic progression during a *rec10-144/rec10-109* asynchronous meiosis

Figure 7.11C demonstrates the horsetail stage occurring between 3-9 hrs. Cells begin the first meiotic division at around 7 hrs, with all cells exhibiting ≥2 nuclei by 24 hrs.

In comparison with a *rec10⁺/rec10⁺* asynchronous meiosis (Figure 4.3B), the temporal profile of meiotic nuclei during a *rec10-144/rec10-109* asynchronous meiosis (Figure 7.11C) demonstrates no significant difference.

A

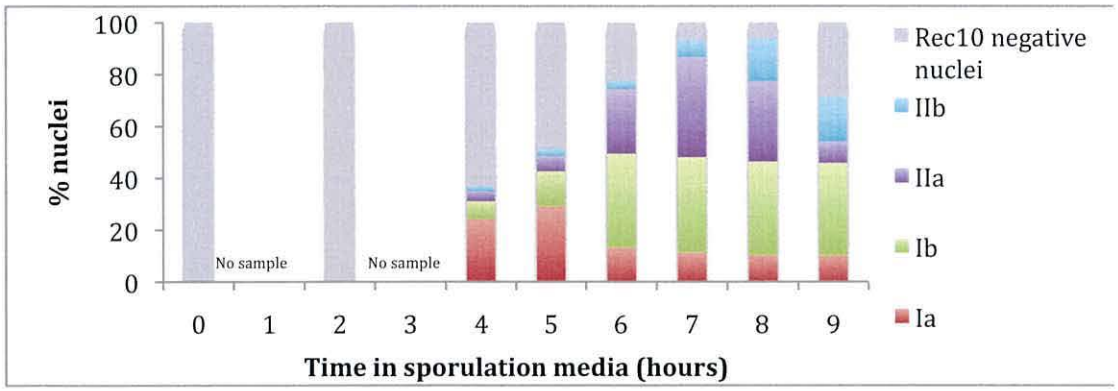

B

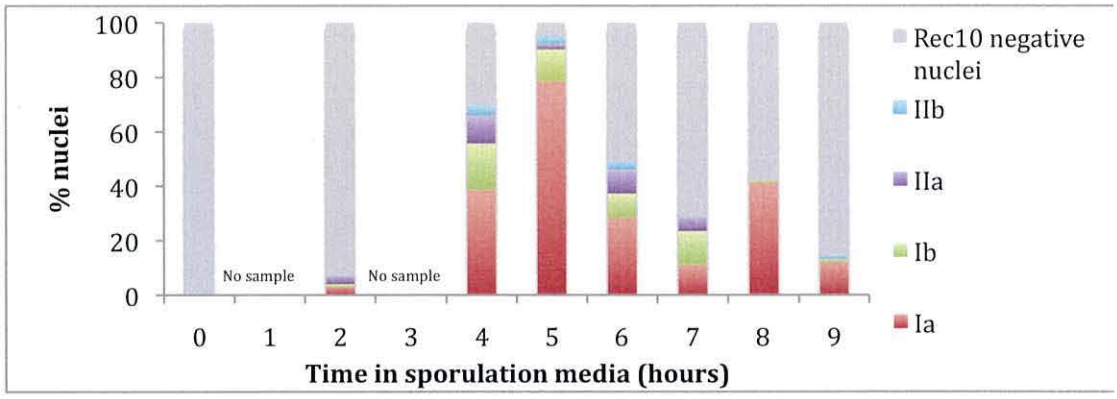

C

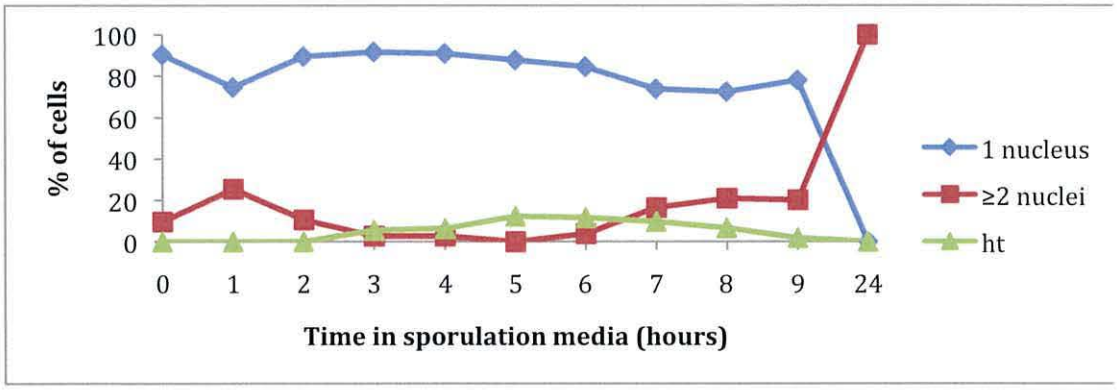

Figure 7.11 Development of LinEs during an asynchronous meiosis of a *rec10-144/rec10-109* heterozygous diploid. (**A**) Proportions of LinE classes scored in *rec10⁺/rec10⁺* diploid asynchronous meiosis*. (**B**) Proportions of LinE classes found in samples taken at hourly intervals after transfer of *rec10-144/rec10-109* culture to sporulation media. ≥80 nuclei were scored for each time point* **. (* - No data was collected for time points 1 and 3 hours; ** These data are a duplication of Figure 4.3A and are represented for case of comparison). (**C**) Analysis of cytological meiotic events in samples taken at hourly intervals after transfer of *rec10-144/rec10-109* culture to sporulation media. ≥80 nuclei were scored for each time point. ht – horsetail nuclei.

7.2.4e LinE formation and development during a *rec10-144/rec10-155* asynchronous meiosis

We have already demonstrated the partial complementation of the *rec10-144* and *rec10-109* alleles with regard to LinE formation (7.2.4d). *rec10-155* and *rec10-175* homozygous mutants fails to form any visible LinEs. We therefore looked at LinE formation in a *rec10-144/rec10-155* and a *rec10-144/rec10-175* heterozygous mutant in order to analyse LinE formation in this heterozygote compared to the *rec10-144*, *rec10-155* and *rec10-175* homozygous mutants.

In Figure 7.8B, class Ia LinEs first become visible at 4 hrs, accounting for ~30% of all recorded nuclei. The frequency of class Ia LinEs increases slightly, by ~10% by 5 hrs and 6 hrs, before returning to ~30% at 7 hrs. A small number (<5%) of class Ib structures are observed between 5-7 hrs. At 8 hrs, only class Ia structures are visible, accounting for ~10% of all recorded nuclei. At 9 hrs, no Rec10-positively stained structures are observed.

In comparison with a *rec10⁺/rec10⁺* asynchronous meiosis (Figure 7.8A), the temporal quantification of LinEs during a *rec10-144/rec10-155* asynchronous meiosis (Figures 7.8B) demonstrates:

- → No class IIa and IIb LinEs are observed during a *rec10-144/rec10-155* asynchronous meiosis.
- → An elevated frequency of class Ia LinEs are observed between 5-7 hrs during a *rec10-144/rec10-155* asynchronous meiosis.
- → A reduced frequency of class Ib structures are observed throughout a *rec10-144/rec10-155* asynchronous meiosis.
- → A reduced frequency of Rec10-positively stained nuclei is observed throughout a *rec10-144/rec10-155* asynchronous meiosis.
- → No LinEs are visible by 9 hrs during a *rec10-144/rec10-155* asynchronous meiosis.

7.2.4f Meiotic progression during a *rec10-144/rec10-155* asynchronous meiosis

Figure 7.8C demonstrates that the horsetail stage occurs between 4-9 hrs, with progression into the first meiotic division beginning at around 8 hrs.

In comparison with a *rec10⁺/rec10⁺* asynchronous meiosis (Figure 4.3B), the temporal profile of meiotic nuclei during a *rec10-144/rec10-155* asynchronous meiosis (Figure 7.8C) demonstrates no significant difference.

A

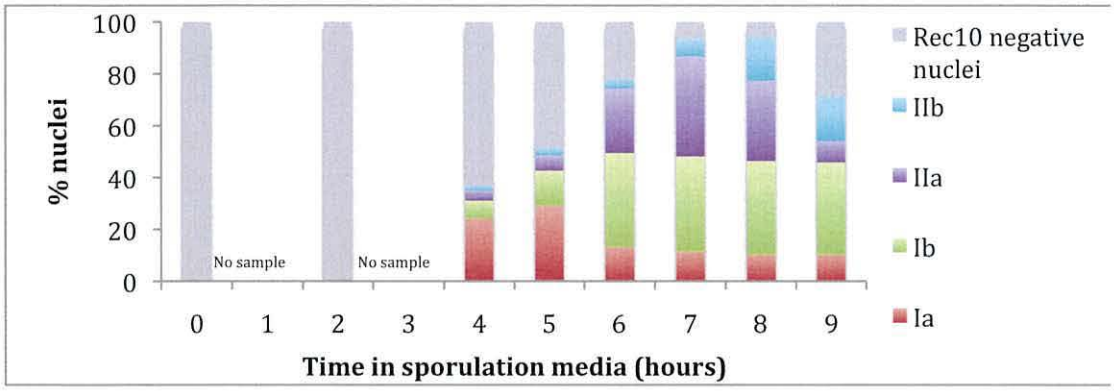

B

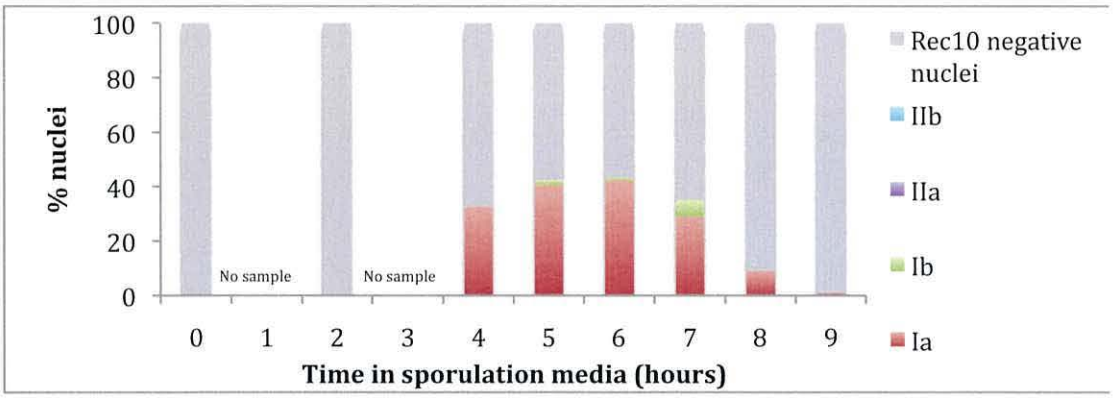

C

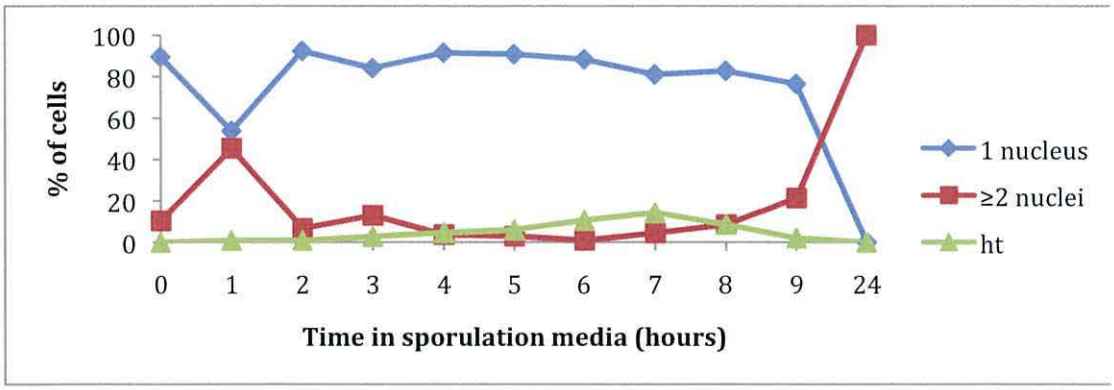

Figure 7.12 Development of LinEs during an asynchronous meiosis of a *rec10-144/rec10-155* heterozygous diploid. (**A**) Proportions of LinE classes scored in *rec10⁺/rec10⁺* diploid asynchronous meiosis*. (**B**) Proportions of LinE classes found in samples taken at hourly intervals after transfer of *rec10-144/rec10-155* culture to sporulation media. ≥80 nuclei were scored for each time point* **. (* - No data was collected for time points 1 and 3 hours; ** These data are a duplication of Figure 4.3A and are represented for case of comparison). (**C**) Analysis of cytological meiotic events in samples taken at hourly intervals after transfer of *rec10-144/rec10-155* culture to sporulation media. ≥80 nuclei were scored for each time point. ht – horsetail nuclei.

7.2.4g LinE formation and development during a *rec10-144/rec10-175* asynchronous meiosis

In Figure 7.13B, we see that class Ia (~60%) and class Ib (~15%) first appear at 4 hrs after the transfer of cells to sporulation media. The frequency of class Ia LinEs remains fairly constant through 4-6 hrs, with the frequency of class Ib LinEs reducing each time. Only class Ia LinEs are visible at 7 hrs (~30%) and 8 hrs (~5%), with no LinEs recorded by 9 hrs.

In comparison with a *rec10⁺/rec10⁺* asynchronous meiosis (Figure 7.13A), the temporal quantification of LinEs during a *rec10-144/rec10-175* asynchronous meiosis (Figures 7.13B) demonstrates:

- → No class IIa or class IIb LinEs are visible during a *rec10-144/rec10-175* asynchronous meiosis.
- → The maximum frequency of Rec10-positively stained nuclei is exhibited at 4 hrs during a *rec10-144/rec10-175* asynchronous meiosis.
- → An elevated frequency of class Ia LinEs is observed between 4-6 hrs during a *rec10-144/rec10-175* asynchronous meiosis.
- → No LinEs are recorded at 9 hrs during a *rec10-144/rec10-175* asynchronous meiosis.

7.2.4h Meiotic progression during a *rec10-144/rec10-175* asynchronous meiosis

The horsetail stage appears to occur between 2-8 hrs, peaking at 5 hrs (Figure 7.13C). Progression into the first meiotic division appears to start at 6 hrs, with ~80% of nuclei exhibiting ≥2 nuclei by 9 hrs.

In comparison with a *rec10⁺/rec10⁺* asynchronous meiosis (Figure 4.3B), the temporal profile of meiotic nuclei during a *rec10-144/rec10-175* asynchronous meiosis (Figure 7.13C) demonstrates:

- → A slight advancement in the horsetail stage (~2 hrs) during a *rec10-144/rec10-175* asynchronous meiosis.
- → An advancement of the first meiotic division, by ~3 hrs during a *rec10-144/rec10-175* asynchronous meiosis.

A

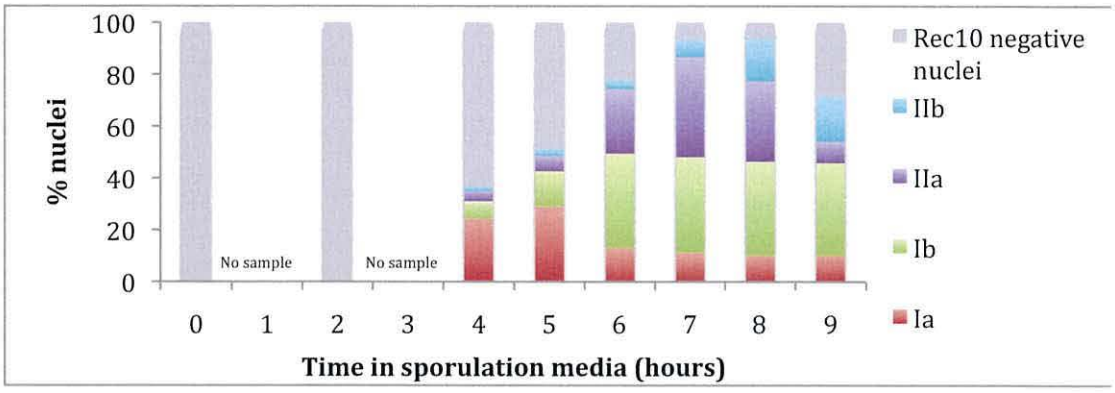

B

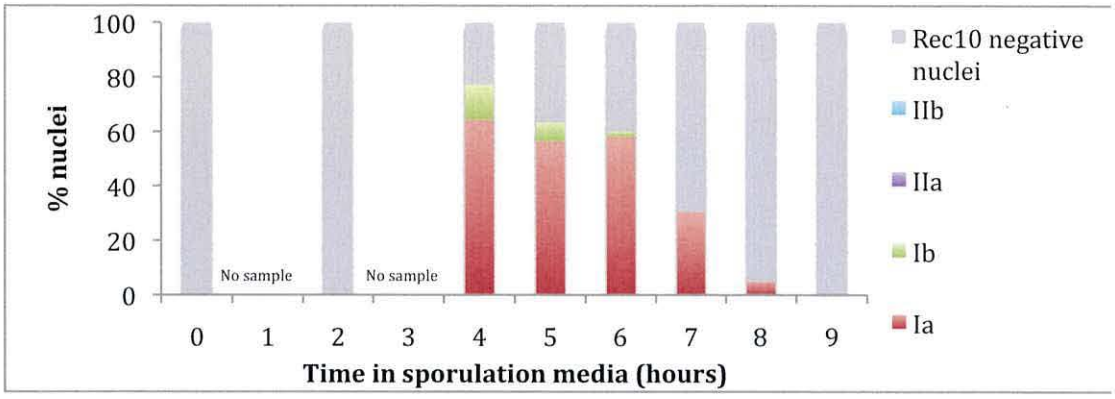

C

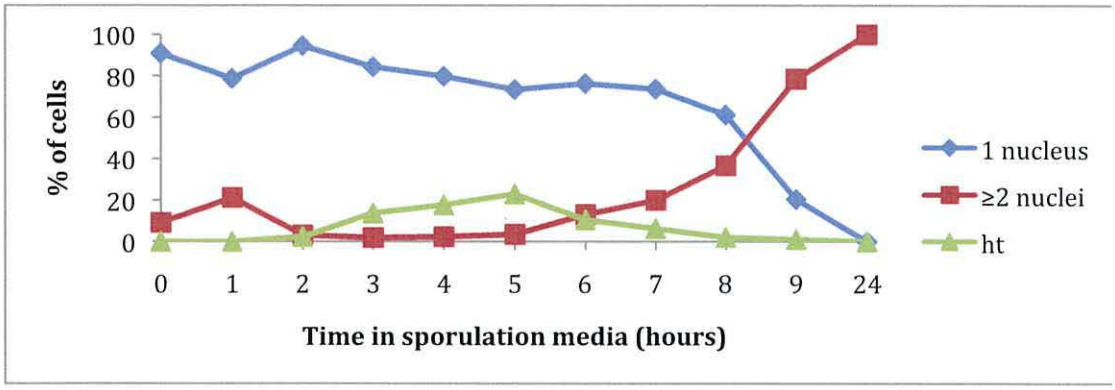

Figure 7.13 Development of LinEs during an asynchronous meiosis of a *rec10-144/rec10-175* heterozygous diploid. (**A**) Proportions of LinE classes scored in *rec10⁺/rec10⁺* diploid asynchronous meiosis*). (**B**) Proportions of LinE classes found in samples taken at hourly intervals after transfer of *rec10-144/rec10-175* culture to sporulation media. ≥80 nuclei were scored for each time point* **. (* - No data was collected for time points 1 and 3 hours; ** These data are a duplication of Figure 4.3A and are represented for case of comparison). (**C**) Analysis of cytological meiotic events in samples taken at hourly intervals after transfer of *rec10-144/rec10-175* culture to sporulation media. ≥80 nuclei were scored for each time point. ht – horsetail nuclei.

7.3 Discussion

7.3.1 Intragenic recombination in *rec10-175* heterozygote crosses

The *rec10-175* homozygous mutant exhibits significant reductions in inter- and intragenic recombination (ELLERMEIER and SMITH 2005; WELLS *et al.,* 2006). The results in Table 1 are in agreement with previous findings, with *rec10-175* homozygous crosses exhibiting substantially reduced recombination frequency observed at all three loci analysed compared with *rec10*$^{+}$ homozygous crosses (*ade6* - ~100-fold; *ura1* - ~100-fold; *lys7* - ~50-100-fold).

Previous studies have demonstrated that *rec10-155* and *rec10-144* homozygote crosses exhibit severe reductions in gene conversion frequencies, however *rec10-155* and *rec10-144* heterozygote crosses appear to have little or no effect on gene conversion frequencies at at least 2 loci - *ade6* and *lys7* (WELLS PH.D.,; WELLS *et al.*, 201X). These data lead to the hypothesis that recombination initiation at these specific loci (*ade6* and *lys7*) suffers little or no defects when LinEs are impaired due to the heterozygosity of *rec10-144* or *rec10-155* (WELLS PH.D.,; WELLS *et al.* 201X).

The data obtained here for *rec10-175* heterozygote crosses at the *ura1* and *lys7* loci are in agreement with the previous findings for *rec10-155*, exhibiting no significant reduction in gene conversions (with the exception of one cross at the *ura1* locus, where a small significant reduction is observed). However, at the *ade6* locus, significant reductions in gene conversion events are exhibited (~4-fold; $P<0.001$ in both cases) in the *rec10-175* heterozygote crosses, although not to the same extent as observed in the *rec10-175* homozygous cross. These data infer a subtle region-specific proficiency for gene conversions in *rec10-175* heterozygote mutants. This region specificity is not highly pronounced, as is the case for rec10-109 homozygous crosses (DEVEAUX and SMITH 1994; ELLERMEIER and SMITH 2005; KRAWCHUK *et al.,* 1999).

We must point out that the *ade6* allele tested in this (and previous) analysis is *ade6-M26*, which is, as previously mentioned, a recombination hotspot. The hotspot activity of *ade6-M26* results in a ~13-fold increase in recombination frequency compared to the non-hotspot allele *of ade6-M375* (GUTZ 1971).

The *rec10-175* heterozygote crosses exhibit a ~4-fold reduction in recombination frequency at the *ade6* locus (Table 1); which is not as low as basal-level recombination. It would therefore be fair to suggest that these data indicate that the reduction in recombination frequency observed in the *rec10-175* heterozygote crosses may be due to a partial loss of *ade6-M26* hotspot activation.

7.3.2 Intergenic recombination analysis in *rec10* mutant heterozygotes – investigating RCP

We have previously discussed the RCP model, which proposes a correlation between LinE associated regions and crossover proficiency (WELLS *et al.*, 201X).

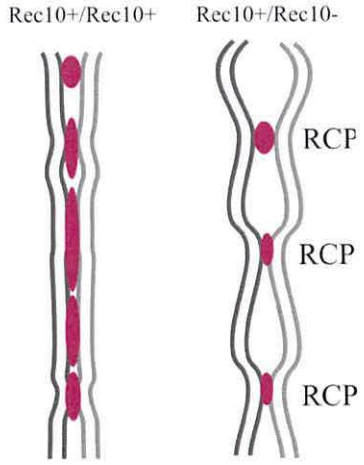

Figure 7.14 Regions of crossover preference model. The left hand image delineates the widespread LinE formation in a *rec10⁺/rec10⁺* meiosis, which exhibits genome-wide crossover proficiency. The right hand image shows the aberrant nature of LinE formation in rec10⁺/rec10⁻ meiosis, which exhibits region-specific crossover proficiency; LinE formation is only seen at specific regions, which the model proposes as being regions of crossover preference. Figure adapted from WELLS et al, (201X).

This model is based on the region-specific crossover proficiency of heterozygous crosses in *rec10* mutants that are defective in LinE formation. Our data appears to correlate with this hypothesis. In Figure 7.4, *rec10-155* heterozygote crosses exhibit wild-type crossover frequencies at the *ade8-arg4* interval, yet at the *ura1-pro1* interval, crossover events are similar to those exhibited in a *rec10-155*

homozygous cross. In Figure 7.7, *rec10-144* heterozygote crosses exhibit wild-type crossover frequencies at the *ade8-arg4* interval. At the *pro2-arg3* interval however, there is a confusing result; one heterozygous cross retains near enough wild-type levels of crossing over, whilst the other heterozygous cross is completely void of any measurable crossover events, like the mutant homozygous cross. This result may be due to: a mating-type effect, with sensitivity to the *rec10-144* mutant only apparent when the mutation occurs in a specific mating type, although this has not been apparent in any other mutant at any other interval; the *ade6-* mutant background bearing some effect on the results, repeating the experiment in *ade6*$^{+}$ strains would eliminate this possibility; or as previously mentioned, it may be due to an unknown auxotrophy in one of the rec10-144 mutant strains. Ideally, the experiment should be repeated with newly constructed strains for clarification of results.

From these data, and unpublished observations (WELLS *et al.*, 201X), using the RCP model (Figure 7.14) we can predict that LinEs preferentially associate with chromatin in the regions of *ade8-arg4*, *ade6-tps16*.

To further this theory, we aim to use FISH to directly label the intervals in question on spread nuclei stained with anti-Rec10, to visualise the correlation patterns between LinEs and the analysed intervals.

In order to correlate with the RCP model, we expect Rec10-stained LinEs in spread nuclei from *rec10*$^{+}$*/rec10*$^{+}$ meioses to co-localise with each one of the FISH-labelled intergenic recombination interval tested; however, we expect Rec10-stained LinEs in spread nuclei from *rec10*$^{+}$*/rec10-155* meioses to co-localise only with the FISH-labelled intergenic recombination intervals where the crossover proficiency of *rec10* heterozygous mutants is similar to the levels of crossovers in wild type crosses. This would further support the RCP theory, where crossover proficiency is predominant in LinE-associated regions. Whilst co-FISH/immunofluorescence eventually worked, time limitations prevented addressing this question in depth. Figure 7.15 gives an example of preliminary images from wild-type meiosis showing co-FISH/Rec10-immunofluorescence.

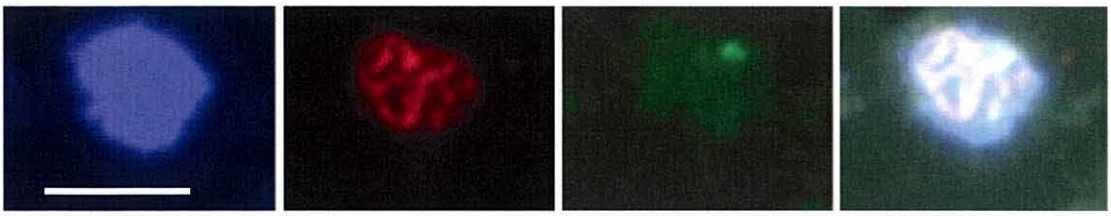

Figure 7.15 Example of FISH-stained Rec10-stained spread nucleus. Cell is stained for DNA (blue), Rec10 (red) and FISH probe (green). These are preliminary experiments, and correlation patterns between Rec10- and FISH- staining are yet to be established. Bar = 5 μm.

7.3.3 LinE development in *rec10-155* and *rec10-175* heterozygote meioses

Figures 7.2 and 7.6 indicate that LinE formation does occur in *rec10-155* and *rec10-175* heterozygote meioses. Semi-dominance of the *rec10* mutant allele on the formation of LinEs is seen in both *rec10-155* and *rec10-175* heterozygote meioses (Figure 7.2 + Figure 7.6); both LinE profiles differ from that of the *rec10⁺/rec10⁺*.

Interestingly, it seems that the *rec10-155* heterozygote exhibits a greater deficiency in LinE development than observed in the *rec10-175* heterozygote; the *rec10-155* heterozygote exhibiting fewer Rec10-positively stained nuclei overall, and an advancement in LinE degradation. These data infer that the remaining portion of the *rec10* gene in the *rec10-155* mutant exerts a stronger negative effect on LinE development than haplo-insufficiency (*rec10-175/rec10⁺*).

The *rec10-155* heterozygous meiosis also exhibits a greater deviation from wild-type in the progression of meiosis than the *rec10-175* heterozygote (Figure 7.2C + Figure 7.6C). These data again suggest that the presence of a truncated *rec10* gene imparts a greater negative effect on meiotic progression than the complete absence of the whole of the *rec10* gene, indicating a dominant negative effect.

7.3.4 Observations on the temporal profile of LinE formation and development in various *rec10-144* heterozygotes

Previous studies have reported the aberrant nature of LinEs in a *rec10-144* mutant (PRYCE *et al.,* 2005), and we have generated a temporal profile of LinE formation and development in a *rec10-144/rec10-144* asynchronous meiosis (Figure 6.3). The semi-dominant nature of the *rec10-144* mutated allele has

previously been mentioned with regard to its effect on meiotic recombination in heterozygous diploids (PRYCE *et al.,* 2005). Therefore, in this study, we wanted to analyse what effect this apparent semi-dominance of the *rec10-144* mutation has on LinE formation and development.

7.3.4a *rec10-144/rec10-109*

Although the *rec10-144* and *rec10-109* homozygous mutants both exhibit highly aberrant LinE formation (as discussed in Chapter 6), it is apparent here that a *rec10-144/rec10-109* heterozygous diploid is able to form more substantial structures, very comparable to all four classes of LinEs observed in a wild type meiosis, although they arguably exhibit a slightly altered morphology (Figure 7.10). The temporal profile of LinE formation is different in a *rec10-144/rec10-109* asynchronous meiosis to that of wild-type (Figure 7.11), yet it is still reasonable to suggest that the *rec10-144* and *rec10-109* mutations act in a somewhat complimentary fashion in the *rec10-144/rec10-109* heterozygous mutant, partly masking each other's negative effect on LinE formation, therefore generating more extensive LinE formation than that seen in either the *rec10-144* or *rec10-109* homozygous mutant. This is consistent with the genetic complementation observed for these alleles for intragenic recombination proficiency (PRYCE *et al.,* 2005), which is why *rec10-144* was originally designated to a distinct complementation group from *rec10-109* (DE VEAUX *et al.,* 1992).

7.3.4b *rec10-144/rec10-155*

The *rec10-144/rec10-155* heterozygote appears to be the most defective *144*-heterozygote in LinE formation (Figure 7.12). It has the least number of Rec10-positively stained nuclei overall, and only class Ia and very few class Ib structures are visible throughout the time course. The *rec10-144/rec10-155* heterozygous mutant appears to inflict a more sever effect on LinE formation than the *rec10⁺/rec10-155* heterozygous mutant (Figure7.6). This indicates that the presence of both the *rec10-155* truncation, and the *rec10-144* mutation has a combined negative effect on LinE formation. The *rec10-144* mutation does appear to exhibit semi-dominance in the *rec10-144/rec10-155* heterozygote, as

we see no advancement in LinE formation (which is seen in a *rec10⁺/rec10-155* heterozygote); no class IIa and IIb structures (which are observed in a *rec10⁺/rec10-155* mutant); no significant difference in meiotic progression (an advancement in meiotic progression is observed in the *rec10⁺/rec10-155* mutant).

Chapter 8

General discussion

8.1 Introduction

S. pombe exhibits a SC-free meiosis, instead forming structures termed LinEs (BÄHLER *et al.*, 1993). LinEs are proposed to be the minimal structures required for proper chromosomal function during MI (BÄHLER *et al.*, 1993). Cytological observations conclude that LinEs do not form along the entire length of the chromosomes (MOLNAR *et al.*, 2003), although their exact chromosomal localisation sites remain unclear. Our observations, made in a synchronised meiosis capable of forming full LinE structures, further clarified previous suggestions that the different LinE structures are in fact different stages of LinE maturation.

The meiosis-specific protein Rec10 is known to be the main component of *S. pombe* LinEs (LORENZ *et al.*, 2004), with Rec25, Rec27, Mek1 and Hop1 also being identified as LinE components (DAVIS *et al.*, 2008; LORENZ *et al.*, 2004). Rec10 is required for meiotic recombination throughout the genome (ELLERMEIER and SMITH 2005), however, significant levels of meiotic recombination can occur in the absence of LinEs (WELLS *et al.*, 2006), indicating that it is not LinEs *per se* which are the Rec10 function essential for recombination.

It is known that the meiotic cohesin complex Rec8-Rec11 is required for wild-type LinE formation (LORENZ *et al.*, 2006; MOLNAR *et al.*, 1995), and that *meu13*, *rec12* and *rec14* mutants all exhibit different temporal profiles of LinE formation compared to the wild-type (MOLNAR *et al.*, 2003). The functions of LinEs however, remain poorly understood.

This study generated several *rec10* C-terminal mutants, with the aim of creating a *rec10* "separation-of-function" mutant, which did not form LinEs but retained wild-type levels of meiotic recombination. Each mutant generated in this study retained the ability to form LinEs, albeit with differing temporal profiles of varying extents to that observed in a wild-type meiosis. Therefore, it remains uncertain whether it is possible to completely separate the recombination and LinE-forming functions of Rec10: consequently it remains unclear whether LinEs

play a direct role in mediating meiotic recombination.

8.2 *rec10-K754R* hotspot-specific suppression of recombination

Genetic analysis of the *rec10* C-terminal mutants generated during this study revealed a remarkable phenotype of the *rec10-K754R* mutant. This mutant appears to not only fail to activate certain recombination hotspots, but in fact the mutation appears to inhibit recombination levels in a hotspot-specific manner. Atf1-Pcr1 is known to facilitate the "opening" of chromatin at recombination hotspots. Loss of Atf1-Pcr1 function results in the loss of hotspot activation, yet basal recombination frequencies are retained. The reduced recombination frequencies observed in the *rec10-K754R* mutant must also be due to a hotspot-specific regulatory factor, as recombination frequencies at the non-hotspot allele are not as dramatically reduced.

In Figure 8.1, we propose a model whereby the *rec10-K754R* mutation causes the Rec10 protein to aberrantly localise to the chromatin subsequent to Atf-Pcr1 in such a way as to "block" the dissociation of Atf1-Pcr1. This "blocking" may result in the absence of a chromatin transition, creating a blockade against Rec12-mediated recombination. This results in Rec12-mediated DSB formation becoming aborted, and a strong reduction in measurable recombination.

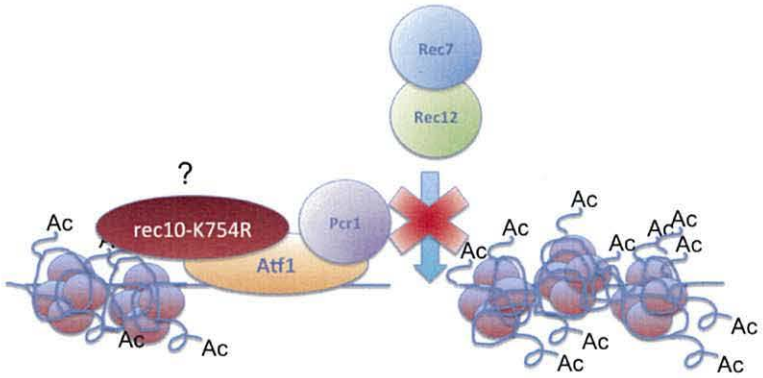

Figure 8.1 Model for *rec10-K754R* hotspot-specific suppression of recombination.

Question mark indicates hypothetical interaction. Red cross indicates inability of Rec7/Rec12 to access the chromatin to mediate DSB formation.

Cytological analysis of LinE formation in the *rec10-K754R* mutant revealed that the K754 residue might be involved in the stabilisation of LinEs or alternatively play a role in regulating their dissociation/degradation, as the temporal profile of LinE development exhibits an advanced degradation/dissociation of LinEs in the *rec10-K754R* mutant. However, the same advancement in LinE degradation/dissociation is also observed in the *rec10-3KR* mutant, which does not exhibit the same reductions in meiotic recombination as the *rec10-K754R* mutant. Therefore, it would be fair to suggest that advancement in the degradation/dissociation of LinEs (as observed in the *rec10-K754R* mutant and the *rec10-3KR* mutant) is not the cause of the hotspot-specific reduction in recombination frequency observed in the *rec10-K754R* mutant. These are independent events.

This study also generated temporal profiles for LinE development in mutants known to exhibit aberrant/temporally different LinEs to those observed in wild-type. Our data for the *rec12Δ* meiosis agrees with previous studies that LinE formation is not dependent on DSB formation; however, we conclude that LinE development and maturation may be dependent upon a process initiated by DSB formation.

8.3 Rec10, Rec25 and Rec27 loading

This study has indicated that LinE formation can be initiated, without subsequent maturation in the absence of Rec27, and we speculate that the apparent dependence on Rec27 previously reported was in fact a *pat1-114* artefact.

Rec25 and Rec27 are known components of LinEs (Davis *et al.*, 2008), and have been proposed to act in a complex with Rec10 (Davis *et al.*, 2008), with the suggestion that their chromosomal localisation may be inter-dependent. The data presented here demonstrates that Rec10 localisation is not completely Rec27-dependent; suggesting that the loading of Rec10, Rec25 and Rec27 may occur in a step-wise manner.

A

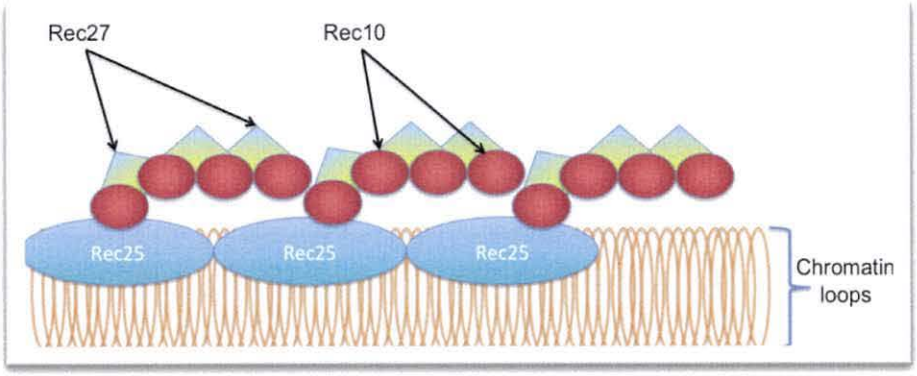

B

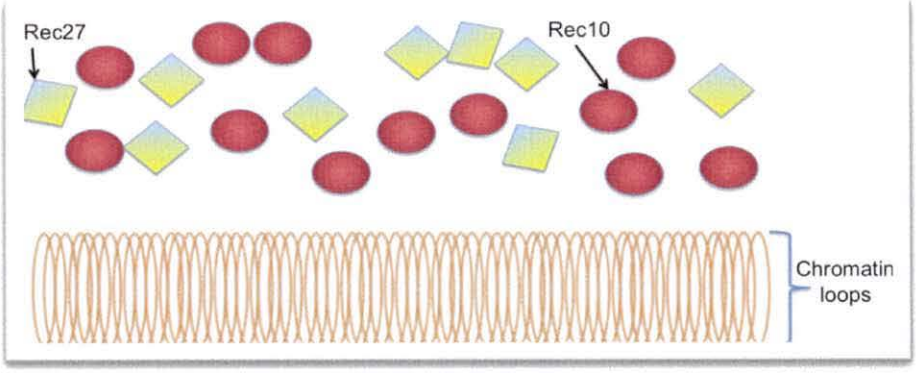

C

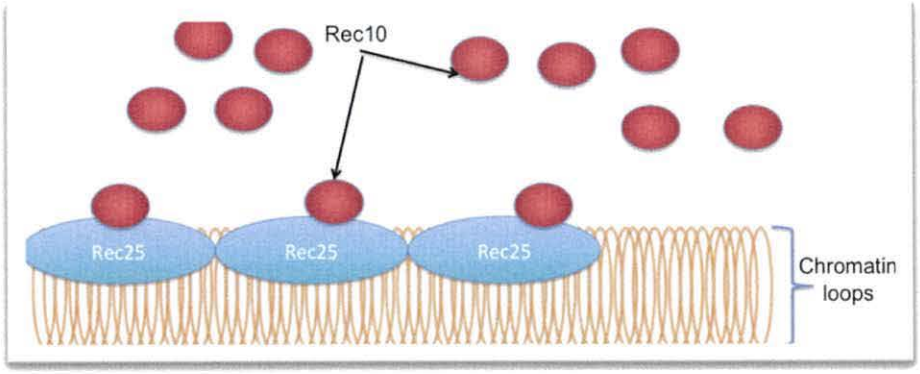

<u>Figure 8.2</u> Model for Rec10, Rec25 and Rec27 loading. (**A**) This model proposes that Rec10 loads onto a Rec25 base platform to initiate LinE formation. Rec27 is subsequently loaded to aid the homo-oligomerisation of Rec10, resulting in the elongation and maturation of LinEs; (**B**) Loss of Rec25 results in failure to load Rec10, and subsequently Rec27, therefore no LinEs are visible; (**C**) Loss of Rec27 results in initial loading of Rec10 onto the Rec25 base platform, but failure to oligomerise, resulting in the dot-like Rec10-positively stained foci observed in a *rec27*Δ mutant.

Figure 8.2 infers two distinct roles for Rec25 and Rec27 in LinE formation; Rec25 may have a role in the loading of Rec10 and subsequent initiation of LinE formation, whilst Rec27 may serve to promote Rec10 homo-oligomerization, resulting in the maturation of LinEs. This model would explain the complete absence of LinEs in a *rec25Δ*, alongside the formation of early dot-like foci in the *rec27Δ*.

8.4 Localisation pattern of Hop1

This study also uncovered the presence of previously unreported structures, which we termed "Hop1 clusters". These structures are observed in regions devoid of Rec10-posisitve LinE staining. As LinEs are proposed to be involved in pairing, lack of pairing in the regions devoid of LinEs may give rise to an elevated probability of inter-sister recombination events; the presence of dense Hop1 staining may be to counteract this phenomenon by suppressing inter-sister events. We also suggest that these Hop1 cluster structures may localise to regions of highly repetitive DNA where suppressing meiotic recombination may be of fundamental importance e.g., telomeres, centromeres and the rDNA locus.

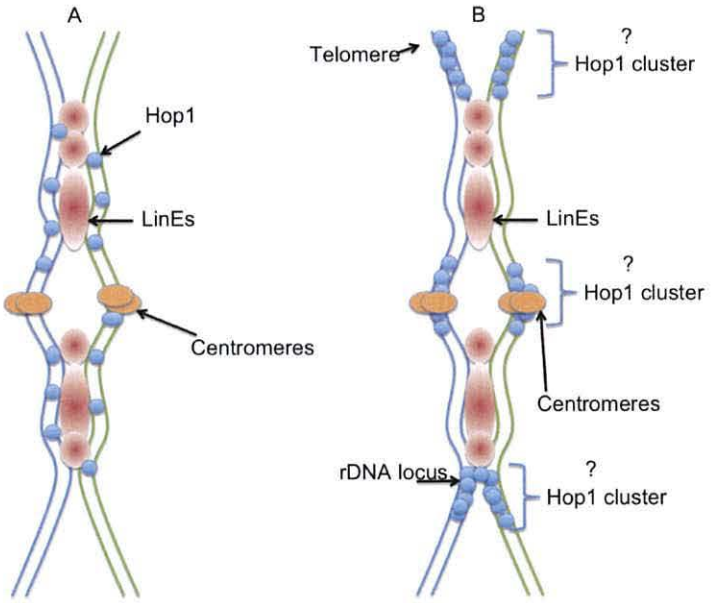

Figure 8.3 Model for Hop1 and LinE localisation patterns. (A) Represents early time point localisation patterns, where Hop1 and LinEs are observed to co-localise. (B) Represents a later time point where Hop1 clusters are observed in specific regions of repetitive DNA, devoid of LinEs.

In Figure 8.3 a model is proposed for the localisation patterns of Hop1 and LinEs. The temporal profile of Hop1 localisation, Hop1/Rec10 co-staining and the appearance of Hop1 cluster structures suggests that Hop1 clusters are formed by a re-organisation of Hop1 localisation throughout the nucleus. The model proposes that Hop1 moves from being LinE-associated, and present throughout the nucleus (Figure 8.3A) to being observed as dense staining within a small region devoid of Rec10 positively stained LinEs (Figure 8.3B).

8.5 Linking Hop1 localisation to RCP model

We have previously mentioned the RCP model (Chapter 7), whereby the study of mutants that are heterozygous for *rec10* alleles (that result in varying degrees of defective LinE formation) demonstrated a region-specific loss of crossover function; these data contributed to the generation of the RCP model, where crossovers preferentially occur in LinE-associated regions (WELLS & MACFARLANE PERS. COMM, THIS STUDY). The data presented in Chapter 7 re-enforces the RCP model.

Loss of Hop1 does not effect LinE formation, although LinEs are required for Hop1 function (LORENZ *et al.,* 2004). A *hop1Δ* heterozygous mutant exhibits RCP despite exhibiting fully formed LinEs (WELLS *et al.*, 201X). These data infer that the presence of neither wild-type levels of Rec10, nor full LinE formation is not sufficient to mediate crossovers on a genome-wide basis and that other associated proteins e.g., Hop1 are also required genome-wide crossover proficiency.

It is inferred that RCPs are still observed in *hop1* heterozygote mutants in order to avoid recombination in certain areas (e.g., centromeres and telomeres) where inter-sister recombination would usually be suppressed in a wild-type strain, or alternatively to ensure the obligate CO event in the absence of CO interference (as exhibited in *S. pombe*). In Figure 8.4 we propose that the localisation of Hop1 clusters facilitate genome-wide crossover proficiency by providing the necessary barriers against inter-sister recombination events at specific regions (we speculate the centromeres and telomeres in this model). The model suggests that recombination machinery only localises to certain areas once inter-sister recombination has been suppressed. Therefore, the model infers that a

combination of LinEs and Hop1 localisation creates optimum environment for crossing over, by both promoting inter-homologue associations, and selectively ensuring lack of inter-sister recombination events.

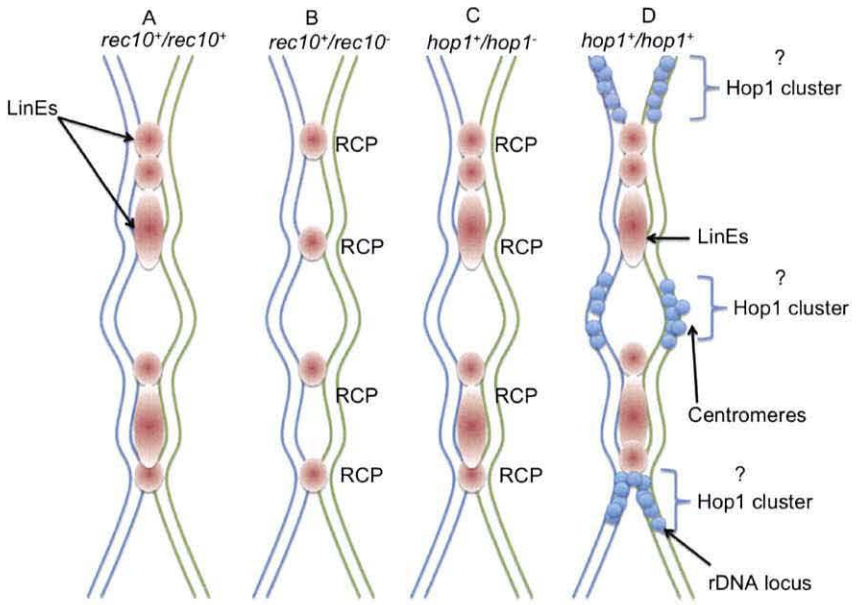

Figure 8.4 Hop1 localisation in relation to the RCP model. (**A**) Fully formed LinEs in a *rec10⁺/rec10⁺* meiosis exhibit no regional preference in crossover proficiency; (**B**) heterozygosity of a *rec10* mutant defective in LinE formation exhibits RCP; (**C**) *hop1* heterozygosity has no ill-effect on LinE formation yet still exhibits RCP; (**D**) *hop1⁺/hop1⁺* forms full LinEs and does not exhibit RCP – here it is speculated that the localisation patterns of Hop1 permit genome-wide crossover proficiency. Figure adapted from WELLS *et al.,* (201X).

References

ALANI, E., R. PADMORE and N. KLECKNER, 1990 Analysis of wild-type and rad50 mutants of yeast suggests an intimate relationship between meiotic chromosome synapsis and recombination. Cell **61:** 419-436.

ALLERS, T., and M. LICHTEN, 2001 Differential timing and control of noncrossover and crossover recombination during meiosis. Cell **106:** 47-57.

ARORA, C., K. KEE, S. MALEKI and S. KEENEY, 2004 Antiviral protein Ski8 is a direct partner of Spo11 in meiotic DNA break formation, independent of its cytoplasmic role in RNA metabolism. Mol Cell **13:** 549-559.

BAHLER, J., P. SCHUCHERT, C. GRIMM and J. KOHLI, 1991 Synchronized meiosis and recombination in fission yeast: observations with pat1-114 diploid cells. Curr Genet **19:** 445-451.

BAHLER, J., T. WYLER, J. LOIDL and J. KOHLI, 1993 Unusual nuclear structures in meiotic prophase of fission yeast: a cytological analysis. J Cell Biol **121:** 241-256.

BAILIS, J. M., and G. S. ROEDER, 1998 Synaptonemal complex morphogenesis and sister-chromatid cohesion require Mek1-dependent phosphorylation of a meiotic chromosomal protein. Genes Dev **12:** 3551-3563.

BASS, H. W., W. F. MARSHALL, J. W. SEDAT, D. A. AGARD and W. Z. CANDE, 1997 Telomeres cluster de novo before the initiation of synapsis: a three-dimensional spatial analysis of telomere positions before and during meiotic prophase. J Cell Biol **137:** 5-18.

BERCHOWITZ, L. E., and G. P. COPENHAVER, 2010 Genetic interference: don't stand so close to me. Curr Genomics **11:** 91-102.

BISHOP, D. K., 1994 RecA homologs Dmc1 and Rad51 interact to form multiple nuclear complexes prior to meiotic chromosome synapsis. Cell **79:** 1081-1092.

BISHOP, D. K., Y. NIKOLSKI, J. OSHIRO, J. CHON, M. SHINOHARA *et al.*, 1999 High copy number suppression of the meiotic arrest caused by a dmc1 mutation: REC114 imposes an early recombination block and RAD54 promotes a DMC1-independent DSB repair pathway. Genes Cells **4:** 425-444.

BISHOP, D. K., D. PARK, L. XU and N. KLECKNER, 1992 DMC1: a meiosis-specific yeast homolog of E. coli recA required for recombination, synaptonemal complex formation, and cell cycle progression. Cell **69:** 439-456.

BISHOP, D. K., and D. ZICKLER, 2004 Early decision; meiotic crossover interference prior to stable strand exchange and synapsis. Cell **117:** 9-15.

BLAT, Y., R. U. PROTACIO, N. HUNTER and N. KLECKNER, 2002 Physical and functional interactions among basic chromosome organizational features govern early steps of meiotic chiasma formation. Cell **111:** 791-802.

BODDY, M. N., P. H. GAILLARD, W. H. MCDONALD, P. SHANAHAN, J. R. YATES, 3RD *et al.*, 2001 Mus81-Eme1 are essential components of a Holliday junction resolvase. Cell **107:** 537-548.

BODDY, M. N., A. LOPEZ-GIRONA, P. SHANAHAN, H. INTERTHAL, W. D. HEYER *et al.*, 2000 Damage tolerance protein Mus81 associates with the FHA1 domain of checkpoint kinase Cds1. Mol Cell Biol **20:** 8758-8766.

BORNER, G. V., N. KLECKNER and N. HUNTER, 2004 Crossover/noncrossover differentiation, synaptonemal complex formation, and regulatory surveillance at the leptotene/zygotene transition of meiosis. Cell **117:** 29-45.

CALLENDER, T. L., and N. M. HOLLINGSWORTH, 2010 Mek1 suppression of meiotic double-strand break repair is specific to sister chromatids, chromosome autonomous and independent of Rec8 cohesin complexes. Genetics **185:** 771-782.

CARBALLO, J. A., A. L. JOHNSON, S. G. SEDGWICK and R. S. CHA, 2008 Phosphorylation of the axial element protein Hop1 by Mec1/Tel1 ensures meiotic interhomolog recombination. Cell **132:** 758-770.

CERVANTES, M. D., J. A. FARAH and G. R. SMITH, 2000 Meiotic DNA breaks associated with recombination in S. pombe. Mol Cell **5:** 883-888.

CHELYSHEVA, L., S. DIALLO, D. VEZON, G. GENDROT, N. VRIELYNCK *et al.*, 2005 AtREC8 and AtSCC3 are essential to the monopolar orientation of the kinetochores during meiosis. J Cell Sci **118:** 4621-4632.

CHEN, X. B., R. MELCHIONNA, C. M. DENIS, P. H. GAILLARD, A. BLASINA *et al.*, 2001 Human Mus81-associated endonuclease cleaves Holliday junctions in vitro. Mol Cell **8:** 1117-1127.

CHENG, C. H., F. M. LIN, Y. H. LO and T. F. WANG, 2007 Tying SUMO modifications to dynamic behaviors of chromosomes during meiotic prophase of Saccharomyces cerevisiae. J Biomed Sci **14:** 481-490.

CHENG, C. H., Y. H. LO, S. S. LIANG, S. C. TI, F. M. LIN *et al.*, 2006 SUMO modifications control assembly of synaptonemal complex and polycomplex in meiosis of Saccharomyces cerevisiae. Genes Dev **20:** 2067-2081.

CHI, P., J. SAN FILIPPO, M. G. SEHORN, G. V. PETUKHOVA and P. SUNG, 2007 Bipartite stimulatory action of the Hop2-Mnd1 complex on the Rad51 recombinase. Genes Dev **21:** 1747-1757.

CHIKASHIGE, Y., D. Q. DING, H. FUNABIKI, T. HARAGUCHI, S. MASHIKO *et al.*, 1994 Telomere-led premeiotic chromosome movement in fission yeast. Science **264:** 270-273.

CHIKASHIGE, Y., D. Q. DING, Y. IMAI, M. YAMAMOTO, T. HARAGUCHI *et al.*, 1997 Meiotic nuclear reorganization: switching the position of centromeres and telomeres in the fission yeast Schizosaccharomyces pombe. EMBO J **16:** 193-202.

CHIKASHIGE, Y., R. KUROKAWA, T. HARAGUCHI and Y. HIRAOKA, 2004 Meiosis induced by inactivation of Pat1 kinase proceeds with aberrant nuclear positioning of centromeres in the fission yeast Schizosaccharomyces pombe. Genes Cells **9:** 671-684.

CHIKASHIGE, Y., C. TSUTSUMI, M. YAMANE, K. OKAMASA, T. HARAGUCHI *et al.*, 2006 Meiotic proteins bqt1 and bqt2 tether telomeres to form the bouquet arrangement of chromosomes. Cell **125:** 59-69.

CICCIA, A., A. CONSTANTINOU and S. C. WEST, 2003 Identification and characterization of the human mus81-eme1 endonuclease. J Biol Chem **278:** 25172-25178.

CICCIA, A., N. MCDONALD and S. C. WEST, 2008 Structural and functional relationships of the XPF/MUS81 family of proteins. Annu Rev Biochem **77:** 259-287.

CIOSK, R., M. SHIRAYAMA, A. SHEVCHENKO, T. TANAKA, A. TOTH *et al.*, 2000 Cohesin's binding to chromosomes depends on a separate complex consisting of Scc2 and Scc4 proteins. Mol Cell **5:** 243-254.

COLEMAN, T. R., and W. G. DUNPHY, 1994 Cdc2 regulatory factors. Curr Opin Cell Biol **6:** 877-882.

COOPER, J. P., Y. WATANABE and P. NURSE, 1998 Fission yeast Taz1 protein is required for meiotic telomere clustering and recombination. Nature **392:** 828-831.

COWAN, C. R., P. M. CARLTON and W. Z. CANDE, 2001 The polar arrangement of telomeres in interphase and meiosis. Rabl organization and the bouquet. Plant Physiol **125:** 532-538.

CREMER, M., J. VON HASE, T. VOLM, A. BRERO, G. KRETH *et al.*, 2001 Non-random radial higher-order chromatin arrangements in nuclei of diploid human cells. Chromosome Res **9:** 541-567.

CROMIE, G., and G. R. SMITH, 2008 Meiotic Recombination in Schizosaccharomyces pombe: A Paradigm for Genetic and Molecular Analysis. Genome Dyn Stab **3:** 195.

CROMIE, G. A., J. C. CONNELLY and D. R. LEACH, 2001 Recombination at double-strand breaks and DNA ends: conserved mechanisms from phage to humans. Mol Cell **8:** 1163-1174.

CROMIE, G. A., R. W. HYPPA, A. F. TAYLOR, K. ZAKHARYEVICH, N. HUNTER *et al.*, 2006 Single Holliday junctions are intermediates of meiotic recombination. Cell **127:** 1167-1178.

CROMIE, G. A., and G. R. SMITH, 2007 Branching out: meiotic recombination and its regulation. Trends Cell Biol **17:** 448-455.

CUNLIFFE, L., S. WHITE and C. J. MCINERNY, 2004 DSC1-MCB regulation of meiotic transcription in Schizosaccharomyces pombe. Mol Genet Genomics **271:** 60-71.

DARWICHE, N., L. A. FREEMAN and A. STRUNNIKOV, 1999 Characterization of the components of the putative mammalian sister chromatid cohesion complex. Gene **233:** 39-47.

DAVIS, L., A. E. ROZALEN, S. MORENO, G. R. SMITH and C. MARTIN-CASTELLANOS, 2008 Rec25 and Rec27, novel linear-element components, link cohesin to meiotic DNA breakage and recombination. Curr Biol **18:** 849-854.

DAVIS, L., and G. R. SMITH, 2001 Meiotic recombination and chromosome segregation in Schizosaccharomyces pombe. Proc Natl Acad Sci U S A **98:** 8395-8402.

DAVIS, L., and G. R. SMITH, 2003 Nonrandom homolog segregation at meiosis I in Schizosaccharomyces pombe mutants lacking recombination. Genetics **163:** 857-874.

DE LOS SANTOS, T., N. HUNTER, C. LEE, B. LARKIN, J. LOIDL *et al.*, 2003 The Mus81/Mms4 endonuclease acts independently of double-Holliday junction resolution to promote a distinct subset of crossovers during meiosis in budding yeast. Genetics **164:** 81-94.

DE VEAUX, L. C., N. A. HOAGLAND and G. R. SMITH, 1992 Seventeen complementation groups of mutations decreasing meiotic recombination in Schizosaccharomyces pombe. Genetics **130:** 251-262.

DEN HAESE, G. J., N. WALWORTH, A. M. CARR and K. L. GOULD, 1995 The Wee1 protein kinase regulates T14 phosphorylation of fission yeast Cdc2. Mol Biol Cell **6:** 371-385.

DEVEAUX, L. C., and G. R. SMITH, 1994 Region-specific activators of meiotic recombination in Schizosaccharomyces pombe. Genes Dev **8:** 203-210.

DEWAR, H., K. TANAKA, K. NASMYTH and T. U. TANAKA, 2004 Tension between two kinetochores suffices for their bi-orientation on the mitotic spindle. Nature **428:** 93-97.

DING, D. Q., N. SAKURAI, Y. KATOU, T. ITOH, K. SHIRAHIGE *et al.*, 2006 Meiotic cohesins modulate chromosome compaction during meiotic prophase in fission yeast. J Cell Biol **174:** 499-508.

DING, D. Q., A. YAMAMOTO, T. HARAGUCHI and Y. HIRAOKA, 2004 Dynamics of homologous chromosome pairing during meiotic prophase in fission yeast. Dev Cell **6:** 329-341.

DOLL, E., M. MOLNAR, G. CUANOUD, G. OCTOBRE, V. LATYPOV *et al.*, 2008 Cohesin and recombination proteins influence the G1-to-S transition in azygotic meiosis in Schizosaccharomyces pombe. Genetics **180:** 727-740.

DORSETT, D., 2009 Cohesin, gene expression and development: lessons from Drosophila. Chromosome Res **17:** 185-200.

EICHINGER, C. S., and S. JENTSCH, 2010 Synaptonemal complex formation and meiotic checkpoint signaling are linked to the lateral element protein Red1. Proc Natl

Acad Sci U S A **107:** 11370-11375.
ELLERMEIER, C., E. C. HIGUCHI, N. PHADNIS, L. HOLM, J. L. GEELHOOD *et al.*, 2010 RNAi and heterochromatin repress centromeric meiotic recombination. Proc Natl Acad Sci U S A **107:** 8701-8705.
ELLERMEIER, C., H. SCHMIDT and G. R. SMITH, 2004 Swi5 acts in meiotic DNA joint molecule formation in Schizosaccharomyces pombe. Genetics **168:** 1891-1898.
ELLERMEIER, C., H. SCHMIDT and G. R. SMITH, 2004 Swi5 acts in meiotic DNA joint molecule formation in Schizosaccharomyces pombe. Genetics **168:** 1891-1898.
ELLERMEIER, C., and G. R. SMITH, 2005 Cohesins are required for meiotic DNA breakage and recombination in Schizosaccharomyces pombe. Proc Natl Acad Sci U S A **102:** 10952-10957.
ENGEBRECHT, J. A., K. VOELKEL-MEIMAN and G. S. ROEDER, 1991 Meiosis-specific RNA splicing in yeast. Cell **66:** 1257-1268.
FARAH, J. A., G. A. CROMIE and G. R. SMITH, 2009 Ctp1 and Exonuclease 1, alternative nucleases regulated by the MRN complex, are required for efficient meiotic recombination. Proc Natl Acad Sci U S A **106:** 9356-9361.
FEENEY, K. M., C. W. WASSON and J. L. PARISH, 2010 Cohesin: a regulator of genome integrity and gene expression. Biochem J **428:** 147-161.
FEKAIRI, S., S. SCAGLIONE, C. CHAHWAN, E. R. TAYLOR, A. TISSIER *et al.*, 2009 Human SLX4 is a Holliday junction resolvase subunit that binds multiple DNA repair/recombination endonucleases. Cell **138:** 78-89.
FERRARI, S. R., J. GRUBB and D. K. BISHOP, 2009 The Mei5-Sae3 protein complex mediates Dmc1 activity in Saccharomyces cerevisiae. J Biol Chem **284:** 11766-11770.
FOX, M. E., J. B. VIRGIN, J. METZGER and G. R. SMITH, 1997 Position- and orientation-independent activity of the Schizosaccharomyces pombe meiotic recombination hot spot M26. Proc Natl Acad Sci U S A **94:** 7446-7451.
FOX, M. E., T. YAMADA, K. OHTA and G. R. SMITH, 2000 A family of cAMP-response-element-related DNA sequences with meiotic recombination hotspot activity in Schizosaccharomyces pombe. Genetics **156:** 59-68.
FUKUSHIMA, K., Y. TANAKA, K. NABESHIMA, T. YONEKI, T. TOUGAN *et al.*, 2000 Dmc1 of Schizosaccharomyces pombe plays a role in meiotic recombination. Nucleic Acids Res **28:** 2709-2716.
GAILLARD, P. H., E. NOGUCHI, P. SHANAHAN and P. RUSSELL, 2003 The endogenous Mus81-Eme1 complex resolves Holliday junctions by a nick and counternick mechanism. Mol Cell **12:** 747-759.
GARTENBERG, M., 2009 Heterochromatin and the cohesion of sister chromatids. Chromosome Res **17:** 229-238.
GASKELL, L. J., F. OSMAN, R. J. GILBERT and M. C. WHITBY, 2007 Mus81 cleavage of Holliday junctions: a failsafe for processing meiotic recombination intermediates? EMBO J **26:** 1891-1901.
GERTON, J. L., J. DERISI, R. SHROFF, M. LICHTEN, P. O. BROWN *et al.*, 2000 Global mapping of meiotic recombination hotspots and coldspots in the yeast Saccharomyces cerevisiae. Proc Natl Acad Sci U S A **97:** 11383-11390.
GERTON, J. L., and J. L. DERISI, 2002 Mnd1p: an evolutionarily conserved protein required for meiotic recombination. Proc Natl Acad Sci U S A **99:** 6895-6900.
GOLDSTEIN, P., 1987 Multiple synaptonemal complexes (polycomplexes): origin, structure and function. Cell Biol Int Rep **11:** 759-796.
GRANT, P. A., D. E. STERNER, L. J. DUGGAN, J. L. WORKMAN and S. L. BERGER, 1998 The SAGA unfolds: convergence of transcription regulators in chromatin-modifying

complexes. Trends Cell Biol **8:** 193-197.
GREGAN, J., P. K. RABITSCH, B. SAKEM, O. CSUTAK, V. LATYPOV *et al.*, 2005 Novel genes required for meiotic chromosome segregation are identified by a high-throughput knockout screen in fission yeast. Curr Biol **15:** 1663-1669.
GRISHCHUK, A. L., R. KRAEHENBUEHL, M. MOLNAR, O. FLECK and J. KOHLI, 2004 Genetic and cytological characterization of the RecA-homologous proteins Rad51 and Dmc1 of Schizosaccharomyces pombe. Curr Genet **44:** 317-328.
GRUBER, S., C. H. HAERING and K. NASMYTH, 2003 Chromosomal cohesin forms a ring. Cell **112:** 765-777.
GUACCI, V., D. KOSHLAND and A. STRUNNIKOV, 1997 A direct link between sister chromatid cohesion and chromosome condensation revealed through the analysis of MCD1 in S. cerevisiae. Cell **91:** 47-57.
GUTZ, H., 1971 Site Specific Induction of Gene Conversion in SCHIZOSACCHAROMYCES POMBE. Genetics **69:** 317-337.
HALL, S. E., G. KETTLER and D. PREUSS, 2003 Centromere satellites from Arabidopsis populations: maintenance of conserved and variable domains. Genome Res **13:** 195-205.
HARPER, L., I. GOLUBOVSKAYA and W. Z. CANDE, 2004 A bouquet of chromosomes. J Cell Sci **117:** 4025-4032.
HARTMAN, T., K. STEAD, D. KOSHLAND and V. GUACCI, 2000 Pds5p is an essential chromosomal protein required for both sister chromatid cohesion and condensation in Saccharomyces cerevisiae. J Cell Biol **151:** 613-626.
HARTSUIKER, E., K. MIZUNO, M. MOLNAR, J. KOHLI, K. OHTA *et al.*, 2009 Ctp1CtIP and Rad32Mre11 nuclease activity are required for Rec12Spo11 removal, but Rec12Spo11 removal is dispensable for other MRN-dependent meiotic functions. Mol Cell Biol **29:** 1671-1681.
HARTSUIKER, E., E. VAESSEN, A. M. CARR and J. KOHLI, 2001 Fission yeast Rad50 stimulates sister chromatid recombination and links cohesion with repair. EMBO J **20:** 6660-6671.
HENDERSON, K. A., K. KEE, S. MALEKI, P. A. SANTINI and S. KEENEY, 2006 Cyclin-dependent kinase directly regulates initiation of meiotic recombination. Cell **125:** 1321-1332.
HENDERSON, K. A., and S. KEENEY, 2005 Synaptonemal complex formation: where does it start? Bioessays **27:** 995-998.
HENRY, J. M., R. CAMAHORT, D. A. RICE, L. FLORENS, S. K. SWANSON *et al.*, 2006 Mnd1/Hop2 facilitates Dmc1-dependent interhomolog crossover formation in meiosis of budding yeast. Mol Cell Biol **26:** 2913-2923.
HERNANDEZ-HERNANDEZ, A., H. RINCON-ARANO, F. RECILLAS-TARGA, R. ORTIZ, C. VALDES-QUEZADA *et al.*, 2008 Differential distribution and association of repeat DNA sequences in the lateral element of the synaptonemal complex in rat spermatocytes. Chromosoma **117:** 77-87.
HIROTA, K., C. S. HOFFMAN, T. SHIBATA and K. OHTA, 2003 Fission yeast Tup1-like repressors repress chromatin remodeling at the fbp1+ promoter and the ade6-M26 recombination hotspot. Genetics **165:** 505-515.
HIROTA, K., K. MIZUNO, T. SHIBATA and K. OHTA, 2008 Distinct chromatin modulators regulate the formation of accessible and repressive chromatin at the fission yeast recombination hotspot ade6-M26. Mol Biol Cell **19:** 1162-1173.
HOLLINGSWORTH, N. M., and S. J. BRILL, 2004 The Mus81 solution to resolution: generating meiotic crossovers without Holliday junctions. Genes Dev **18:** 117-125.

HOLLINGSWORTH, N. M., and B. BYERS, 1989 HOP1: a yeast meiotic pairing gene. Genetics **121:** 445-462.
HOLLINGSWORTH, N. M., L. GOETSCH and B. BYERS, 1990 The HOP1 gene encodes a meiosis-specific component of yeast chromosomes. Cell **61:** 73-84.
HOLLINGSWORTH, N. M., and A. D. JOHNSON, 1993 A conditional allele of the Saccharomyces cerevisiae HOP1 gene is suppressed by overexpression of two other meiosis-specific genes: RED1 and REC104. Genetics **133:** 785-797.
HONG, E. J., and G. S. ROEDER, 2002 A role for Ddc1 in signaling meiotic double-strand breaks at the pachytene checkpoint. Genes Dev **16:** 363-376.
HOOKER, G. W., and G. S. ROEDER, 2006 A Role for SUMO in meiotic chromosome synapsis. Curr Biol **16:** 1238-1243.
HUNTER, N., and N. KLECKNER, 2001 The single-end invasion: an asymmetric intermediate at the double-strand break to double-holliday junction transition of meiotic recombination. Cell **106:** 59-70.
HYPPA, R. W., G. A. CROMIE and G. R. SMITH, 2008 Indistinguishable landscapes of meiotic DNA breaks in rad50+ and rad50S strains of fission yeast revealed by a novel rad50+ recombination intermediate. PLoS Genet **4:** e1000267.
HYPPA, R. W., and G. R. SMITH, 2010 Crossover invariance determined by partner choice for meiotic DNA break repair. Cell **142:** 243-255.
IINO, Y., and M. YAMAMOTO, 1985 Negative control for the initiation of meiosis in Schizosaccharomyces pombe. Proc Natl Acad Sci U S A **82:** 2447-2451.
IP, S. C., U. RASS, M. G. BLANCO, H. R. FLYNN, J. M. SKEHEL *et al.*, 2008 Identification of Holliday junction resolvases from humans and yeast. Nature **456:** 357-361.
IP, S. C., U. RASS, M. G. BLANCO, H. R. FLYNN, J. M. SKEHEL *et al.*, 2008 Identification of Holliday junction resolvases from humans and yeast. Nature **456:** 357-361.
ISSHIKI, T., N. MOCHIZUKI, T. MAEDA and M. YAMAMOTO, 1992 Characterization of a fission yeast gene, gpa2, that encodes a G alpha subunit involved in the monitoring of nutrition. Genes Dev **6:** 2455-2462.
IVANOV, D., A. SCHLEIFFER, F. EISENHABER, K. MECHTLER, C. H. HAERING *et al.*, 2002 Eco1 is a novel acetyltransferase that can acetylate proteins involved in cohesion. Curr Biol **12:** 323-328.
JONES, G. H., 1984 The control of chiasma distribution. Symp Soc Exp Biol **38:** 293-320.
KADYK, L. C., and L. H. HARTWELL, 1992 Sister chromatids are preferred over homologs as substrates for recombinational repair in Saccharomyces cerevisiae. Genetics **132:** 387-402.
KADYK, L. C., and L. H. HARTWELL, 1993 Replication-dependent sister chromatid recombination in rad1 mutants of Saccharomyces cerevisiae. Genetics **133:** 469-487.
KAN, F., M. K. DAVIDSON and W. P. WAHLS, 2011 Meiotic recombination protein Rec12: functional conservation, crossover homeostasis and early crossover/non-crossover decision. Nucleic Acids Res **39:** 1460-1472.
KASSIR, Y., N. ADIR, E. BOGER-NADJAR, N. G. RAVIV, I. RUBIN-BEJERANO *et al.*, 2003 Transcriptional regulation of meiosis in budding yeast. Int Rev Cytol **224:** 111-171.
KATIS, V. L., M. GALOVA, K. P. RABITSCH, J. GREGAN and K. NASMYTH, 2004 Maintenance of cohesin at centromeres after meiosis I in budding yeast requires a kinetochore-associated protein related to MEI-S332. Curr Biol **14:** 560-572.
KAWASHIMA, S. A., T. TSUKAHARA, M. LANGEGGER, S. HAUF, T. S. KITAJIMA *et al.*, 2007 Shugoshin enables tension-generating attachment of kinetochores by loading Aurora to centromeres. Genes Dev **21:** 420-435.

KEENEY, S., 2001 Mechanism and control of meiotic recombination initiation. Curr Top Dev Biol **52:** 1-53.

KEENEY, S., C. N. GIROUX and N. KLECKNER, 1997 Meiosis-specific DNA double-strand breaks are catalyzed by Spo11, a member of a widely conserved protein family. Cell **88:** 375-384.

KHASANOV, F. K., G. V. SAVCHENKO, E. V. BASHKIROVA, V. G. KOROLEV, W. D. HEYER *et al.*, 1999 A new recombinational DNA repair gene from Schizosaccharomyces pombe with homology to Escherichia coli RecA. Genetics **152:** 1557-1572.

KITAJIMA, T. S., S. A. KAWASHIMA and Y. WATANABE, 2004 The conserved kinetochore protein shugoshin protects centromeric cohesion during meiosis. Nature **427:** 510-517.

KITAJIMA, T. S., Y. MIYAZAKI, M. YAMAMOTO and Y. WATANABE, 2003 Rec8 cleavage by separase is required for meiotic nuclear divisions in fission yeast. EMBO J **22:** 5643-5653.

KJÆRULFF *et al.*, 2005, Constitutive Activation of the fission yeast Pheromone-Responsive Pathway Induces Ectopic Meiosis and Reveals Ste11 as a Mitogen-Activated Protein Kinase Target.

KLECKNER, N., 2006 Chiasma formation: chromatin/axis interplay and the role(s) of the synaptonemal complex. Chromosoma **115:** 175-194.

KLEIN, F., P. MAHR, M. GALOVA, S. B. BUONOMO, C. MICHAELIS *et al.*, 1999 A central role for cohesins in sister chromatid cohesion, formation of axial elements, and recombination during yeast meiosis. Cell **98:** 91-103.

KLEIN, H. L., and L. S. SYMINGTON, 2009 Breaking up just got easier to do. Cell **138:** 20-22.

KON, N., M. D. KRAWCHUK, B. G. WARREN, G. R. SMITH and W. P. WAHLS, 1997 Transcription factor Mts1/Mts2 (Atf1/Pcr1, Gad7/Pcr1) activates the M26 meiotic recombination hotspot in Schizosaccharomyces pombe. Proc Natl Acad Sci U S A **94:** 13765-13770.

KON, N., S. C. SCHROEDER, M. D. KRAWCHUK and W. P. WAHLS, 1998 Regulation of the Mts1-Mts2-dependent ade6-M26 meiotic recombination hot spot and developmental decisions by the Spc1 mitogen-activated protein kinase of fission yeast. Mol Cell Biol **18:** 7575-7583.

KOSZUL, R., K. P. KIM, M. PRENTISS, N. KLECKNER and S. KAMEOKA, 2008 Meiotic chromosomes move by linkage to dynamic actin cables with transduction of force through the nuclear envelope. Cell **133:** 1188-1201.

KOSZUL, R., and N. KLECKNER, 2009 Dynamic chromosome movements during meiosis: a way to eliminate unwanted connections? Trends Cell Biol **19:** 716-724.

KRAWCHUK, M. D., L. C. DEVEAUX and W. P. WAHLS, 1999 Meiotic chromosome dynamics dependent upon the rec8(+), rec10(+) and rec11(+) genes of the fission yeast Schizosaccharomyces pombe. Genetics **153:** 57-68.

KROGH, B. O., and L. S. SYMINGTON, 2004 Recombination proteins in yeast. Annu Rev Genet **38:** 233-271.

KUGOU, K., T. FUKUDA, S. YAMADA, M. ITO, H. SASANUMA *et al.*, 2009 Rec8 guides canonical Spo11 distribution along yeast meiotic chromosomes. Mol Biol Cell **20:** 3064-3076.

LATYPOV, V., M. ROTHENBERG, A. LORENZ, G. OCTOBRE, O. CSUTAK *et al.*, 2010 Roles of Hop1 and Mek1 in meiotic chromosome pairing and recombination partner choice in Schizosaccharomyces pombe. Mol Cell Biol **30:** 1570-1581.

LEU, J. Y., P. R. CHUA and G. S. ROEDER, 1998 The meiosis-specific Hop2 protein of S. cerevisiae ensures synapsis between homologous chromosomes. Cell **94:** 375-386.

LI, J., G. W. HOOKER and G. S. ROEDER, 2006 Saccharomyces cerevisiae Mer2, Mei4 and

Rec114 form a complex required for meiotic double-strand break formation. Genetics **173:** 1969-1981.

LIN, F. M., Y. J. LAI, H. J. SHEN, Y. H. CHENG and T. F. WANG, 2010 Yeast axial-element protein, Red1, binds SUMO chains to promote meiotic interhomologue recombination and chromosome synapsis. EMBO J **29:** 586-596.

LIU, H., and J. H. NAISMITH, 2008 An efficient one-step site-directed deletion, insertion, single and multiple-site plasmid mutagenesis protocol. BMC Biotechnol **8:** 91.

LOIDL, J., 2006 S. pombe linear elements: the modest cousins of synaptonemal complexes. Chromosoma **115:** 260-271.

LORENZ, A., A. ESTREICHER, J. KOHLI and J. LOIDL, 2006 Meiotic recombination proteins localize to linear elements in Schizosaccharomyces pombe. Chromosoma **115:** 330-340.

LORENZ, A., J. L. WELLS, D. W. PRYCE, M. NOVATCHKOVA, F. EISENHABER *et al.*, 2004 S. pombe meiotic linear elements contain proteins related to synaptonemal complex components. J Cell Sci **117:** 3343-3351.

LORENZ, A., S. C. WEST and M. C. WHITBY, 2010 The human Holliday junction resolvase GEN1 rescues the meiotic phenotype of a Schizosaccharomyces pombe mus81 mutant. Nucleic Acids Res **38:** 1866-1873.

LYDALL, D., Y. NIKOLSKY, D. K. BISHOP and T. WEINERT, 1996 A meiotic recombination checkpoint controlled by mitotic checkpoint genes. Nature **383:** 840-843.

LYNN, A., R. SOUCEK and G. V. BORNER, 2007 ZMM proteins during meiosis: crossover artists at work. Chromosome Res **15:** 591-605.

MALEKI, S., M. J. NEALE, C. ARORA, K. A. HENDERSON and S. KEENEY, 2007 Interactions between Mei4, Rec114, and other proteins required for meiotic DNA double-strand break formation in Saccharomyces cerevisiae. Chromosoma **116:** 471-486.

MANCERA, E., R. BOURGON, A. BROZZI, W. HUBER and L. M. STEINMETZ, 2008 High-resolution mapping of meiotic crossovers and non-crossovers in yeast. Nature **454:** 479-485.

MAO-DRAAYER, Y., A. M. GALBRAITH, D. L. PITTMAN, M. COOL and R. E. MALONE, 1996 Analysis of meiotic recombination pathways in the yeast Saccharomyces cerevisiae. Genetics **144:** 71-86.

MARSHALL, R. R., M. MURPHY, D. J. KIRKLAND and K. S. BENTLEY, 1996 Fluorescence in situ hybridisation with chromosome-specific centromeric probes: a sensitive method to detect aneuploidy. Mutat Res **372:** 233-245.

MARSTON, A. L., and A. AMON, 2004 Meiosis: cell-cycle controls shuffle and deal. Nat Rev Mol Cell Biol **5:** 983-997.

MARTIN-CASTELLANOS, C., M. BLANCO, A. E. ROZALEN, L. PEREZ-HIDALGO, A. I. GARCIA *et al.*, 2005 A large-scale screen in S. pombe identifies seven novel genes required for critical meiotic events. Curr Biol **15:** 2056-2062.

MARTINI, E., R. L. DIAZ, N. HUNTER and S. KEENEY, 2006 Crossover homeostasis in yeast meiosis. Cell **126:** 285-295.

MENEELY, P. M., A. F. FARAGO and T. M. KAUFFMAN, 2002 Crossover distribution and high interference for both the X chromosome and an autosome during oogenesis and spermatogenesis in Caenorhabditis elegans. Genetics **162:** 1169-1177.

MICHAELIS, C., R. CIOSK and K. NASMYTH, 1997 Cohesins: chromosomal proteins that prevent premature separation of sister chromatids. Cell **91:** 35-45.

MILMAN, N., E. HIGUCHI and G. R. SMITH, 2009 Meiotic DNA double-strand break repair requires two nucleases, MRN and Ctp1, to produce a single size class of Rec12 (Spo11)-oligonucleotide complexes. Mol Cell Biol **29:** 5998-6005.

MIMITOU, E. P., and L. S. SYMINGTON, 2009 Nucleases and helicases take center stage in homologous recombination. Trends Biochem Sci **34:** 264-272.
MIZUNO, K., Y. EMURA, M. BAUR, J. KOHLI, K. OHTA *et al.*, 1997 The meiotic recombination hot spot created by the single-base substitution ade6-M26 results in remodeling of chromatin structure in fission yeast. Genes Dev **11:** 876-886.
MIZUNO, K., T. HASEMI, T. UBUKATA, T. YAMADA, E. LEHMANN *et al.*, 2001 Counteracting regulation of chromatin remodeling at a fission yeast cAMP response element-related recombination hotspot by stress-activated protein kinase, cAMP-dependent kinase and meiosis regulators. Genetics **159:** 1467-1478.
MORIGASAKI *et al.*, 2008 Fission yeast TOR complex 2 activates the AGC-family Gad8 kinase essential for stress resistance and cell cycle control.
MOLNAR, M., J. BAHLER, J. KOHLI and Y. HIRAOKA, 2001 Live observation of fission yeast meiosis in recombination-deficient mutants: a study on achiasmate chromosome segregation. J Cell Sci **114:** 2843-2853.
MOLNAR, M., J. BAHLER, M. SIPICZKI and J. KOHLI, 1995 The rec8 gene of Schizosaccharomyces pombe is involved in linear element formation, chromosome pairing and sister-chromatid cohesion during meiosis. Genetics **141:** 61-73.
MOLNAR, M., E. DOLL, A. YAMAMOTO, Y. HIRAOKA and J. KOHLI, 2003 Linear element formation and their role in meiotic sister chromatid cohesion and chromosome pairing. J Cell Sci **116:** 1719-1731.
MOORE, D. P., A. W. PAGE, T. T. TANG, A. W. KERREBROCK and T. L. ORR-WEAVER, 1998 The cohesion protein MEI-S332 localizes to condensed meiotic and mitotic centromeres until sister chromatids separate. J Cell Biol **140:** 1003-1012.
MUNOZ, I. M., K. HAIN, A. C. DECLAIS, M. GARDINER, G. W. TOH *et al.*, 2009 Coordination of structure-specific nucleases by human SLX4/BTBD12 is required for DNA repair. Mol Cell **35:** 116-127.
MUNZ, P., 1994 An analysis of interference in the fission yeast Schizosaccharomyces pombe. Genetics **137:** 701-707.
NABESHIMA, K., Y. KAKIHARA, Y. HIRAOKA and H. NOJIMA, 2001 A novel meiosis-specific protein of fission yeast, Meu13p, promotes homologous pairing independently of homologous recombination. EMBO J **20:** 3871-3881.
NASMYTH, K., 2001 Disseminating the genome: joining, resolving, and separating sister chromatids during mitosis and meiosis. Annu Rev Genet **35:** 673-745.
NASMYTH, K., and C. H. HAERING, 2005 The structure and function of SMC and kleisin complexes. Annu Rev Biochem **74:** 595-648.
NEALE, M. J., J. PAN and S. KEENEY, 2005 Endonucleolytic processing of covalent protein-linked DNA double-strand breaks. Nature **436:** 1053-1057.
NEIMAN *et al.*, 1993 Functional homology of protein kinases required for sexual differentiation in Schizosaccharomyces pombe and Saccharomyces cerevisiae suggests a conserved signal transduction module in eukaryotic organisms.
NIMMO, E. R., A. L. PIDOUX, P. E. PERRY and R. C. ALLSHIRE, 1998 Defective meiosis in telomere-silencing mutants of Schizosaccharomyces pombe. Nature **392:** 825-828.
NIU, H., X. LI, E. JOB, C. PARK, D. MOAZED *et al.*, 2007 Mek1 kinase is regulated to suppress double-strand break repair between sister chromatids during budding yeast meiosis. Mol Cell Biol **27:** 5456-5467.
NIU, H., L. WAN, B. BAUMGARTNER, D. SCHAEFER, J. LOIDL *et al.*, 2005 Partner choice during meiosis is regulated by Hop1-promoted dimerization of Mek1. Mol Biol Cell **16:** 5804-5818.
NIWA, O., M. SHIMANUKI and F. MIKI, 2000 Telomere-led bouquet formation facilitates

homologous chromosome pairing and restricts ectopic interaction in fission yeast meiosis. EMBO J **19:** 3831-3840.

NONAKA, N., T. KITAJIMA, S. YOKOBAYASHI, G. XIAO, M. YAMAMOTO *et al.*, 2002 Recruitment of cohesin to heterochromatic regions by Swi6/HP1 in fission yeast. Nat Cell Biol **4:** 89-93.

NURSE, P., 1985 Yeast aids cancer research. Nature **313:** 631-632.

NURSE, P., 1997 Regulation of the eukaryotic cell cycle. Eur J Cancer **33:** 1002-1004.

OCTOBRE, G., A. LORENZ, J. LOIDL and J. KOHLI, 2008 The Rad52 homologs Rad22 and Rti1 of Schizosaccharomyces pombe are not essential for meiotic interhomolog recombination, but are required for meiotic intrachromosomal recombination and mating-type-related DNA repair. Genetics **178:** 2399-2412.

OHTA, K., A. NICOLAS, M. FURUSE, A. NABETANI, H. OGAWA *et al.*, 1998 Mutations in the MRE11, RAD50, XRS2, and MRE2 genes alter chromatin configuration at meiotic DNA double-stranded break sites in premeiotic and meiotic cells. Proc Natl Acad Sci U S A **95:** 646-651.

OHTA, K., T. SHIBATA and A. NICOLAS, 1994 Changes in chromatin structure at recombination initiation sites during yeast meiosis. EMBO J **13:** 5754-5763.

OSMAN, F., J. DIXON, C. L. DOE and M. C. WHITBY, 2003 Generating crossovers by resolution of nicked Holliday junctions: a role for Mus81-Eme1 in meiosis. Mol Cell **12:** 761-774.

PAGE, S. L., and R. S. HAWLEY, 2004 The genetics and molecular biology of the synaptonemal complex. Annu Rev Cell Dev Biol **20:** 525-558.

PARISI, S., M. J. MCKAY, M. MOLNAR, M. A. THOMPSON, P. J. VAN DER SPEK *et al.*, 1999 Rec8p, a meiotic recombination and sister chromatid cohesion phosphoprotein of the Rad21p family conserved from fission yeast to humans. Mol Cell Biol **19:** 3515-3528.

PAWLOWSKI, W. P., I. N. GOLUBOVSKAYA, L. TIMOFEJEVA, R. B. MEELEY, W. F. SHERIDAN *et al.*, 2004 Coordination of meiotic recombination, pairing, and synapsis by PHS1. Science **303:** 89-92.

PENG, Z., W. WANG, A. SCHETTINO, B. LEUNG and M. MCLEOD, 2003 Inactivation of Ran1/Pat1 kinase bypasses the requirement for high-level expression of mei2 during fission yeast meiosis. Curr Genet **43:** 178-185.

PETES, T. D., 1980 Unequal meiotic recombination within tandem arrays of yeast ribosomal DNA genes. Cell **19:** 765-774.

PEZZA, R. J., O. N. VOLOSHIN, F. VANEVSKI and R. D. CAMERINI-OTERO, 2007 Hop2/Mnd1 acts on two critical steps in Dmc1-promoted homologous pairing. Genes Dev **21:** 1758-1766.

PINEDA-KRCH, M., and R. J. REDFIELD, 2005 Persistence and loss of meiotic recombination hotspots. Genetics **169:** 2319-2333.

PONTICELLI, A. S., E. P. SENA and G. R. SMITH, 1988 Genetic and physical analysis of the M26 recombination hotspot of Schizosaccharomyces pombe. Genetics **119:** 491-497.

PONTICELLI, A. S., and G. R. SMITH, 1989 Meiotic recombination-deficient mutants of Schizosaccharomyces pombe. Genetics **123:** 45-54.

PONTICELLI, A. S., and G. R. SMITH, 1992 Chromosomal context dependence of a eukaryotic recombinational hot spot. Proc Natl Acad Sci U S A **89:** 227-231.

PRIELER, S., A. PENKNER, V. BORDE and F. KLEIN, 2005 The control of Spo11's interaction with meiotic recombination hotspots. Genes Dev **19:** 255-269.

PRYCE, D. W., A. LORENZ, J. B. SMIRNOVA, J. LOIDL and R. J. MCFARLANE, 2005 Differential activation of M26-containing meiotic recombination hot spots in

Schizosaccharomyces pombe. Genetics **170:** 95-106.
PRYCE, D. W., and R. J. MCFARLANE, 2009 The meiotic recombination hotspots of Schizosaccharomyces pombe. Genome Dyn **5:** 1-13.
RABITSCH, K. P., J. GREGAN, A. SCHLEIFFER, J. P. JAVERZAT, F. EISENHABER *et al.*, 2004 Two fission yeast homologs of Drosophila Mei-S332 are required for chromosome segregation during meiosis I and II. Curr Biol **14:** 287-301.
ROCKMILL, B., and G. S. ROEDER, 1988 RED1: a yeast gene required for the segregation of chromosomes during the reductional division of meiosis. Proc Natl Acad Sci U S A **85:** 6057-6061.
ROCKMILL, B., and G. S. ROEDER, 1990 Meiosis in asynaptic yeast. Genetics **126:** 563-574.
ROCKMILL, B., M. SYM, H. SCHERTHAN and G. S. ROEDER, 1995 Roles for two RecA homologs in promoting meiotic chromosome synapsis. Genes Dev **9:** 2684-2695.
ROEDER, G. S., 1997 Meiotic chromosomes: it takes two to tango. Genes Dev **11:** 2600-2621.
ROTHENBERG, M., J. KOHLI and K. LUDIN, 2009 Ctp1 and the MRN-complex are required for endonucleolytic Rec12 removal with release of a single class of oligonucleotides in fission yeast. PLoS Genet **5:** e1000722.
SAKUNO, T., and Y. WATANABE, 2009 Studies of meiosis disclose distinct roles of cohesion in the core centromere and pericentromeric regions. Chromosome Res **17:** 239-249.
SARTORI, A. A., C. LUKAS, J. COATES, M. MISTRIK, S. FU *et al.*, 2007 Human CtIP promotes DNA end resection. Nature **450:** 509-514.
SAUVAGEAU, S., A. Z. STASIAK, I. BANVILLE, M. PLOQUIN, A. STASIAK *et al.*, 2005 Fission yeast rad51 and dmc1, two efficient DNA recombinases forming helical nucleoprotein filaments. Mol Cell Biol **25:** 4377-4387.
SCHERTHAN, H., J. BAHLER and J. KOHLI, 1994 Dynamics of chromosome organization and pairing during meiotic prophase in fission yeast. J Cell Biol **127:** 273-285.
SCHMIDT, C. K., N. BROOKES and F. UHLMANN, 2009 Conserved features of cohesin binding along fission yeast chromosomes. Genome Biol **10:** R52.
SCHUCHERT, P., M. LANGSFORD, E. KASLIN and J. KOHLI, 1991 A specific DNA sequence is required for high frequency of recombination in the ade6 gene of fission yeast. EMBO J **10:** 2157-2163.
SCHWACHA, A., and N. KLECKNER, 1994 Identification of joint molecules that form frequently between homologs but rarely between sister chromatids during yeast meiosis. Cell **76:** 51-63.
SCHWACHA, A., and N. KLECKNER, 1997 Interhomolog bias during meiotic recombination: meiotic functions promote a highly differentiated interhomolog-only pathway. Cell **90:** 1123-1135.
SHIMANUKI, M., F. MIKI, D. Q. DING, Y. CHIKASHIGE, Y. HIRAOKA *et al.*, 1997 A novel fission yeast gene, kms1+, is required for the formation of meiotic prophase-specific nuclear architecture. Mol Gen Genet **254:** 238-249.
SJOGREN, C., and L. STROM, 2010 S-phase and DNA damage activated establishment of sister chromatid cohesion--importance for DNA repair. Exp Cell Res **316:** 1445-1453.
SMITH, G. R., M. N. BODDY, P. SHANAHAN and P. RUSSELL, 2003 Fission yeast Mus81.Eme1 Holliday junction resolvase is required for meiotic crossing over but not for gene conversion. Genetics **165:** 2289-2293.
SPIREK, M., A. ESTREICHER, E. CSASZAR, J. WELLS, R. J. MCFARLANE *et al.*, 2010 SUMOylation is required for normal development of linear elements and wild-type meiotic recombination in Schizosaccharomyces pombe. Chromosoma **119:** 59-72.

STEINER, W. W., R. W. SCHRECKHISE and G. R. SMITH, 2002 Meiotic DNA breaks at the S. pombe recombination hot spot M26. Mol Cell **9:** 847-855.
STEINER, W. W., and G. R. SMITH, 2005 Natural meiotic recombination hot spots in the Schizosaccharomyces pombe genome successfully predicted from the simple sequence motif M26. Mol Cell Biol **25:** 9054-9062.
STEINER, W. W., and G. R. SMITH, 2005 Optimizing the nucleotide sequence of a meiotic recombination hotspot in Schizosaccharomyces pombe. Genetics **169:** 1973-1983.
SUGIMOTO, A., Y. IINO, T. MAEDA, Y. WATANABE and M. YAMAMOTO, 1991 Schizosaccharomyces pombe ste11+ encodes a transcription factor with an HMG motif that is a critical regulator of sexual development. Genes Dev **5:** 1990-1999.
SUGIYAMA, A., K. TANAKA, K. OKAZAKI, H. NOJIMA and H. OKAYAMA, 1994 A zinc finger protein controls the onset of premeiotic DNA synthesis of fission yeast in a Mei2-independent cascade. EMBO J **13:** 1881-1887.
SVENDSEN, J. M., A. SMOGORZEWSKA, M. E. SOWA, B. C. O'CONNELL, S. P. GYGI *et al.*, 2009 Mammalian BTBD12/SLX4 assembles a Holliday junction resolvase and is required for DNA repair. Cell **138:** 63-77.
SYM, M., and G. S. ROEDER, 1994 Crossover interference is abolished in the absence of a synaptonemal complex protein. Cell **79:** 283-292.
SYM, M., and G. S. ROEDER, 1995 Zip1-induced changes in synaptonemal complex structure and polycomplex assembly. J Cell Biol **128:** 455-466.
SZANKASI, P., W. D. HEYER, P. SCHUCHERT and J. KOHLI, 1988 DNA sequence analysis of the ade6 gene of Schizosaccharomyces pombe. Wild-type and mutant alleles including the recombination host spot allele ade6-M26. J Mol Biol **204:** 917-925.
SZOSTAK, J. W., 1983 A rapid procedure for the construction of linear yeast plasmids. Methods Enzymol **101:** 245-252.
TANABE, H., F. A. HABERMANN, I. SOLOVEI, M. CREMER and T. CREMER, 2002 Non-random radial arrangements of interphase chromosome territories: evolutionary considerations and functional implications. Mutat Res **504:** 37-45.
TAVASSOLI, M., M. SHAYEGHI, A. NASIM and F. Z. WATTS, 1995 Cloning and characterisation of the Schizosaccharomyces pombe rad32 gene: a gene required for repair of double strand breaks and recombination. Nucleic Acids Res **23:** 383-388.
TEASE, C., and M. A. HULTEN, 2004 Inter-sex variation in synaptonemal complex lengths largely determine the different recombination rates in male and female germ cells. Cytogenet Genome Res **107:** 208-215.
TONAMI, Y., H. MURAKAMI, K. SHIRAHIGE and M. NAKANISHI, 2005 A checkpoint control linking meiotic S phase and recombination initiation in fission yeast. Proc Natl Acad Sci U S A **102:** 5797-5801.
TRAVERS, A., 1999 Chromatin modification: how to put a HAT on the histones. Curr Biol **9:** R23-25.
TRELLES-STICKEN, E., J. LOIDL and H. SCHERTHAN, 1999 Bouquet formation in budding yeast: initiation of recombination is not required for meiotic telomere clustering. J Cell Sci **112 (Pt 5):** 651-658.
TSUBOUCHI, H., and G. S. ROEDER, 2002 The Mnd1 protein forms a complex with hop2 to promote homologous chromosome pairing and meiotic double-strand break repair. Mol Cell Biol **22:** 3078-3088.
TSUBOUCHI, T., A. J. MACQUEEN and G. S. ROEDER, 2008 Initiation of meiotic chromosome synapsis at centromeres in budding yeast. Genes Dev **22:** 3217-3226.
TSUBOUCHI, T., and G. S. ROEDER, 2005 A synaptonemal complex protein promotes

homology-independent centromere coupling. Science **308:** 870-873.
UENO, M., T. NAKAZAKI, Y. AKAMATSU, K. WATANABE, K. TOMITA *et al.*, 2003 Molecular characterization of the Schizosaccharomyces pombe nbs1+ gene involved in DNA repair and telomere maintenance. Mol Cell Biol **23:** 6553-6563.
UHLMANN, F., 2000 Chromosome cohesion: a polymerase for chromosome bridges. Curr Biol **10:** R698-700.
UHLMANN, F., 2003 Chromosome cohesion and separation: from men and molecules. Curr Biol **13:** R104-114.
UHLMANN, F., F. LOTTSPEICH and K. NASMYTH, 1999 Sister-chromatid separation at anaphase onset is promoted by cleavage of the cohesin subunit Scc1. Nature **400:** 37-42.
USUI, T., T. OHTA, H. OSHIUMI, J. TOMIZAWA, H. OGAWA *et al.*, 1998 Complex formation and functional versatility of Mre11 of budding yeast in recombination. Cell **95:** 705-716.
VAN DEN BOSCH, M., K. VREEKEN, J. B. ZONNEVELD, J. A. BRANDSMA, M. LOMBAERTS *et al.*, 2001 Characterization of RAD52 homologs in the fission yeast Schizosaccharomyces pombe. Mutat Res **461:** 311-323.
VAN DEN BOSCH, M., J. B. ZONNEVELD, K. VREEKEN, F. A. DE VRIES, P. H. LOHMAN *et al.*, 2002 Differential expression and requirements for Schizosaccharomyces pombe RAD52 homologs in DNA repair and recombination. Nucleic Acids Res **30:** 1316-1324.
VERDUN, R. E., and J. KARLSEDER, 2007 Replication and protection of telomeres. Nature **447:** 924-931.
VIRGIN, J. B., J. METZGER and G. R. SMITH, 1995 Active and inactive transplacement of the M26 recombination hotspot in Schizosaccharomyces pombe. Genetics **141:** 33-48.
VON WETTSTEIN, D., 1984 The synaptonemal complex and genetic segregation. Symp Soc Exp Biol **38:** 195-231.
WAHLS, W. P., E. R. SIEGEL and M. K. DAVIDSON, 2008 Meiotic recombination hotspots of fission yeast are directed to loci that express non-coding RNA. PLoS One **3:** e2887.
WAHLS, W. P., and G. R. SMITH, 1994 A heteromeric protein that binds to a meiotic homologous recombination hot spot: correlation of binding and hot spot activity. Genes Dev **8:** 1693-1702.
WAIZENEGGER, I. C., S. HAUF, A. MEINKE and J. M. PETERS, 2000 Two distinct pathways remove mammalian cohesin from chromosome arms in prophase and from centromeres in anaphase. Cell **103:** 399-410.
WATANABE, T., K. MIYASHITA, T. T. SAITO, T. YONEKI, Y. KAKIHARA *et al.*, 2001 Comprehensive isolation of meiosis-specific genes identifies novel proteins and unusual non-coding transcripts in Schizosaccharomyces pombe. Nucleic Acids Res **29:** 2327-2337.
WATANABE, Y., and T. S. KITAJIMA, 2005 Shugoshin protects cohesin complexes at centromeres. Philos Trans R Soc Lond B Biol Sci **360:** 515-521, discussion 521.
WATANABE, Y., and P. NURSE, 1999 Cohesin Rec8 is required for reductional chromosome segregation at meiosis. Nature **400:** 461-464.
WELLS, J.L., 2006 Schizosaccharomyces pombe meiotic linear elements. PhD thesis.
WELLS, J. L., D. W. PRYCE, A. ESTREICHER, J. LOIDL and R. J. MCFARLANE, 2006 Linear element-independent meiotic recombination in Schizosaccharomyces pombe. Genetics **174:** 1105-1114.
WELLS, J. L., D. W. PRYCE and R. J. MCFARLANE, 2006 Homologous chromosome pairing in Schizosaccharomyces pombe. Yeast **23:** 977-989.

WENDT, K. S., and J. M. PETERS, 2009 How cohesin and CTCF cooperate in regulating gene expression. Chromosome Res **17:** 201-214.
WEST, S. C., 2009 The search for a human Holliday junction resolvase. Biochem Soc Trans **37:** 519-526.
WHITBY, M. C., 2005 Making crossovers during meiosis. Biochem Soc Trans **33:** 1451-1455.
WILKINSON, M. G., M. SAMUELS, T. TAKEDA, W. M. TOONE, J. C. SHIEH *et al.*, 1996 The Atf1 transcription factor is a target for the Sty1 stress-activated MAP kinase pathway in fission yeast. Genes Dev **10:** 2289-2301.
WILLER, M., L. HOFFMANN, U. STYRKARSDOTTIR, R. EGEL, J. DAVEY *et al.*, 1995 Two-step activation of meiosis by the mat1 locus in Schizosaccharomyces pombe. Mol Cell Biol **15:** 4964-4970.
WOLTERING, D., B. BAUMGARTNER, S. BAGCHI, B. LARKIN, J. LOIDL *et al.*, 2000 Meiotic segregation, synapsis, and recombination checkpoint functions require physical interaction between the chromosomal proteins Red1p and Hop1p. Mol Cell Biol **20:** 6646-6658.
YAMADA, T., K. MIZUNO, K. HIROTA, N. KON, W. P. WAHLS *et al.*, 2004 Roles of histone acetylation and chromatin remodeling factor in a meiotic recombination hotspot. EMBO J **23:** 1792-1803.
YAMAMOTO, A., and Y. HIRAOKA, 2003 Monopolar spindle attachment of sister chromatids is ensured by two distinct mechanisms at the first meiotic division in fission yeast. EMBO J **22:** 2284-2296.
YAMAMOTO, A., R. R. WEST, J. R. MCINTOSH and Y. HIRAOKA, 1999 A cytoplasmic dynein heavy chain is required for oscillatory nuclear movement of meiotic prophase and efficient meiotic recombination in fission yeast. J Cell Biol **145:** 1233-1249.
YAMAMOTO, M., 1996 Regulation of meiosis in fission yeast. Cell Struct Funct **21:** 431-436.
YANOWITZ, J., 2010 Meiosis: making a break for it. Curr Opin Cell Biol **22:** 744-751.
YOKOBAYASHI, S., M. YAMAMOTO and Y. WATANABE, 2003 Cohesins determine the attachment manner of kinetochores to spindle microtubules at meiosis I in fission yeast. Mol Cell Biol **23:** 3965-3973.
YOUNG, J. A., R. W. HYPPA and G. R. SMITH, 2004 Conserved and nonconserved proteins for meiotic DNA breakage and repair in yeasts. Genetics **167:** 593-605.
YOUNG, J. A., R. W. SCHRECKHISE, W. W. STEINER and G. R. SMITH, 2002 Meiotic recombination remote from prominent DNA break sites in S. pombe. Mol Cell **9:** 253-263.
ZICKLER, D., 1973 Fine structure of chromosome pairing in ten Ascomycetes: meiotic and premeiotic (mitotic) synaptonemal complexes. Chromosoma **40:** 401-416.
ZICKLER, D., 2006 From early homologue recognition to synaptonemal complex formation. Chromosoma **115:** 158-174.
ZICKLER, D., and N. KLECKNER, 1998 The leptotene-zygotene transition of meiosis. Annu Rev Genet **32:** 619-697.
ZICKLER, D., and N. KLECKNER, 1999 Meiotic chromosomes: integrating structure and function. Annu Rev Genet **33:** 603-754.